Unclassified

AD 746314

DOCUMENT CONTROL DATA · R & D		
(Security classification of title, body of abstract and indexing annotation must be entered when the overall report is classified)		
1. ORIGINATING ACTIVITY (Corporate author) Radiophysics Laboratory Thayer School of Engineering Dartmouth College, Hanover, N.H.03755		2a. REPORT SECURITY CLASSIFICATION __Unclassified__ 2b. GROUP

3. REPORT TITLE

TRAVELLING IONOSPHERIC DISTURBANCES

4. DESCRIPTIVE NOTES (Type of report and inclusive dates)
Scientific. Final. 1967 Oct 1 - 1971 Sep 30   Approved 72 Apr 26

5. AUTHOR(S) (First name, middle initial, last name)

Carlos H.J. Calderón
Millett G. Morgan

6. REPORT DATE 1971 October 31	7a. TOTAL NO. OF PAGES 174	7b. NO. OF REFS 13
8a. CONTRACT OR GRANT NO. F19628-68-C-0099 b. PROJECT, TASK, AND WORK UNIT NO. 5631-11-01 c. DOD ELEMENT 61102F d. DOD SUBELEMENT 685631	9a. ORIGINATOR'S REPORT NUMBER(S) 9b. OTHER REPORT NO(S) (Any other numbers that may be assigned this report) AFCRL-72-0234	

10. DISTRIBUTION STATEMENT

A - Approved for public release; distribution unlimited.

11. SUPPLEMENTARY NOTES Submitted in partial fulfillment of the requirements for a Doctorate in Engineering Sciences, Dartmouth College Hanover, New Hampshire	12. SPONSORING MILITARY ACTIVITY Air Force Cambridge Research Laboratories (LI) L.G. Hanscom Field Bedford, Massachusetts 01730

13. ABSTRACT

A general study of travelling ionospheric disturbances (T.I.D.'s) has been undertaken.

In the theoretical aspect, the gravity-wave resonant mode $\vec{k} \cdot \vec{B}_0 = 0$ has been studied and the concept of an ionospheric predictive function has been introduced.

In the experimental aspect, the digital data processing portion of the Dartmouth ionosonde network has been brought into operation and seven T.I.D. events have been analyzed with it. The data have been interpreted in light of Hooke's theory and substantial agreement has been found.

Further investigation, both theoretical and experimental, of the $\vec{k} \cdot \vec{B}_0 = 0$ mode, and the adoption of the iso-height contour presentation of the data rather than the iso-ionic fashion which is conventional in the T.I.D. field, are recommended.

Still greater automation in the Dartmouth ionospheric data processing system and the operation of a fourth semi-mobile station, are also recommended.

DD FORM NOV 65 1473

Unclassified

1a

Unclassified

14 KEY WORDS	LINK A		LINK B		LINK C	
	ROLE	WT	ROLE	WT	ROLE	WT
Ionosphere						
Ionospheric sounding						
Ionospheric irregularities						
Travelling ionospheric disturbances						

Unclassified

TRAVELLING IONOSPHERIC DISTURBANCES

by

Carlos H.J. Calderón and Millett G. Morgan

Radiophysics Laboratory
Thayer School of Engineering
Dartmouth College
Hanover, New Hampshire 03755

FINAL REPORT
1967 October 1 - 1971 September 30
1971 October 31

Submitted in partial fulfillment of the requirements for a
Doctorate in Engineering Sciences, Dartmouth College,
Hanover, New Hampshire.

Contract Monitor: Charles M. Rush
Ionospheric Physics Laboratory

Prepared
for

AIR FORCE CAMBRIDGE RESEARCH LABORATORIES
AIR FORCE SYSTEMS COMMAND
UNITED STATES AIR FORCE
BEDFORD, MASSACHUSETTS   01730

TABLE OF CONTENTS

I. INTRODUCTION

A. THE IONOSPHERE

The upper atmosphere is ionized by solar radiation. As the radiation penetrates the atmosphere, it encounters increasing density of ionizable material but is increasingly attenuated by the atmosphere above, and these opposing effects produce a maximum in free electron density at about 300 km. This ionized region of the atmosphere is known as the ionosphere. The free electrons in the ionosphere interact with radiowaves of frequencies up to 100 MHz or so, and significantly affect their propagation.

Although the peak of electron density occurs at a height of about 300 km, subsidiary peaks or "layers" occur at lower levels due to variation with height of the atmospheric composition.

The traditional classification of the ionospheric regions and layers as given, for example, by DAVIES (1965), is:

Height range (km)	Region	Layers
50 - 90	D	D
90 -130	E	E_1, E_2, E_s
130 - up	F	F_1, $F_{1\frac{1}{2}}$, F_2

The simplest possible type of ionized layer that has been derived theoretically is the so-called Chapman layer which results from assuming:

a) an atmosphere with only one type of gas

b) plane stratification

c) parallel rays of monochromatic, ionizing, solar radiation

.

1

d) an isothermal atmosphere.

It can then be shown that the rate of production of ion pairs when the angle to the sun from the zenith is χ, is given at level ζ by:

$$q(\chi, \zeta) = q_0 \exp[1 - \zeta - \sec\chi \ \exp(-\zeta)] \qquad (1)$$

where q_0 is the maximum rate of production of ion pairs at level $\zeta = 0$ when the sun is overhead, and

$$\zeta = \frac{h - h_0}{H} \qquad (2)$$

where h is the height above the ground, h_0 is the height of maximum ion production and H is the scale height of the ionosphere given by

$$H = \frac{kT_0}{Mg} \qquad (3)$$

where k is Boltzmann's constant, T_0 is the uniform temperature of the atmosphere, M is the mean molecular mass of the atmospheric gas, and g is the constant acceleration of gravity.

Assuming that the removal of electrons is due to a recombination process described by

$$\frac{dN}{dt} = q - \alpha N^2 \qquad (4)$$

where N is the electron number density, t is time, and α is the

recombination coefficient; and also assuming that equilibrium has been reached, there results:

$$N(\zeta) = N_O \exp \frac{1}{2} [1 - \zeta - \sec \chi \exp(-\zeta)] \qquad (5)$$

where N_O is the maximum electron number density at level $\zeta = 0$ when the sun is overhead. This expression is known as the Chapman law. In its derivation, the recombination coefficient is taken to be independent of height. In view of this simplifying assumption, and the four previous ones, it is surprising that the E and F_1 layers do in fact approximately follow the Chapman law. In Figure 1, the expression for $N(\zeta)$ is plotted against ζ for several values of the solar zenith angle χ.

B. RADIO WAVES IN THE IONOSPHERE

The existence of the ionosphere was postulated by Kennelly and Heaviside in 1902 to account for the success of Marconi's trans-Atlantic radio experiment. However its existence was not confirmed beyond reasonable doubt until 1925 when in a single year six independent methods of measuring the height of the ionosphere were published and (or) used. Most of the knowledge now existing about the ionosphere has been and is being obtained by means of radio techniques. It is appropriate, therefore, to review the general aspects of radio waves propagating in the ionosphere. Perhaps the most complete treatment of this topic is that by BUDDEN (1961). Generalized treatments of radio waves in magneto-plasmas are also available such as that by STIX (1962).

In the presence of the earth's magnetic field, the ionospheric magneto-plasma acts as a bi-refringent medium, decomposing a plane polarized wave into "ordinary" and "extra-ordinary" waves and changing the direction of energy flow away from the direction of phase propagation.

For the present purpose it will suffice to limit consideration to the propagation of radio waves of the order of a few megahertz, and it will not be necessary to take into account the motion of the neutral particles, the pressure gradients of the atmospheric constituents, or the frictional effects of collisions. With these simplifications and the assumption of small plane wave disturbances (entirely

equivalent to cold-plasma, collisionless wave-theory) it can be shown that the dispersion equation of the characteristic waves, i.e., the waves which can propagate in the medium, is given by:

$$n^2 = 1 - \frac{2X(1-X)}{2(1-X)-Y^2\sin^2\theta \pm \sqrt{Y^4\sin^4\theta + 4(1-X)^2Y^2\cos^2\theta}} \qquad (6)$$

which is known as the Appleton-Hartree equation. Here n is the refractive index of the ionosphere for the radio wave; θ is the angle between the earth's magnetic field and the direction of the wave-normal;

$$X = \frac{\omega_p^2}{\omega^2} \qquad (7)$$

where ω is the angular frequency of the radio wave, ω_p is the local angular plasma frequency given by

$$\omega_p^2 = \frac{Ne^2}{\epsilon_o m} \qquad (8)$$

where ϵ_o is the permittivity of free space, e is the charge of an electron, m its mass; and

$$Y = \frac{\omega_H}{\omega} \qquad (9)$$

where ω_H is the electron angular gyrofrequency given by

$$\omega_H = \frac{eB_o}{m} \qquad (10)$$

where B_o is the earth's magnetic field, taken to be constant.

In general, the Appleton-Hartree dispersion relation
yields four possible values for the refractive index n, once
a particular set of values for X, Y, and θ has been chosen.
These occur in pairs which have the same magnitude but opposite
sign. Each of these two pairs describes different types of
waves, whereas each component of a given pair represents the
same type of wave but with opposite directions of propagation.

In addition to the phase-velocity described by the Appleton-
Hartree dispersion relation, it is useful to consider the polar-
ization of the characteristic waves. The polarization of a
plane wave travelling in the z-direction in the ionosphere is
defined by the ratio R of the transverse electric field com-
ponents

$$R = \frac{E_x}{E_y} \tag{11}$$

when the coordinate system is chosen so that B_o lies in the
yz-plane. Using the parameters of the dispersion relation,
the polarization becomes:

$$R = -\frac{i}{2Y \cos \theta} \left[\frac{Y^2 \sin^2 \theta}{1 - X} \mp \sqrt{\frac{Y^4 \sin^4 \theta}{(1 - X)^2} + 4 Y^2 \cos^2 \theta} \right] \tag{12}$$

The reflection condition for the case of a radio wave
vertically incident upon the ionosphere is obtained by setting
$n = 0$ in the dispersion relation and solving for X,

with + sign: $X = 1$ (13)

with − sign: $X = 1 - Y$ (14a)

  or $X = 1 + Y$ (14b)

Equation (13) shows that for one of the characteristic waves, the wave is reflected as in the absence of a background magnetic field, i.e., $Y = 0$. This wave is called the ordinary wave. Equations (14) show that the height of reflection of the other wave (called extraordinary) is dependent on the magnitude, but not on the direction of the earth's magnetic field. For waves of frequency greater than the gyrofrequency the height of reflection is given by $X = 1 - Y$ whereas for frequencies below the gyrofrequency the condition is $X = 1 + Y$.

C. THE IONOSONDE

The most widely used instrument for investigating the ionosphere by radio is the ionosonde. This is essentially a pulsed radar device in which the probing frequency is swept from about 2 MHz up to 20 MHz.

The equipment is designed to measure directly the time taken for a pulse of radio waves to travel up to the ionosphere from the ground (or down to it from a satellite) and back, as a function of frequency. This time is used to define the radar range to the reflection ight. Assuming group-propagation at the speed of light it defines h', the so-called "virtual height" of the ionosphere, given by

$$h' = 0.5 \ ct \tag{15}$$

where c is the speed of light in free space and t is the echo delay time. The resulting photographic record of virtual height versus frequency is known as an ionogram.

Although the radar pulse travels progressively slower as it penetrates the ionosphere, it is generally possible to compute from an ionogram, the electron number density N(h) as a function of "true-height" h and so provide an electron density height-profile of the ionosphere.

The relation between true height h and virtual height h' is as follows

$$h' = \int_0^h \mu' dh \tag{16}$$

where the group refractive index μ' is given by

$$\mu' = \frac{d}{d\omega}\ (n\omega) \qquad\qquad (17)$$

The inversion of equation (16) is complicated by the fact that μ', defined through equations (17), (6), (7), and (8), is an unknown function of h. The solution may be effected in either of two ways, as classified by THOMAS (1959):

(a) Model or comparison methods in which the layer is assumed to have an $N(h)$ profile such that substitution in equation (16) gives an integral which can be evaluated analytically. The calculated $h'(f)$ curve is then compared with the observed one and the parameters of the assumed distribution obtained.

(b) Integral equation methods which may be divided into two categories: in the first, the equation is inverted directly to give an analytic solution; and in the second, the integral is replaced by a discrete sum over a number of sufficiently small frequency-intervals.

Model or comparison methods have the basic disadvantage that the shape of the layer is assumed a priori and, therefore, they need not be discussed any further.

Both integral equation methods suffer from the inherent instrumental limitation that there are no observations of $h'(f)$ below some

value of the probing frequency. Direct inversion methods are unwieldly except when the magnetic field of the earth is neglected and even when it is not, they apply exactly only on the magnetic equator ($\theta = 90°$). A second fundamental limitation of all integral equation methods is that it is necessary to assume that the plasma density is a monotonically increasing function of height. A more recent, simpler and faster integral equation method due to TITHERIDGE (1967) has been adopted here and is described in the next section.

D. THE OVERLAPPING POLYNOMIAL METHOD OF ANALYSIS OF IONOGRAMS

In this method, the true heights of reflection at a series of frequencies f_1, f_2, f_3, ..., f_n are calculated from the measured virtual heights at these same frequencies. When computing the real height h_i at the frequency f_i, the real height curve between the frequencies f_{i-2} and f_{i+1} is represented by a five-term polynomial in the plasma frequency f_N. The polynomial is required to pass through the real heights f_{i-2}, f_{i-1}, and f_i, and to give the observed virtual height at the frequencies f_{i-1}, f_i, and f_{i+1}. These conditions define a set of five polynomial coefficients at each frequency, giving the value of h_i in terms of h_{i-2}, h_{i-1}, h'_{i-1}, h'_i, and h'_{i+1}.

The polynomial used in calculating h_i extends only down to the height h_{i-2}. The contribution of the ionization below this height to the values of h'_{i-1}, h'_i, h'_{i+1} must therefore be allowed for separately. This is done by the method used in the normal lamination analysis of ionograms, i.e., by the replacement of integral (16) by a discrete sum over a number of sufficiently small frequency intervals.

E. TRAVELLING IONOSPHERIC DISTURBANCES

Iso-ionic contours are height-contours of constant electron density in the ionosphere. Perturbations of the normal equilibrium conditions create ripples of horizontal gradients in these contours. Anomalous reflections then appear on ionograms and records of other radio wave observing stations depending upon ionospheric reflection. Spaced receiving sites often exhibit time delays between them in the occurrence of similar phases of perturbations, thereby demonstrating horizontal propagation of them.

The most successful interpretation of these observations is that which attributes travelling ionospheric disturbances (T.I.D.'s) to corresponding perturbations of the neutral gas associated with the passage of internal atmospheric gravity waves. This interpretation is consistent with T.I.D.'s in so many respects that there is little doubt about its basic correctness, HOOKE (1968).

F. INTERNAL ATMOSPHERIC GRAVITY WAVES

The theory of internal gravity waves has been studied extensively by HINES (1960). The analysis is based on an idealized model in which the atmosphere is taken to be stationary in the absence of such waves, and to be uniform in both temperature and composition. Superimposed wave motions are assumed to have only perturbation magnitude, in that terms of second and higher orders are neglected in the equations governing the motion. Changes are assumed to occur adiabatically and the gravitational field is taken to be constant both in direction and magnitude.

Under these assumptions, it can be shown that atmospheric oscillations are governed by the following dispersion relation:

$$\omega^4 - \omega^2 C_s^2 \ (k_h^2 + k_z^2) + i\omega^2 \gamma g k_z + (\gamma-1)g^2 k_h^2 = 0 \qquad (18)$$

where ω is the angular frequency of the wave, γ is the specific heats ratio of air, g is the acceleration of gravity, k_h and k_z are the horizontal and vertical components of the phase propagation vector $\vec{k}$ (or angular wave number), and C_s is the speed of sound given by

$$C_s^2 = \gamma H g \qquad (19)$$

where H is, again, the scale height of the atmosphere as defined in equation (3). Hines confined his attention

to the case that k_h is purely real so that equation (18) reveals two possibilities: either k_z is purely imaginary or

$$k_z = k_{zr} + i/2H \qquad (20)$$

where k_{zr} is purely real.

The first alternative corresponds to horizontally propagating "surface" waves having vertical attenuation. The second alternative corresponds to "internal" waves which possess a vertical component of propagation. Substituting equation (20) into (18) results in the dispersion relation for internal waves which may be cast in the following form:

$$\frac{1 - \frac{\omega_g^2}{\omega^2}}{1 - \frac{\omega_a^2}{\omega^2}} \, n_h^2 + \frac{1}{1 - \frac{\omega_a^2}{\omega^2}} \, n_{zr}^2 = 1 \qquad (21)$$

where

$$\omega_g^2 \approx \frac{(\gamma - 1)g^2}{C_s^2} \qquad (22)$$

$$\omega_a^2 = \frac{\gamma g}{4H} \qquad (23)$$

$$n_h = \frac{C_s k_h}{\omega} \qquad (24)$$

and $\qquad n_{zr} = \frac{C_s k_{zr}}{\omega} \qquad (25)$

Since γ is less than 2 it follows that $\omega_g < \omega_a$. From equation (21) it can be shown that there exists a gap in the frequency spectrum

$$\omega_g < \omega < \omega_a \qquad (26)$$

in which no internal waves can be propagated. This indicates that two distinct sequences of internal waves can occur. The one at high frequencies, $\omega > \omega_a$ ($T < T_a$), and the other at low frequencies, $\omega < \omega_g$ ($T > T_g$) where $T = 2\pi/\omega$ and $T_g = 2\pi/\omega_g$. The two sequences have been termed by Hines "internal acoustic" waves and "internal gravity" waves.

In Figure 2, contours of constant period in the $n_h - n_{zr}$ domain are shown for the internal gravity wave mode. From these, the directions of phase propagation and energy flow can be readily determined, STIX (1962). The direction of phase propagation is that of the radius vector (n_h, n_{zr}) drawn from the origin to any particular point in the n_h vs. n_{zr} domain. The direction of energy propagation is that of the normal to the corresponding constant period contour, drawn at the tip of the radius vector (n_h, n_{zr}). It is seen that energy may propagate in directions radically different from the corresponding phase normals, by as much as 90° when the asymptotes of the period-contours are approached, and for the longer periods the flow tends to be nearly horizontal.

G. TRAVELLING IONOSPHERIC DISTURBANCES AND GRAVITY WAVES

In a perturbation treatment of the ionospheric irregularities caused by internal atmospheric gravity waves, HOOKE (1968) arrived at several important conclusions. In the F2-region, the main effect of the gravity wave is to impart the component of motion of the neutral gas which is parallel to the magnetic field, to the ionized component. Up to the F1-ledge, the effect of gravity waves on the rate of chemical processes is important and at any point, gravity waves affect the rate of photoionization by altering both the neutral gas number density and the ionizing radiation flux at that point.

At heights at or above the height of the F2-peak, the amplitude of the perturbation in electron number density N' at (x, y, z, t) is given by

$$|N'| = N_0(z)U_b(z_0)\sin I \ \exp[k_{zi}(z-z_0)]\omega^{-1}\sqrt{\left(\frac{1}{N_0}\frac{\partial N_0}{\partial z} + k_{zi}\right)^2 + \left(\frac{k_{br}}{\sin I}\right)^2}$$

$$(27)$$

assuming that it is caused by an internal atmospheric gravity wave producing neutral gas velocities along the earth's magnetic field given by

$$u_b = U_b(z_0)\exp[k_{zi}(z-z_0)]\exp i(\omega t - k_x x - k_y y - k_{zr}z)$$

$$(28)$$

where

$$k_{zi} = \frac{1}{2H} \qquad (29)$$

II. THEORETICAL WORK

A. GRAVITY WAVE RESONANCE CONDITION $\vec{k} \cdot \vec{B}_O = 0$

There is ample evidence that travelling ionospheric disturbances (T.I.D.'s) are caused by the passage of internal atmospheric gravity waves, HINES (1960).

The nature of the interaction of gravity waves with the ionosphere has been studied in detail by HOOKE (1968). Previously, HINES (1955) had sought to explain T.I.D.'s as caused by the resonant response of the ionosphere and found two conditions: $\vec{k} \cdot \vec{k} = 0$ and $\vec{k} \cdot \vec{B}_O = 0$, where $\vec{k}$ is the gravity-wave complex propagation vector and $\vec{B}_O$ is the magnetic field of the earth. Since $\vec{k}$ is in general complex, $\vec{k} \cdot \vec{k} = 0$ does not necessarily imply that $\vec{k} = \vec{0}$. The condition $\vec{k} \cdot \vec{B}_O = 0$ means that $\vec{k}$ must lie in a plane perpendicular to $\vec{B}_O$.

Neither author analyzed the case $\vec{k} \cdot \vec{B}_O = 0$ which is the subject of the present section. Hines's gravity wave dispersion relation is generalized so as to include horizontal attenuation or growth. It is then found that the frequency gap between the internal "acoustic" and "gravity" modes persists. However, the internal gravity wave mode no longer encompasses all frequencies under ω_g, the Väisälä-Brunt frequency, but becomes a band limited by $\omega_g \sin A$ and ω_g, where A is the magnitude of the magnetic dip angle.

17

1. Mathematical Development

The basic assumptions are those of HINES (1955). The atmosphere is taken to be an isothermal, stationary medium, permeated by a uniform magnetic field $\vec{B}_o$ and subject to a constant gravitational acceleration $\vec{g}$.

The analysis is based on three fluid equations: the conservation of mass, the adiabatic equation, and the equation of motion; and three electromagnetic equations: the two Maxwell's equations and a tensorial Ohm's law.

In the equation of conservation of mass, the source term is set equal to zero; in the equation of motion the effect of gravity is included but the electric and magnetic forces are set equal to zero.

In Ampere's law, the displacement current is neglected, and in the conductivity tensor $\overline{\overline{\sigma}}$, the fact that the longitudinal conductivity σ_o is several orders of magnitude larger than the transverse conductivities will be used.

HINES (1955) showed that the foregoing conditions amount to assuming that hydrodynamic oscillations of the ionosphere dominate the basic disturbance, though secondary electromagnetic effects may play an important part in the observations. The medium considered is the simplest one but still retains the essential features of the ionosphere.

Under the conditions listed above, the pertinent equations are:

$$\frac{\partial \rho}{\partial t} + \nabla \cdot (\rho \vec{v}) = 0 \tag{30}$$

$$\frac{d}{dt} (p\rho^{-\gamma}) = 0 \tag{31}$$

$$\rho \frac{d\vec{v}}{dt} = - \nabla p + \rho \vec{g} \tag{32}$$

$$\nabla \times \vec{E} = - \frac{\partial \vec{B}}{\partial t} \tag{33}$$

$$\nabla \times \vec{B} = \mu_o \vec{J} \tag{34}$$

$$\vec{J} = \overline{\overline{\sigma}} \cdot (\vec{E} + \vec{v} \times \vec{B}_o) \tag{35}$$

where p is pressure, ρ is density, $\vec{v}$ is the velocity of a fluid element, γ is the specific heats ratio of the fluid, $\vec{E}$ and $\vec{B}$ are the electric and magnetic fields, μ_o is the magnetic permeability of free space, and $\vec{J}$ is the current density.

The geometry adopted here is shown in Figure 3. The z-axis is taken in the vertical direction with $\vec{g} = - g\hat{z}$, $\vec{B}_o$ is a constant magnetic field in the yz-plane and $\vec{k}$ is a propagation vector in an arbitrary direction.

Assuming now that small changes of the form exp $[i(\omega t - \vec{k} \cdot \vec{r})]$ take place in all variables but that the pressure and density also vary as exp $(- z/H)$, where H is the scale height of the atmosphere, the fluid equations yield

$$[\omega^2 \overline{\overline{I}} - c_s^2 \vec{k}\vec{k} - i\vec{k}\vec{g} - i(\gamma-1)\vec{g}\vec{k}] \cdot \vec{v} = 0 \tag{36}$$

where $\overline{\overline{I}}$ is the unit tensor, and, again

$$c_s^2 = \gamma g H \tag{19}$$

defines the speed of sound in the medium. Equation (36) can

also be written as

$$\omega^4 - \omega^2 C_s^2 (k_x^2 + k_y^2 + k_z^2) + (\gamma-1)g^2 (k_x^2 + k_y^2) + i\gamma g\omega^2 k_z = 0 \quad (37)$$

which is, of course, Hines's dispersion relation. Applying the same analysis to the electromagnetic equations it follows that

$$(k^2 \bar{\bar{I}} - \vec{k}\vec{k} + i\omega\mu_o\bar{\bar{\sigma}}) \cdot \vec{E} = i\omega\mu_o\sigma_o\bar{\bar{I}} \times \vec{B}_o \cdot \vec{v} \quad (38)$$

HINES (1955) showed that hydromagnetic resonance occurs for either of the cases

$$\vec{k} \cdot \vec{k} = 0 \quad (39a)$$

or

$$\vec{k} \cdot \vec{B}_o = 0 \quad (39b)$$

which are obtained by setting the determinant of the left hand side of equation (38) equal to zero and neglecting the transverse conductivities.

Case a) was discussed by HINES (1955) and need not be repeated here.

In order to simplify the algebra, the following definitions are recalled

$$\omega_g^2 = \frac{(\gamma-1)g^2}{C_s^2} \quad (22)$$

$$\omega_a^2 = \frac{\gamma g}{4H} \quad (23)$$

also

$$n = \frac{C_s k}{\omega} \qquad (40)$$

so that equation (37) becomes

$$1 - (n_x^2 + n_y^2 + n_z^2) + \frac{\omega_g^2}{\omega^2}(n_x^2 + n_y^2) + i\,2\,\frac{\omega_a}{\omega}\,n_z = 0 \qquad (41)$$

Calculations become even simpler using a new coordinate system (ξ, η, ζ) obtained by a counterclockwise rotation of the (x,y,z) system about the x-axis through the dip angle, A. The ξ- and x-axes are identical. The η-axis lies along the magnetic field $\vec{B}_o$, and the ζ-axis completes the right handed rectangular system. Equations (39b) and (41) then become, respectively,

$$n_\eta = 0 \qquad (42)$$

and

$$1 - (n_\xi^2 + n_\zeta^2) + \frac{\omega_g^2}{\omega^2}(n_\xi^2 + n_\zeta^2 \sin^2 A) + i\,2\,\frac{\omega_a}{\omega}\,n_\zeta \cos A = 0 \qquad (43)$$

Assuming that n_ξ is real, then n_ζ must be complex, thus

$$n_\zeta = n_{\zeta r} + i\,n_{\zeta i} \qquad (44)$$

where

$$r_{\zeta i} = \frac{\frac{\omega_a}{\omega}\cos A}{1 - \frac{\omega_g^2}{\omega^2}\sin^2 A} \qquad (45)$$

and

$$n_{\zeta r}^2 + \frac{1 - \frac{\omega_a^2}{\omega^2}}{1 - \frac{\omega_g^2}{\omega^2}\sin^2 A}\,n_\xi^2 = \frac{1 - \frac{\omega_g^2}{\omega^2}\sin^2 A - \frac{\omega_a^2}{\omega^2}\cos^2 A}{\left(1 - \frac{\omega_g^2}{\omega^2}\sin^2 A\right)^2} \qquad (46)$$

Note that equations (45) and (46) reduce exactly to those of internal gravity waves when $A = 0°$ except that equation (46) would apply only to the vertical plane perpendicular to the magnetic field. Careful inspection of equation (46) reveals again, in close analogy with Hines's internal waves, that two modes of waves may be recognized: "gravity" and "acoustic". The following tabulation delineates the situation:

Angular frequency range		Comments
0	to $\omega_g \sin A$	no solution
$\omega_g \sin A$	to ω_g	gravity mode
ω_g	to $\sqrt{\omega_g^2 \sin^2 A + \omega_a^2 \cos^2 A}$	no solution
$\sqrt{\omega_g^2 \sin^2 A + \omega_a^2 \cos^2 A}$	to ∞	acoustic mode

Figures 4 and 5 show the variation of $k_{\zeta i}$ as a function of magnetic angle and period for selected periods and angles, respectively.

Figures 6 through 8 show plots of $n_{\zeta r}$ vs. n_ξ for selected periods and for angles of 15°, 45°, and 75°.

2. Results

This simplified analysis shows the feasibility of the resonant gravity wave mode $\vec{k} \cdot \vec{B}_o = 0$. The main feature of this mode is its confinement to a band $\omega_g \sin A < \omega < \omega_g$ which rules out periods greater than T_g Csc A from magnetic latitudes greater than A. Away from the magnetic equator, the propagation band is rather narrow, e.g., at $A = 30°$ it is only $T_g < T < 2T_g$.

The indices of refraction n_ξ and $n_{\zeta r}$ are entirely analogous to those given by HINES (1960) so that the phase and group velocities still bear the same relationship: for the longer periods, the energy flow is nearly horizontal, radically different from the corresponding phase flow.

As opposed to resonance mode $\vec{k} \cdot \vec{k} = 0$, mode $\vec{k} \cdot \vec{B}_o = 0$ exhibits both vertical and horizontal phase shifts and attenuation or growth.

B. IONOSPHERIC PREDICTIVE FUNCTION

HOOKE (1968) has shown that in the F2-region the amplitude of the electron number density variation produced by an internal atmospheric wave is described by equations (27) through (29), repeated here:

$$|N'| = N_o(z)U_b(z_o)\sin I \exp[k_{zi}(z - z_o)]\omega^{-1}\sqrt{\left(\frac{1}{N_o}\frac{\partial N_o}{\partial z} + k_{zi}\right)^2 + \left(\frac{k_{br}}{\sin I}\right)^2}$$

(27)

$$u_b = U_b(z_o)\exp[k_{zi}(z - z_o)]\exp i(\omega t - k_x x - k_y y - k_{zr}z)$$

(28)

$$k_{zi} = \frac{1}{2H}$$

(29)

The full electron density variation is given by

$$N' = |N'|\exp i\left[\omega t - k_x x - k_y y - k_{zr}z + \frac{\pi}{2} - \tan^{-1}\frac{k_{br}/\sin I}{\frac{1}{N_o}\frac{\partial N_o}{\partial z} + k_{zi}}\right]$$

(47)

In order to obtain an expression for isoionic contours, the height variation of contours of constant N, it is necessary to set

$$N_o(z) + \text{Re}(N') = \text{constant}$$

(48)

and solve for z. This proves to be a cumbersome inversion

which is carried through only because one may wish to compare the theoretical expressions with experimental data which have commonly been presented in the form of iso-ionic contours. There is no fundamental reason to choose iso-ionic contours over iso-height contours, the variation of N at constant height, nor greater difficulty presenting the data under either scheme. Hence, as far as T.I.D. work is concerned, it is much more satisfactory to present experimental data as iso-height contours so that they can be readily compared to the available theory.

The derivation of the gravity wave mode assumed constancy in the value of the scale height H. The fact is that in the region of interest, say 200 to 300 km, H varies from 48 to 60 km so that the theory is imperfect. If, however, the ionosphere is approximated by successive horizontal layers 10 km thick, then H remains constant within 2.5% in each slab, and the theory may be reasonably applied to each slab.

Equation (27) suggests the possibility of predicting the electron density variation at one level when the variation is known at some other level. For levels z_1 and z_2, the ratio of the variation at frequency ω is given by

$$\frac{|N'(z_2)|}{|N'(z_1)|} = \frac{N_o(z_2)}{N_o(z_1)} \exp\left(k_{zi}(z_2-z_1)\right) \sqrt{\frac{\left(\frac{1}{N_o}\frac{\partial N_o}{\partial z}\Big|_{z_2} + k_{zi}\right)^2 + \left(\frac{k_{br}}{\sin I}\right)^2}{\left(\frac{1}{N_o}\frac{\partial N_o}{\partial z}\Big|_{z_1} + k_{zi}\right)^2 + \left(\frac{k_{br}}{\sin I}\right)^2}}$$

$$(49)$$

where k_{br} encompasses the frequency dependence.

As it stands, equation (49) may be thought of as a predictive function for an ionospheric layer of thickness $z_2 - z_1$ and centered about $(z_1 + z_2)/2$. For an input, $|N'(z_1)|$, $|N'(z_2)|$ is predicted. Therefore we may input an observed $|N'(z_1)|$, predict $|N'(z_2)|$ as well as observe $|N'(z_2)|$, and compare the predicted and observed values of $|N'(z_2)|$. This can be done in a revealing manner by Fourier decomposing the predicted and observed functions and examining their ratio at each harmonic frequency. To the extent that confidence in the theory can be established in this way, predictions can be made to heights above (or below) available observations.

With this perspective, and by analogy, Prof. Morgan has suggested the possibility of developing a horizontal predictive function in which the observation points are at the same height but are horizontally displaced.

III. EXPERIMENTAL WORK

A. DARTMOUTH IONOSONDE NETWORK

The Dartmouth ionosonde network consists basically of three vertical-incidence ionosondes operating independently at locations roughly determining an equilateral triangle 150 km on a side, as shown in Figure 9.

Typical operating characteristics of these sounders are as follows: one frequency-sweep every 2 minutes, 100 pulses per second, Gaussian pulse envelope, and logarithmic frequency sweep from about 1.6 to 20 MHz in approximately 20 seconds.

The ionosondes were designed and built at the Dartmouth Radiophysics Laboratory and a description of them will be published by Prof. Morgan and Mr. Pratt so they will not be dealt with further here. An outstanding characteristic of them is their ability to run one-week between film changes and their ability to run months at a time without any other attention.

The ionograms are produced in motion-picture format and each weekly film is inspected by viewing it as an accelerated motion picture. If a possible T.I.D. is detected, the corresponding ionograms are digitized by projection and tracing on a Grafacon 1010A tablet in conjunction with a Spiras-65 computer. The digital data are transferred into paper tape which is then processed by the Dartmouth Time Sharing System to convert virtual height to true height by the overlapping

27

polynomial method previously described. The data are then plotted by a Complot DP-1-1 digital plotter, again in conjunction with the Spiras-65 computer. If the resulting plot confirms the existence of a T.I.D. of interest, the data are further processed for finer detail and computation of speed, direction, power spectra, and comparison with the ionospheric predictive function associated with the T.I.D.

1. Hardware

In what follows, a very brief description of the data processing equipment and interfacing will be given.

The ionogram film projector is a Vanguard M-16C "motion analyzer" which is a movie projector capable of a wide range of speed, both forward and backward with the added facility of frame-by-frame projection. Two front-surfaced mirrors are used to project the image onto the translucent screen of the Grafacon 1010A digitizer from beneath. By means of a spring-loaded tapered pin in the sprocket holes, the projector produces a high degree of registration from frame to frame.

The Grafacon digitizer consists essentially of a tablet with a mesh of imbedded wires and a stylus capable of recognizing its position on the tablet. The xy-coordinates of the stylus position are given by two binary numbers of 10 bits each, picked up from the imbedded wire mesh.

The interfacing of the digitizer and the Spiras-65 computer has involved the building and interconnection of twenty-three level-changing circuits for the twenty data bits and three control bits; additional interconnection within the computer; and adjustment of the power supply circuit of the extension unit of the computer.

The Complot DP-1-1 plotter is a conventional digital plotter. The interfacing of the plotter and the Spiras-65 computer has required the modification of the internal circuits of the former and the addition of circuits to the latter.

The input circuits of the plotter were altered to accept the computer pulses. Four cards were added to the computer: two input/output gating, one input/output controller, and one special-purpose card. The first three were standard cards while the special-purpose card was designed and built at Dartmouth. This card allows enough time for the plotter to perform its functions.

The Spiras-65 computer is a small multipurpose computer with an 8k memory attended by a model 33 ASR teletype unit.

All of the interfacing circuits, modifications, and wiring lists, are appended to the "Small Computer Interfacing" volume at the Radiophysics Laboratory.

2. Software

The main data digitizing program is named "Ionogram Scaling". It is written in Spiras-65 machine language because only 4k of memory was available until recently. This program simply allows the operator to scale ionograms in an automatic fashion. Its main features are visual time-check facility, calibration for both scale and orthogonality in the ionograms, determination of the critical frequency, automatic recording of virtual heights at a preset number of frequencies, and memory dump of coded data on paper tape. Two slight variations of this program have also been written: "Critical Frequencies" and "2-Virtual Heights/Ionogram". The former records on paper tape only the critical frequency of each ionogram while the latter records any two virtual heights per ionogram.

The plotting program is called "Plot" and is also written in Spiras-65 machine language. It accepts coded data in paper tape, loads it, sorts the data, then plots the first pair of characters in each line by printing disconnected diamonds, and finally plots corresponding pairs of characters by means of a continuous line unless there is no value present and the line is broken.

The memory printouts of the above programs are given in Appendix A. Two paper-tape copies of each program are also kept at the Radiophysics Laboratory.

The rest of the programs are written in BASIC language and carried through in the Dartmouth Time Sharing System.

The method of overlapping polynomials is performed essentially by two programs: "JET" which calculates a fixed set of coefficients corresponding to the magnetic latitude of the Dartmouth ionosonde network and need be done only once, and either "JET-1" or "JET-2" which convert virtual heights into true heights and present the results in the form of iso-height contours with different grades of detail.

The "TID" program takes a set of two contours per station and by means of crosscorrelation and autocorrelation techniques, determines the main T.I.D. characteristics: speed, azimuth, wavefront-inclination, power spectra, and comparison with the ionospheric predictive function.

The BASIC programs are also given in Appendix A and two tapes of each are kept at the Radiophysics Laboratory.

B. OBSERVATIONS

The Dartmouth three-station ionosonde network commenced operation late in 1968. All of the 1969 ionograms have been visually inspected by motion-picture projection. Of some 38 likely events, only 7 turned out to be travelling ionospheric irregularities and these are treated in the next subsection.

The possibility of a simultaneous observation with the Canadian satellite-borne ionosondes was actively pursued on a suggestion of Prof. Morgan. The actual results were not satisfactory but the basic ideas of much of the work described, evolved from that endeavor. The lack of success was essentially due to the poor quality of the satellite data used: by the Canadian laboratory's own standards, most of the data qualified as guesses, their lowest contours were quite distant in height from our highest contours so as to render the application of the ionospheric predictive function quite doubtful, and finally, the data, theirs and ours, were presented in the form of iso-ionic contours which required inversion of the ionospheric predictive function for comparison with Hooke's theory.

Dr. J.H.W. Unger of the Bell Telephone Laboratories called to our attention the fact that Dr. J.V. Evans had modified the incoherent backscatter radar at the Millstone Hill Observatory in northeastern Massachusetts to obtain electron-density height profiles up to 600 km or more in two minutes and by this means had observed one substantial T.I.D. This provided an excellent opportunity to test our measurements and related assumptions, and a comparative analysis was undertaken immediately and is reported in subsection 2.

1. Routine

As has already been said, the analysis of all the iono-grams corresponding to the year 1969 resulted in finding seven events. It should be noted that occasionally a likely T.I.D. had to be discarded when one of the three stations was not in proper operating condition.

The general treatment of the data has also already been described but a brief description of the velocity determination and spectral analysis are in order here.

The T.I.D. is assumed to be essentially a wave packet centered about a dominant period component, the phase velocity of which is constant in magnitude and direction throughout the space and time of observation.

Any change in the shape of the T.I.D. is considered slow enough that its effect on time-delay determination is negligible.

The techniques used to determine the various speeds are basically those of JONES (1969) and are pictorially presented in Figure 10. Corresponding pairs of iso-height contours of the three stations are first stripped of any linear trends that may be present. The apparent speeds v_{A1} and v_{A2}, at a given height, are determined by dividing the distances from Highgate Springs and Errol to Hanover by their corresponding time lags. The apparent horizontal speed v_{AH} is then calculated from the geometric construction shown in the upper part of Figure 10. The apparent vertical speed at each station is computed by dividing the difference in height of the iso-height contours by their corresponding time lag obtained at each of the three

stations and an average of the three speeds is taken as v_{AV}, the apparent vertical speed of the T.I.D. Finally, the true speed v is obtained from v_{AH} and v_{AV} by means of the geometric construction depicted in the lower part of Figure 10.

Enough data are scaled so as to completely encompass the T.I.D. in time. After subtracting constant and linear terms, zeros are added beyond the time limits of the data in order to increase the recurrence period in a standard Fourier analysis and obtain finer detail by closer harmonic spacing. The power spectra of two selected contours at the Hanover station are obtained and the ionospheric predictive function for the spectral frequency range that contains 75% of the total energy is computed. This experimental predictive function is then compared with its theoretical estimate.

The following is a list of the T.I.D.'s recorded:

1969 E.S.T. (U.T. minus 5 hrs)	v	ϕ	ψ	T	K_p
Jan 13, 10:00 – 14:00	45.6	164.6	74.7	59	0
Mar 02, 10:00 – 14:00	64.6	34.3	15.2	50	1
Apr 29, 13:30 – 17:30	247.2	171.3	64.6	116	3
Sep 05, 09:00 – 13:00	327.1	169.7	19.4	100	5 –
Nov 15, 11:00 – 15:00	55.2	156.6	74.6	190	0 +
Nov 17, 08:16 – 12:16	52.2	179.8	66.8	190	0 +
Dec 10, 10:00 – 14:00	61.9	180.5	65.9	67.9	1 +

Here v is the true speed in m/s, ϕ is the East-of-North azimuth in degrees towards which the T.I.D. was travelling, ψ is the inclination of the wave normal below the horizontal in degrees, T is the dominant period in minutes and K_p is the planetary 3-hour magnetic index. A rough estimate of the accuracy in the

measurements of a T.I.D. with average characteristics yields a 10° uncertainty in the azimuth and inclination, and a 20% tolerance in the speed. The error involved in the determination of the dominant period should be around 2.5%.

No statistical analysis of such a small population may be made. However, some points should be noted. The fact that most T.I.D.'s occurred at around noon merely reflects an observational bias since the electron density variations are proportional to the equilibrium density value and this achieves a maximum at about noon time. The speeds, inclinations, and dominant periods are all well within the range of observed T.I.D.'s reported by other workers. With regard to the azimuth of the irregularities it should be noted that all but one were travelling essentially southward, not in disagreement with other reports, see for example GEORGES (1968). Also, except for the T.I.D.'s of April and September, all events took place under extremely quiet magnetic conditions. A sudden commencement was recorded on September 5, 1969 at 08:34 E.S.T.

Figures 11 through 59 show the critical frequencies, iso-height contours, power spectra and ionospheric predictive functions. The iso-height contours have not been smoothed and their finest roughness corresponds to the two minute data sampling period.

As can be seen from the figures, the critical frequency or maximum ordinary-ray frequency reflected, foF2, varies in a manner closely following the highest iso-height contours. This is because, at times of large ionization, the height of the maximum electron density does not change markedly during the passage of a T.I.D. although the magnitude of the density at the maximum does change. Thus, the foF2 curve is equivalent to an iso-height density contour at

the height of the maximum. Because the echo delay sharply increases as the ionogram approaches foF2, that frequency is a parameter which can be readily followed when scanning the ionograms as accelerated motion pictures, and periodic variation of it is a clue to the presence of a T.I.D. However, because the plasma frequency is proportional to the square root of the electron density, a perturbation of electron density such as ten percent, appears as about half as much in frequency. Furthermore, at night the unperturbed electron density is an order of magnitude less than in the daytime so that the frequency is about one-third as much and a ten percent variation in electron density is but two percent in frequency.

Before the advantage of presenting the data as iso-height contours had become apparent, the seven T.I.D.'s found in the 1969 data had been reduced and presented as iso-ionic contours. Because this is the conventional method of presentation, these results are included in Figures 50 through 101.

2. T.I.D. Observed at Millstone Hill

EVANS (1970), using special techniques to obtain N(h) profiles in two minutes with the incoherent scatter radar at the Millstone Hill Observatory in northeastern Massachusetts, has so far detected one substantial T.I.D. A particularly clear section of this T.I.D., first noted by him and called to the author's attention by J.H.W. Unger of the Bell Telephone Laboratory (Whippany, N.J.), occurred from about 20:00 to 22:00 E.S.T., May 28, 1970 and is the subject of this subsection. Due to the low values of electron densities at the time, it is not feasible to calculate true heights from the ionograms recorded by the Dartmouth ionosonde network, and virtual heights corresponding to 2 and 2.5 MHz are used.

Figure 102 shows the set of virtual height iso-ionic contours recorded by the ionosonde network at 2 and 2.5 MHz. The U.T. interval shown corresponds to the local standard time interval mentioned above. In Figure 103, the corresponding true height iso-ionic contours obtained at the Millstone Hill station are seen.

The horizontal direction and apparent horizontal speed, are obtained from a cross-correlation of the 2 MHz contours of the Dartmouth stations, while the apparent vertical speed is computed from a cross-correlation of the two Millstone Hill contours.

With the horizontal direction and apparent horizontal speed, it is possible to determine spatial variations of the

T.I.D. Figure 104 shows the virtual height iso-ionic contours
for 2 and 2.5 MHz over Hanover at 02:00 U.T., May 29, 1970,
assuming invariance in the lateral direction and showing ± 500 km
of lateral extent.

The dominant period of the T.I.D. was 92 min; its true
speed, 332 m/s; the azimuth ϕ toward which it was moving, 194°
East of North; and the inclination of the normal to the wave-
front, 29.5° below the horizontal. From the dominant period
and apparent horizontal veloc cy which was 381 m/s, a dominant
apparent horizontal wavelength of some 2100 km is obtained.

The predicted lag in the observation times at Millstone
Hill relative to Hanover may be calculated from the geometry
shown in Figure 105 and it is found to be 5 minutes. However,
the actual lag, found by cross-correlating the 2 MHz contours at
Hanover and Millstone Hill, is 10 minutes.

After considerable effort dedicated to explaining this
discrepancy, it seems that values of foF2 obtained with an
ionosonde at Millstone and used for normalizing the radar, are
in question. Because a periodic variation appears in foF2 as
a T.I.D. passes, use of erroneous values can introduce a
phase-shift in the radar data. Unfortunately, none of the
stations of the Dartmouth network provides unambiguous values
of foF2 during the period under consideration and neither does
the ionosonde at the Lowell Technological Institute near
Millstone. However, MONTES (1971), using a four-station doppler
sounding array in northern New Jersey, has found this T.I.D. in

his data and obtains a speed and azimuth in substantial agreement with our values. Unfortunately, due to the low electron density, he has data only on one of his frequencies and cannot provide information with which the time-lag relative to Hanover could be obtained. The observation of the event by his station array as well as by the Dartmouth stations, establishes the lateral extent of the T.I.D. wavefront as being at least 320 km.

The ratio $|N'(z_2)/N'(z_1)|$, determined experimentally, and its theoretical value determined from equation (49), have been compared for this event. Five iso-height contours for 231, 240, 249, 258, and 267 km recorded by EVANS (1971) with the Millstone radar, have been used. In Figure 106, two iso-height contours corresponding to 240 and 258 km are illustrated, while Figure 107 shows their corresponding normalized power spectra.

In the computation of equation (49), the equilibrium density values were taken as the average values at the 240 and 258 km contours. The slopes at 240 km and 258 km were obtained by taking the difference of the average values at 249 and 231 km, and 267 and 258 km, respectively, and dividing by 18 km. The value $0.5 \times 10^{-5} \text{km}^{-1}$ has been taken for k_{zi} $(= \frac{1}{2H})$. The assumption of a constant phase velocity, allows the computation of k_{br} as a function of frequency.

In order to reduce the effects of noise, only a band of frequencies where most (75%) of the energy of the signal lies, is used. The result of dividing the experimental ratio $|N'(z_2)/N'(z_1)|$ by its theoretical estimate is shown in Figure 108.

Inspection of Figure 108 reveals good agreement between theory and experiment throughout most of the frequency range. It can be seen that the ratio of the theoretical predictive function, as derived from Hooke's theory, to the experimentally determined predictive function, is quite close to unity at all points. The small apparent over-all attenuation is of little significance for it could be easily removed by adjusting the value of k_{zi}. The small emphasis at both ends of the spectrum may be due in part to the broadening of the signal spectrum, and in part, to residual non-T.I.D. variations in the data.

IV. CONCLUSIONS

In the theoretical aspect of this work, there have been two achievements. Firstly, the characteristics of the gravity wave resonant mode $\vec{k} \cdot \vec{B}_0 = 0$ have been studied. Its existence should now be sought experimentally either as T.I.D.'s or perhaps as some permanent feature. In the case of non-equatorial latitudes, the bandpass feature of this mode could be detected. Secondly, using Hooke's results, the concept of an ionospheric predictive function is introduced. If accepted by other workers in the T.I.D. field, the iso-height contour presentation of T.I.D. data should become standard instead of the traditional iso-ionic presentation. Although experimental agreement with theoretically determined predictive functions has been found to be very good, the basic theoretical model used could be progressively improved by including the effects of viscosity, a constant background wind, and by relaxing the adiabatic condition.

In the experimental aspect, the data processing system has been brought into full operation and seven large T.I.D.'s have been found and analyzed. The data processing system could be refined further by changing from paper to magnetic tape or, even better, the SPIRAS-65 computer could be directly linked to the Dartmouth Time Sharing System, thus avoiding a few steps. The Dartmouth Time Sharing System is used for the true-height computations and the spectral computations. Now that the SPIRAS computer has an 8k memory, the spectral computations could be done with it. However, it is unlikely that it could accommodate the true-height computations without still more memory. A fourth ionosonde station, possibly semi-mobile, would be highly

42

desirable. Inasmuch as the observed T.I.D.'s travelled predominantly from north to south, it could be placed north or south of the three-station network to check the propagation of T.I.D.'s with theoretical predictions based upon the parameters determined experimentally by the three-station network. It could also be placed east or west of the three-station network to investigate the lateral extent of T.I.D.'s.

The routine search for T.I.D.'s should be continued in order to obtain a sufficiently large number of events for statistical analysis. Though not included here, a BASIC program has recently been developed to search automatically for a T.I.D., given the values of foF2 scaled by means of the SPIRAS-65 program, "critical frequencies" and this should greatly assist in finding nighttime events and smaller daytime events than those discussed here.

The Dartmouth ionosonde network is especially well-suited for the continuous monitoring of the ionosphere at a particular time of day (noon, sunrise, sunset, etc.). Understanding ionospheric behavior at these times may provide additional insight into the T.I.D. field.

V. APPENDIX: COMPUTER PROGRAMS

A total of eight computer programs are presented here. The first four: "Ionogram Scaling", "Plot", "2-virtual heights/ionogram", and "Critical frequencies", are written in SPIRAS-65 machine language and appear under the headings: "SPIRAS", "SPIRES", "SPIRIS", and "SPIRUS", respectively. The leftmost number of each line corresponds to the address of the next number while the following numbers are stored in successive locations. Thus, in "SPIRAS", 000110 is stored at location 001000 while 000160 is at 001007. It should be noted that the number system used in this language is octal.

The last four programs are: "JET", "JET-1", "JET-2", and "TID", written in BASIC language and require no additional comment.

44

SPIRAS

IONOGRAM SCALING

```
001000: 000110,000222,076041,101002,040000,177775,103102,000160
001010: 000200,000050,000333,005140,176175,000040,000053,004140
001020: 176031,001041,000040,000036,026001,000307,000000,002161
001030: 001445,005100,176002,076025,177773,002175,004200,177770
001040: 076020,076017,177741,000171,000000,101002,000100,177775
001050: 102102,177771,002127,076005,076004,076003,177754,002121
001060: 000171,000000,001043,077760,177772,070000,072142,000000
001070: 174000,110000,113152,050000,106152,020000,034475,044000
001100: 136552,044000,072552,014000,115112,050000,052552,014000
001110: 012552,000000,000000,000000,000000,000000,000000,000000
001120: 000000,000000,000000,000000,000000,000000,000000,070000
001130: 170512,050000,176552,000000,072142,070000,175512,104000
001140: 176552,004000,174512,154000,072152,174000,174410,000000
001150: 107742,074000,042040,104000,174424,100000,176040,013700
001160: 174210,174000,174630,070000,072142,010000,174512,170000
001170: 072162,110000,174532,044000,112552,004100,004176,074000
001200: 076040,040700,035040,101700,076030,052100,105210,010100
001210: 004270,116100,107152,002121,000020,000000,000130,000020
001220: 101002,040100,177775,103102,001054,001154,007034,167765
001230: 027764,003774,177765,100000,000010,117757,102100,111154
001240: 071044,111651,021777,071626,071641,001351,005200,171443
001250: 131652,071626,071641,000316,001767,003776,177772,051773
001260: 021771,111774,051772,021772,111776,051774,021776,111773
001270: 051775,021775,002122,000271,001776,031770,111772,002122
001300: 000271,001771,031767,111771,002122,000270,002246,031766
001310: 000110,000372,002122,000271,001776,031765,131653,121756
001320: 013664,001401,023727,003777,177772,071626,051773,021727
001330: 002521,051774,002322,011770,041727,021726,002126,111726
001340: 053744,004140,176002,006001,177772,113744,053743,021353
001350: 111726,053743,000270,000000,001352,035777,113744,043743
001360: 001141,023744,002721,001042,000040,000044,001043,045777
001370: 025777,000261,001777,113744,051726,004140,176001,003777
001400: 000240,000015,071626,051773,021725,002521,051774,021724
001410: 002322,011770,041725,053727,000200,000001,176002,176005
001420: 177761,000200,177777,177756,002000,121725,011767,041724
001430: 002322,011765,001401,004040,177745,025777,000261,001777
001440: 003777,177740,176003,035777,000261,001777,000110,005215
001450: 025777,000261,001777,005001,171521,111215,051554,005100
001460: 171513,111215,001044,051655,005100,171511,111215,001050
001470: 051655,005100,171506,111215,001054,051233,005100,171503
001500: 111215,041557,171513,111215,041560,171513,111215,041651
001510: 171513,111215,041652,021215,102100,111663,071044,071541
001520: 171243,111001,071044,111372,071044,071574,111447,025777
001530: 111777,051372,021561,111651,021777,115777,051447,004100
001540: 171546,111447,071044,001150,071044,171556,115777,001545
001550: 041564,071044,002121,001445,041564,071044,000261,001777
001560: 000100,000000,171535,111447,071044,001150,071044,071574
```

SPIRAS   (CONTINUED)

```
001570: 111154,071044,C00000,000171,000000,131554,002121,071044
001600: 003777,177775,177770,101005,016000,176001,177774,C71631
001610: 101005,016000,177770,071631,101005,016000,177764,101105
001620: 103205,005100,177760,005200,177755,000171,000000,177753
001630: 000171,000000,111657,021635,000100,000000,177775,177770
001640: 000171,000000,000100,000000,177775,C0C100,000000,177775
001650: 177767,002000,000005,000035,021530,112600,054000,000002
001660: 000010,C00250,003250,000207,000060,000000,000072,000144
001670: 000211,000251,000313,000345,000376,C00431,000454,000501
001700: 000525,000551,000612,000654,C00707,000741,000770,C01015
001710: 001041,001063,001104,C01123,001143,001150,C01176,001213
001720: 001230,001246,C00540,000740,176140,002300,176400,0C0520
```

SPIRES

PLOT

```
001000: 131576,002121,000026,001777,003777,177774,105102,102002
001010: 000221,000110,002000,021777,021776,002121,000130,000200
001020: 022177,003777,177775,071100,051003,005100,171123,041003
001030: 000050,175572,005100,171040,041031,022200,006001,171023
001040: 110200,025777,000261,001777,000130,177770,122211,035777
001050: 000261,001777,006001,177772,171073,002000,002000,002000
001060: 002000,002000,002000,002000,002000,002000,002000,002000
001070: 002000,002000,002000,111775,000040,000014,171013,000171
001100: 001024,101002,040000,177775,103102,001051,001144,000050
001110: 003060,101002,040000,177775,103202,001251,001351,000030
001120: 000117,041120,171077,102002,000023,111214,071230,131222
001130: 111220,071237,111215,071230,131223,111213,071237,111216
001140: 021153,131216,111210,071237,131221,111211,071237,131216
001150: 111210,071237,000100,000000,176001,176004,131224,111212
001160: 071237,177757,131225,111210,071237,111212,021201,131216
001170: 111212,071237,131221,111213,071237,131216,111212,071237
001200: 000100,000000,176001,176040,131225,111211,071237,177757
001210: 000001,000002,000004,000010,000020,000040,000005,000006
001220: 000011,000012,000106,001700,000360,001130,000310,000171
001230: 001241,102105,101005,100000,177775,177771,000171,001505
001240: 071230,003777,177775,177772,002121,021775,021774,111214
001250: 071230,111776,051012,001560,000270,000014,031773,011213
001260: 002521,051213,021771,111012,021265,000111,004540,005100
001270: 176024,051775,005100,176014,002324,041775,021775,002721
001300: 004040,176003,111210,071237,176003,002334,111211,071237
001310: 111215,071230,071335,111214,071230,131213,111213,071237
001320: 111774,041213,021774,000201,001771,176002,176001,176031
001330: 111266,041255,021266,171255,000171,001313,131212,111213
001340: 071237,131212,111215,071237,131212,111217,071237,131212
001350: 111221,071237,131212,111220,071237,131212,111212,071237
001360: 171334,131774,111212,071237,002121,021774,000110,002001
001370: 021373,021460,000111,004542,005100,171417,051775,002324
001400: 041775,021775,002721,005400,171415,004040,176003,111210
001410: 071237,176003,002334,111211,071237,111215,071230,111373
001420: 041255,021373,021424,000111,004542,005100,171435,051775
001430: 002324,041775,021775,071510,176005,111214,071230,131213
001440: 111213,071237,111774,041213,021774,051771,004100,171417
001450: 111214,071230,131774,002121,021774,111212,071237,000110
001460: 002002,041210,000050,002014,005100,176003,041463,004001
001470: 171370,131775,002121,021775,111211,071237,002000,131222
001500: 111212,071237,000130,001414,111210,071237,000000,000171
001510: 001434,002721,004100,176004,111213,131213,071237,171553
001520: 005140,176003,002334,111211,176001,111210,021550,002721
001530: 001543,001355,021767,031765,111213,021770,111765,000114
001540: 001575,001560,001441,041767,005100,176004,002324,000110
001550: 000002,071237,111213,071230,111770,051210,021770,005100
001560: 171563,002121,171542,111424,051255,021567,000111,004626
```

SPIRES   (CONTINUED)

001570: 004100,171507,111215,071230,171507,000000,004000,021000
001600: 025000,033000,056400,073400,077400,176001,177774,071631

SPIRIS

2-VIRTUAL HEIGHTS/IONOGRAM

```
001000: 000110,000222,076041,101002,040000,177775,103102,000160
001010: 000200,000050,000333,005140,176176,000040,000053,004140
001020: 176031,001041,000040,000035,026001,000307,000035,002161
001030: 001445,005100,176002,076025,177773,002175,004200,177770
001040: 076020,076017,177741,000171,001507,101002,000100,177775
001050: 102102,177771,002127,076005,076004,076003,177754,002121
001060: 000171,001042,001043,077760,177772,070000,072142,000000
001070: 174000,110000,113152,050000,106152,020000,034476,044000
001100: 136552,044000,072552,014000,115112,050000,052552,074000
001110: 012552,000000,000000,000000,000000,000000,000000,000000
001120: 000000,000000,000000,000000,000000,000000,000000,170000
001130: 170512,050000,176552,000000,072142,070000,176142,104000
001140: 176552,004000,174512,164000,072152,174000,174410,000000
001150: 107742,074000,042040,104000,174424,100000,176040,013700
001160: 174210,174000,174630,070000,072142,010000,174512,170000
001170: 072152,110000,174532,044000,112552,004100,004176,074000
001200: 076040,040700,035040,101700,076030,052100,105210,010100
001210: 004270,115100,107152,002121,000020,020000,000130,000020
001220: 101002,040100,177775,103102,001054,001154,007034,167765
001230: 027764,003774,177765,100000,000010,117757,102100,111154
001240: 071044,000110,002002,021777,071556,071545,001351,005200
001250: 171342,000130,000006,071556,071545,000316,001767,003776
001260: 177772,051773,021771,111774,051772,021772,111776,051774
001270: 021776,111773,051775,021775,002122,000271,001776,031770
001300: 111772,002122,000271,001771,031767,111771,002122,000270
001310: 002246,031756,000110,000372,002122,000271,001776,031765
001320: 131405,071556,071545,051773,021725,002521,051774,021724
001330: 121725,011767,041724,002322,011755,001401,000025,001777
001340: 006001,171321,000110,000014,041777,021777,005001,171443
001350: 103100,001550,001050,036003,071411,026031,000110,000120
001360: 071411,026024,000040,000002,001560,000270,000074,026016
001370: 001460,046015,001556,000270,000030,071425,001050,026007
001400: 116005,071425,046004,102100,171436,177776,000064,021000
001410: 000171,001361,001544,001354,035005,001560,000010,000012
001420: 001560,000040,000000,177764,000171,001402,001560,000270
001430: 000012,001244,036001,000040,000126,177756,000110,000207
001440: 071044,071545,171244,111001,071044,071522,131405,111242
001450: 026003,111362,026012,000110,004542,026004,041343,026014
001460: 027773,000116,004525,071533,000100,000010,176003,071511
001470: 111362,027773,111777,000050,004542,004100,177754,071511
001500: 006001,177745,071511,071522,000110,000224,071044,000000
001510: 000171,001503,000110,000215,071044,000110,000012,071044
001520: 177767,000171,001504,002121,000130,000100,071044,003777
001530: 177775,177767,000171,001464,001545,041513,071044,001460
001540: 001153,041513,071044,177766,000171,001255,000100,000000
001550: 177775,000100,000000,177775,177767,000171,001322,101005
001560: 016000,176001,177774,071503,101005,016000,177770,071503
```

SPIRIS   (CONTINUED)

```
001570:  101005,016000,177764,101105,103205,005100,177760,005200
001600:  177756,177753,000171,001564,000110,000002,025001,000100
001610:  000000,177775,177767,000060,101005,016000,177764,101105
```

SPIROS

CRITICAL FREQUENCIES

```
001000: 000110,000222,076041,101002,040000,177775,103102,000160
001010: 000200,000050,000333,005140,176176,000040,000053,004140
001020: 176031,001041,000040,000036,026001,000307,000000,002161
001030: 001445,005100,176002,076025,177773,002175,004200,177770
001040: 076020,076017,177741,000171,000000,101002,000100,177775
001050: 102102,177771,002127,076005,076004,076003,177754,002121
001060: 000171,000000,001043,077760,177772,070000,072142,000000
001070: 174000,110000,113152,050000,106152,020000,034476,044000
001100: 136552,044000,072552,014000,115112,050000,052552,074000
001110: 012552,000000,000000,000000,000000,000000,000000,000000
001120: 000000,000000,000000,000000,000000,000000,000000,170000
001130: 170512,050000,176552,000000,072142,070000,176142,104000
001140: 176552,004000,174512,164000,072152,174000,174410,000000
001150: 107742,074000,042040,104000,174424,100000,176040,013700
001160: 174210,174000,174630,070000,072142,010000,174512,170000
001170: 072162,110000,174532,044000,112552,004100,004176,074000
001200: 076040,040700,035040,101700,076030,052100,105210,010100
001210: 004270,116100,107152,002121,000020,000000,000130,000020
001220: 101002,040100,177775,103102,001054,001154,007034,167765
001230: 027764,003774,177765,100000,000010,117757,102100,111154
001240: 071044,111651,021777,071625,071641,001351,005200,171443
001250: 131652,071625,071641,000316,001767,003776,177772,051773
001260: 021771,111774,051772,021772,111776,051774,021775,111773
001270: 051775,021775,002122,000271,001775,031770,111772,002122
001300: 000271,001771,031767,111771,002122,000270,002246,031766
001310: 000110,000372,002122,000271,001776,031765,131653,121766
001320: 013664,001401,023727,003777,177772,071625,051773,021727
001330: 002521,051774,002322,011770,041727,021726,002126,111726
001340: 053730,004140,176002,006001,177772,113730,053727,021353
001350: 111726,053727,000270,000000,001352,035777,002721,000050
001360: 000015,004140,176005,002721,001044,000040,000160,176006
001370: 002721,000050,000015,001045,000040,000500,045777,025777
001400: 000261,001777,171446,000000,000000,000000,000000,000000
001410: 000000,000000,000000,000000,000000,000000,000000,000000
001420: 000000,000000,000000,000000,000000,000000,000000,000000
001430: 000000,000000,000000,000000,000000,000000,000000,000000
001440: 000000,000000,000000,035777,000261,001777,000110,005215
001450: 025777,000261,001777,005001,171521,111215,051654,005100
001460: 171513,111215,001044,051655,005100,171511,111215,001050
001470: 051655,005100,171506,111215,001054,051233,005100,171503
001500: 111215,041657,171513,111215,041660,171513,111215,041661
001510: 171513,111215,041662,021215,102100,111663,071044,071641
001520: 171243,111001,071044,111401,071044,071574,111447,025777
001530: 111777,051401,021561,111651,021777,115777,051447,004100
001540: 171546,111447,071044,001150,071044,171556,115777,001543
001550: 041664,071044,002121,001445,041664,071044,000261,001777
001560: 000100,000000,171535,111447,071044,001150,071044,071574
```

SP1ROS   (CONTINUED)

```
001570: 111154,071044,000000,000171,000000,131664,002121,071044
001600: 003777,177775,177770,101005,016000,176001,177774,071631
001610: 101005,016000,177770,071631,101005,016000,177764,101105
001620: 103205,005100,177760,005200,177756,000171,000000,177753
001630: 000171,000000,111657,021635,000100,000000,177775,177770
001640: 000171,000000,000100,000000,177775,000100,000000,177775
001650: 177767,002000,000006,000035,021530,112600,054000,000002
001660: 000010,000250,003250,000207,000060,000000,000072,000144
001670: 000211,000251,000313,000345,000376,000431,000454,000501
001700: 000525,000551,000612,000654,000707,000741,000770,001015
001710: 001041,001063,001104,001123,001143,001160,001176,001213
001720: 001230,001246,000000,000000,000000,000000,000000,000000
```

JET

```
100 'THIS PROGRAM COMPUTES THREE SETS OF QUANTITIES NECESSARY FOR THE
110 'CONVERSION OF VIRTUAL HEIGHTS INTO TRUE HEIGHTS ACCORDING TO THE
120 'OVERLAPPING POLYNOMIAL METHOD BY J.E. TITHERIDGE.
130 'THE FIRST SET CONSISTS OF TEST FREQUENCIES BETWEEN 2 AND 1. MHZ,
140 'EVERY 0.25 MHZ, AND IS STORED IN FILE "FREQ".
150 'THE SECOND SET CONSISTS OF AN ARRAY OF FIVE COEFFICIENTS FOR
160 'EACH FREQUENCY AND IS STORED IN FILE "COEF".
170 'THE LAST SET CORRESPONDS TO AVERAGE GROUP REFRACTIVE INDICES FOR
180 'ALL TEST FREQUENCIES AND ASSOCIATED PLASMA FREQUENCIES. THIS SET
190 'IS STORED IN FILE "GRIN".
200 FILES FREQ%:COEF%:GRIN%
210 DIM F(49),X(5),W(5),Z(5,5),L(5,5),C(5,1),P(49,5),A(5,1),E(49,49)
220 FOR I=0 TO 49
230 LET F(I)=2+(I-1)/4
240 NEXT I
250 MAT WRITE#1:F
260 LET H1=1.434*COS((90+74)*ATN(1)/45)
270 LET H2=1.434*SIN((90+74)*ATN(1)/45)
280 MAT READ X
290 DATA .04691009, .23076534, .5, .76923466, .95308992
300 MAT READ W
310 DATA .11846344, .23931434, .23444444, .23931434, .11846344
320 DEF FNX(F,P)=P↑2/F↑2
330 DEF FNT(F)=H2↑2/F↑2
340 DEF FNL(F)=H1↑2/F↑2
350 DEF FNI(F,P)=1-FNX(F,P)
360 DEF FNA(F,P)=2*FNX(F,P)*FNI(F,P)
370 DEF FNB(F,P)=2*FNI(F,P)-FNT(F)+SQR(FNT(F)↑2+4*FNI(F,P)↑2*FNL(F))
380 DEF FNU(F,P)=SQR(1-FNA(F,P)/FNB(F,P))
390 DEF FNC(F,P)=(1-FNU(F,P)↑2)↑2/FNU(F,P)
400 DEF FND(F,P)=1/FNX(F,P)+.5*FNT(F)/FNI(F,P)↑2
410 DEF FNE(F,P)=2*FNI(F,P)↑3*FNL(F)-FNX(F,P)*FNT(F)↑2
420 DEF FNG(F,P)=FNA(F,P)*FNI(F,P)*SQR(FNT(F)↑2+4*FNI(F,P)↑2*FNL(F))
430 DEF FNM(F,P)=FNU(F,P)+FNC(F,P)*(FND(F,P)+FNE(F,P)/FNG(F,P))
440 FOR I=2 TO 49
450 LET A1=F(I-1)/F(I)
460 LET A2=F(I-2)/F(I)
470 FOR J=1 TO 3
480 LET F=F(I-2+J)
490 FOR K=1 TO 4
500 LET Z=0
510 FOR R=1 TO 5
520 LET T(R)=X(R)*SQR(1-(F(I-2)/F)↑2)
530 LET G(R)=F/F(I)*SQR(1-T(R)↑2)
540 LET P=F*SQR(1-T(R)↑2)
550 LET Z=Z+FNM(F,P)*T(R)*W(R)*G(R)↑(K-2)
560 NEXT R
570 LET B(J,K)=K*(F/F(I))↑2*SQR(1-(F(I-2)/F)↑2)*Z
580 NEXT K
590 NEXT J
```

JET   (CONTINUED)

```
600 MAT Z=ZER
610 LET Z(1,1)=1
620 LET Z(1,2)=1
630 FOR M=2 TO 5
640 LET Z(M,1)=(A2-1)*A2↑(M-2)
650 NEXT M
660 FOR N=2 TO 5
670 LET Z(N,2)=(A1-1)*A1↑(N-2)
680 NEXT N
690 LET Z(2,3)=B(1,1)
700 LET Z(2,4)=B(2,1)
710 LET Z(2,5)=B(3,1)
720 FOR X=3 TO 5
730 FOR Y=3 TO 5
740 LET Z(X,Y)=B(X-2,Y-1)-B(X-2,Y-2)
750 NEXT Y
760 NEXT X
770 MAT L=INV(Z)
780 LET C(1,1)=1
790 MAT A=L*C
800 FOR Z=1 TO 5
810 LET P(I,Z)=A(Z,1)
820 NEXT Z
830 NEXT I
840 MAT WRITE #2:P
850 FOR I=4 TO 49
860 FOR J=2 TO I-1
870 LET E(I,J)=(FNM(F(I),F(J))+FNM(F(I),F(J-1)))/2
880 IF J<I-3 THEN 900
890 LET E(I,J)=(E(I,J)+2*FNM(F(I),(F(J-1)+F(J))/2))/3
900 NEXT J
910 NEXT I
920 MAT WRITE #3:E
930 END
```

```
JET-1

100 'THIS PROGRAM COMPUTES PLASMA LOG DENSITIES FROM VIRTUAL HEIGHTS
110 'STORED IN FILE "VH&CF" BY MEANS OF THE TITHERIDGE OVERLAPPING
120 'POLYNOMIAL METHOD. IT USES THREE SETS OF QUANTITIES, PREVIOUSLY
130 'COMPUTED BY "JET", STORED IN FILES "FREQ", "COEF", AND "GRIN".
140 'THE OUTPUT OF THIS PROGRAM IS A SET OF STRINGS EQUAL TO THE
150 'NUMBER OF IONOGRAMS STORED AT "VH&CF". THE FIRST TWO CHARACTERS
160 'OF EACH STRING REPRESENT THE VALUE OF THE CRITICAL FREQUENCY
170 'AND THE FOLLOWING PAIRS REPRESENT PLASMA LOG DENSITIES FOR
180 'HEIGHTS OF 200,220,240,...KM
190 MARGIN 242
200 LET H=1.484
210 FILE # 1:"FREQ"
220 FILE # 2:"COEF"
230 FILE # 3:"GRIN"
240 FILE # 4:"VHYCF"
250 DIM F(49),P(49,5),E(49,49),A(120),V(49),H(49),K(49),N(49),D(20)
260 MAT READ #1:F
270 MAT READ #2:P
280 MAT READ #3:E
290 IF END#4 THEN 1000
300 LINPUT #4:A$
310 CHANGE A$ TO A
320 LET C=((A(1)-48)*32+A(2)-48)/64
330 IF C=0 THEN 980
340 FOR I=1 TO 49
350 IF C-F(I)<=0 THEN 370
360 NEXT I
370 LET N=I-1
380 MAT V=ZER
390 FOR J=3 TO A(0) STEP 2
400 LET V((A(0)-J+1)/2)=(A(J)-48)*32+A(J+1)-48
410 NEXT J
420 MAT H=ZER
430 FOR I=1 TO 13
440 LET H(I)=V(I)
450 NEXT I
460 FOR J=14 TO N STEP 2
470 IF J+1>N THEN 520
480 LET H(J)=(V((J+12)/2)+V((J+14)/2))/2
490 LET H(J+1)=V((J+14)/2)
500 NEXT J
510 GO TO 530
520 LET H(N)=V((N+14)/2)
530 MAT K=ZER
540 LET K(1)=H(1)
550 FOR I=1 TO 4
560 LET R(I)=H(I)-K(1)
570 NEXT I
580 LET K(2)=(P(2,1)*K(1)+P(2,3)*R(1)+P(2,4)*R(2)+P(2,5)*R(3))/(1-P(2
590 LET K(3)=P(3,1)*K(1)+P(3,2)*K(2)+P(3,3)*R(2)+P(3,4)*R(3)+P(3,5)*R
```

JET-1   (CONTINUED)

```
600 FOR I=4 TO N
610 LET S1=P(I,1)*K(I-2)
620 LET S2=P(I,2)*K(I-1)
630 LET C3=0
640 LET C4=0
650 LET C5=0
660 FOR J=2 TO I-2
670 LET C3=C3+E(I-1,J)*(K(J)-K(J-1))
680 LET C4=C4+E(I,J)*(K(J)-K(J-1))
690 LET C5=C5+E(I+1,J)*(K(J)-K(J-1))
700 NEXT J
710 LET S3=P(I,3)*(H(I-1)-H(1)-C3)
720 LET S4=P(I,4)*(H(I)-H(1)-C4)
730 LET S5=P(I,5)*(H(I+1)-H(1)-C5)
740 LET K(I)=S1+S2+S3+S4+S5
750 IF I<N THEN 770
760 LET K(N)=S1+S2+S3+S4+P(I,5)*1.5*H(N)
770 NEXT I
780 FOR I=1 TO N
790 LET V(I)=F(I)↑2*1E6/90.5
800 NEXT I
810 FOR L=200 TO 20*INT(K(N)/20) STEP 20
820 FOR I=2 TO N
830 IF K(I)>L THEN 850
840 NEXT I
850 LET D(L/20 -9)=N(I-1)+(N(I)-N(I-1))/(K(I)-K(I-1))*(L-K(I-1))
850 LET D(L/20-9)=600*(LOG(D(L/20-9))-LOG(10↑5.5))/LOG(10↑.75)
870 NEXT L
880 LET H(0)=2+2*(INT(K(N)/20)-9)
890 FOR I=1 TO INT(K(N)/20)-9
900 LET H(2*I+1)=INT(D(I)/32)+48
910 LET H(2*I+2)=INT(D(I)-32*INT(D(I)/32)+48)
920 NEXT I
930 LET H(1)=50*C/32+48
940 LET H(2)=50*C-32*INT(50*C/32)+48
950 CHANGE H TO B$
960 PRINT B$
970 GO TO 290
980 PRINT "00"
990 GO TO 290
1000 PRINT "00"
1010 END
```

JET-2

```
100 'THIS PROGRAM COMPUTES PLASMA LOG DENSITIES FROM VIRTUAL HEIGHTS
110 'STORED IN FILE "VH&CF" BY MEANS OF THE TITHERIDGE OVERLAPPING
120 'POLYNOMIAL METHOD. IT USES THREE SETS OF QUANTITIES, PREVIOUSLY
130 'COMPUTED BY "JET", STORED IN FILES "FREQ", "COEF", AND "GRIN".
140 'THE OUTPUT OF THIS PROGRAM IS A SET OF STRINGS EQUAL TO THE
150 'NUMBER OF IONOGRAMS STORED AT "VH&CF". THE FIRST TWO CHARACTERS
160 'OF EACH STRING REPRESENT THE VALUE OF THE CRITICAL FREQUENCY
170 'AND THE FOLLOWING PAIRS REPRESENT PLASMA LOG DENSITIES FOR
180 'HEIGHTS OF HO,HO+5,....,HO+35 KM.
190 PRINT "HO":
200 INPUT HO
210 MARGIN 242
220 LET H=1.484
230 FILE # 1:"FREQ"
240 FILE # 2:"COEF"
250 FILE # 3:"GRIN"
260 FILE # 4:"VHYCF"
270 DIM F(49),P(49,5),E(49,49),A(120),V(49),H(49),K(49),N(49),D(20)
280 MAT READ #1:F
290 MAT READ #2:P
300 MAT READ #3:E
310 IF END#4 THEN 1020
320 LINPUT #4:AS
330 CHANGE AS TO A
340 LET C=((A(1)-48)*32+A(2)-48)/64
350 IF C=0 THEN 1000
360 FOR I=1 TO 49
370 IF C-F(I)<=0 THEN 390
380 NEXT I
390 LET N=I-1
400 MAT V=ZER
410 FOR J=3 TO A(0) STEP 2
420 LET V((A(0)-J+1)/2)=(A(J)-48)*32+A(J+1)-48
430 NEXT J
440 MAT H=ZER
450 FOR I=1 TO 13
460 LET H(I)=V(I)
470 NEXT I
480 FOR J=14 TO N STEP 2
490 IF J+1>N THEN 540
500 LET H(J)=(V((J+12)/2)+V((J+14)/2))/2
510 LET H(J+1)=V((J+14)/2)
520 NEXT J
530 GO TO 550
540 LET H(N)=V((N+14)/2)
550 MAT K=ZER
560 LET K(1)=H(1)
570 FOR I=1 TO 4
580 LET R(I)=H(I)-K(1)
590 NEXT I
```

JET-2   (CONTINUED)

```
600 LET K(2)=(P(2,1)*K(1)+P(2,3)*R(1)+P(2,4)*R(2)+P(2,5)*R(3))/(1-P(2,2))
610 LET K(3)=P(3,1)*K(1)+P(3,2)*K(2)+P(3,3)*R(2)+P(3,4)*R(3)+P(3,5)*R(4)
620 FOR I=4 TO N
630 LET S1=P(I,1)*K(I-2)
640 LET S2=P(I,2)*K(I-1)
650 LET C3=0
660 LET C4=0
670 LET C5=0
680 FOR J=2 TO I-2
690 LET C3=C3+E(I-1,J)*(K(J)-K(J-1))
700 LET C4=C4+E(I,J)*(K(J)-K(J-1))
710 LET C5=C5+E(I+1,J)*(K(J)-K(J-1))
720 NEXT J
730 LET S3=P(I,3)*(H(I-1)-H(1)-C3)
740 LET S4=P(I,4)*(H(I)-H(1)-C4)
750 LET S5=P(I,5)*(H(I+1)-H(1)-C5)
760 LET K(I)=S1+S2+S3+S4+S5
770 IF I<N THEN 790
780 LET K(N)=S1+S2+S3+S4+P(I,5)*1.5*H(N)
790 NEXT I
800 FOR I=1 TO N
810 LET N(I)=F(I)+2*1E6/R0.5
820 NEXT I
830 FOR L=HO TO HO+35 STEP 5
840 FOR I=2 TO N
850 IF K(I)>L THEN 870
860 NEXT I
870 LET D((L-HO)/5+1)=N(I-1)+(N(I)-N(I-1))/(K(I)-K(I-1))*(L-K(I-1))
880 LET D((L-HO)/5+1)=600*(LOG(D((L-HO)/5+1))-LOG(10↑5.5))/LOG(10↑.75)
890 NEXT L
900 LET H(0)=4+2/5*(L-HO)
910 FOR I=1 TO 8
920 LET H(2*I+1)=INT(D(I)/32)+48
930 LET H(2*I+2)=INT(D(I)-32*INT(D(I)/32)+48)
940 NEXT I
950 LET H(1)=50*C/32+48
960 LET H(2)=50*C-32*INT(50*C/32)+48
970 CHANGE H TO B$
980 PRINT B$
990 GO TO 310
1000 PRINT "00"
1010 GO TO 310
1020 PRINT "00"
1030 END
```

TID

```
100 'THIS PROGRAM COMPUTES THE NORMALIZED POWER SPECTRA OF A T.I.D.
110 'AT THE TOP AND BOTTOM OF AN IONOSPHERIC LAYER. THIS LAYER IS
120 '10 KM THICK AND IS CENTERED ABOUT HO. THE RATIO OF THE EXPE-
130 'RIMENTAL TO THEORETICAL IONOSPHERIC PREDICTIVE FUNCTIONS IS
140 'ALSO CALCULATED USING HOOKE'S FORMULA. IT THEN DETERMINES THE
150 'SPEED V OF THE T.I.D., ITS AZIMUTH PHI, AND ITS INCLINATION
160 'PSI. TWO ALTERNATIVE COMPONENT DESCRIPTIONS ARE PRESENTED:
170 'X,Y,Z (EAST,NORTH,UP), AND 1,2,3 WHICH CORRESPOND TO EAST,
180 'MAGNETIC FIELD DIRECTION, AND THE THIRD DIRECTION MAKES THE
190 'SYSTEM CARTESIAN. T IS THE DOMINANT PERIOD OF THE T.I.D. AND
200 'UA,UB,UC ARE THE APPARENT VERTICAL SPEEDS AT HANOVER, HIGH-
210 'GATE SPRINGS AND ERROL RESPECTIVELY.
220 MARGIN 242
230 FILE#1:"OPTIMO"
240 DIM A(13),B(2,363),H(6,121),G(2,6),F(6,121),D(5,30)
250 LET P4=ATN(1)
260 PRINT "STARTING COLUMN":
270 INPUT IO
280 PRINT "AVERAGE HEIGHT":
290 INPUT HO
300 FOR J=1 TO 363
310 LINPUT = 1:A$
320 CHANGE A$ TO A
330 LET B(1,J)=(A(2*IO+1)-48)*32+A(2*IO+2)-48
340 LET B(2,J)=(A(2*IO+5)-48)*32+A(2*IO+6)-48
350 LET M1=B(1,J)/363
360 LET M2=((A(2*IO+3)-48)*32+A(2*IO+4)-48)/363
370 LET M3=B(2,J)/363
380 LET M4=((A(2*IO+7)-48)*32+A(2*IO+8)-48)/363
390 NEXT J
400 LET M1=10↑(5.5+.75*M1/600)
410 LET M2=10↑(5.5+.75*M2/600)
420 LET M3=10↑(5.5+.75*M3/600)
430 LET M4=10↑(5.5+.75*M4/600)
440 FOR J=1 TO 121
450 LET H(1,J)=B(1,J)
460 LET H(2,J)=B(2,J)
470 LET H(3,J)=B(1,J+121)
480 LET H(4,J)=B(2,J+121)
490 LET H(5,J)=B(1,J+242)
500 LET H(6,J)=B(2,J+242)
510 NEXT J
520 FOR I=1 TO 6
530 FOR J=1 TO 121
540 LET G(1,I)=G(1,I)+H(I,J)/121
550 LET G(2,I)=G(2,I)+J*H(I,J)/121
560 NEXT J
570 NEXT I
580 FOR I=1 TO 6
590 FOR K=1 TO 121
```

```
TID        (CONTINUED)

600 LET Z=2*(243-3*X)/120
610 LET Y=6*(122-2*X)/120/122
620 LET F(I,K)=H(I,K)-Z*G(1,I)+Y*G(2,I)
630 NEXT K
640 NEXT I
650 FOR I=1 TO 3
660 FOR K=-5 TO 5
670 FOR J=1-K*(1-SGN(K))/2 TO 121-K*(1+SGN(K))/2
680 LET D(I,K+5)=D(I,K+5)+F(2*I-1,J+K)*F(2*I,J)/121
690 NEXT J
700 NEXT K
710 NEXT I
720 FOR I=1 TO 3
730 LET Y2=-1E10
740 FOR K=0 TO 9
750 IF D(I,K)<Y2 THEN 780
760 LET Y2=D(I,K)
770 LET X2=K-5
780 NEXT K
790 LET X1=X2-1
800 LET X3=X2+1
810 LET Y1=D(I,X1+5)
820 LET Y3=D(I,X3+5)
830 LET N=X1↑2*(Y2-Y3)+X2↑2*(Y3-Y1)+X3↑2*(Y1-Y2)
840 LET D=X1*(Y2-Y3)+X2*(Y3-Y1)+X3*(Y1-Y2)
850 LET T(I)=N/D*50
860 LET U(I)=10000/T(I)
870 NEXT I
880 FOR I=4 TO 5
890 FOR K=-15 TO 15
900 FOR J=1-K*(1-SGN(K))/2 TO 121-K*(1+SGN(K))/2
910 LET D(I,K+15)=D(I,K+15)+F(2*I-4,J)*F(2,J+K)/121
920 NEXT J
930 NEXT K
940 NEXT I
950 FOR I=4 TO 5
960 LET Y2=-1E10
970 FOR K=0 TO 29
980 IF D(I,K)<Y2 THEN 1010
990 LET Y2=D(I,K)
1000 LET X2=K-15
1010 NEXT K
1020 LET X1=X2-1
1030 LET X3=X2+1
1040 LET Y1=D(I,X1+15)
1050 LET Y3=D(I,X3+15)
1060 LET N=X1↑2*(Y2-Y3)+X2↑2*(Y3-Y1)+X3↑2*(Y1-Y2)
1070 LET D=X1*(Y2-Y3)+X2*(Y3-Y1)+X3*(Y1-Y2)
1080 LET T(I)=N/D*50
1090 NEXT I
```

TID   (CONTINUED)

```
1100 LET U(4)=163265/T(4)
1110 LET U(5)=143700/T(5)
1120 LET W=1.05839
1130 LET S=SIN(W)
1140 LET C=COS(W)
1150 LET B=2.63837
1160 LET U(6)=ABS(U(4)*U(5)*S/SQR(U(4)↑2+U(5)↑2-2*U(4)*U(5)*C))
1170 LET A=ATN(SQR((U(4)/U(5))↑2-1))
1180 LET AO=(B+(1-SGN(U(4)))*2*P4+SGN(U(5))*A)*45/P4
1190 LET U(7)=(U(1)*T(1)+U(2)*T(2)+U(3)*T(3))/(T(1)+T(2)+T(3))
1200 LET R=(U(6)*U(7))↑2/(U(6)↑2+U(7)↑2)
1210 LET U(8)=SQR(R)
1220 LET GO=ATN(U(6)/U(7))*45/P4
1230 LET V(1)=R/U(6)*SIN(AO*P4/45)
1240 LET V(2)=R/U(6)*COS(AO*P4/45)
1250 LET V(3)=-R/U(7)
1260 LET I=74*P4/45
1270 LET V(4)=V(2)*COS(I)-V(3)*SIN(I)
1280 LET V(5)=V(2)*SIN(I)+V(3)*COS(I)
1290 DIM X(120),Y(120),P(3,121),L(242)
1300 FOR K=0 TO 120
1310 FOR J=1 TO 121-K
1320 LET Y(K)=Y(K)+P(1,J)*P(1,J+K)/900
1330 LET Y(K)=Y(K)+P(2,J)*P(2,J+K)/900
1340 NEXT J
1350 NEXT K
1360 FOR M=0 TO 120
1370 FOR K=0 TO 120
1380 LET P(1,M)=P(1,M)+Y(K)*COS(3*P4*M*K/900)*2/900
1390 LET P(2,M)=P(2,M)+Y(K)*COS(3*P4*M*K/900)*2/900
1400 NEXT K
1410 NEXT M
1420 FOR M=1 TO 120
1430 IF P1>P(1,M) THEN 1450
1440 LET P1=P(1,M)
1450 LET T1=1800/M
1460 IF P2>P(2,M) THEN 1480
1470 LET P2=P(2,M)
1480 LET T2=1800/M
1490 NEXT M
1500 FOR M=0 TO 120
1510 LET PO=PO+P(1,M)
1520 NEXT M
1530 FOR M=0 TO 120
1540 LET EO=EO+P(1,M)
1550 LET MO=M
1560 IF EO>.75*PO THEN 1530
1570 NEXT M
1580 LET K9=.5/(.12*MO+24)
1590 LET D1=((M2-M1)/10/M1+K9)↑2
```

```
TID        (CONTINUED)

1600 LET D2=((M4-M3)/10/M3+K9)↑2
1610 LET S9=SIN(74*P4/45)
1620 DIM K(120)
1630 FOR M=0 TO 120
1640 LET X=V(4)/U(3)↑2*M/144/S9
1650 LET K1=SQR((D2+X↑2)/(D1+X↑2))
1660 LET K(M)=M3/M1*EXP(10*K9)*K1
1670 NEXT M
1680 FOR M=0 TO 120
1690 IF M>M0 THEN 1710
1700 LET P(3,M)=K(M)/SQR(P(2,M)/P(1,M))*100+400
1710 LET P(1,M)=P(1,M)/P1*200
1720 LET P(2,M)=P(2,M)/P2*200+200
1730 NEXT M
1740 LET L(0)=6
1750 FOR J=1 TO 121
1760 FOR I=1 TO 3
1770 LET L(2*I-1)=P(4-I,J-1)/32+48
1780 LET L(2*I)=P(4-I,J-1)-32*INT(P(4-I,J-1)/32)+48
1790 NEXT I
1800 CHANGE L TO L$
1810 PRINT L$
1820 NEXT J
1830 PRINT "00"
1840 LET V=INT(10*U(3)+.5)/10
1850 LET A0=INT(10*A0+.5)/10-360*INT(A0/360)
1860 LET C0=INT(10*C0+.5)/10
1870 FOR I=1 TO 5
1880 LET V(I)=INT(10*V(I)+.5)/10
1890 NEXT I
1900 PRINT "V=";V;" M/SEC","PHI=";A0;"DEG","PSI=";C0;"DEG"
1910 PRINT " VX=";V(1);" M/SEC","VY=";V(2);" M/SEC","VZ=";V(3);" M/SEC"
1920 PRINT " V1=";V(1);" M/SEC","V2=";V(4);" M/SEC","V3=";V(5);" M/SEC"
1930 PRINT " T=";INT(5*(T1+T2)+.5)/10;" MIN","HO=";HO;"KM"
1940 FOR I=1 TO 3
1950 LET U(I)=INT(U(I)*10+.5)/10
1960 NEXT I
1970 PRINT " UA=";U(1);" M/SEC","UB=";U(2);" M/SEC","UC=";U(3);" M/SEC"
1980 END
```

VI. BIBLIOGRAPHY

Budden, K.G., [1961], "Radio Waves in the Ionosphere",
University Press at Cambridge

Davies, K., [1965], "Ionospheric Radio Propagation",
National Bureau of Standards Monograph 80,
U.S. Government Printing Office

Evans, J.V., [1970], ESD-TR-70-357, Technical Note 1970-20

Evans, J.V., [1971], Private communication

Georges, T.M., [1968], J. Atmosph. Terr. Phys. 30, 735

Hines, C.O., [1955], J. Atmosph. Terr. Phys. 7, 14

Hines, C.O., [1960], Can. J. Phys. 38, 1441

Hooke, W.H., [1968], J. Atmosph. Terr. Phys. 30, 795

Jones, J.E., [1969], E.S.S.A. Tech. Rep. ERL 142-SOL 11

Montes, H.A., [1971], Private communication

Thomas, J.O., [1959], Proc. IRE, 47, 162

Titheridge, J.E., [1967], Radio Science, vol. 2 (new series),
1169

Stix, T.H., [1962], "The Theory of Plasma Waves", McGraw-Hill
Book Co.

VII. ACKNOWLEDGMENTS

FIGURE 1. NORMALIZED CHAPMAN LAW

$X = 80°$

$60°$

$40°$

$20°$

$0°$

N/N_0
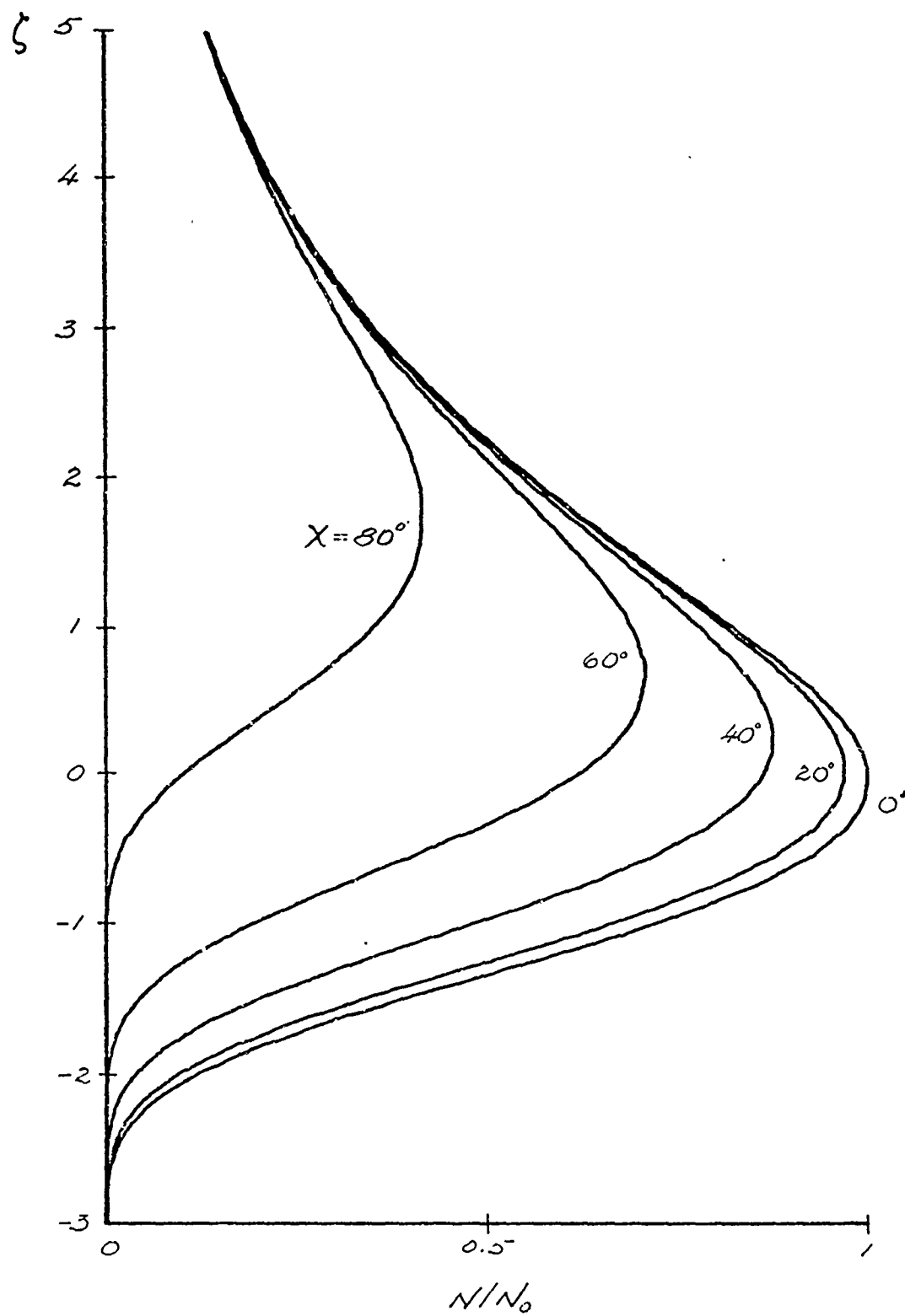
FIGURE 2. CONTOURS OF CONSTANT PERIOD T/T_g IN THE n_{zr} VS n_h DOMAIN
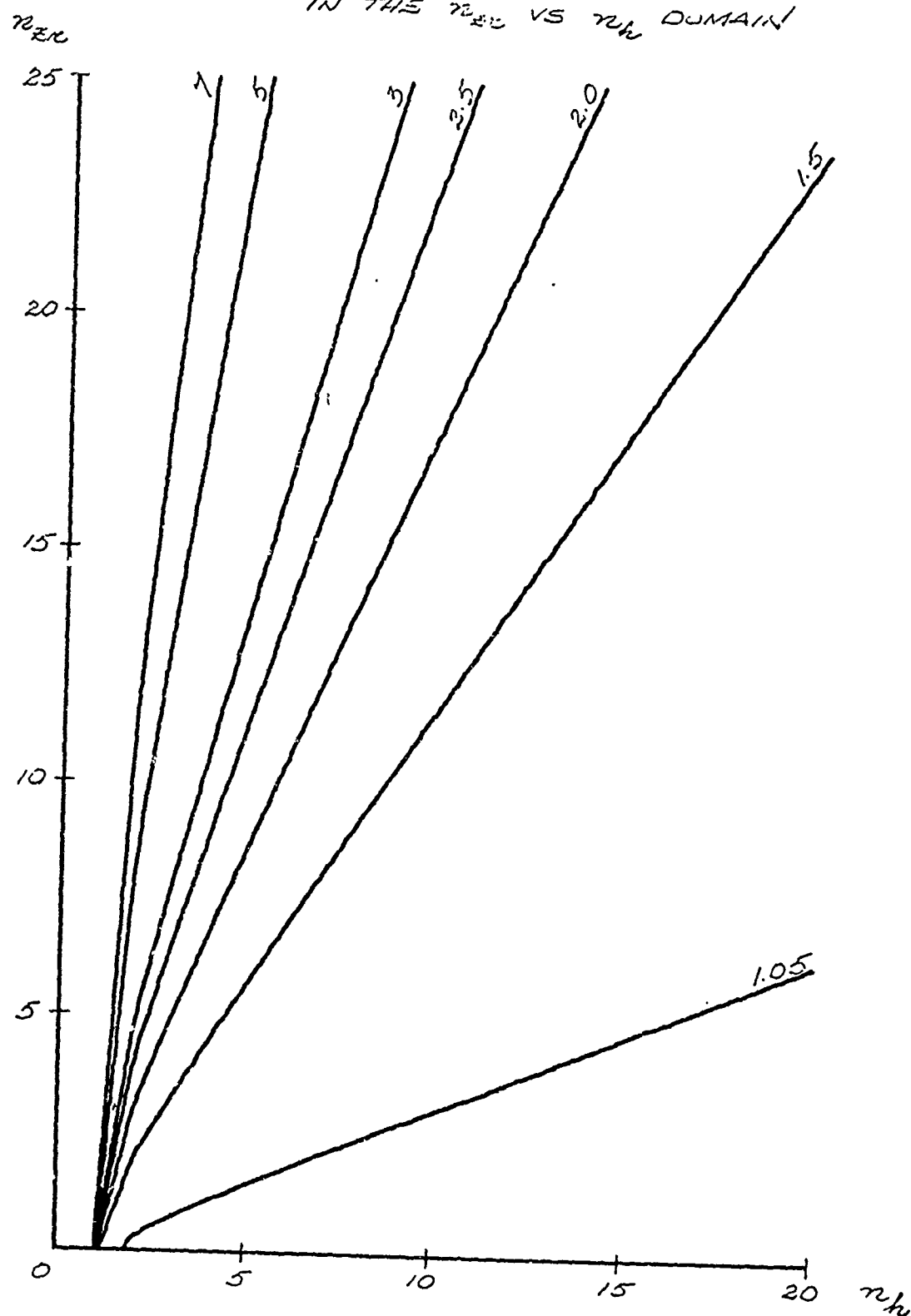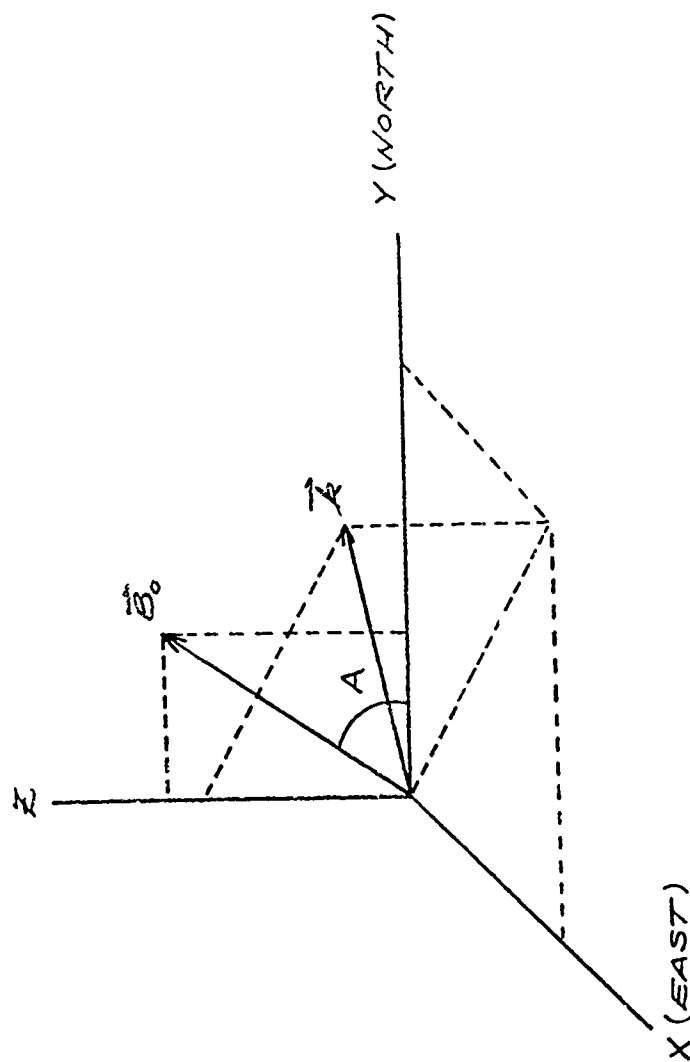
FIGURE 3 GEOMETRY UNDER CONSIDERATION
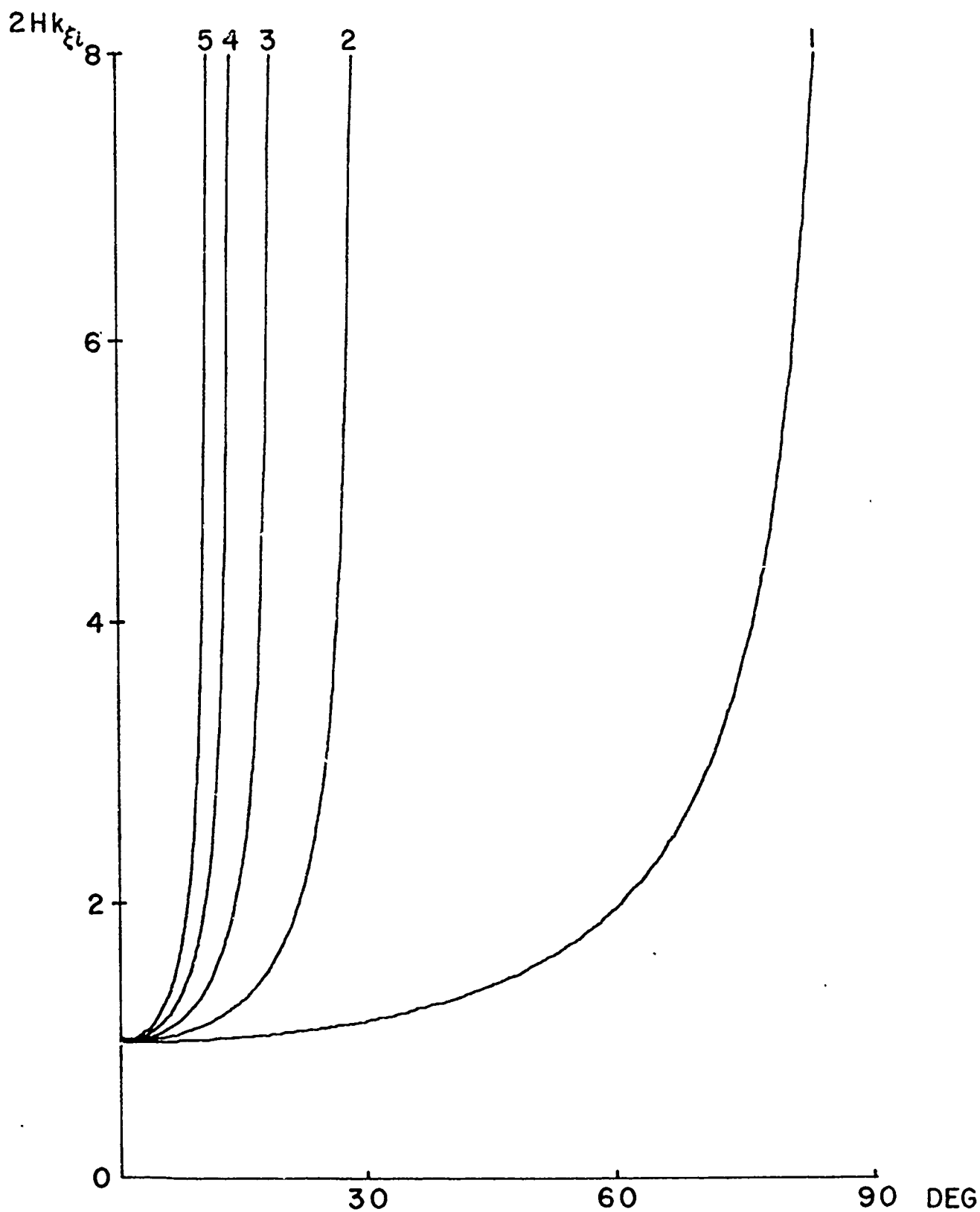
FIGURE 4   GRAPH OF $k_{\xi i}/(1/2H)$ VS ANGLE A

WITH PERIOD T/T_g AS A PARAMETER

68
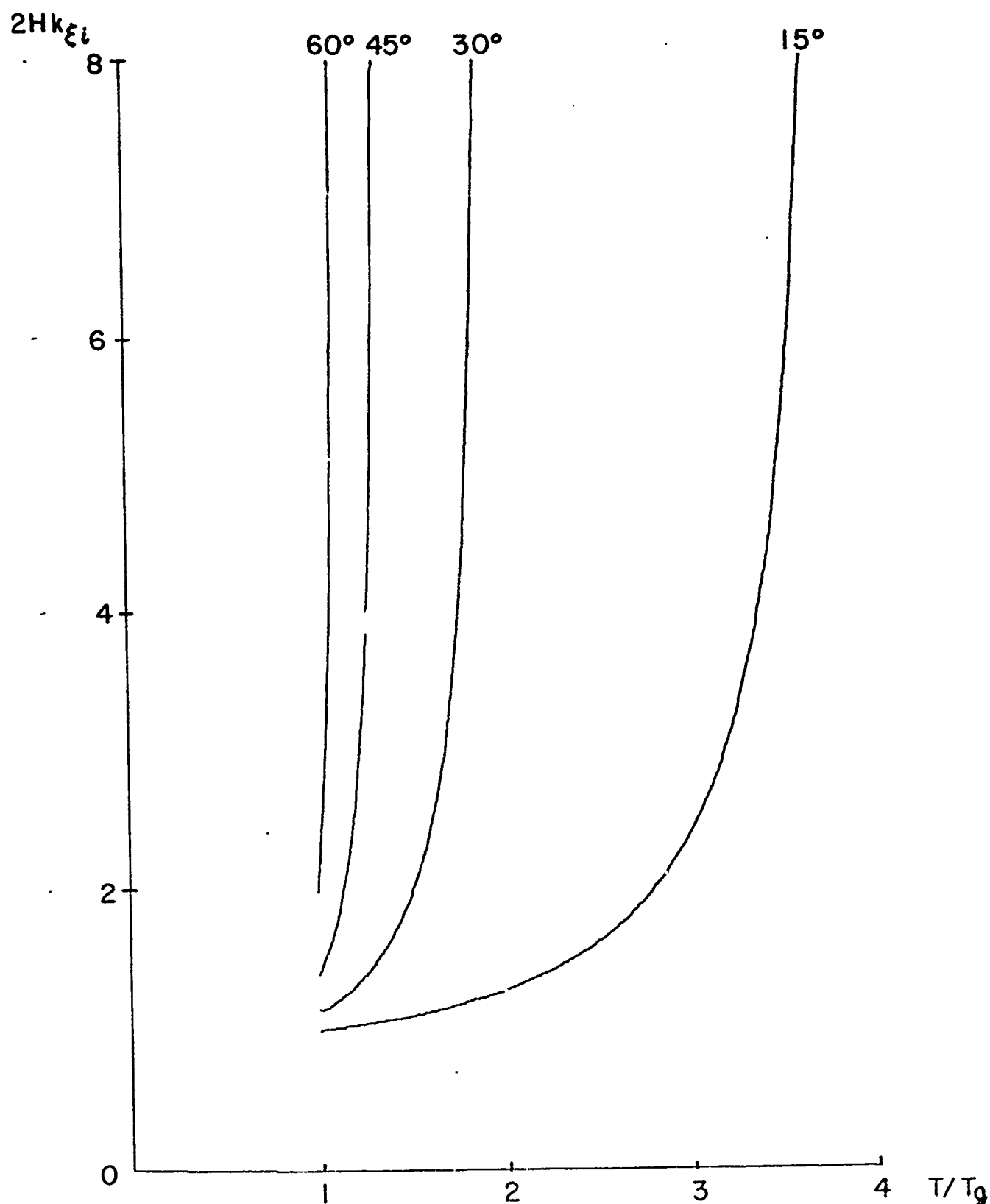
FIGURE 5   GRAPH OF $k_{\xi i}/(1/2H)$ VS PERIOD T/T_g

WITH ANGLE A   AS PARAMETER

69
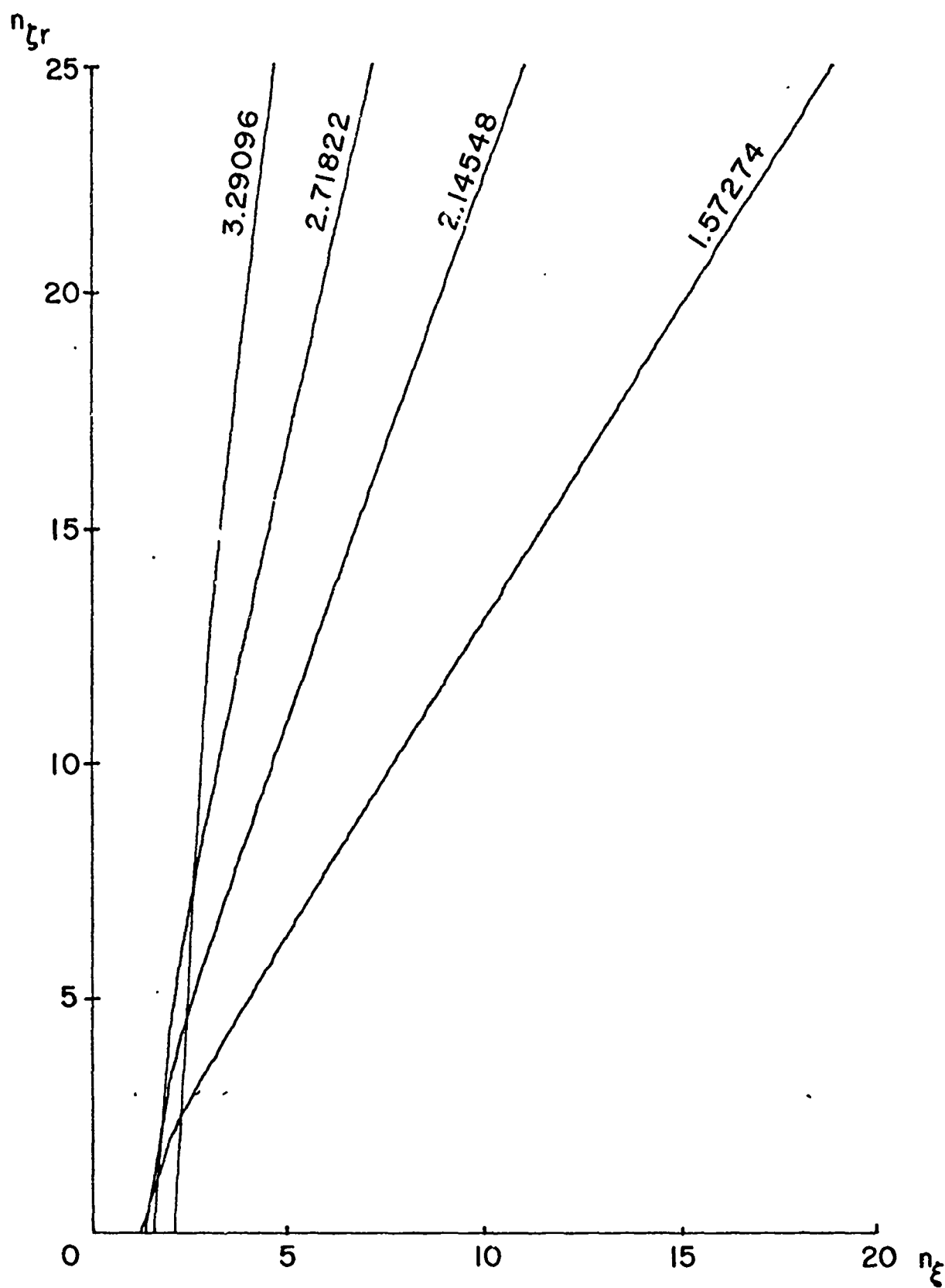
FIGURE 6   CONTOURS OF CONSTANT PERIOD T/T_g

IN $n_{\zeta r}$ VS n_ξ DOMAIN FOR $A = 15°$

70
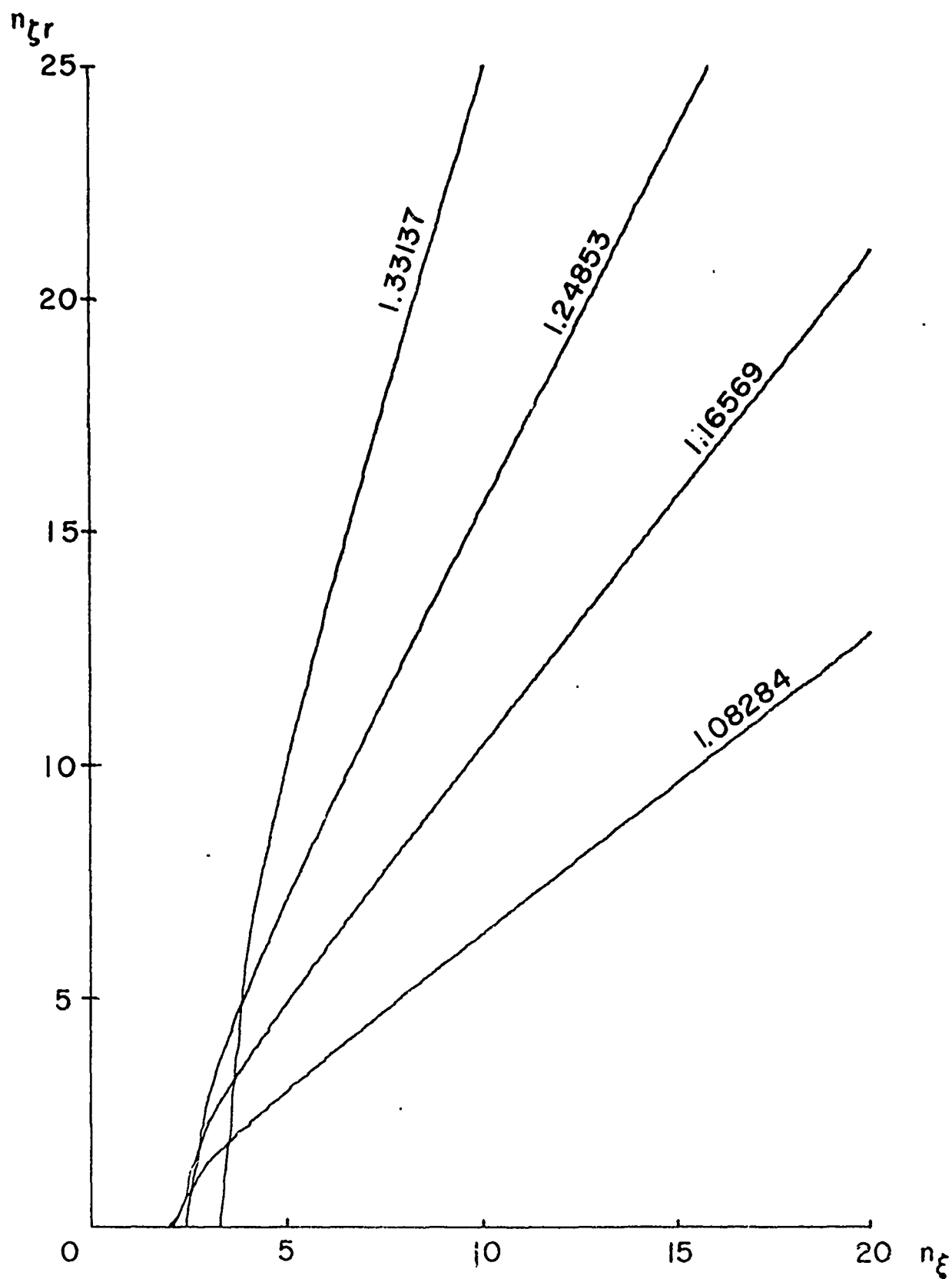
FIGURE 7   CONTOURS OF CONSTANT PERIOD T/T$_g$

IN n$_{\zeta r}$ VS n$_\xi$ DOMAIN FOR A = 45°
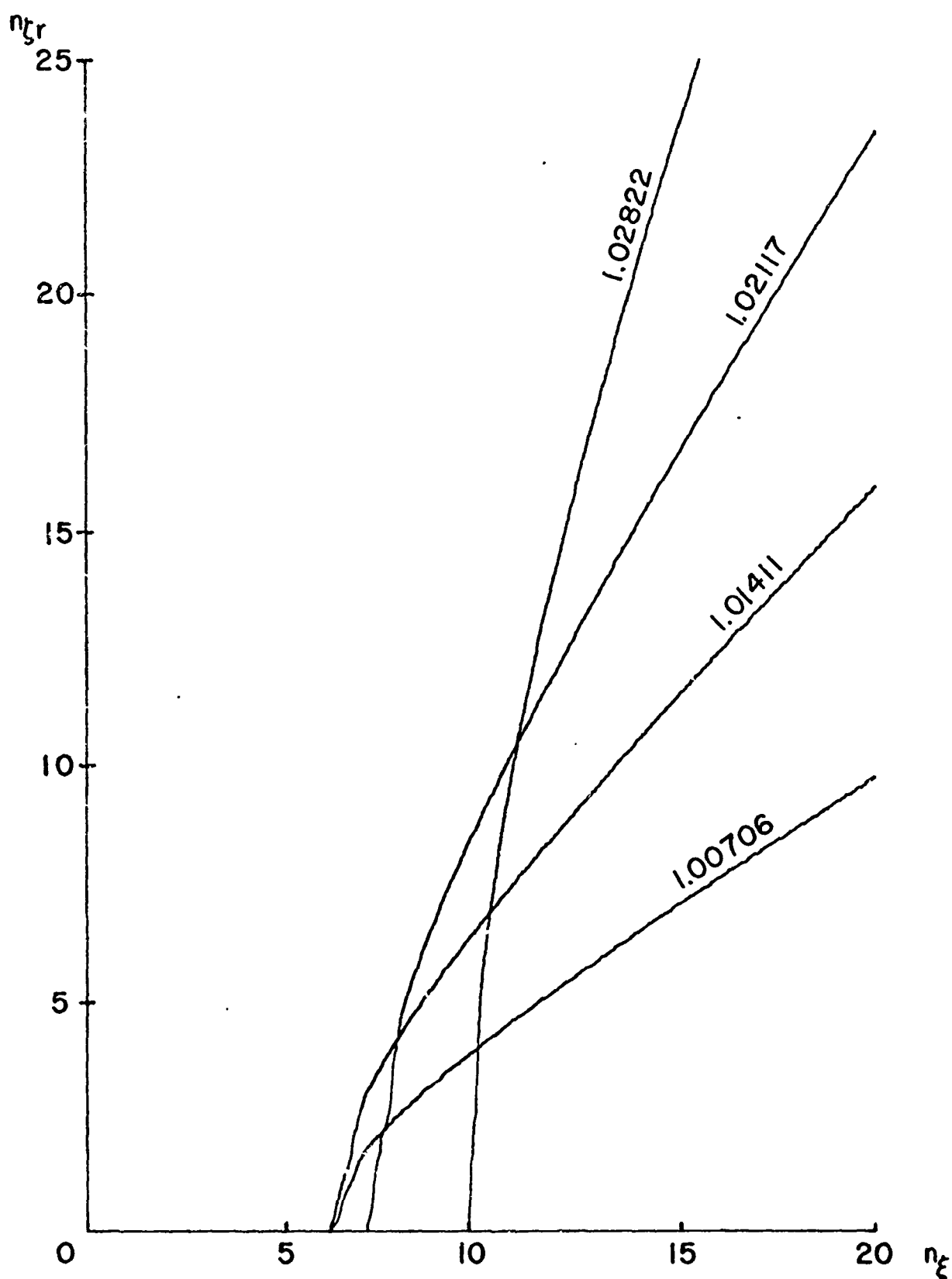
FIGURE 8 CONTOURS OF CONSTANT PERIOD T/T_g IN $n_{\zeta r}$ VS n_ξ DOMAIN FOR $A = 75°$

72

HANOVER, N.H. (HA)   43°41'30"N   72°11'18"W

HIGHGATE SPRINGS, VT. (HI)   45°00'47"N   73°05'11"W

ERROL, N.H. (ER)   44°47'30"N   71°07'30"W
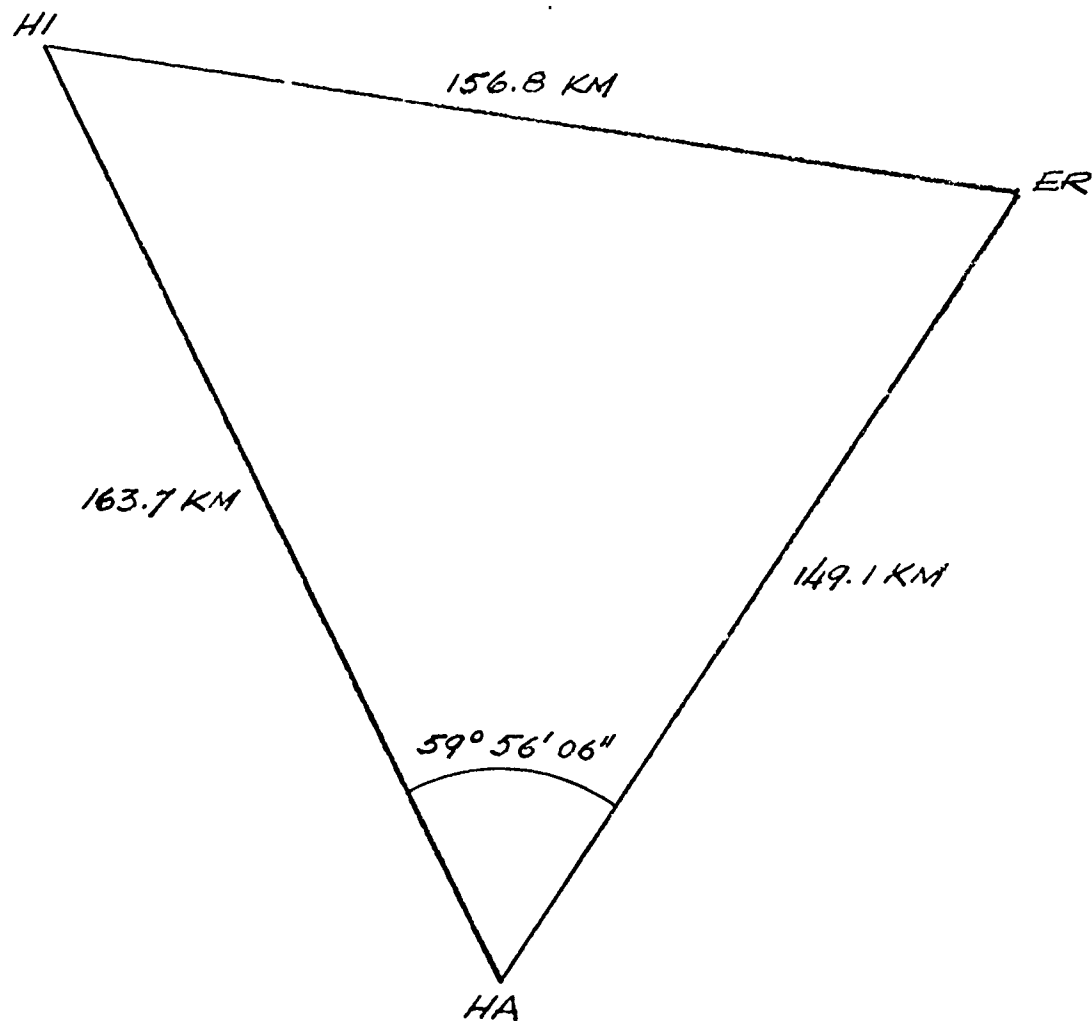
FIGURE 9   GEOMETRY FOR THE DARTMOUTH THREE-STATION IONOSONDE NETWORK

73

FIGURE 10   GEOMETRIC   DETERMINATION
OF THE VELOCITY OF A T. I. D.
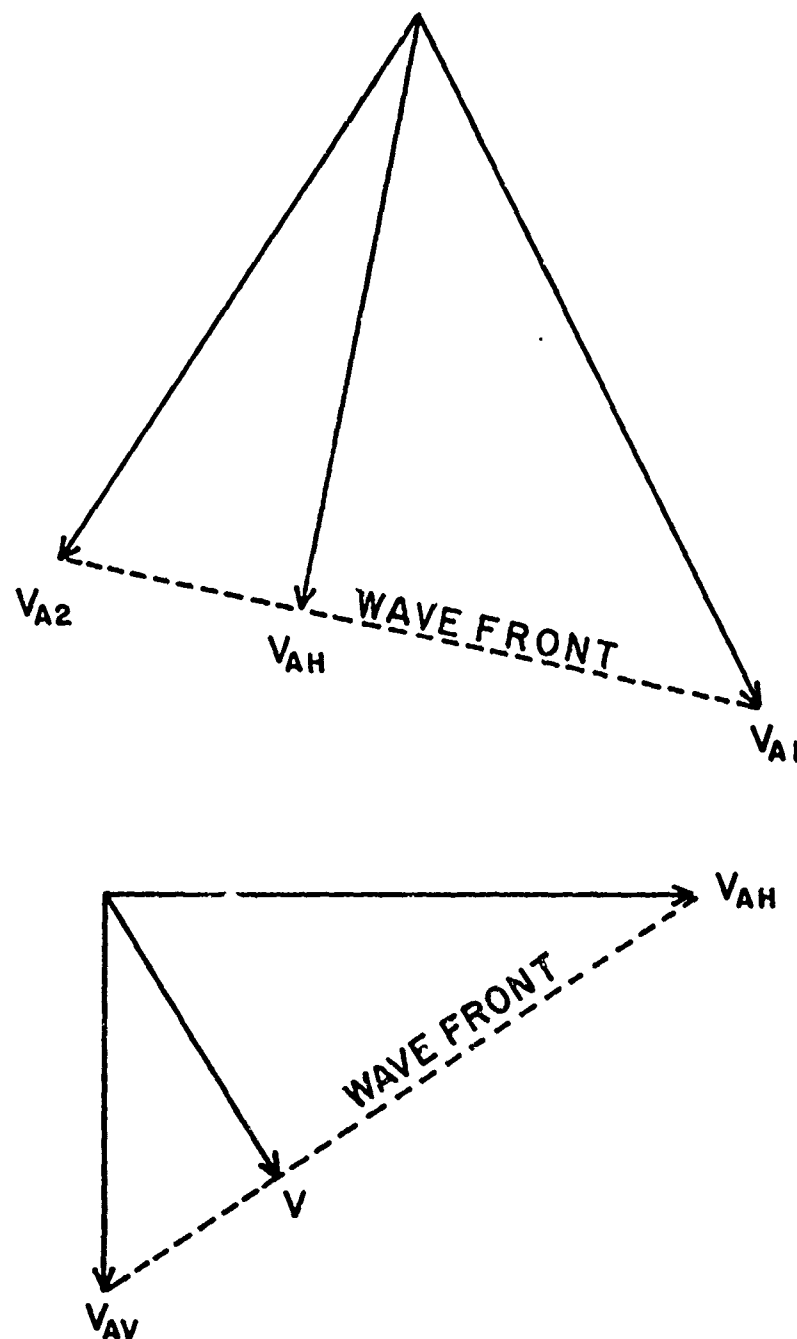
FIGURE 11. CRITICAL FREQUENCIES AND ISO-HEIGHT CONTOURS
HANOVER, JAN 13, 1969, 10:00 - 14:00 EST

FIGURE 12. CRITICAL FREQUENCIES AND ISO-HEIGHT CONTOURS
HIGHGATE SPRINGS, JAN' 13, 1969, 10:00-14:00 EST
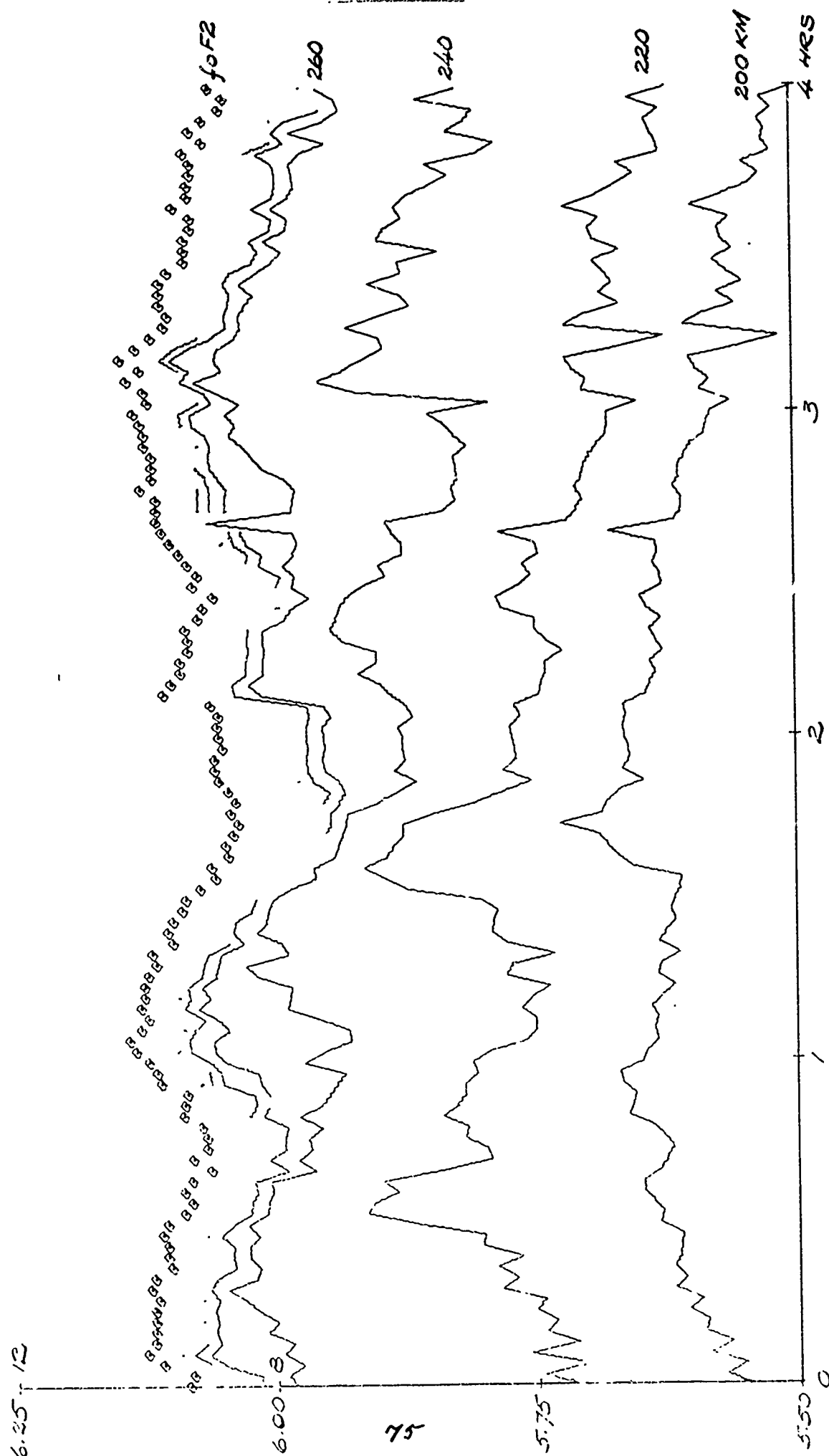
FIGURE 13. VERTICAL FREQUENCIES AND ISO-HEIGHT CONTOURS

SAGOL, Jan 13, 1969, 10:00-14:00 EST
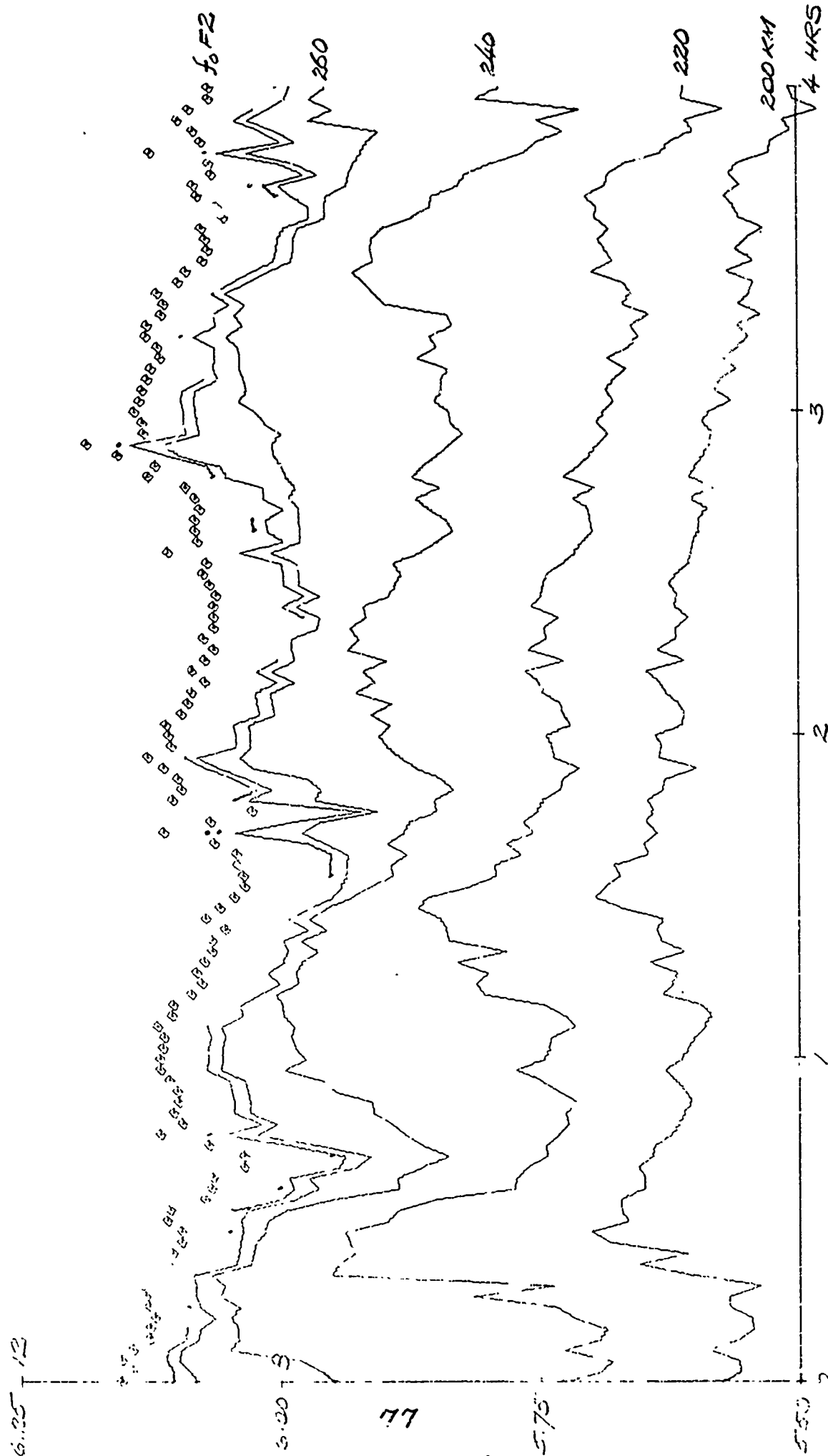
FIGURE 14. CRITICAL FREQUENCIES AND ISO-HEIGHT CONTOURS
HANOVER, JAN 13, 1969, 10:00 - 14:00 EST
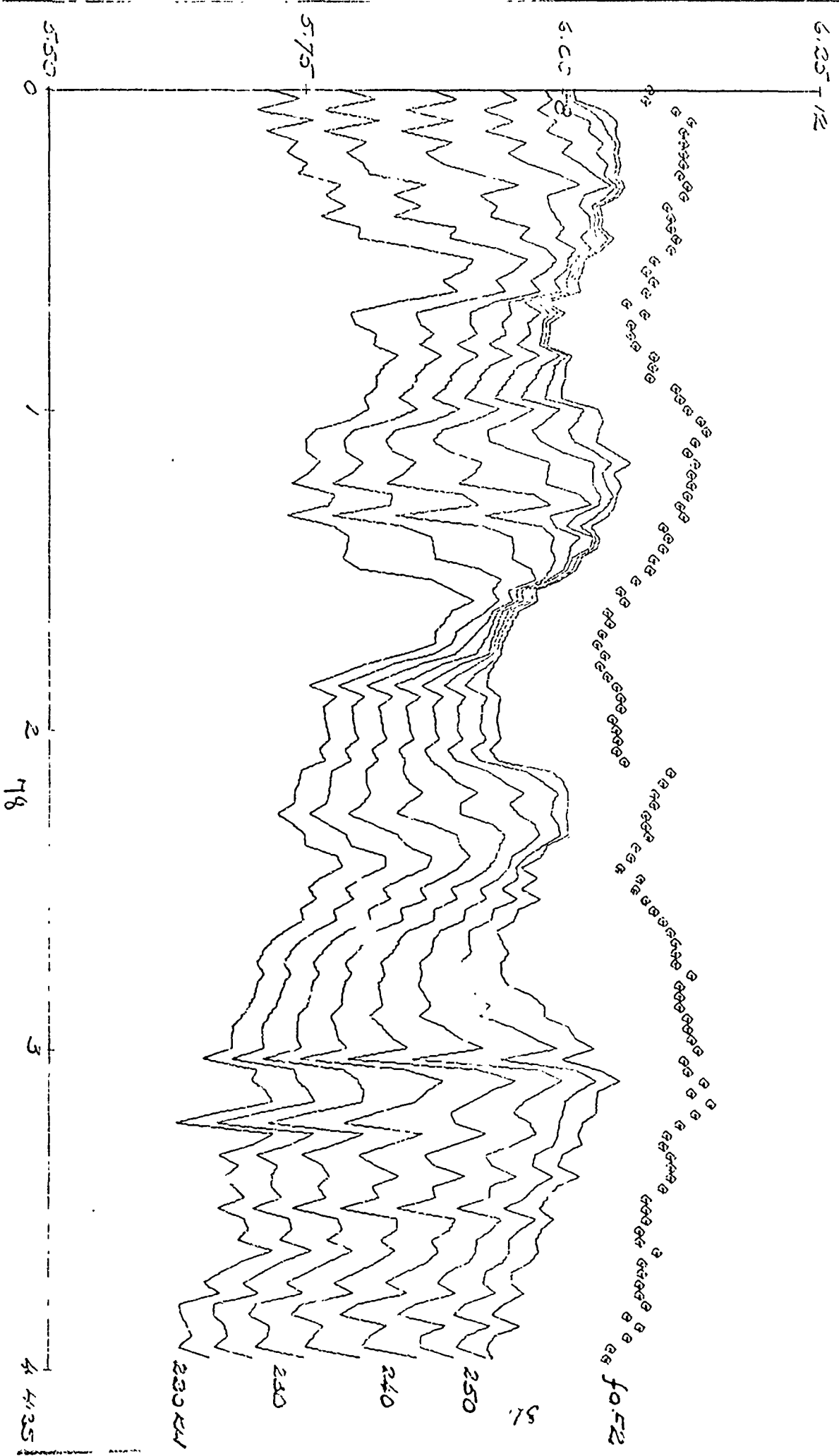
FIGURE 15. CRITICAL FREQUENCIES AND ISO-HEIGHT CONTOURS

HIGHGATE SPRINGS, JAN 13, 1969, 10:00-14:00 EST
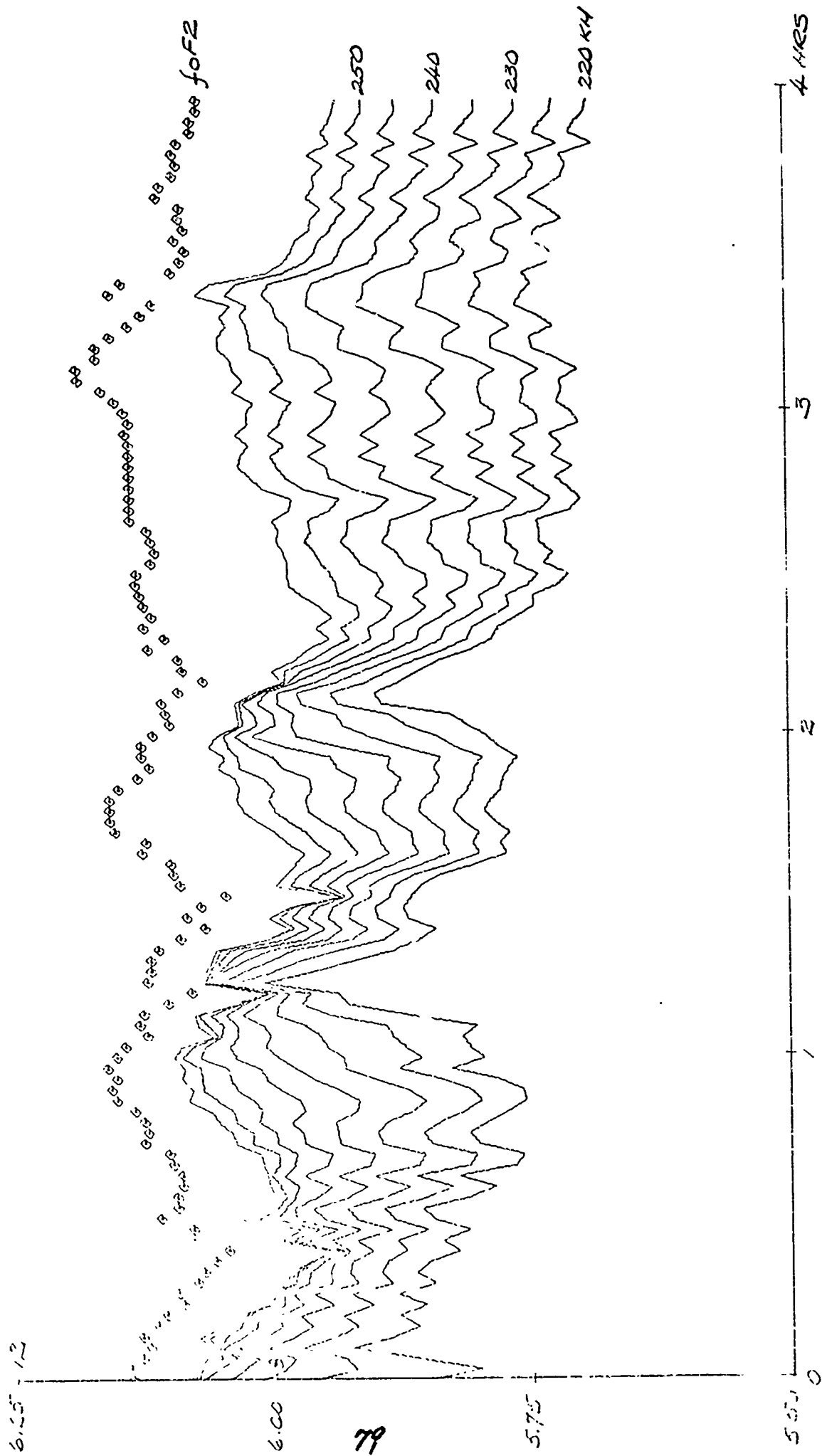
FIGURE 16. CRITICAL FREQUENCIES AND ISO-HEIGHT CONTOURS

ERROL, JAN 13, 1959, 10:00-14:10 EST
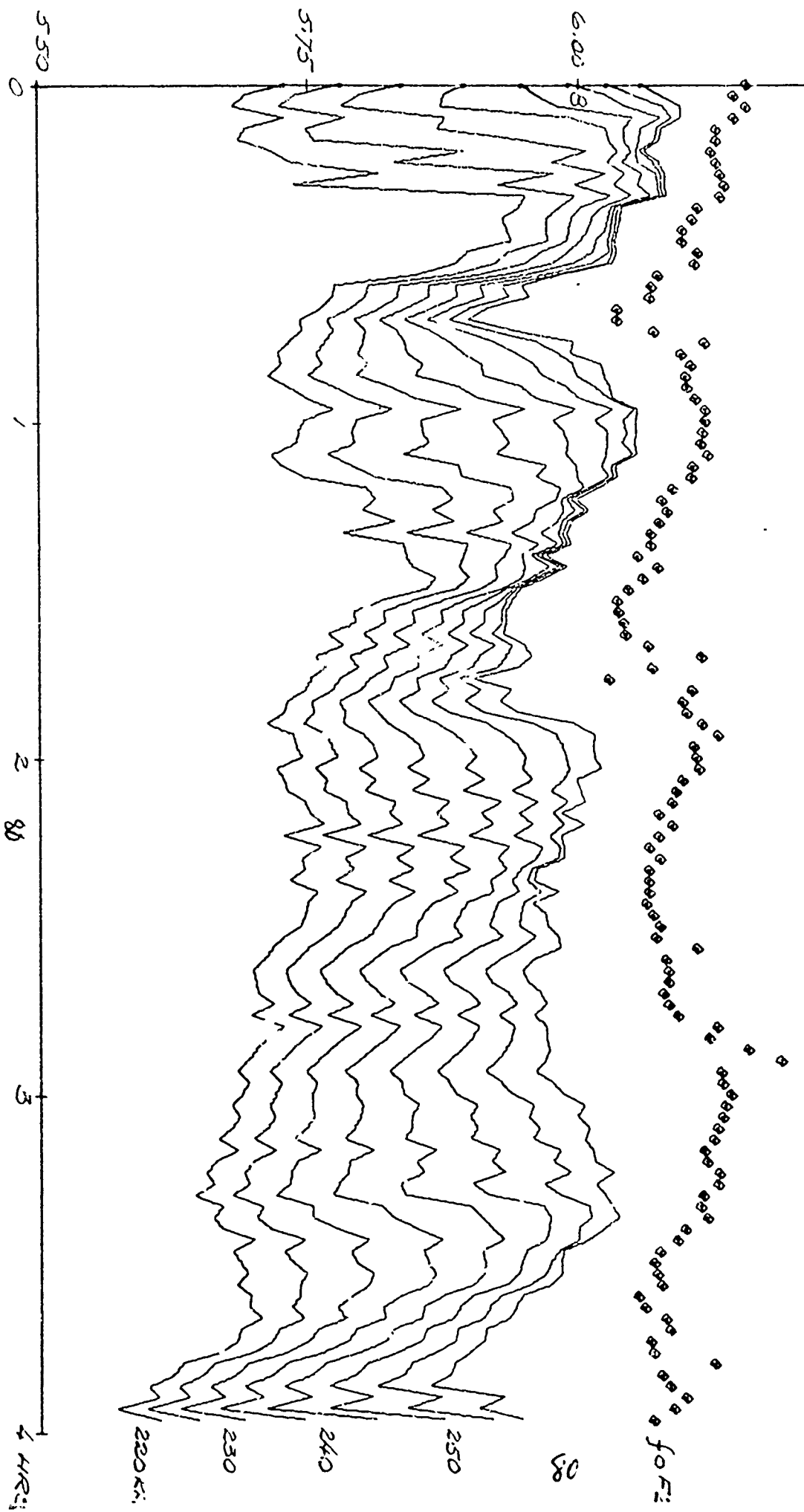
FIGURE 17. NORMALIZED POWER SPECTRA AND IONOSPHERIC PREDICTIVE FUNCTIONS

HANOVER, JAN 13, 1969, 10:00-14:00 EST

GGGGGG THEORETICAL / EXPERIMENTAL PREDICTIVE FUNCTIONS

250 KM
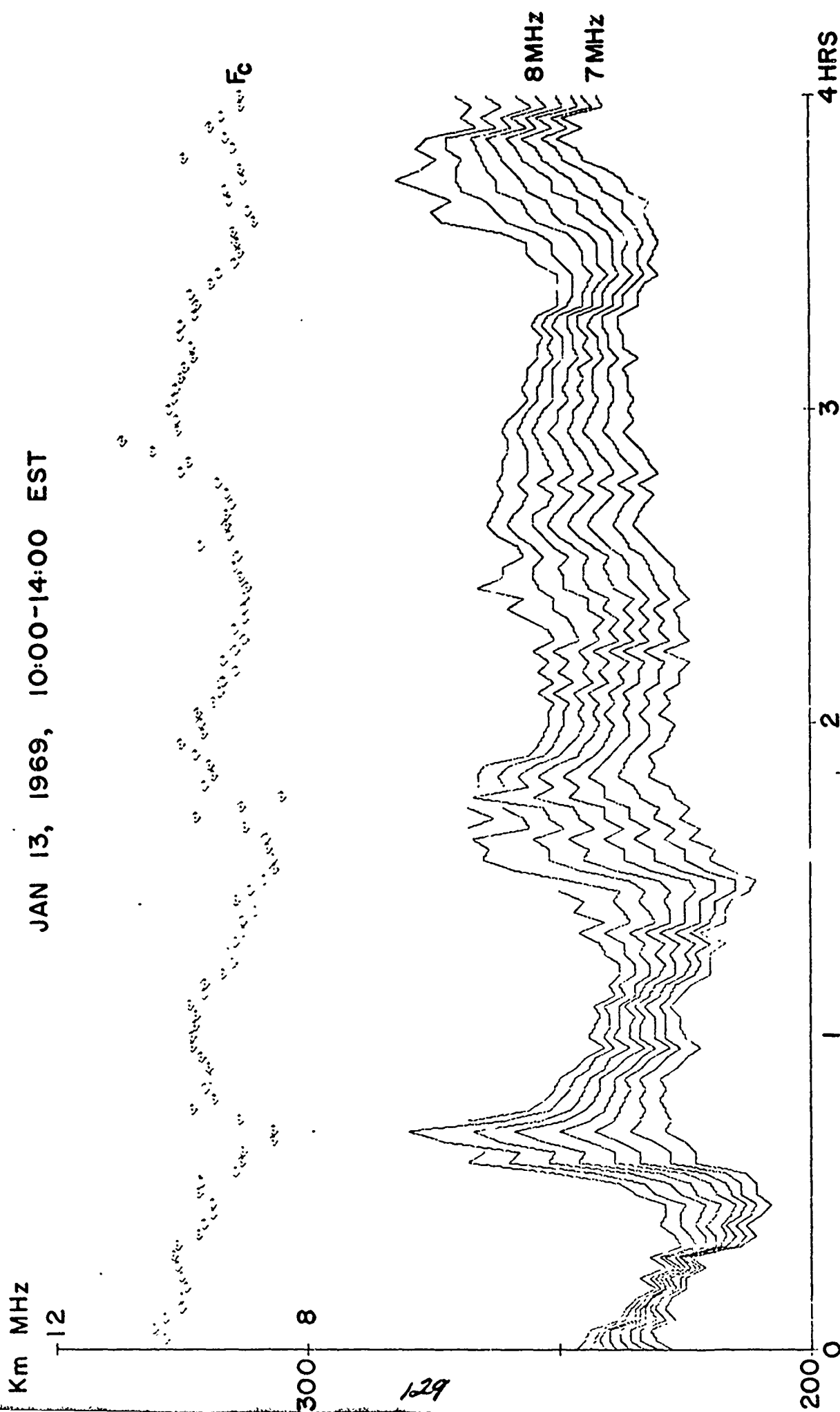
240 KM

1/60   1/50   1/20   1/5 KM⁻¹
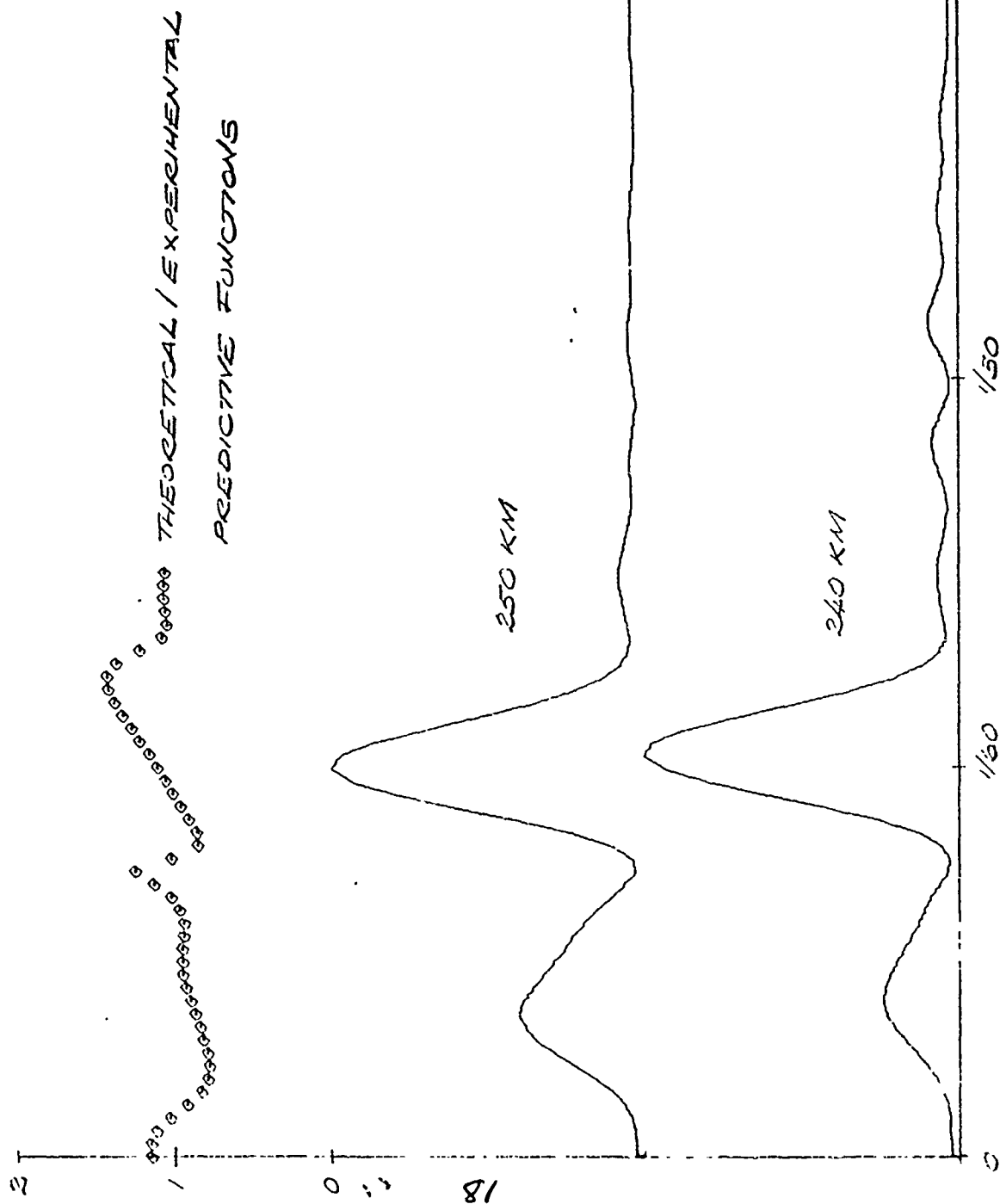
FIGURE 18. CRITICAL FREQUENCIES AND ISO-HEIGHT CONTOURS
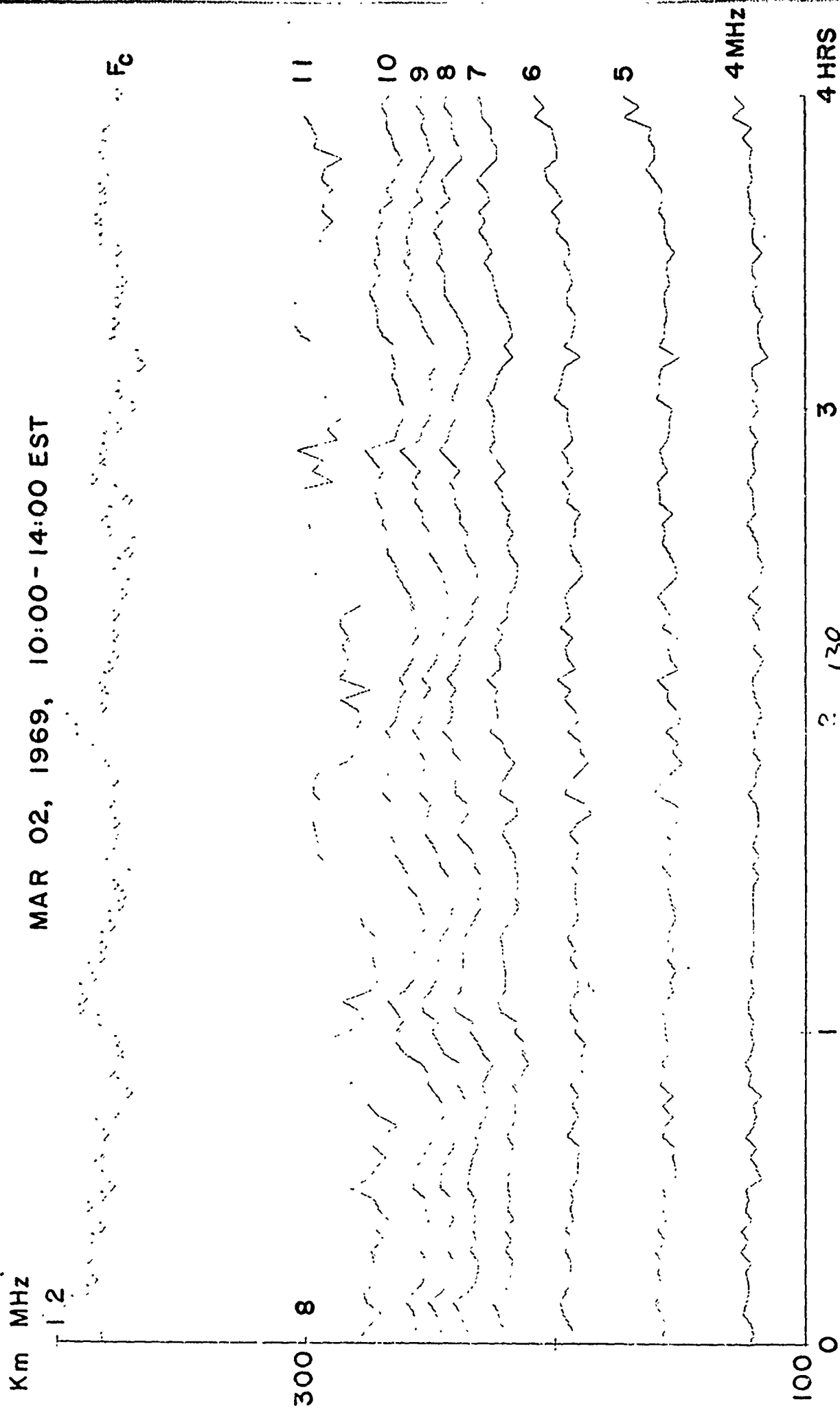
HANOVER, MAR 02, 1959, 10:00 - 14:00 EST
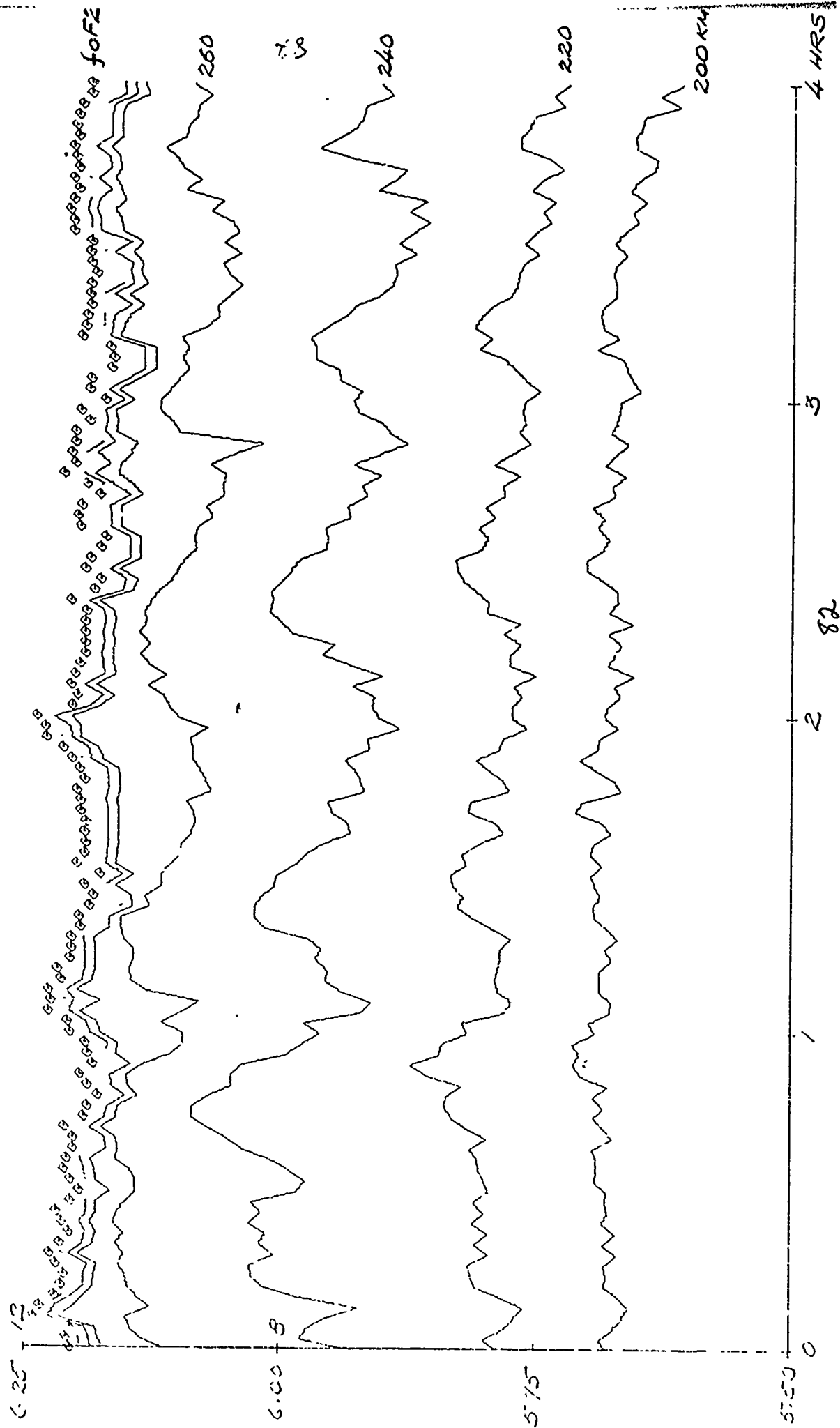
FIGURE 19. CRITICAL FREQUENCIES AND ISO-HEIGHT CONTOURS

HIGHGATE SPRINGS, MAR 02, 1969, 10:00-14:00 EST
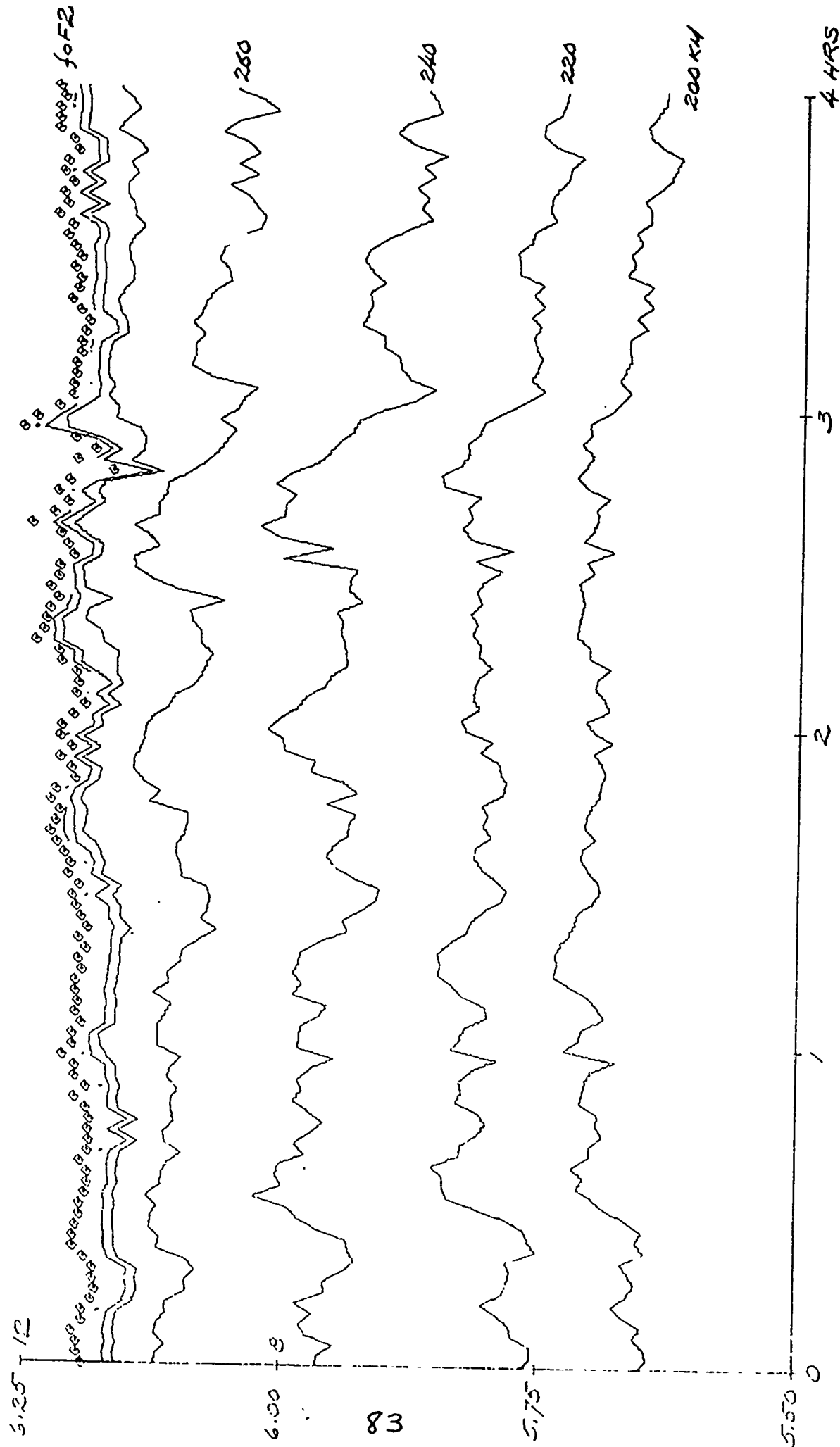
FIGURE 20. CRITICAL FREQUENCIES AND ISO-HEIGHT CONTOURS

ERROL, MAR 02, 1969, 10:00–14:00 EST
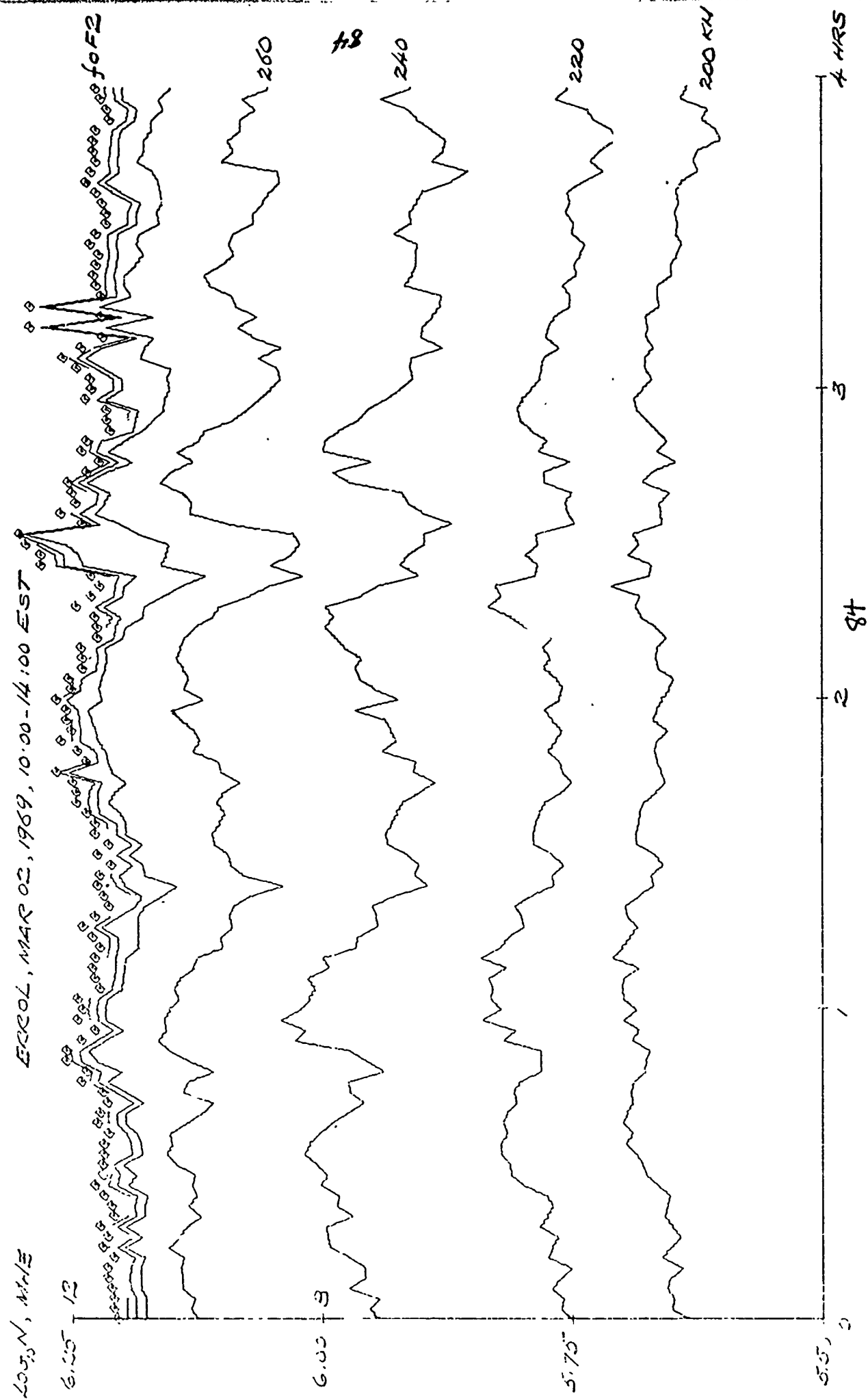
FIGURE 21. CRITICAL FREQUENCIES AND ISO-HEIGHT CONTOURS

HANOVER, MAR 02, 1969, 10:00-14:00 EST
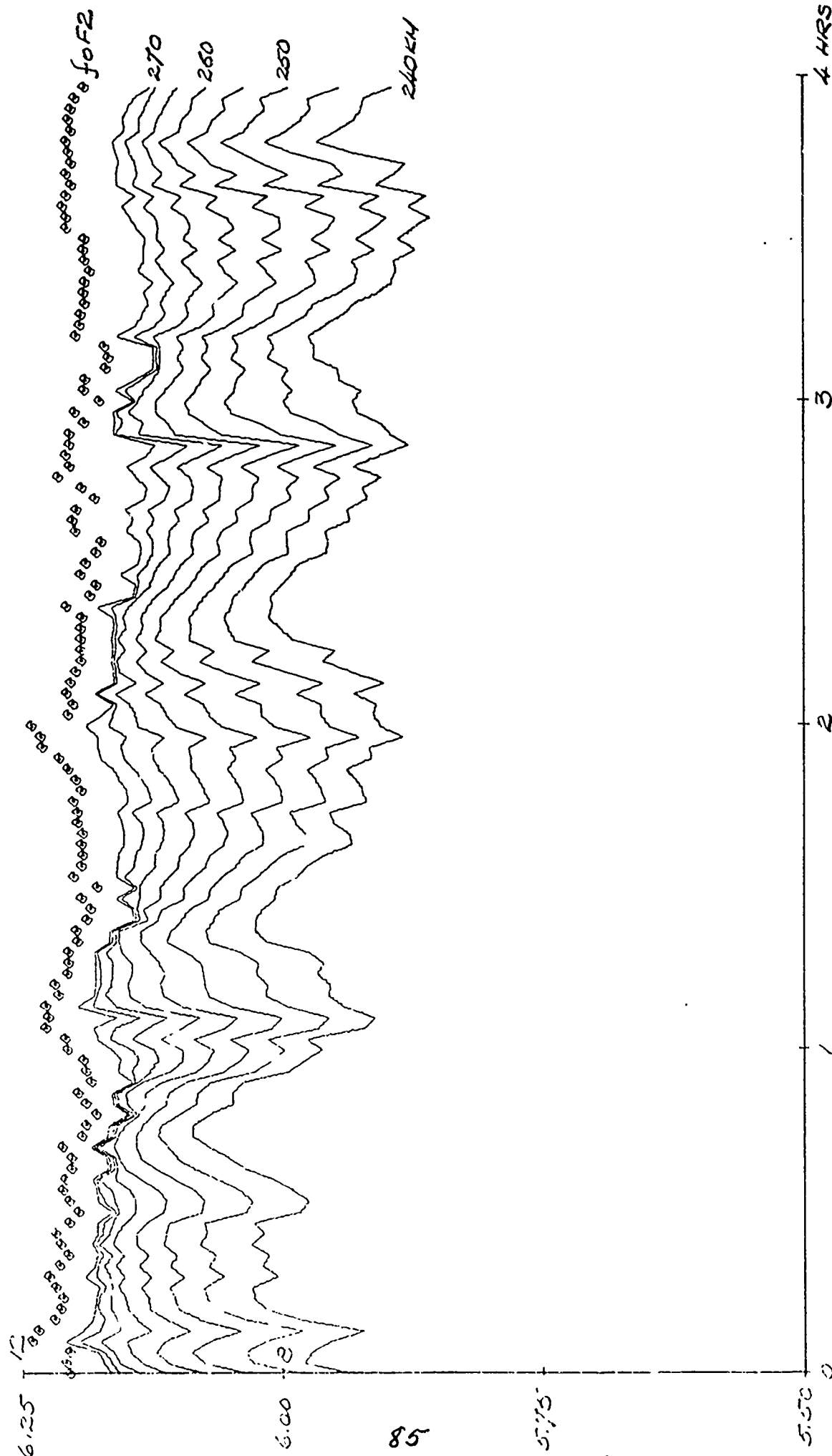
FIGURE 22. CRITICAL FREQUENCIES AND ISO-HEIGHT CONTOURS

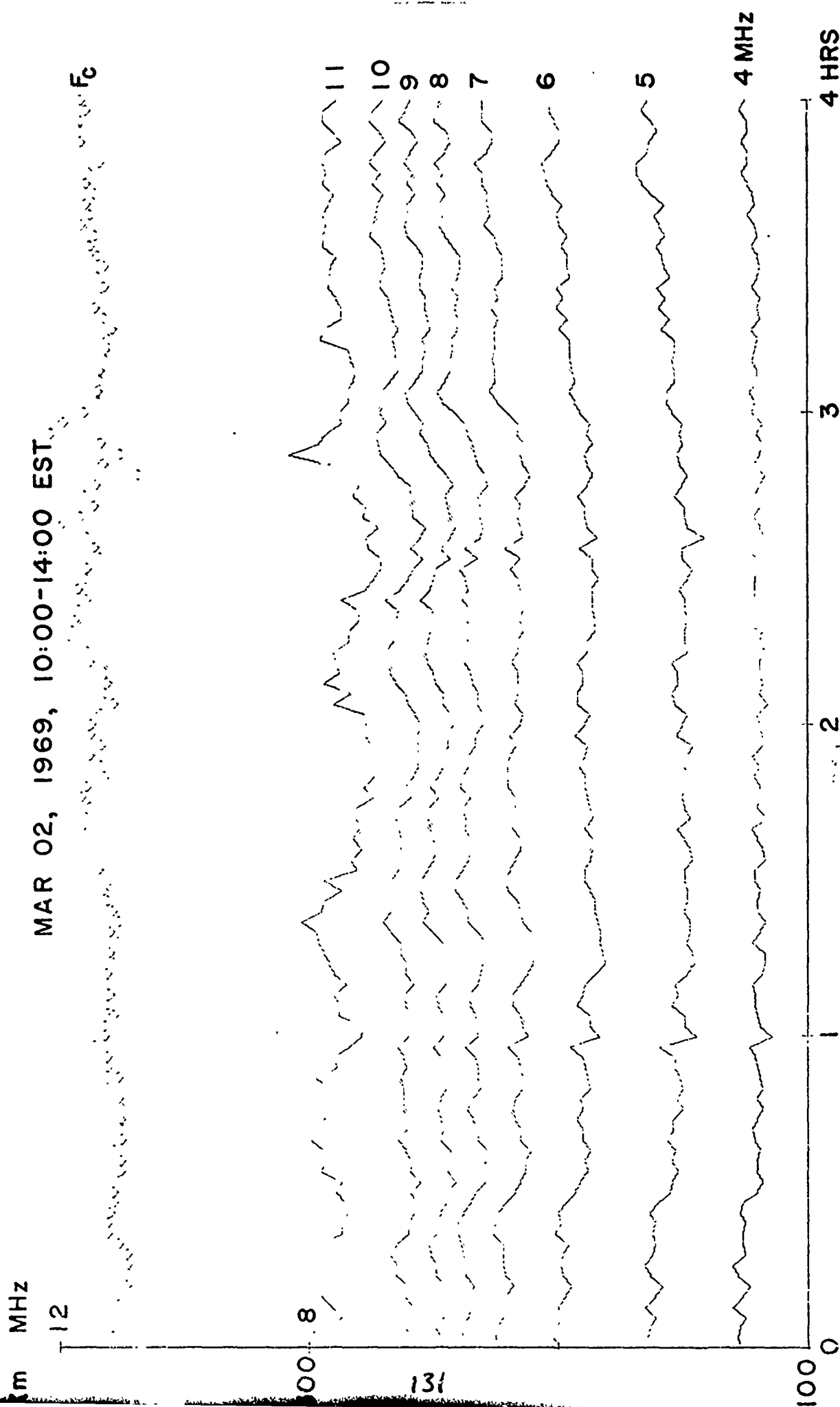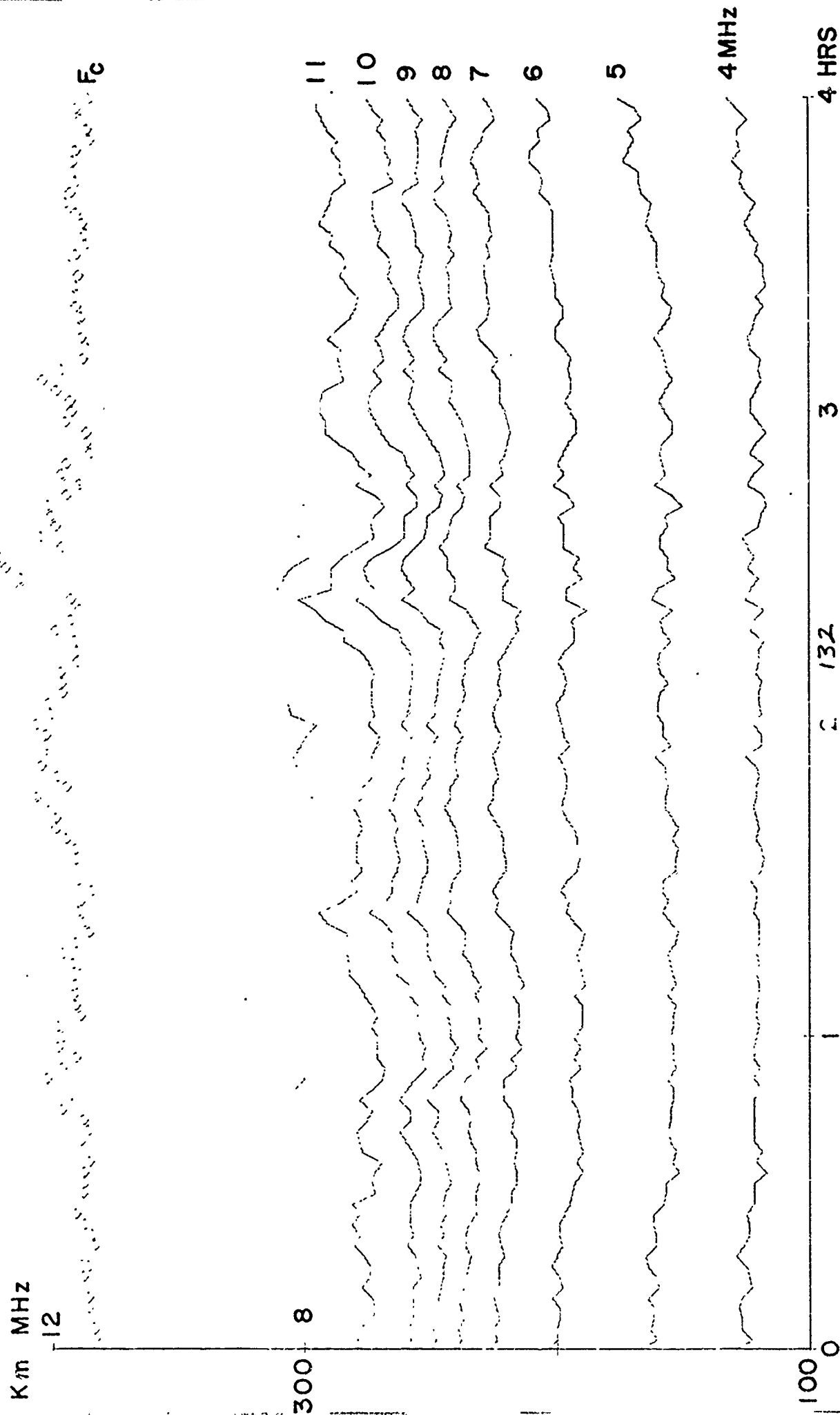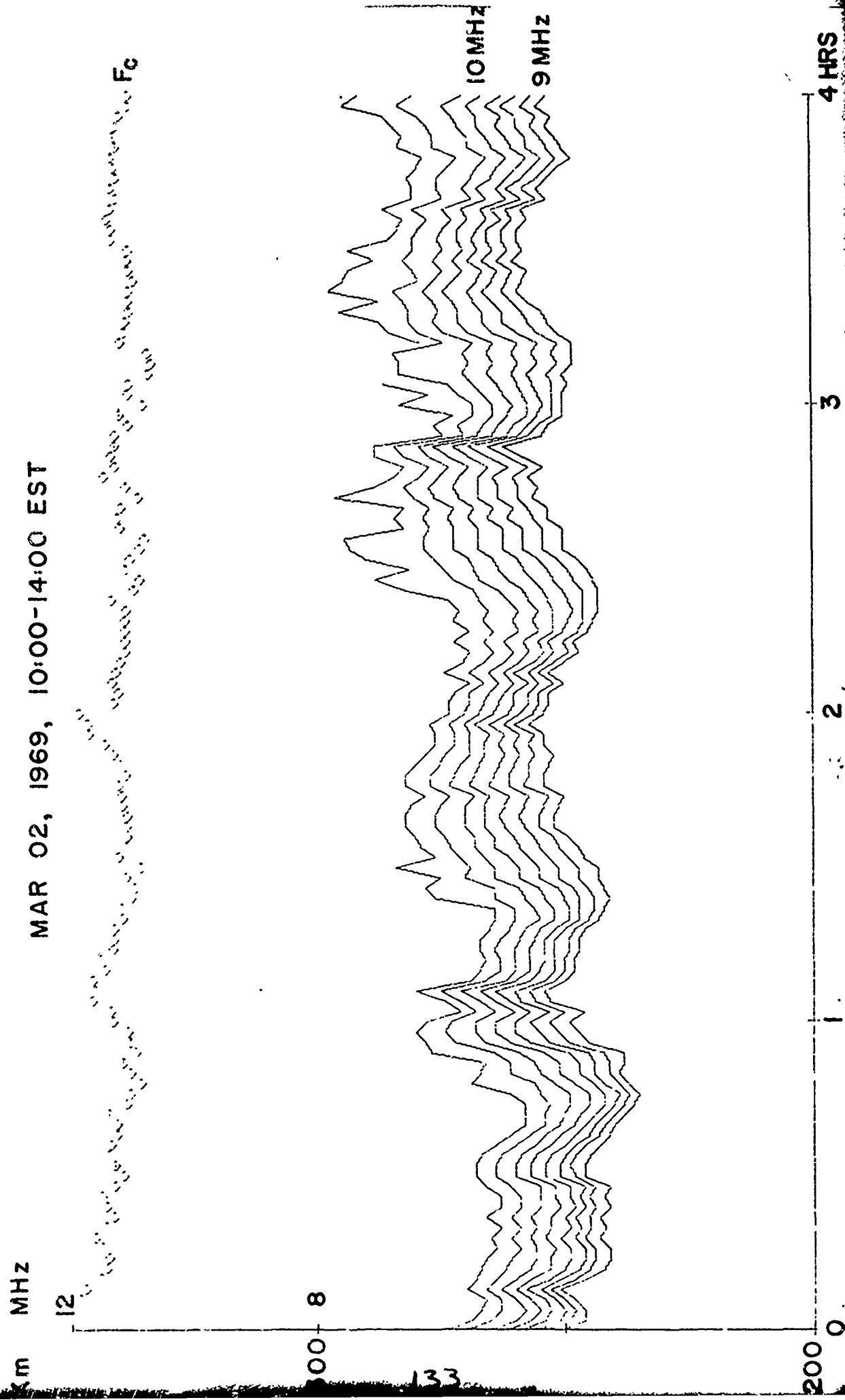HIGHGATE SPRINGS, MAR 02, 1969, 10:00 ~ 14:00 EST

$43°N, MHz$

f_0F2

270

98

260

250

240KM

4 HRS
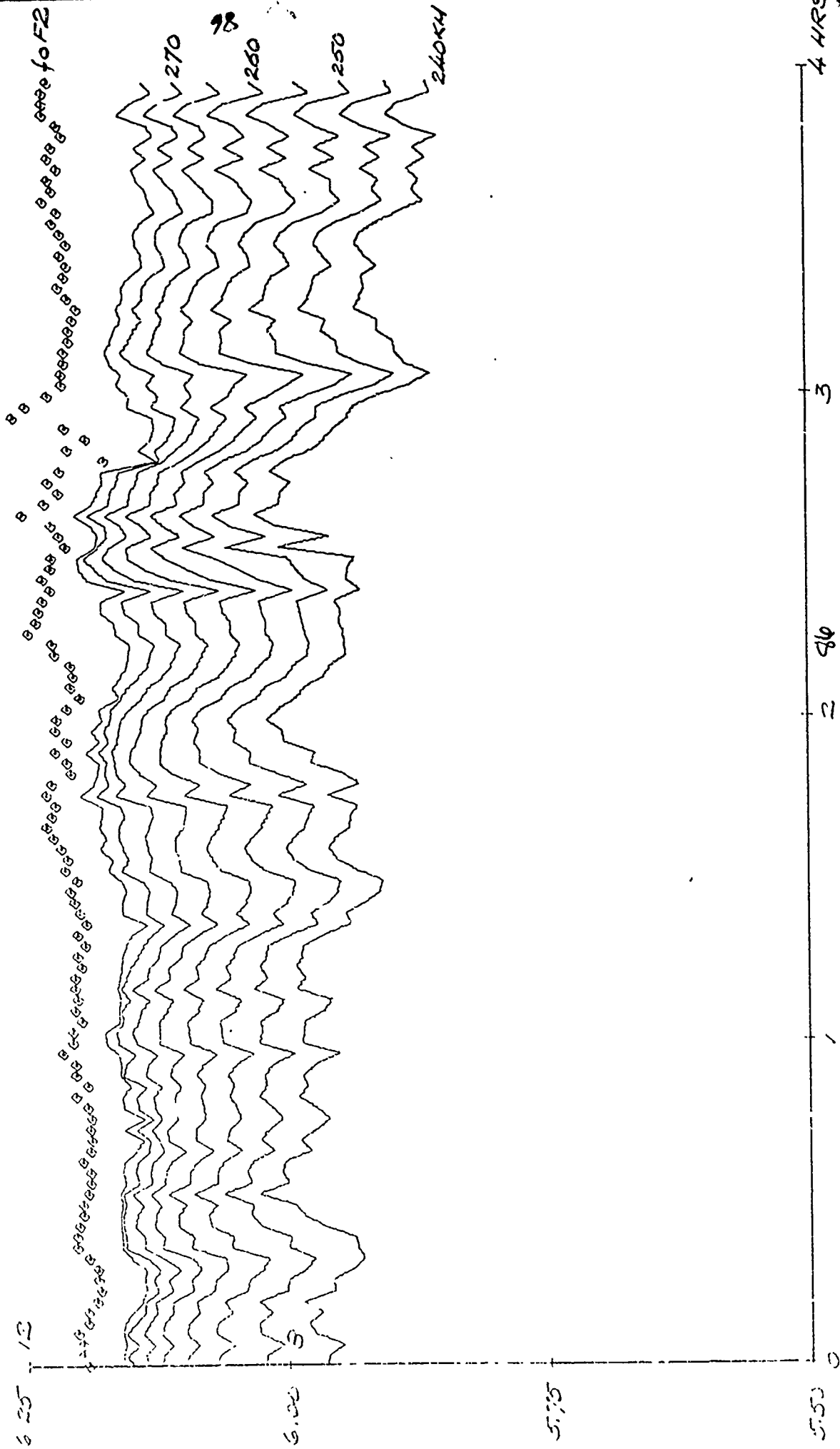
FIGURE 23 CRITICAL FREQUENCIES AND ISO-HEIGHT CONTOURS

ERROL, MAR 22, 1969, 10.00-14:00 EST
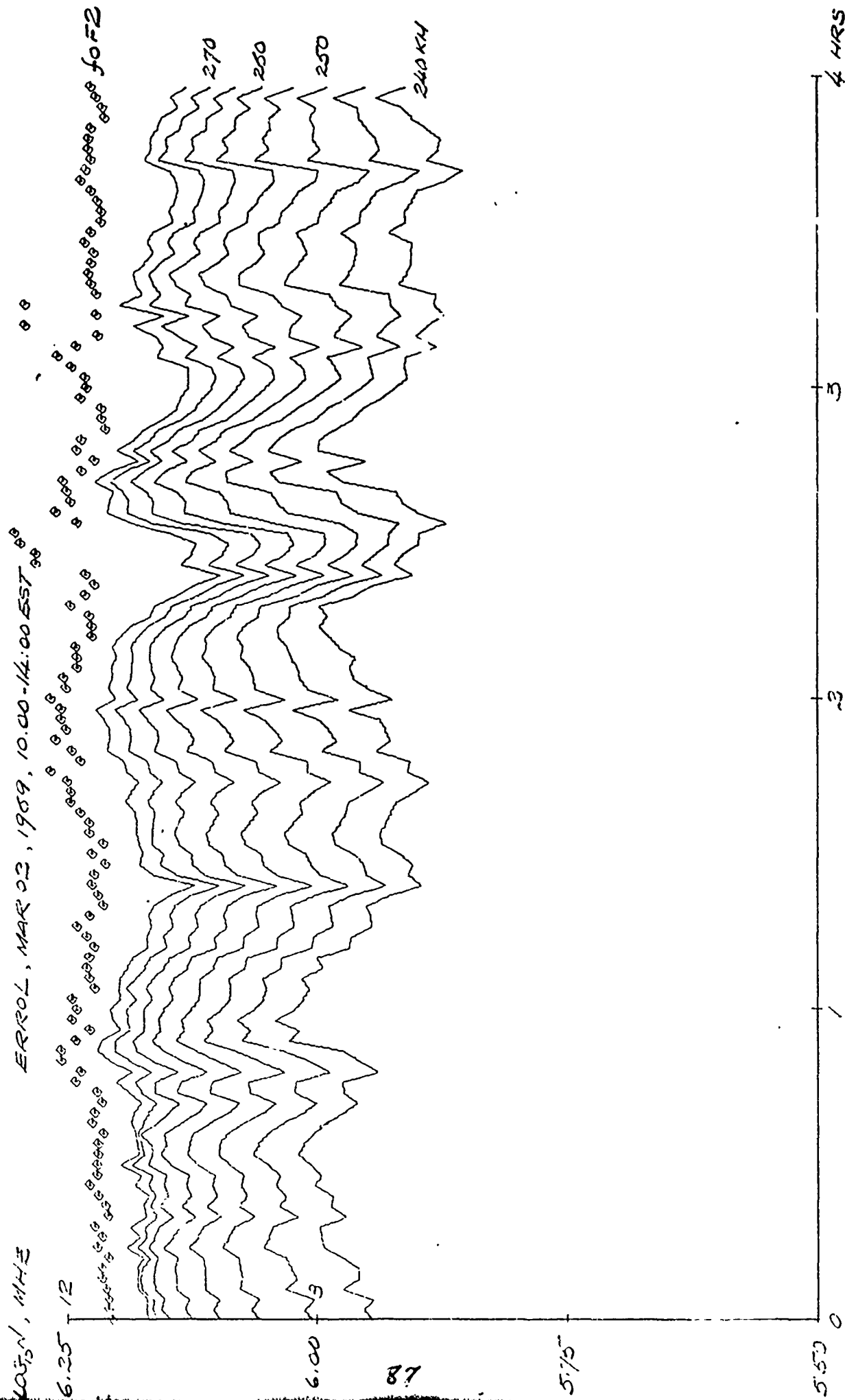
FIGURE 24. NORMALIZED POWER SPECTRA AND IONOSPHERIC PREDICTIVE FUNCTIONS

HANOVER, MAR 02, 1967, 10:00 - 14:00 EST

THEORETICAL/EXPERIMENTAL

PREDICTIVE FUNCTIONS
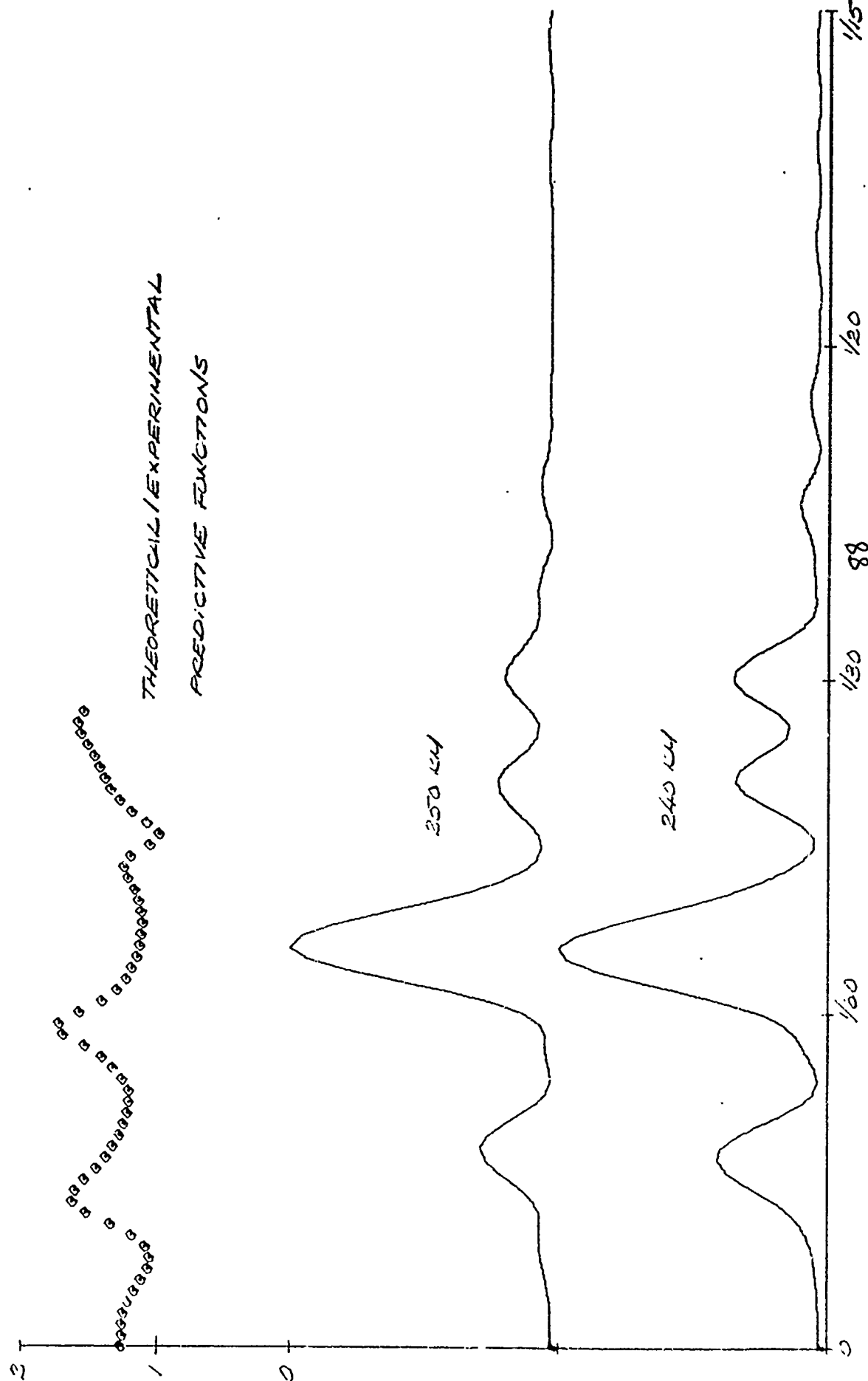
FIGURE 25   CRITICAL FREQUENCIES AND ISO-HEIGHT CONTOURS

HANOVER, APR 29, 1969, 13:30 - 17:30 EST
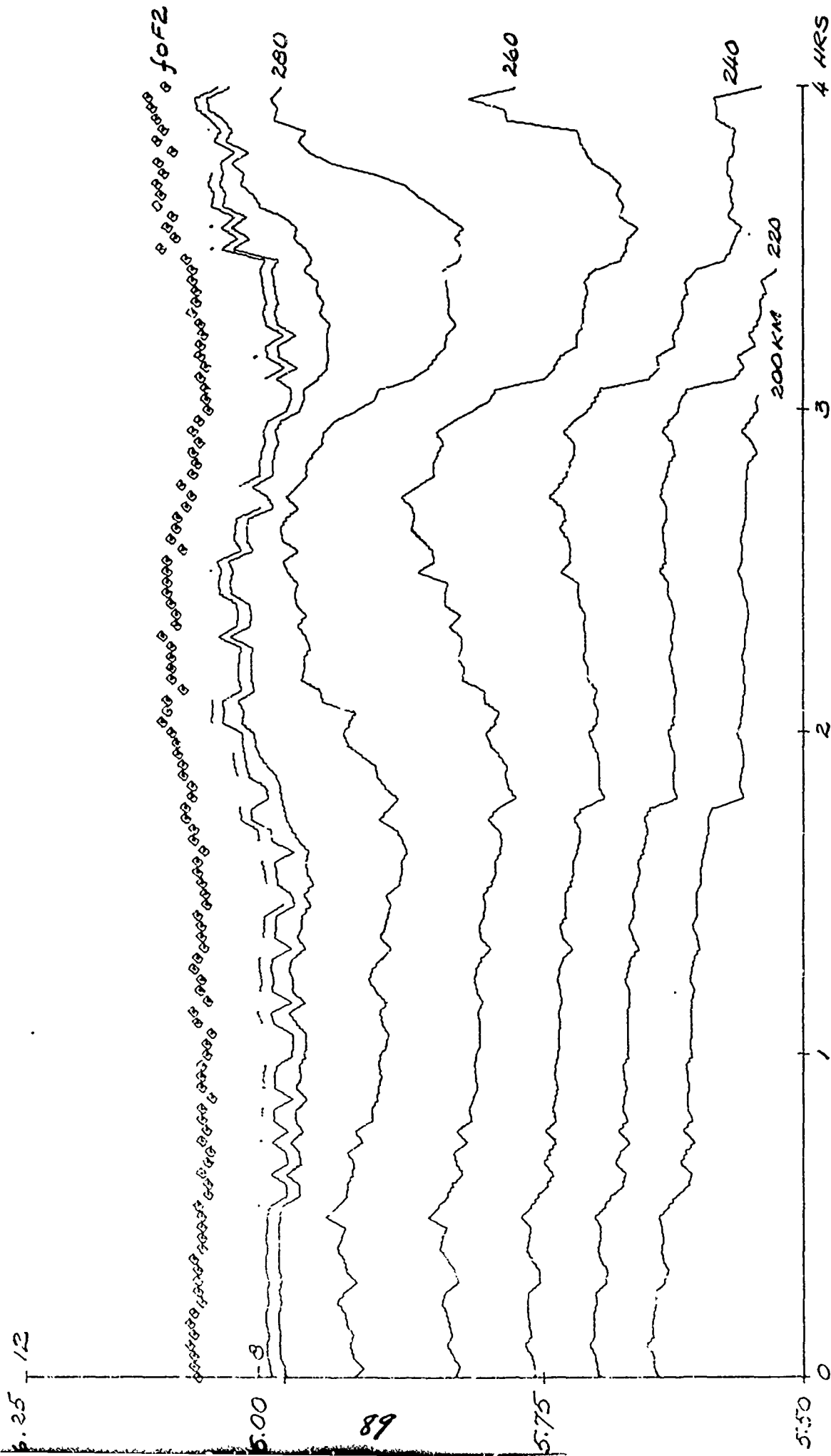
FIGURE 26 CRITICAL FREQUENCIES AND ISO-HEIGHT CONTOURS

HIGHGATE SPRINGS, APR 29, 1969, 13:30 - 17:30 EST
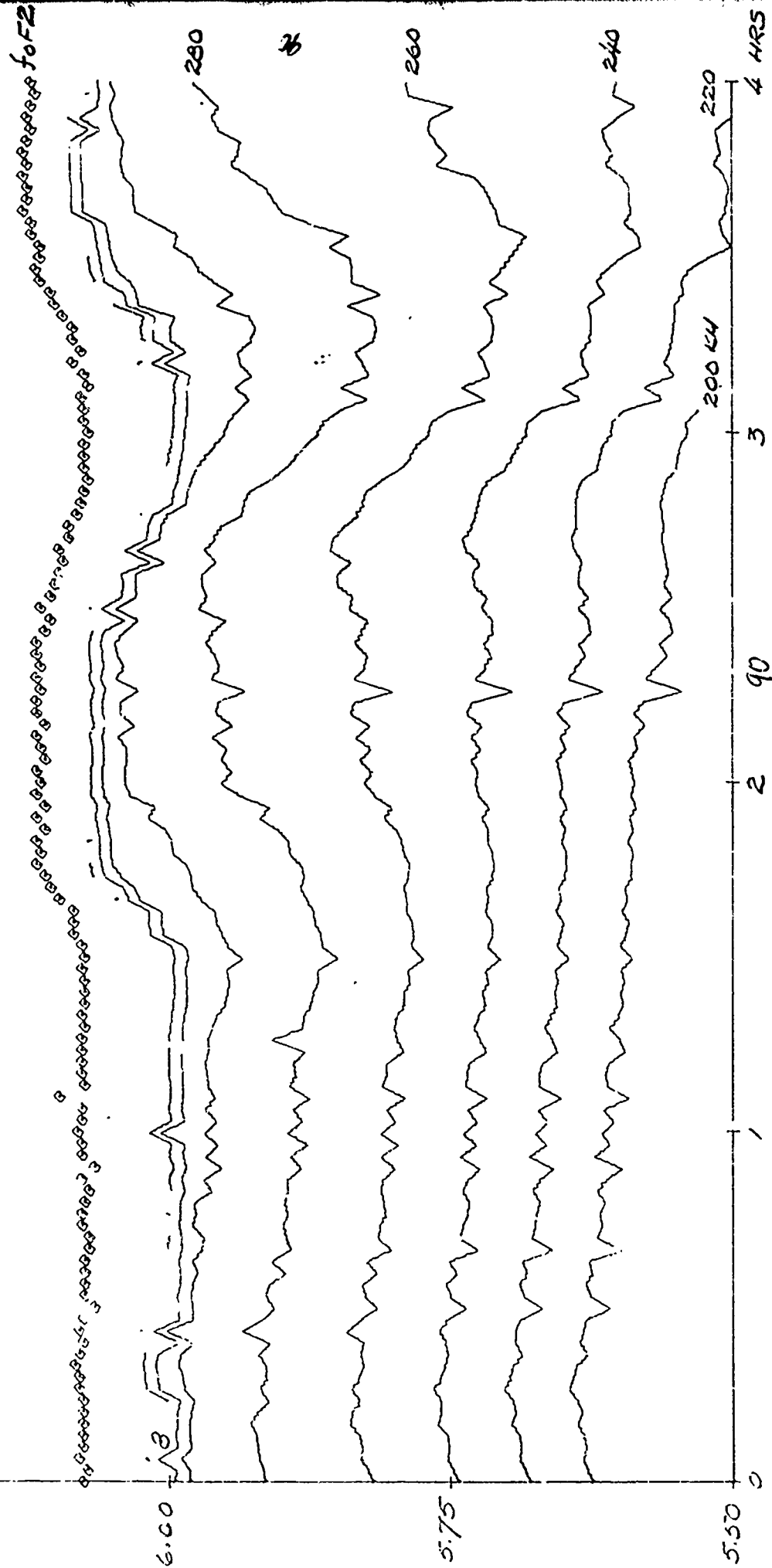
FIGURE 27. CRITICAL FREQUENCIES AND ISO-HEIGHT CONTOURS
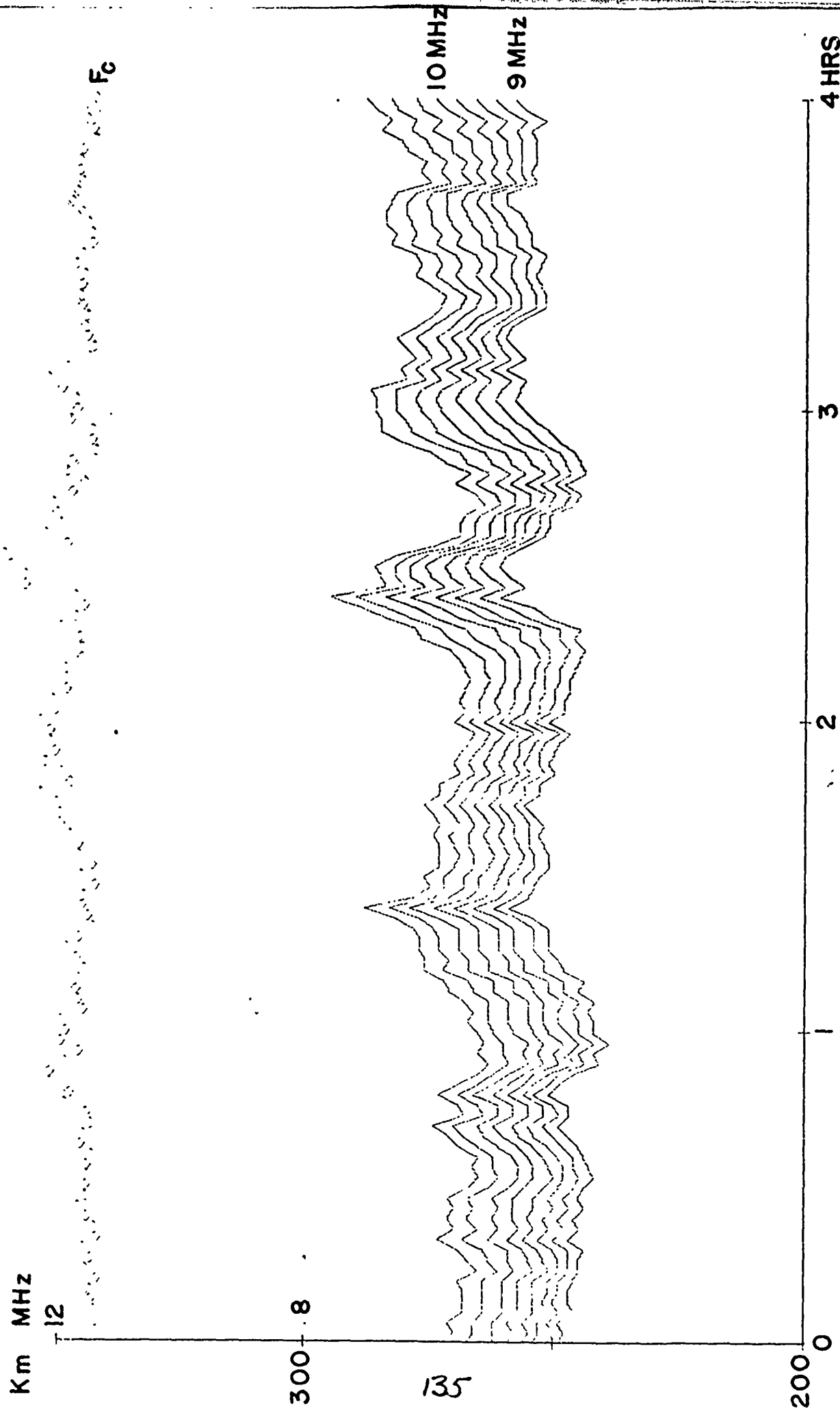
ERROL, APR 29, 1969, 13:30-17:30 EST
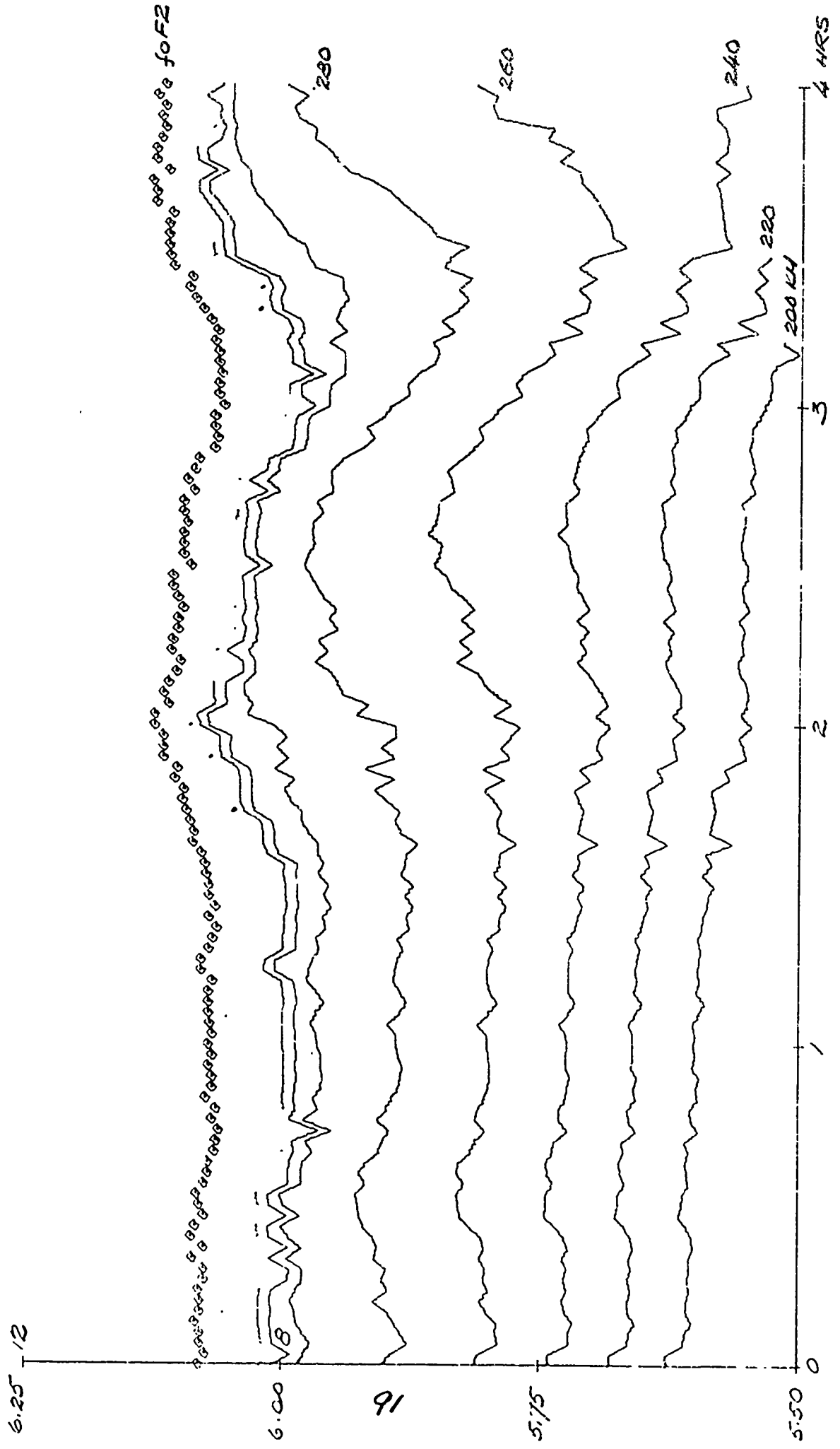
FIGURE 28. CRITICAL FREQUENCIES AND ISO-HEIGHT CONTOURS
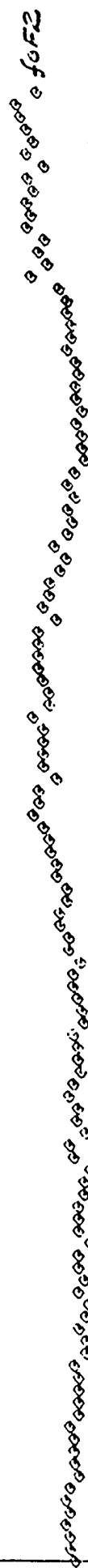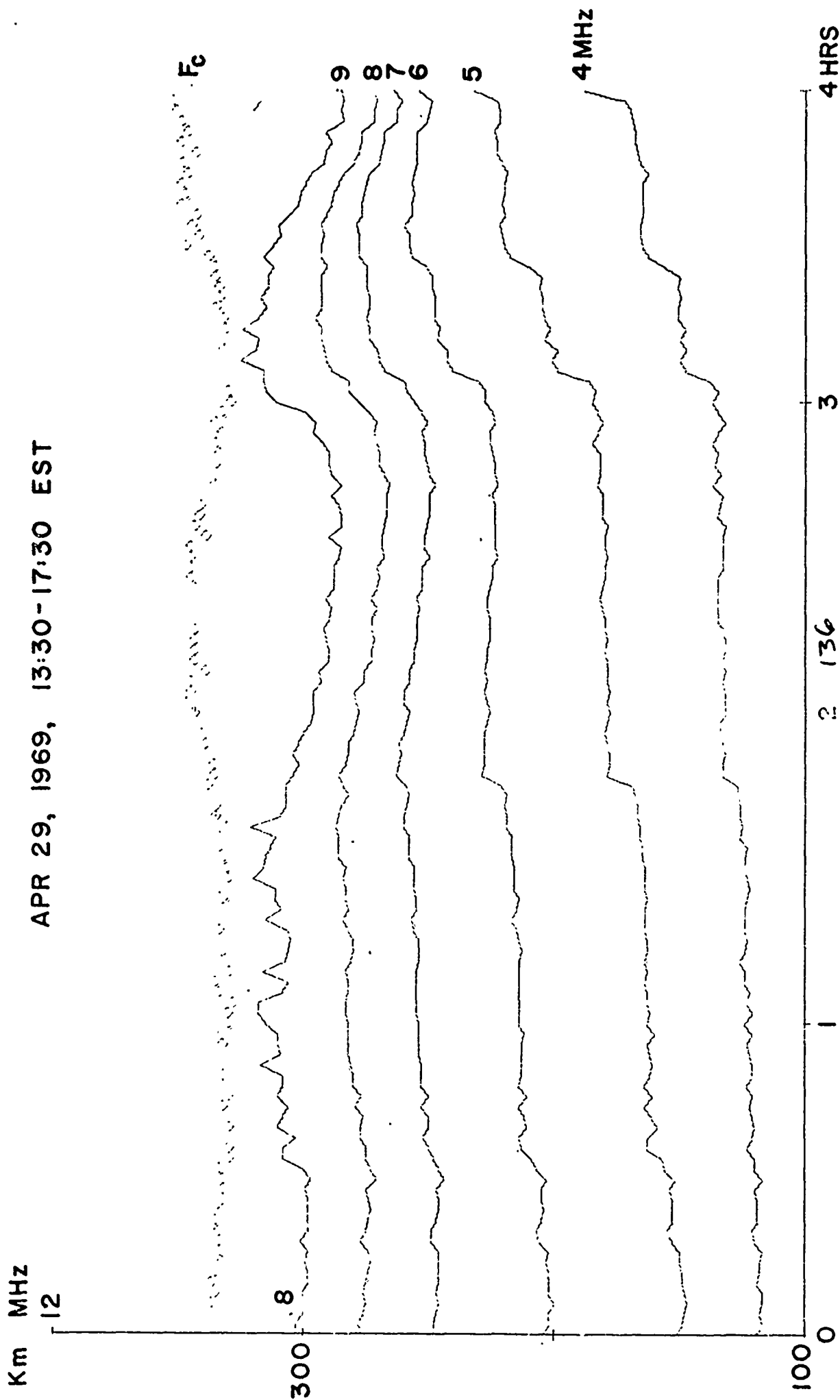
HANOVER, APR 29, 1969, 13:30 - 17:30 EST

FIGURE 29. CRITICAL FREQUENCIES AND ISO-HEIGHT CONTOURS
HIGHGATE SPRINGS, APR. 29, 1969, 19:30 - 17:30 EST
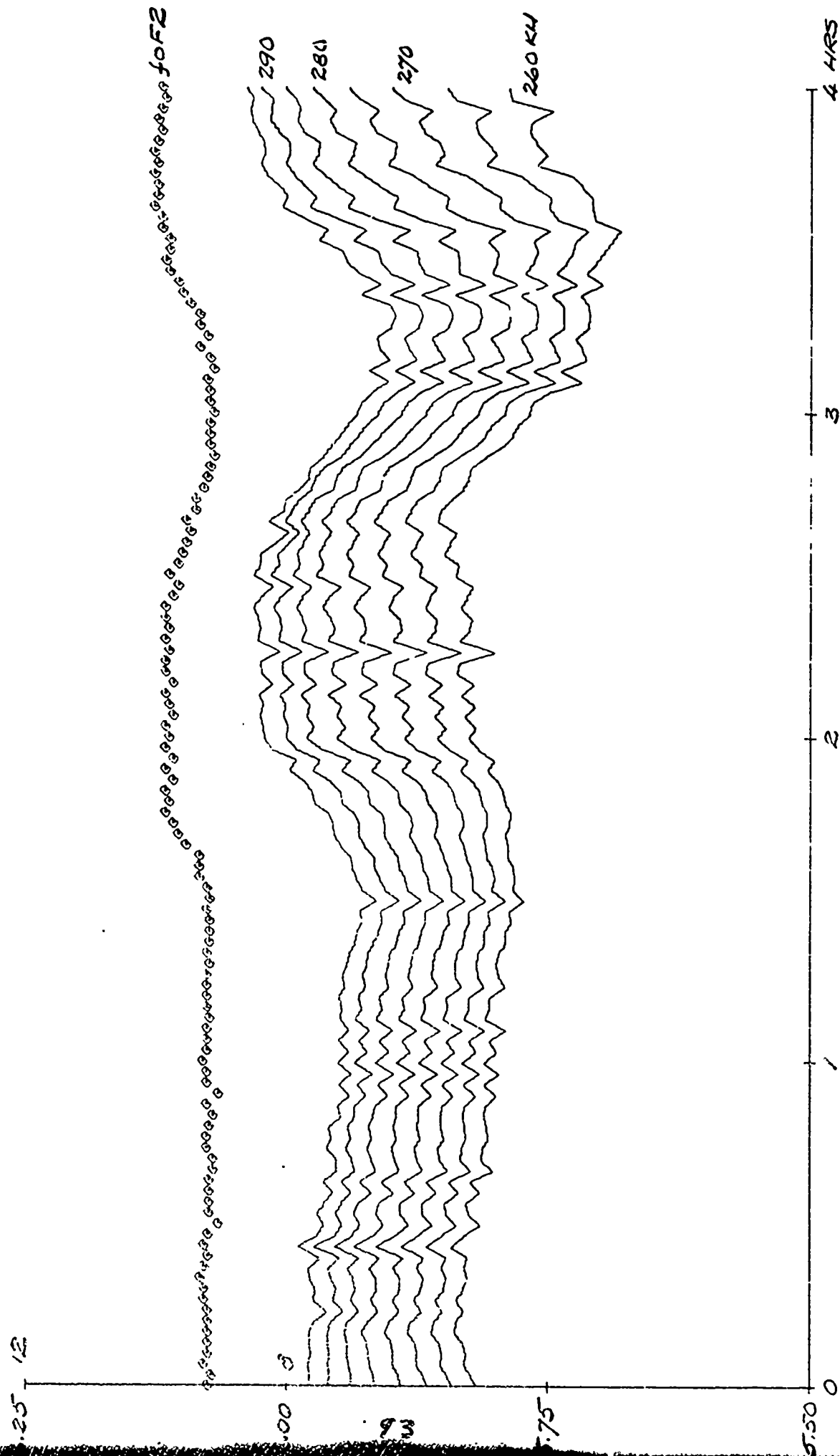
FIGURE 30. CRITICAL FREQUENCIES AND 150-HEIGHT CONTOURS

ERROL, APR 29, 1969, 13:30 - 17:30 EST

FIGURE 31. NORMALIZED POWER SPECTRA AND IONOSPHERIC PREDICTIVE FUNCTIONS

HANOVER, APR 29, 1969, 13:30 – 17:30 EST
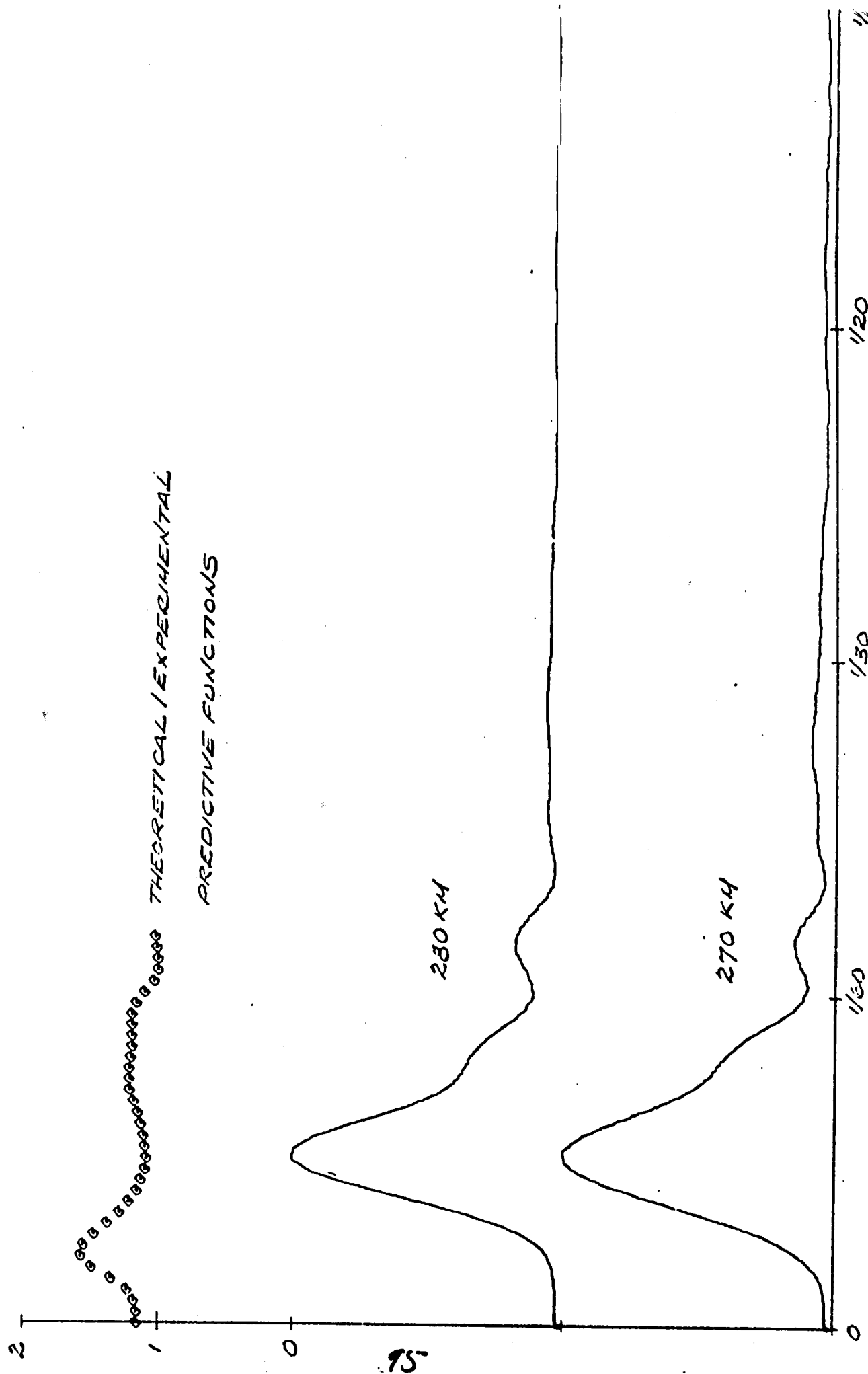
FIGURE 32 CRITICAL FREQUENCIES AND ISO-HEIGHT CONTOURS

HANOVER, SEP 05, 1969, 09:00 - 13:00 EST
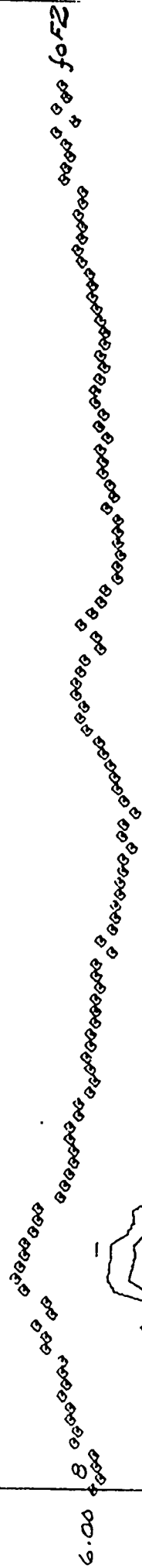
FIGURE 33. CRITICAL FREQUENCIES AND ISO-HEIGHT CONTOURS

HIGHGATE SPRINGS, SEP 05, 1969, 09:00-13:00 EST
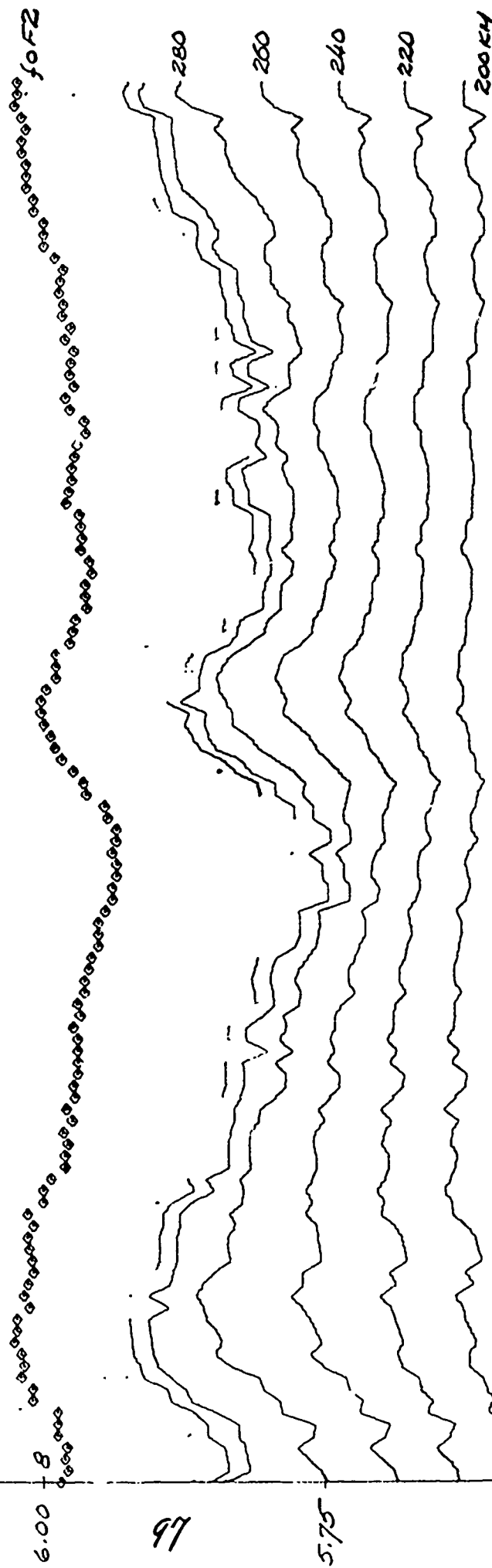
$LOG_{10}N'$, MHz

FIGURE 34 CRITICAL FREQUENCIES AND ISO-HEIGHT CONTOURS

ERCOL, SEP 05, 1969, 09:00 - 13:00 EST
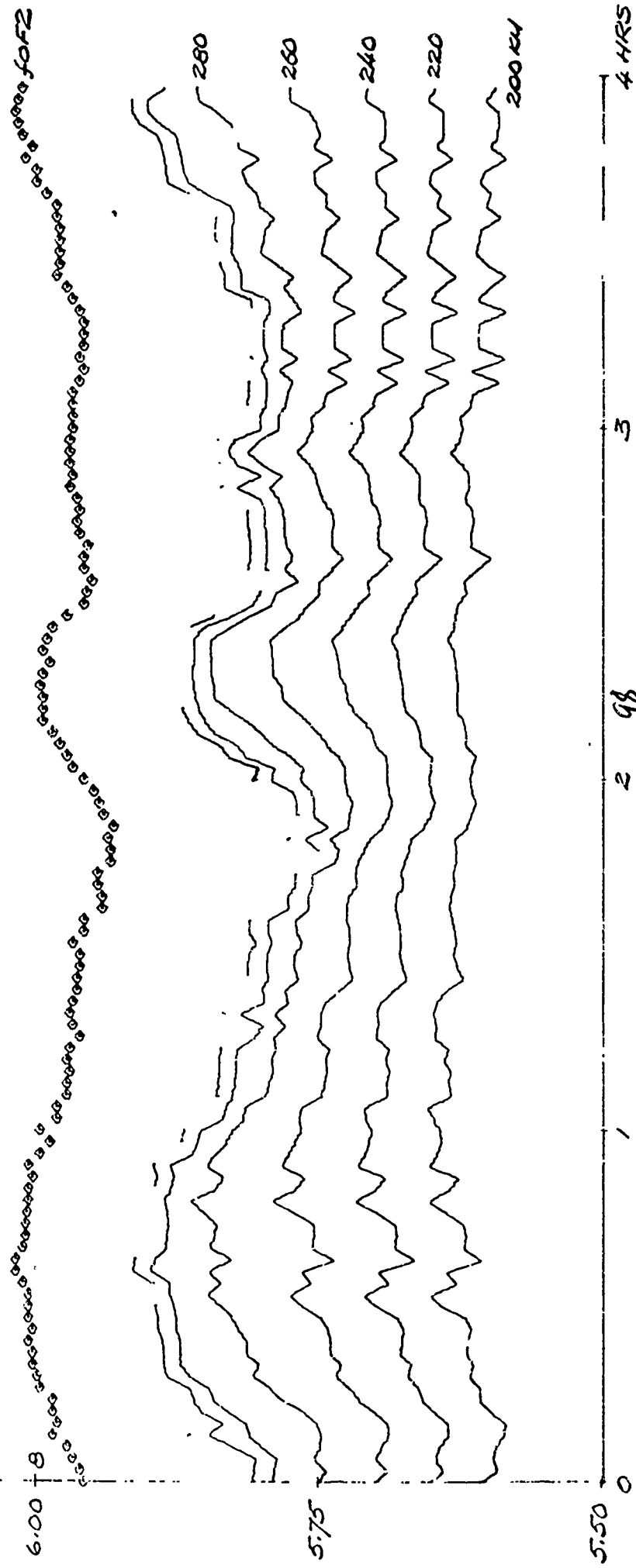
FIGURE 35 CRITICAL FREQUENCIES AND ISO-HEIGHT CONTOURS

HANOVER, SEP 05, 1989, 09:00 - 13:00 EST
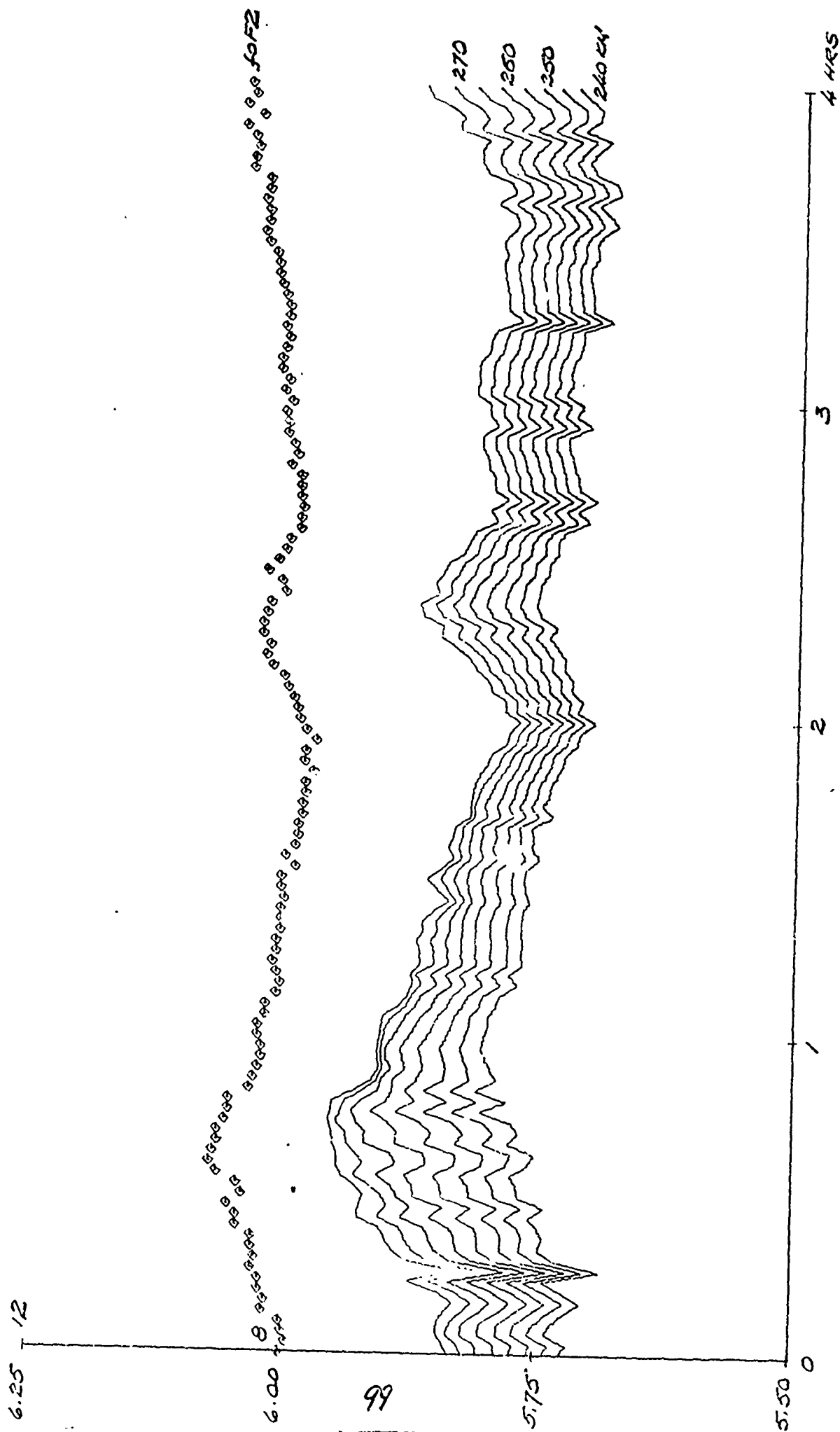
FIGURE 36 CRITICAL FREQUENCIES AND ISO-HEIGHT CONTOURS

HIGHGATE SPRINGS, SEP 05, 1959, 09:00 - 13:00 EST
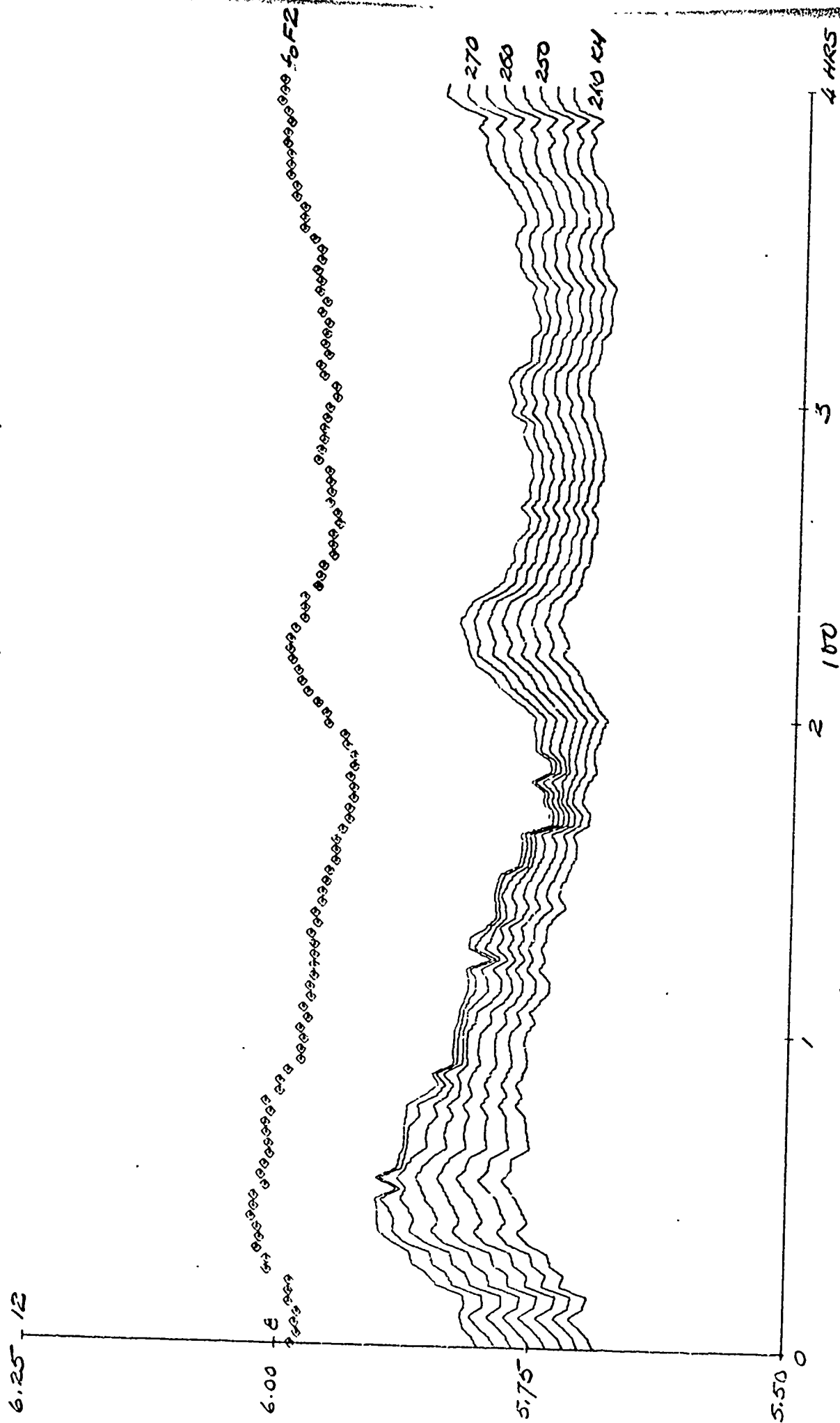
FIGURE 37 CRITICAL FREQUENCIES AND ISO-HEIGHT CONTOURS

ERROL, SEP 05, 1969, 09:00 - 13:00 EST
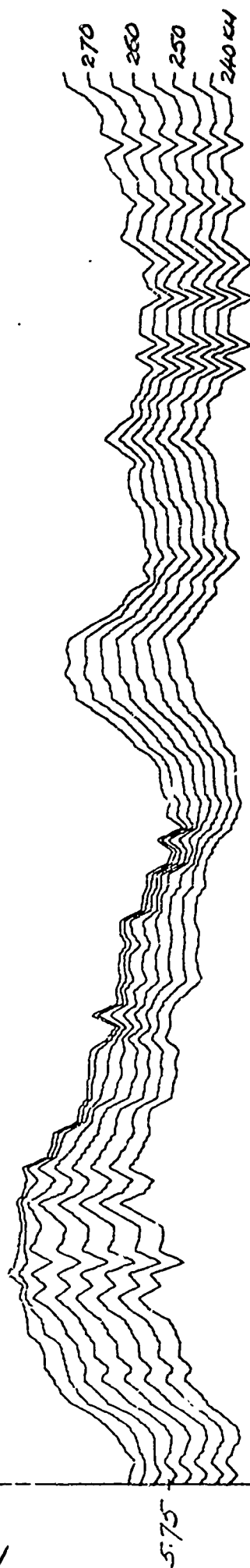
FIGURE 38. NORMALIZED POWER SPECTRA AND IONOSPHERIC PREDICTIVE FUNCTIONS
HANOVER, SEP 05, 1969, 09:00 - 13:00 GST
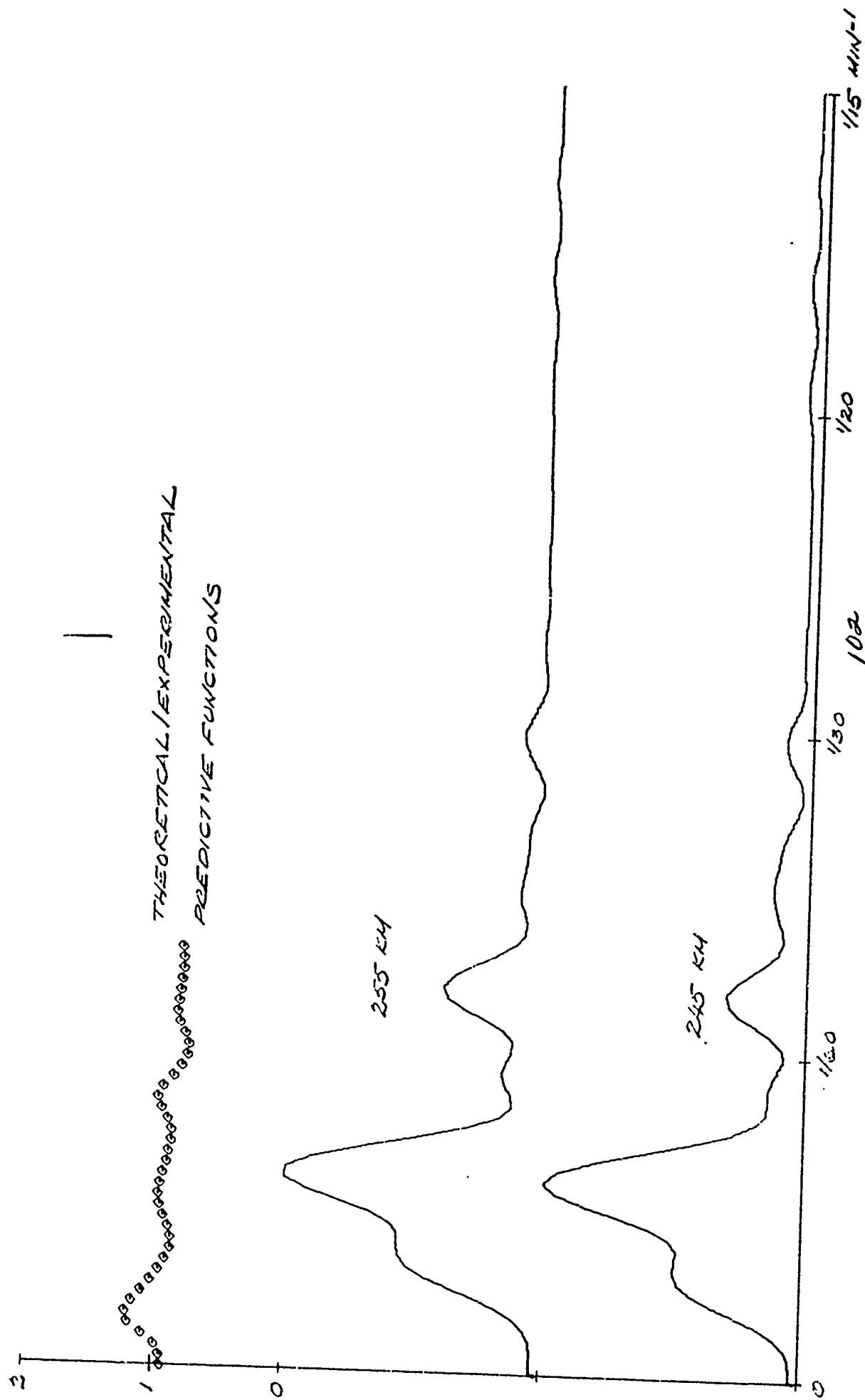
FIGURE 39 CRITICAL FREQUENCIES AND ISO-HEIGHT CONTOURS

HANOVER, NOV 15, 1969, 11:00-15:00 EST
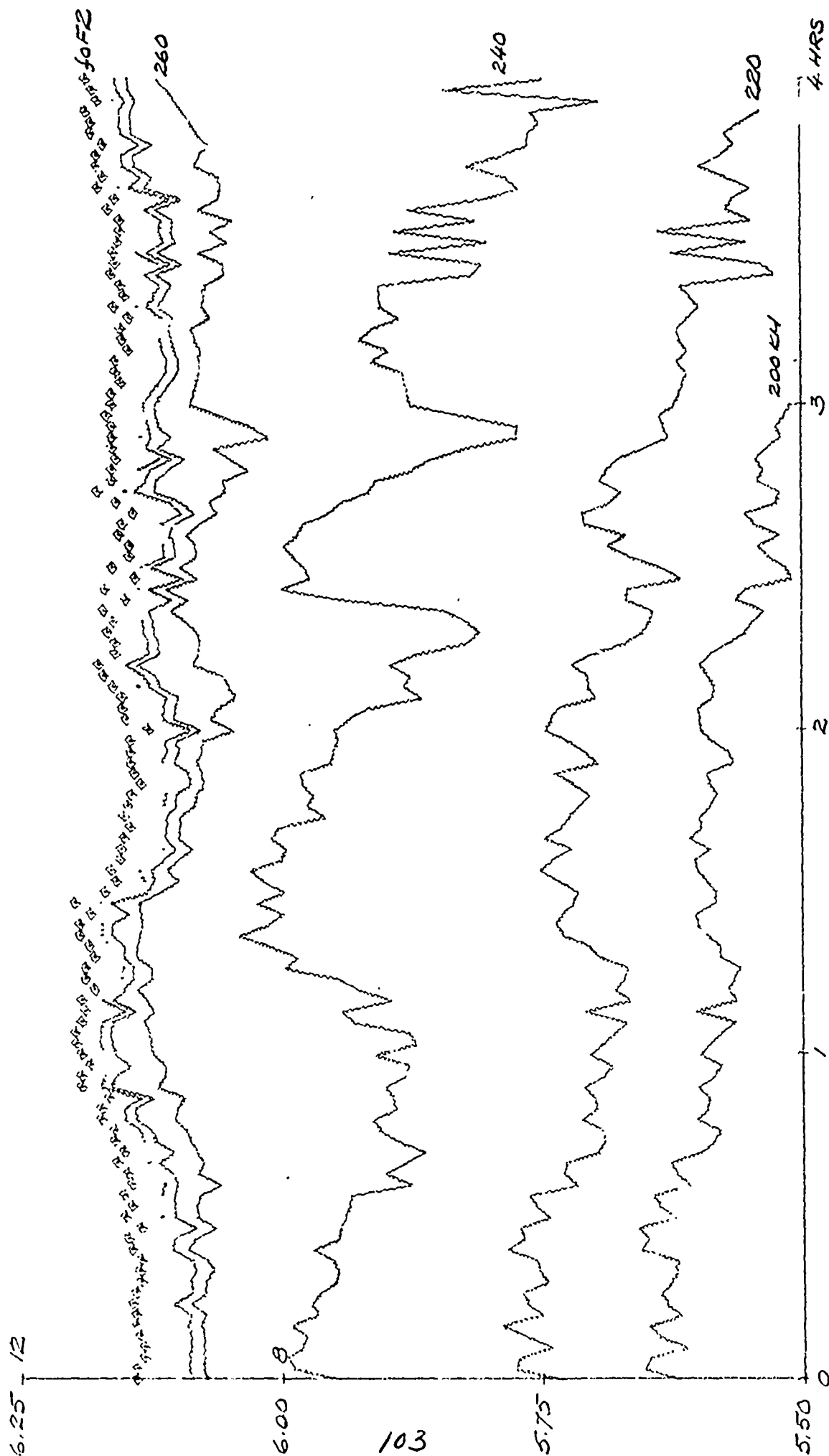
FIGURE 40 CRITICAL FREQUENCIES AND ISO-HEIGHT CONTOURS

HIGHGATE SPRINGS, NOV 15, 1969, 11:00-15:00 EST
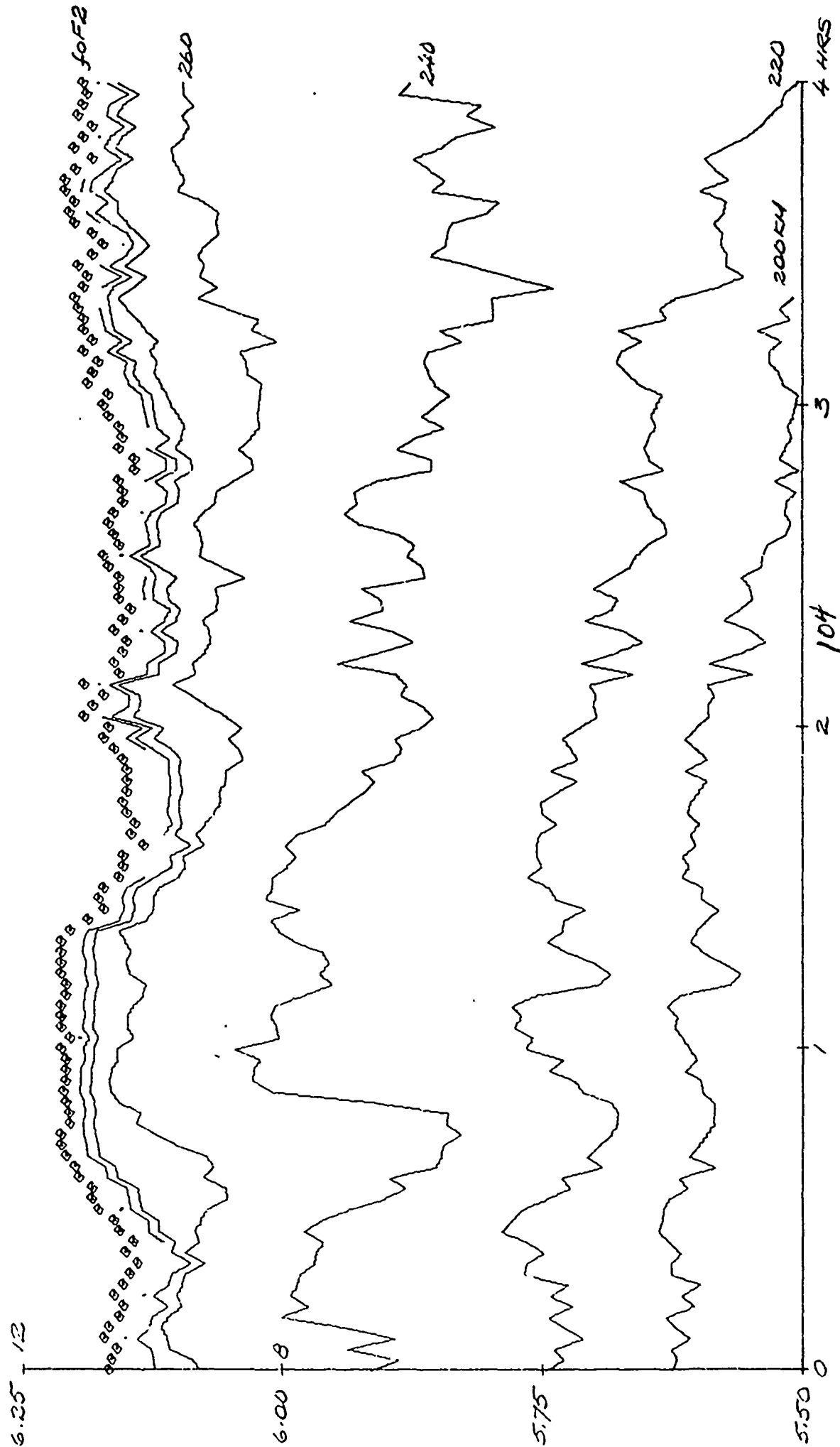
FIGURE 4. CRITICAL FREQUENCIES AND ISO-HEIGHT CONTOURS

ERCOL, NOV 15, 1967, 11:00-15:00 EST
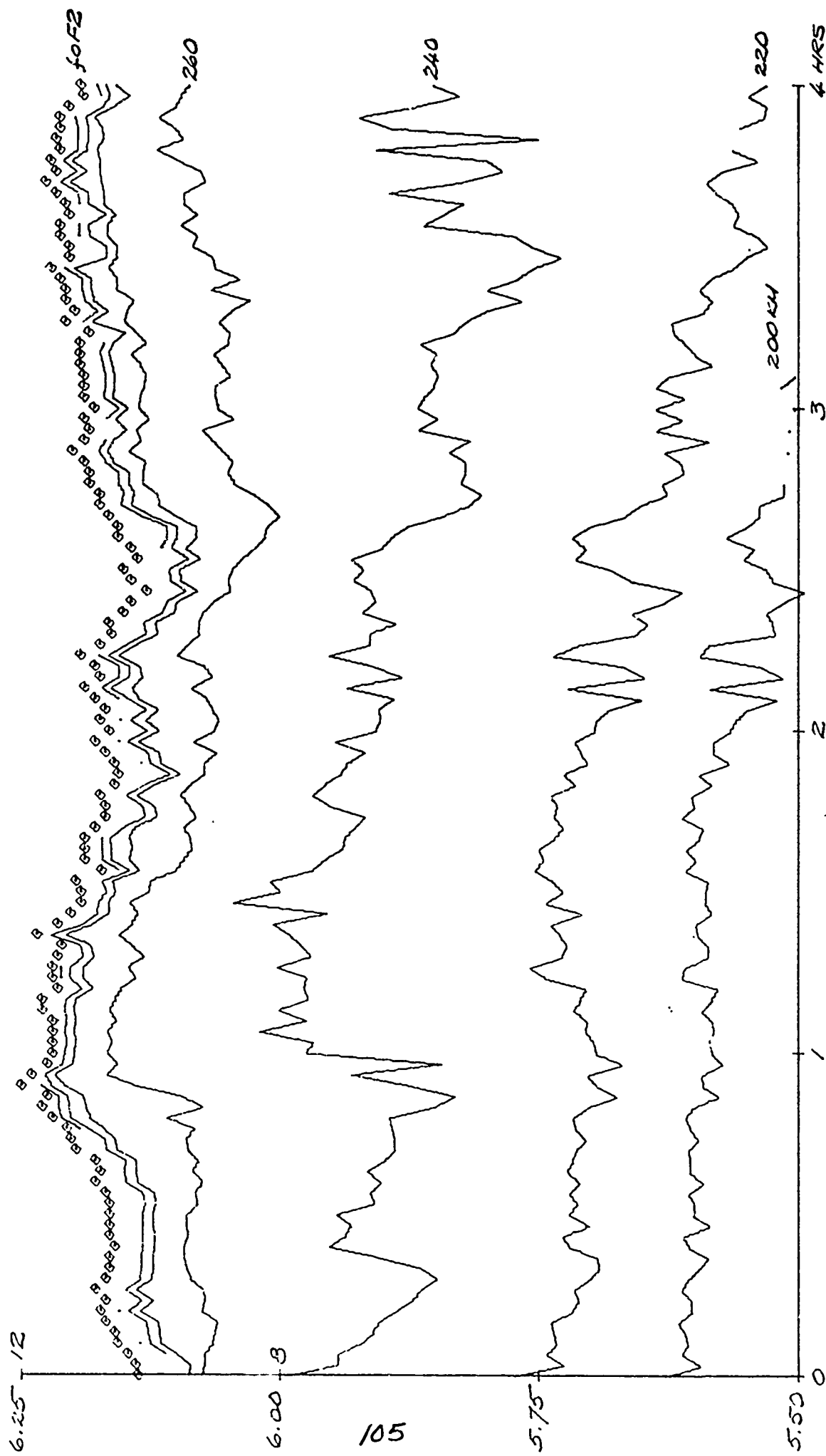
FIGURE 4.3 CRITICAL FREQUENCIES AND 150-HEIGHT CONTOURS

HANOVER, Nov 15, 1967, 11:00 - 15:00 EST
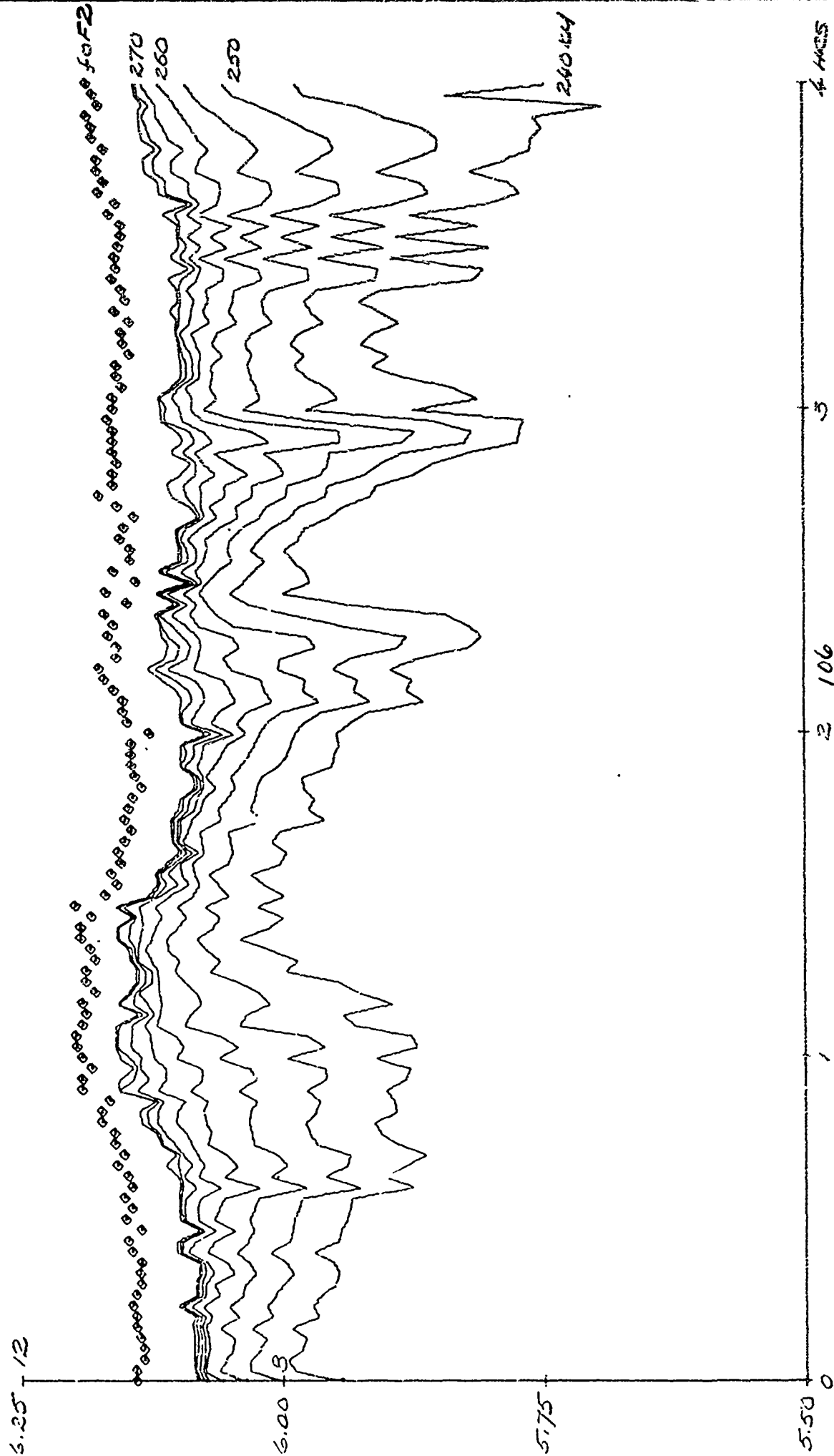
FIGURE 43 CRITICAL FREQUENCIES AND ISO-HEIGHT CONTOURS

HIGHGATE SPRINGS, NOV 15, 1969, 11:00~15:00 EST
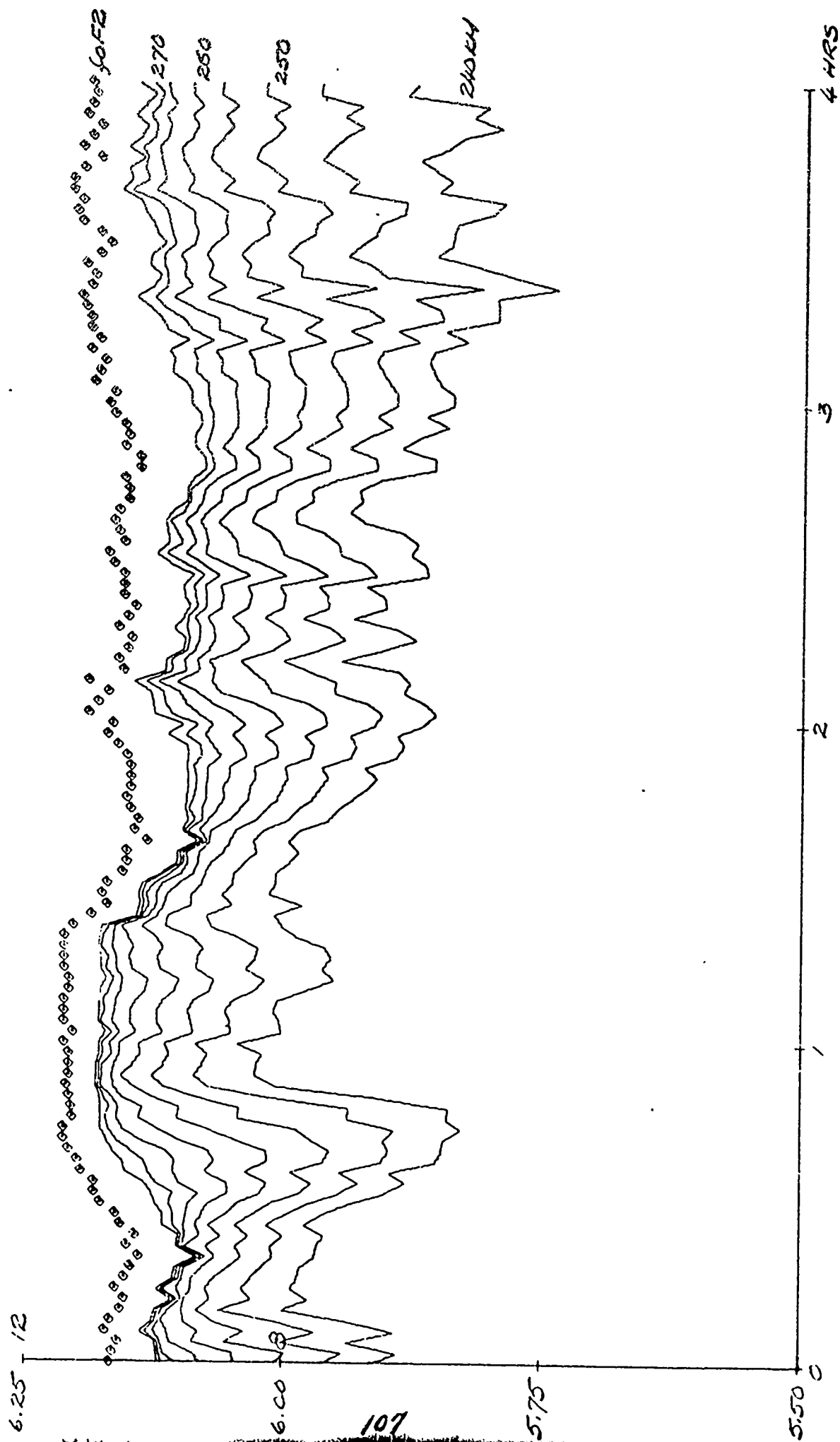
FIGURE 44 CRITICAL FREQUENCIES AND ISO-HEIGHT CONTOURS
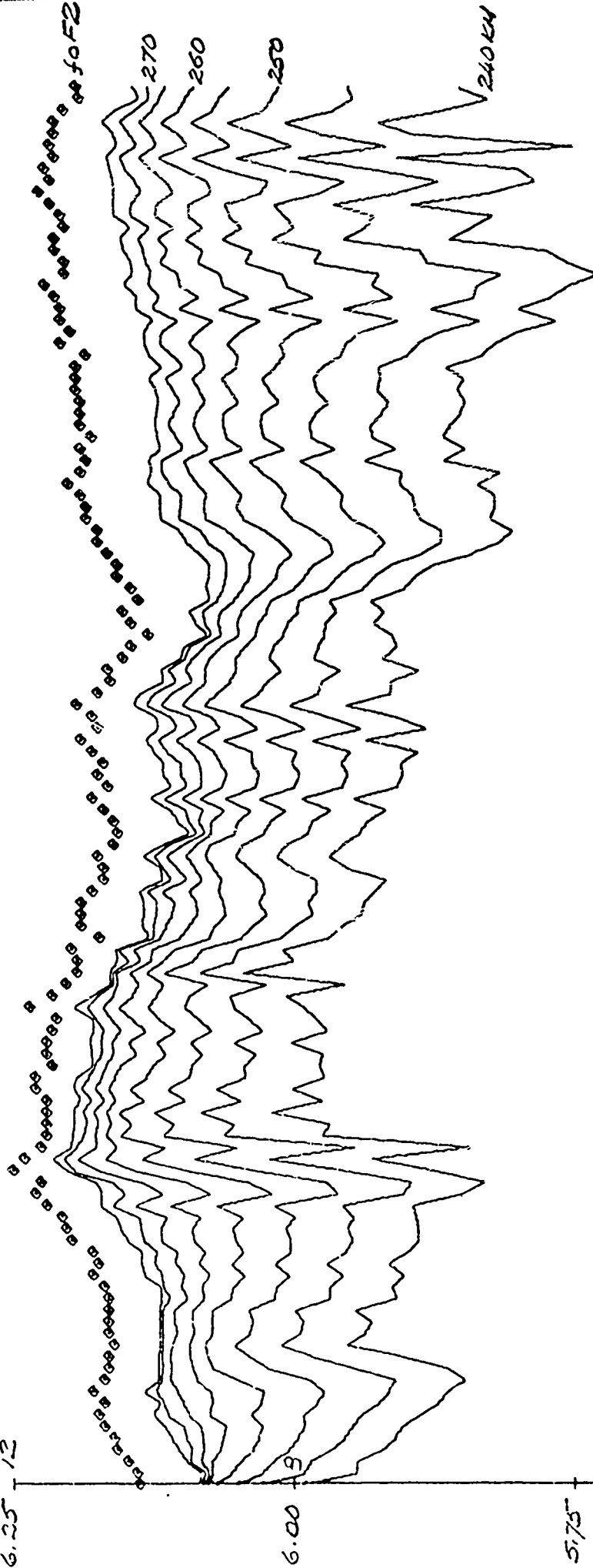
ERROL, Nov 15, 1969, 11:00-15:00 EST

FIGURE 45. NORMALIZED POWER SPECTRA AND IONOSPHERIC PREDICTIVE FUNCTIONS

HANOVER, NOV 15, 1969, 11:00-15:00 EST

THEORETICAL / EXPERIMENTAL PREDICTIVE FUNCTIONS

250 KM

240 KM

109
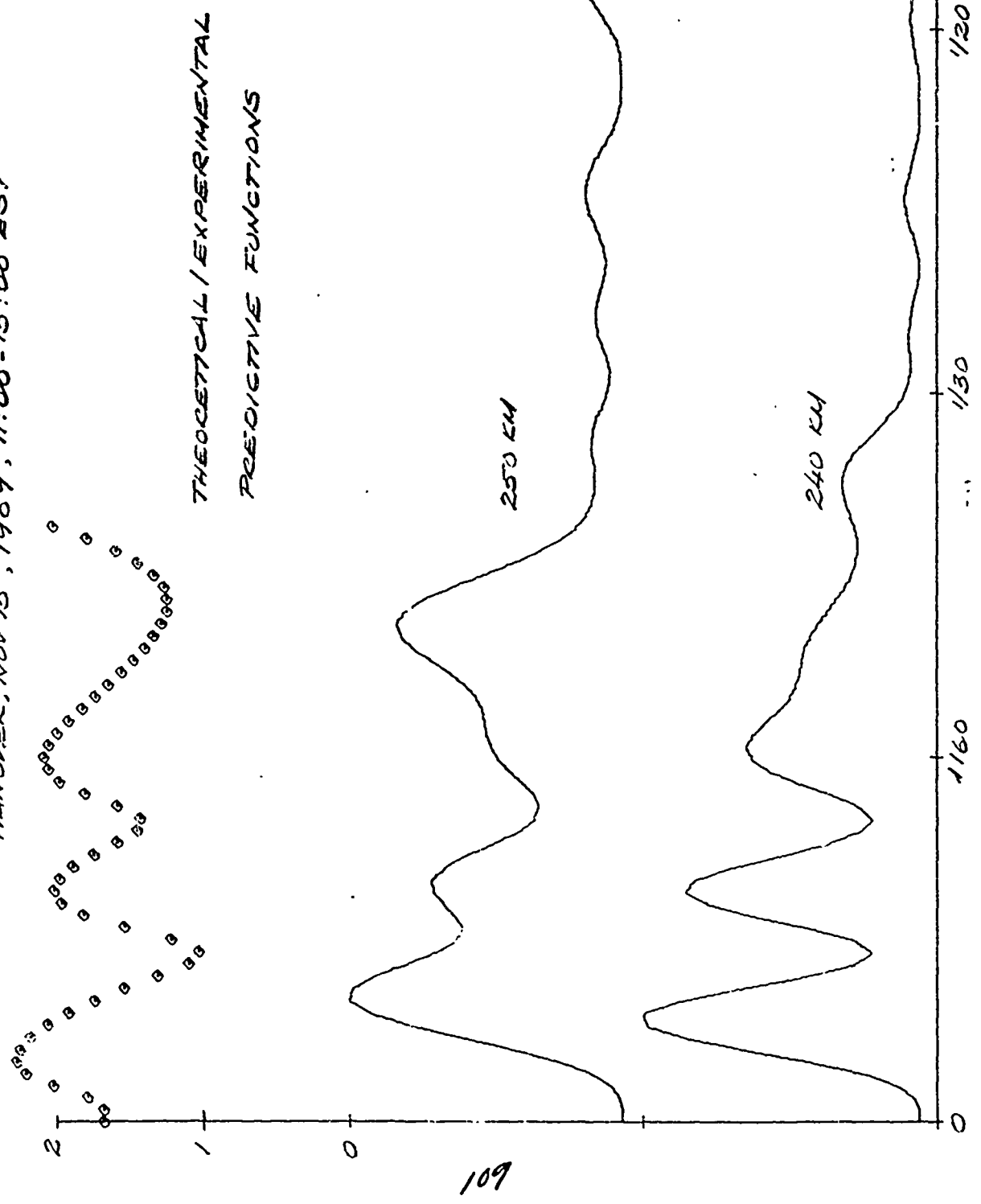
FIGURE 46 CRITICAL FREQUENCIES AND ISO-HEIGHT CONTOURS

HANOVER, NOV 17, 1969, 08:16-12:16 EST
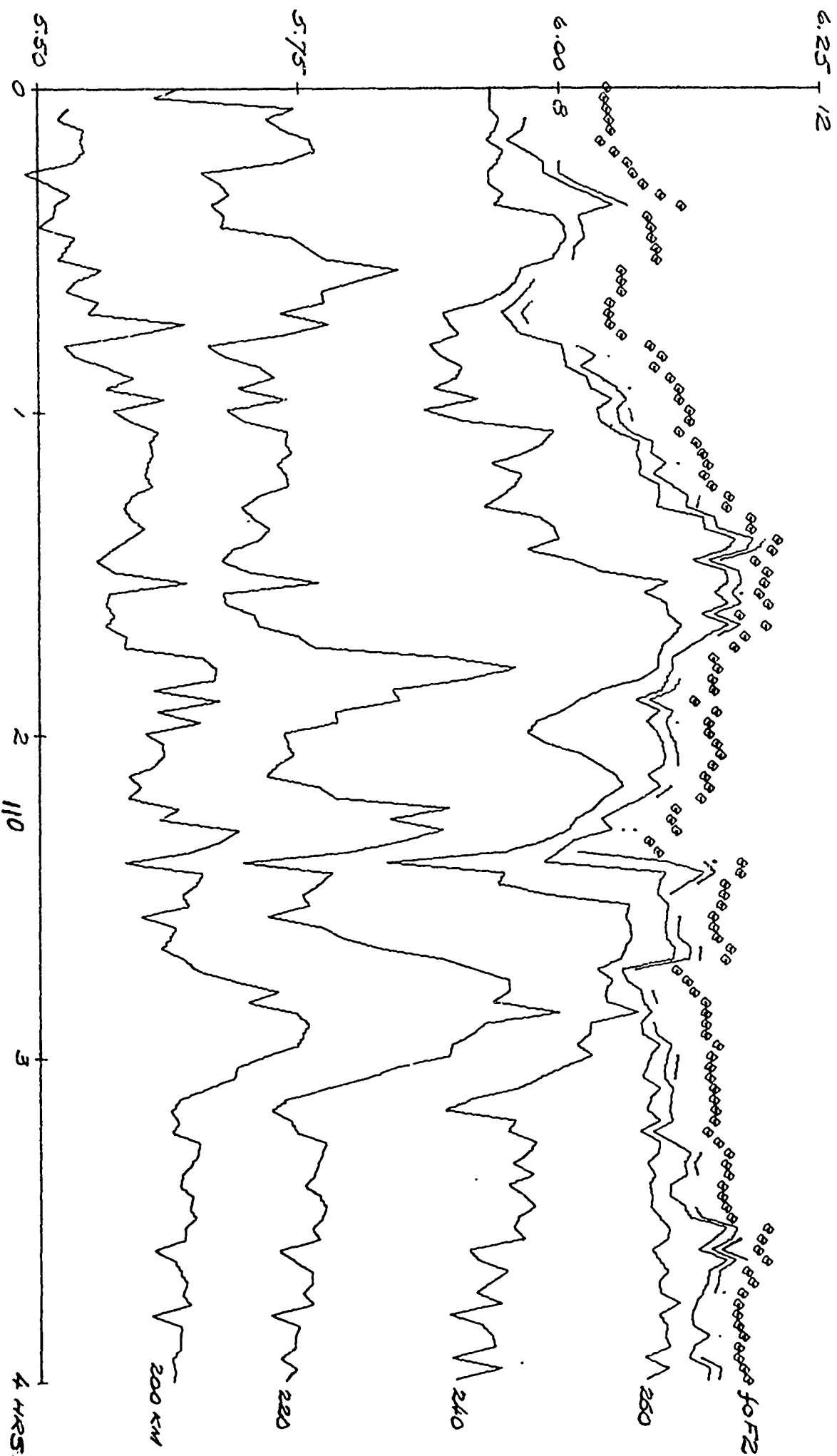
FIGURE 47 CRITICAL FREQUENCIES AND 150-HEIGHT CONTOURS

HIGHGATE SPRINGS, Nov 17, 1969, 08:16 – 12:16 EST
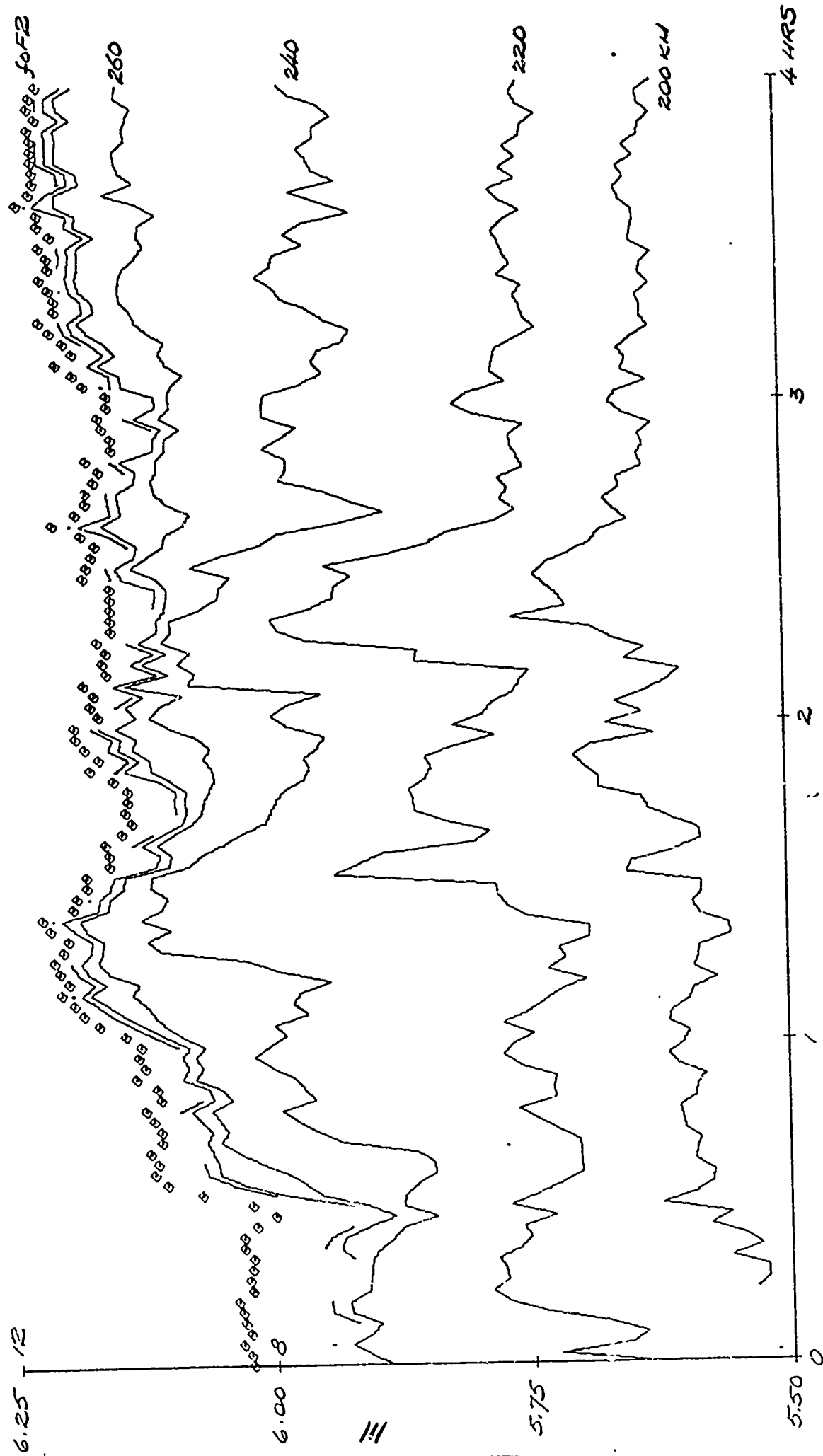
FIGURE 48 CRITICAL FREQUENCIES AND ISO-HEIGHT CONTOURS

ERROL, NOV 17, 1969, 08:16 - 12:16 EST
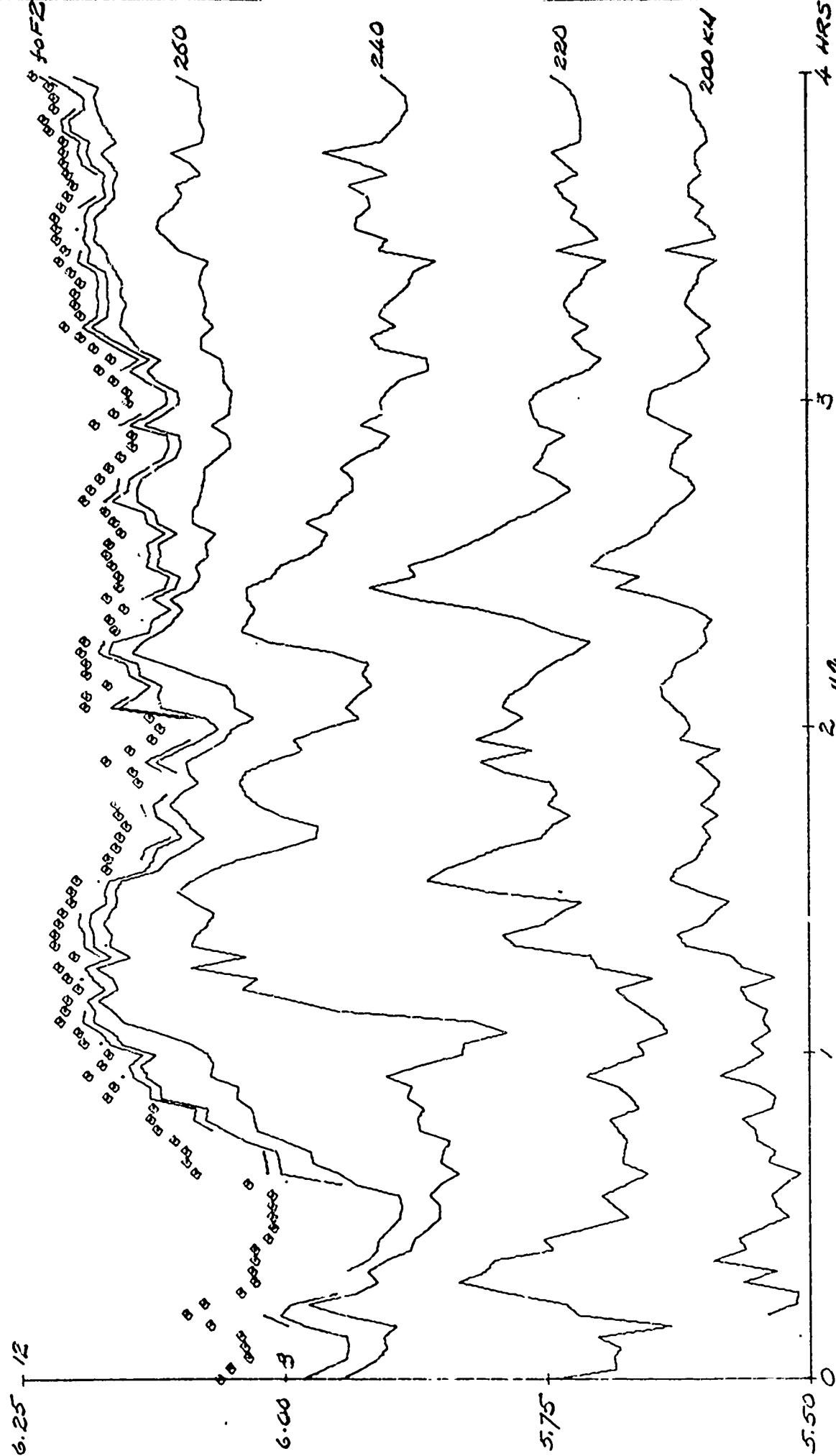
FIGURE 49 CRITICAL FREQUENCIES AND ISO-HEIGHT CONTOURS

HANOVER, NOV 17, 1969, 08:16-12.16 EST

FIGURE 50 CRITICAL FREQUENCIES AND ISO-HEIGHT CONTOURS

HIGHGATE SPRINGS, Nov 17, 1969, 08:16-12:16 EST
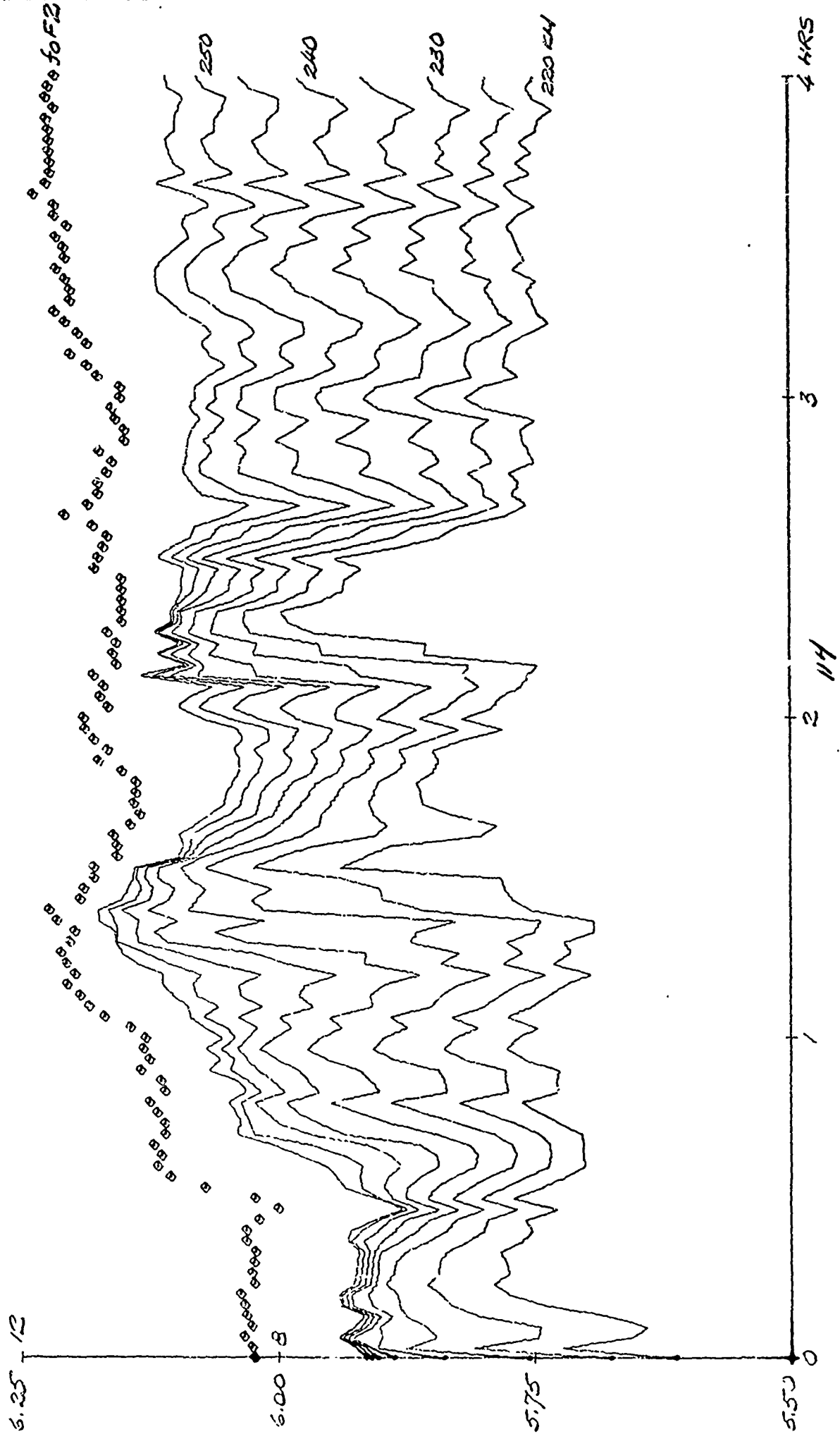
FIGURE 51 CRITICAL FREQUENCIES AND ISO-HEIGHT CONTOURS

ERCOL, NOV 17, 1969, 08:16-12:16 EST
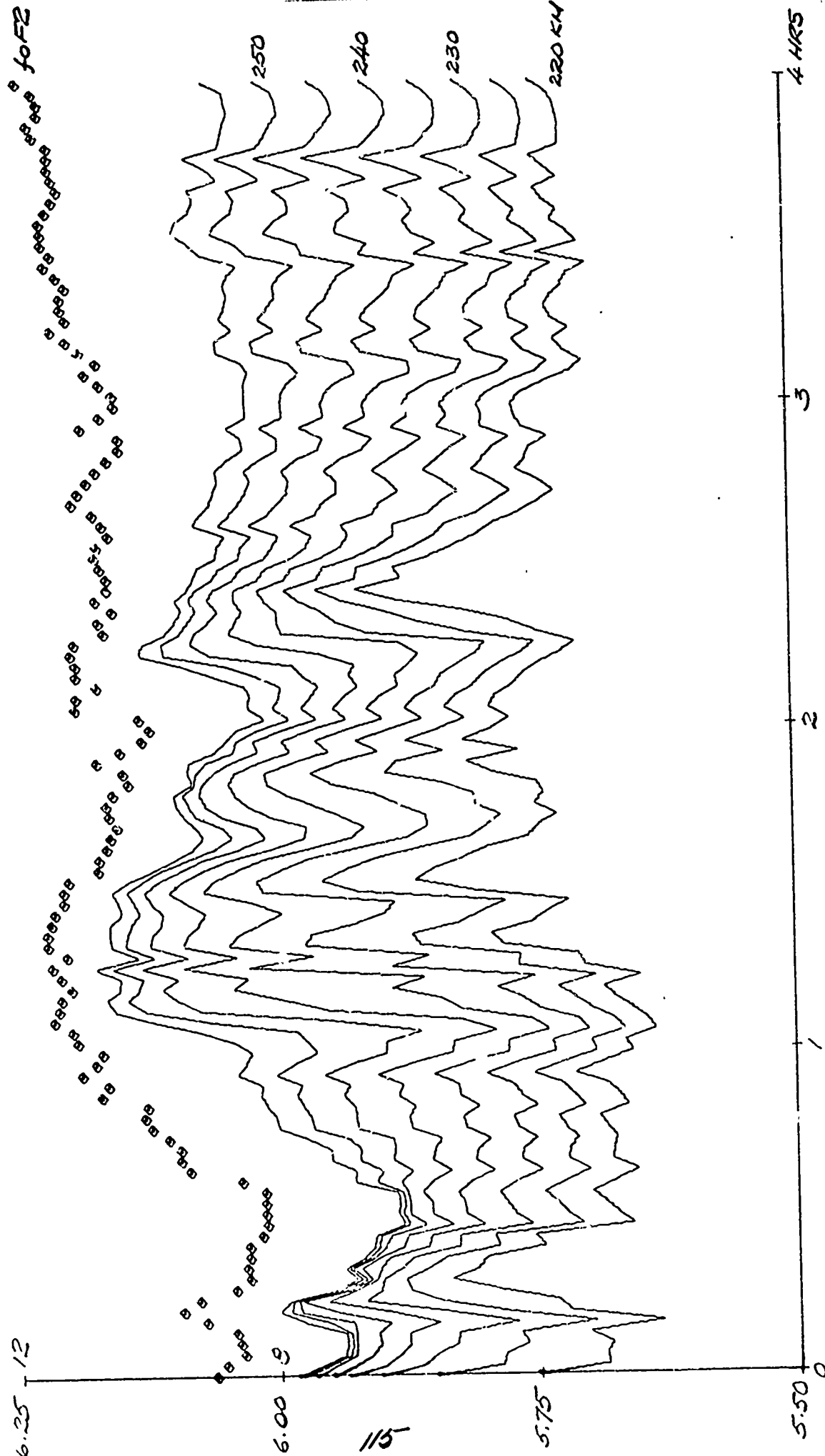
FIGURE 5.2 NORMALIZED POWER SPECTRA AND IONOSPHERIC PREDICTIVE FUNCTIONS

HANOVER, NOV 15, 1959, 08:16 - 12:15 EST

THEORETICAL / EXPERIMENTAL
PREDICTIVE FUNCTIONS

245 KM

235 KM
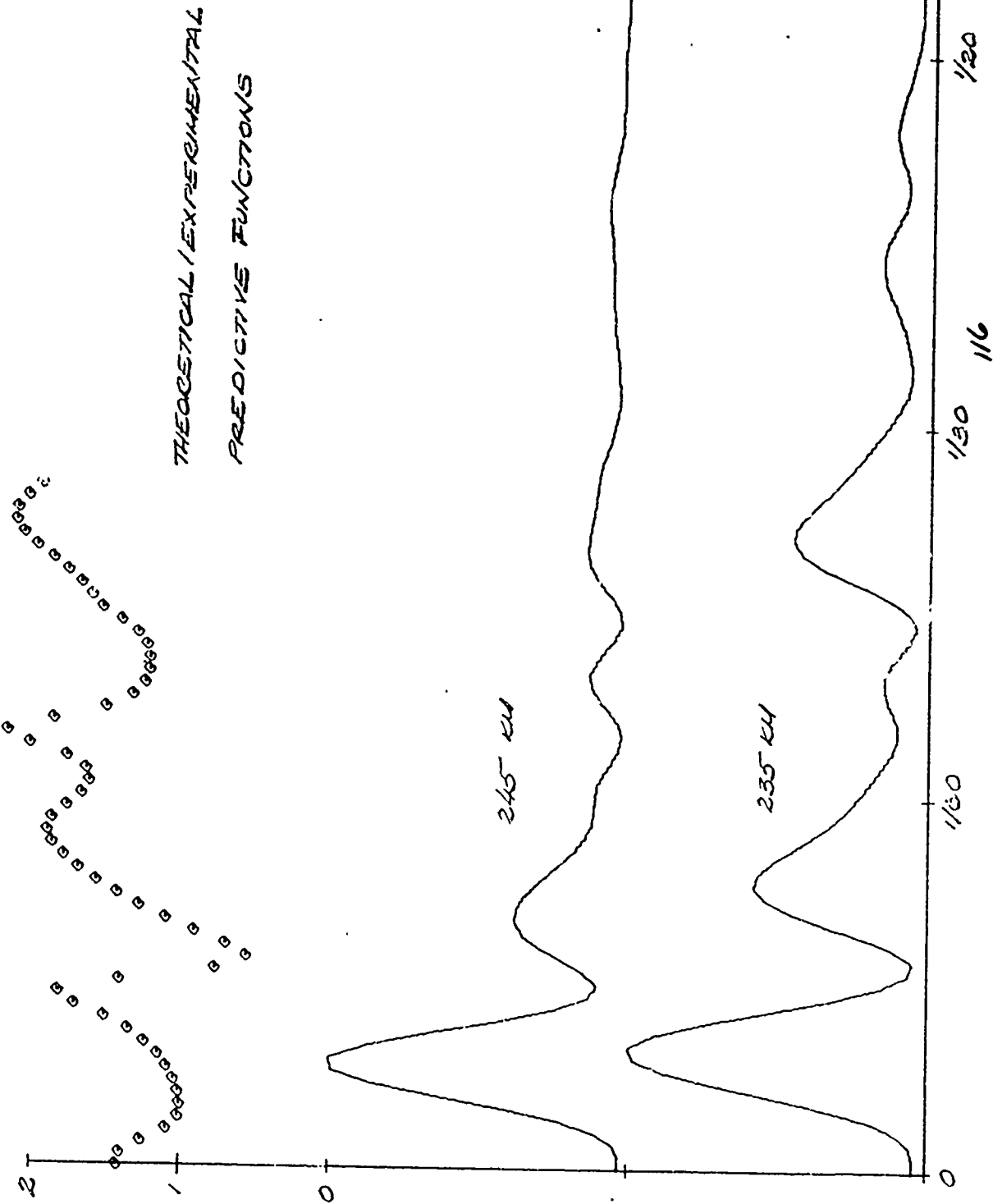
FIGURE 53 CRITICAL FREQUENCIES AND ISO-HEIGHT CONTOURS

HANOVER, DEC 10, 1959, 10:00-14:00 EST
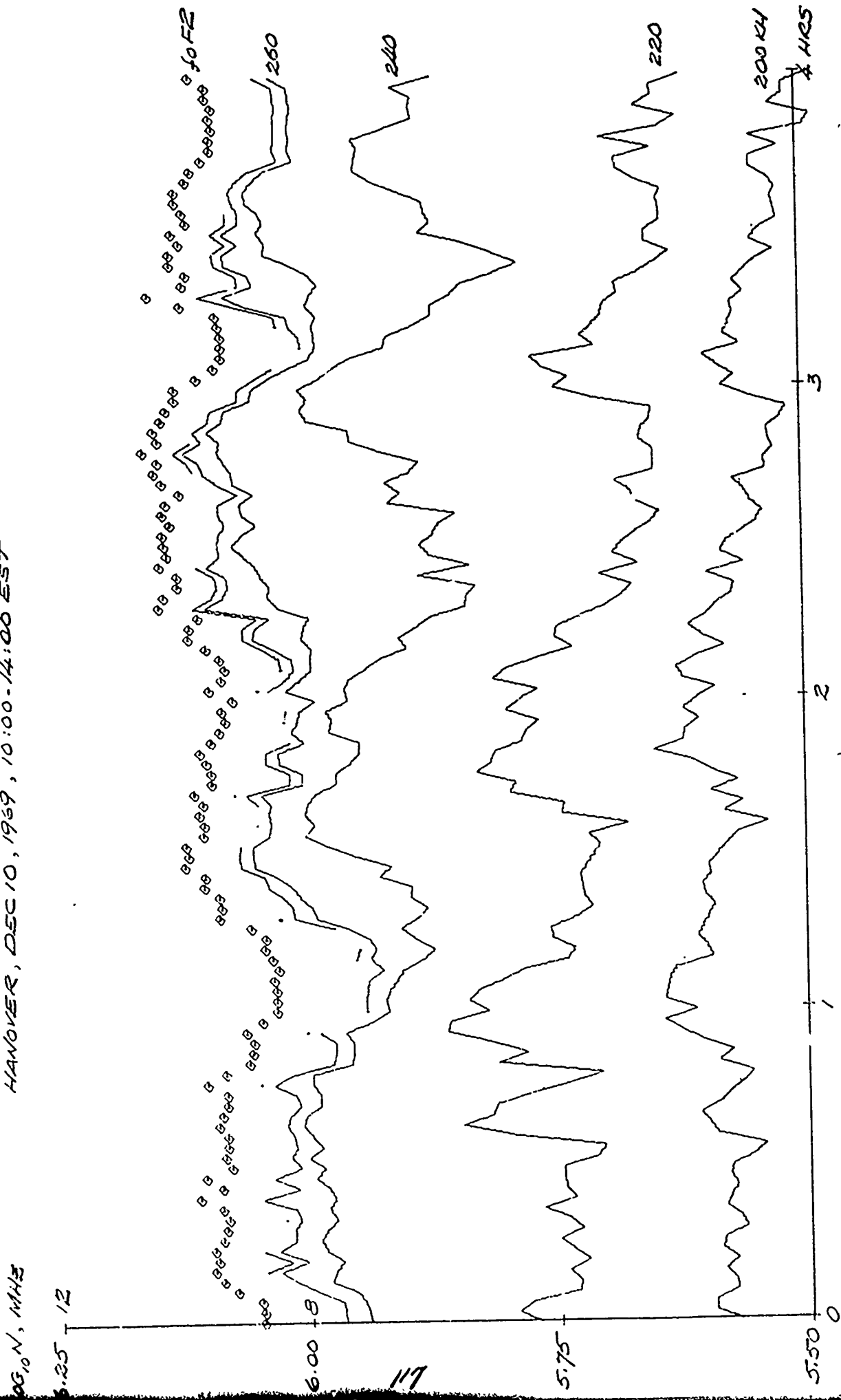
FIGURE 54 CRITICAL FREQUENCIES AND ISO-HEIGHT CONTOURS

HIGHGATE SPRINGS, DEC 10, 1964, 10:00-14:00 EST
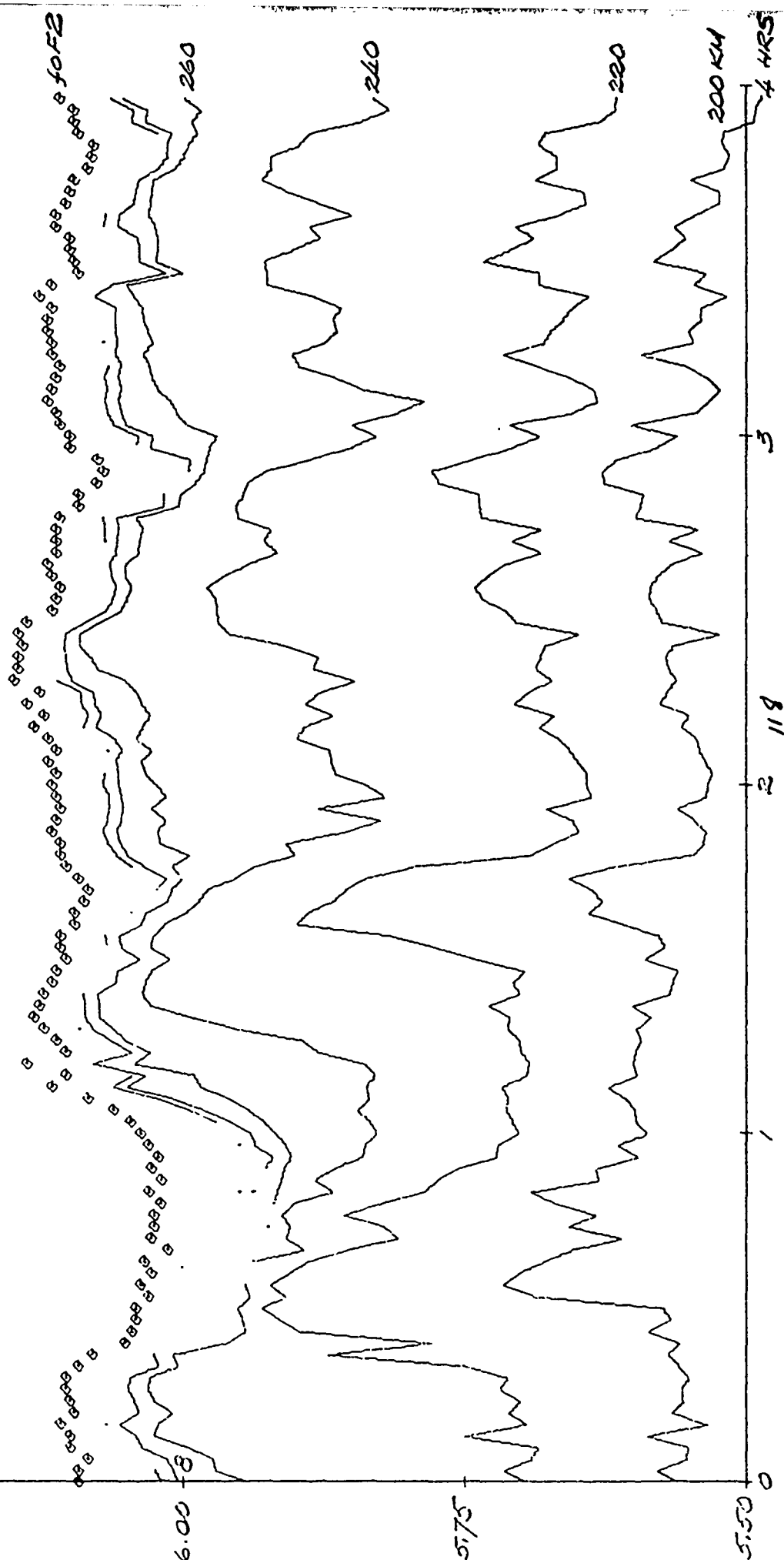
FIGURE 55 CRITICAL FREQUENCIES AND ISO-HEIGHT CONTOURS

ERROL, DEC 10, 1969, 10:00-14:00 EST
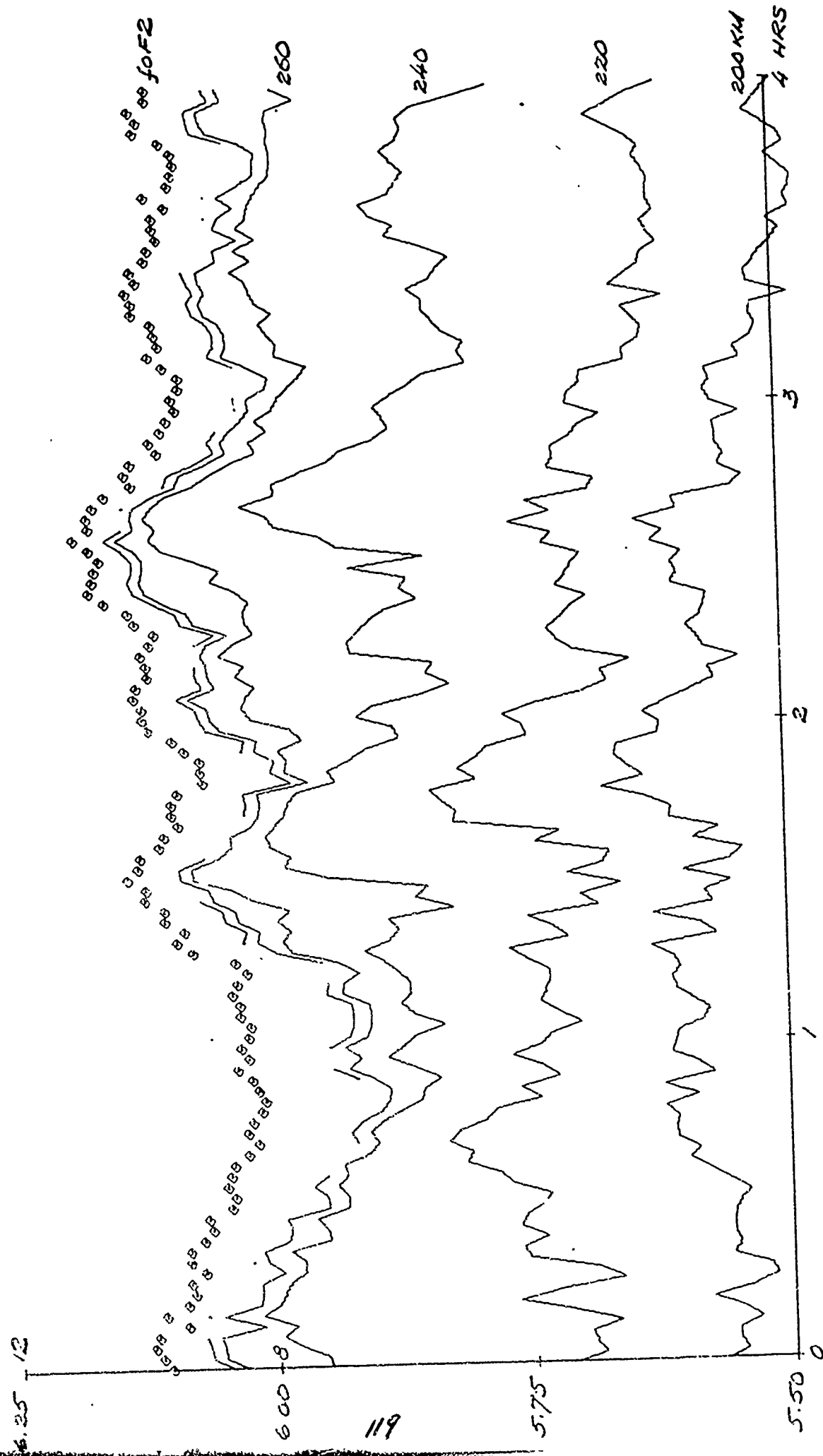
FIGURE 5b CRITICAL FREQUENCIES AND ISO-HEIGHT CONTOURS

HANOVER, DEC 10, 1969, 10:00-14:00 EST
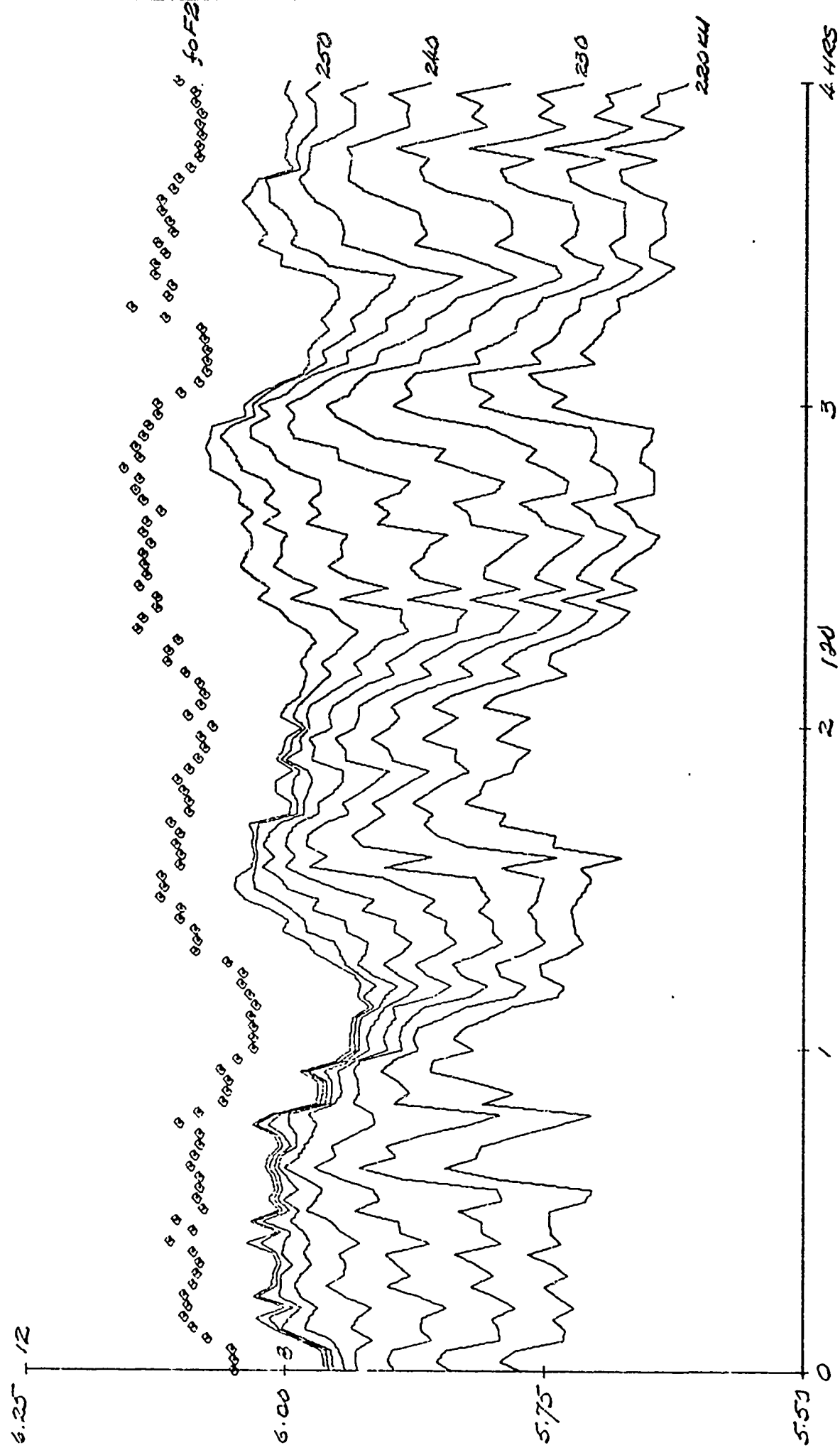
Log₁₀N, MHz

FIGURE 57 CRITICAL FREQUENCIES AND 150-HEIGHT CONTOURS

HIGHGATE SPRINGS, DEC 10, 1969, 10:00-14:00 EST
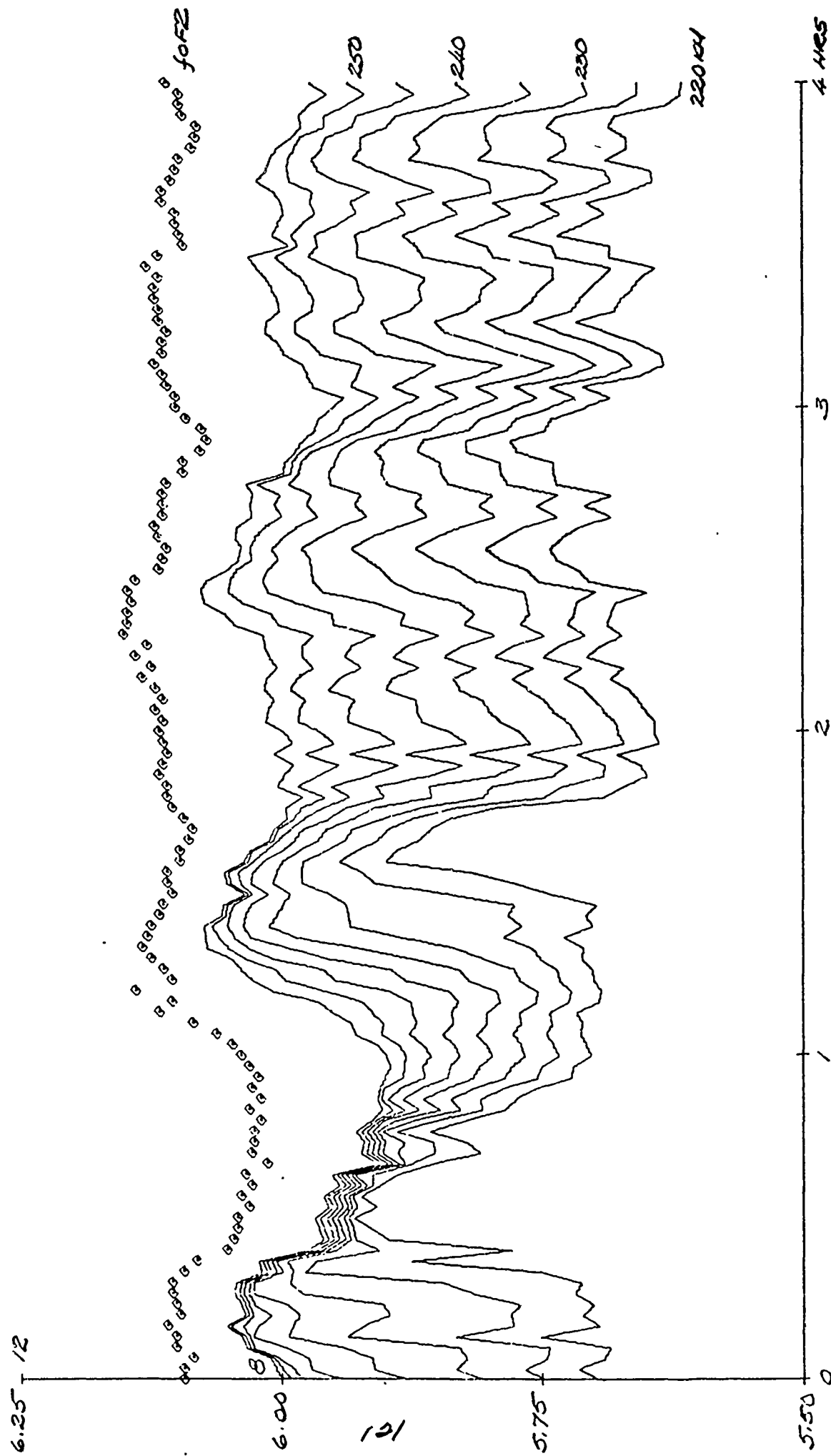
FIGURE 58 CRITICAL FREQUENCIES AND ISO-HEIGHT CONTOURS
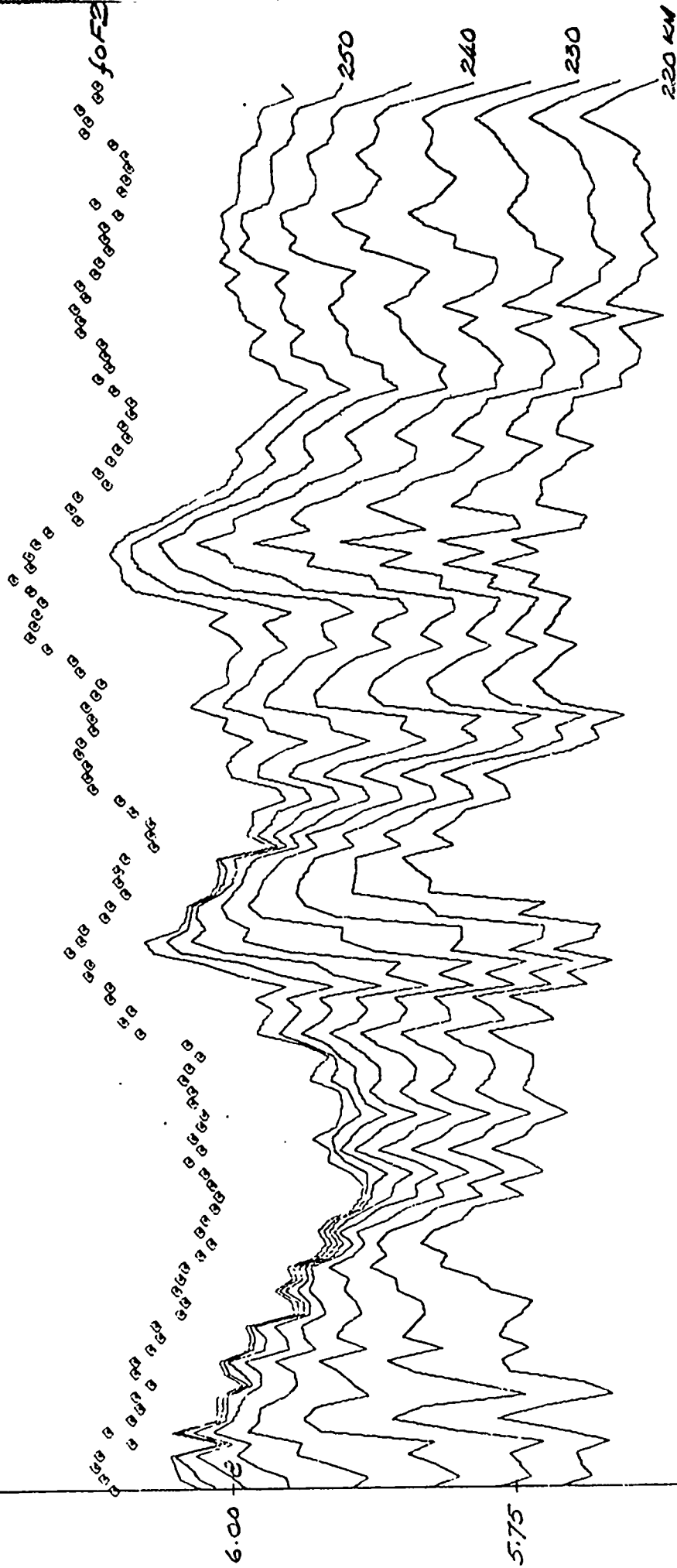
ERROL, DEC 10, 1969, 10:00-14:00 EST

FIGURE 59 NORMALIZED POWER SPECTRA AND IONOSPHERIC PREDICTIVE FUNCTIONS

HANOVER, DEC 10, 1969, 10:00-14:00 EST

THEORETICAL/EXPERIMENTAL PREDICTIVE FUNCTIONS

240 KM

230 KM

1/5 MIN⁻¹

1/20

1/30

1/60

0

123
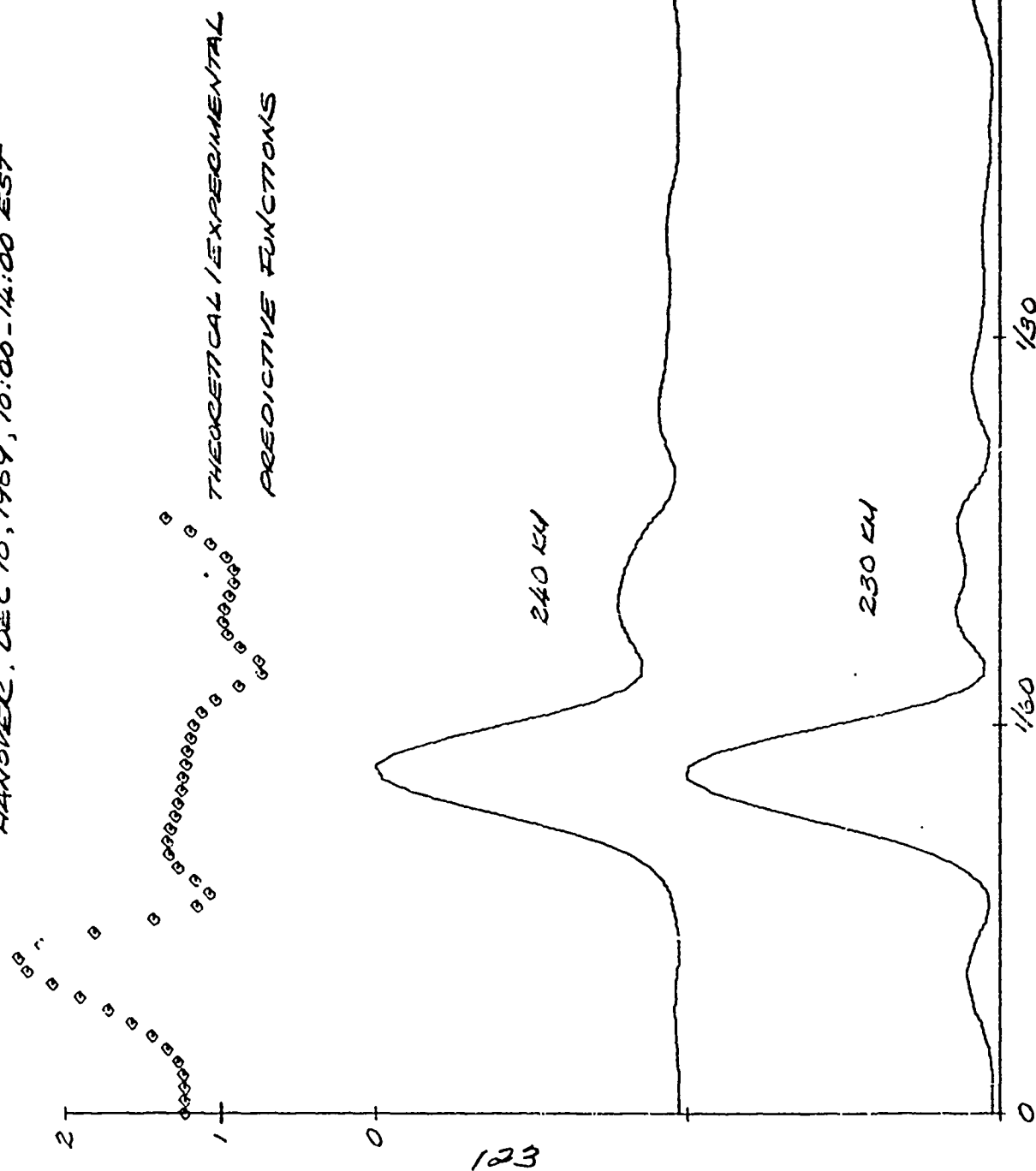
FIGURE 60   CRITICAL FREQUENCIES AND ISOIONIC CONTOURS

HANOVER

JAN 13, 1969, 10:00–14:00 EST
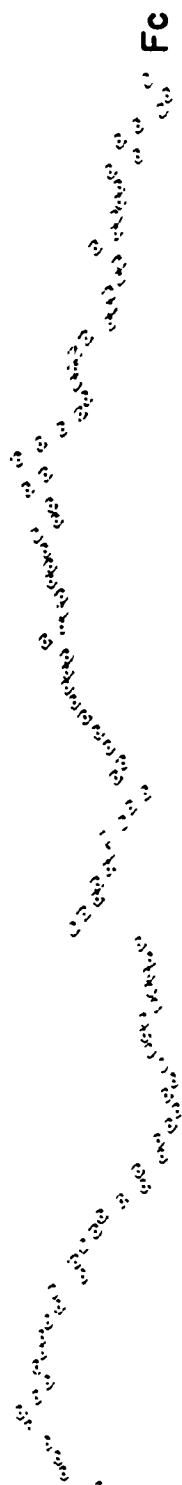
FIGURE 61   CRITICAL FREQUENCIES AND ISOIONIC CONTOURS

HIGHGATE SPRINGS
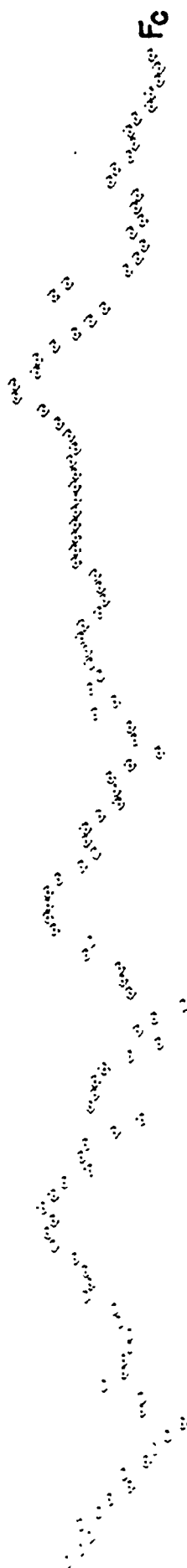
JAN 13, 1969, 10:00-14:00 EST

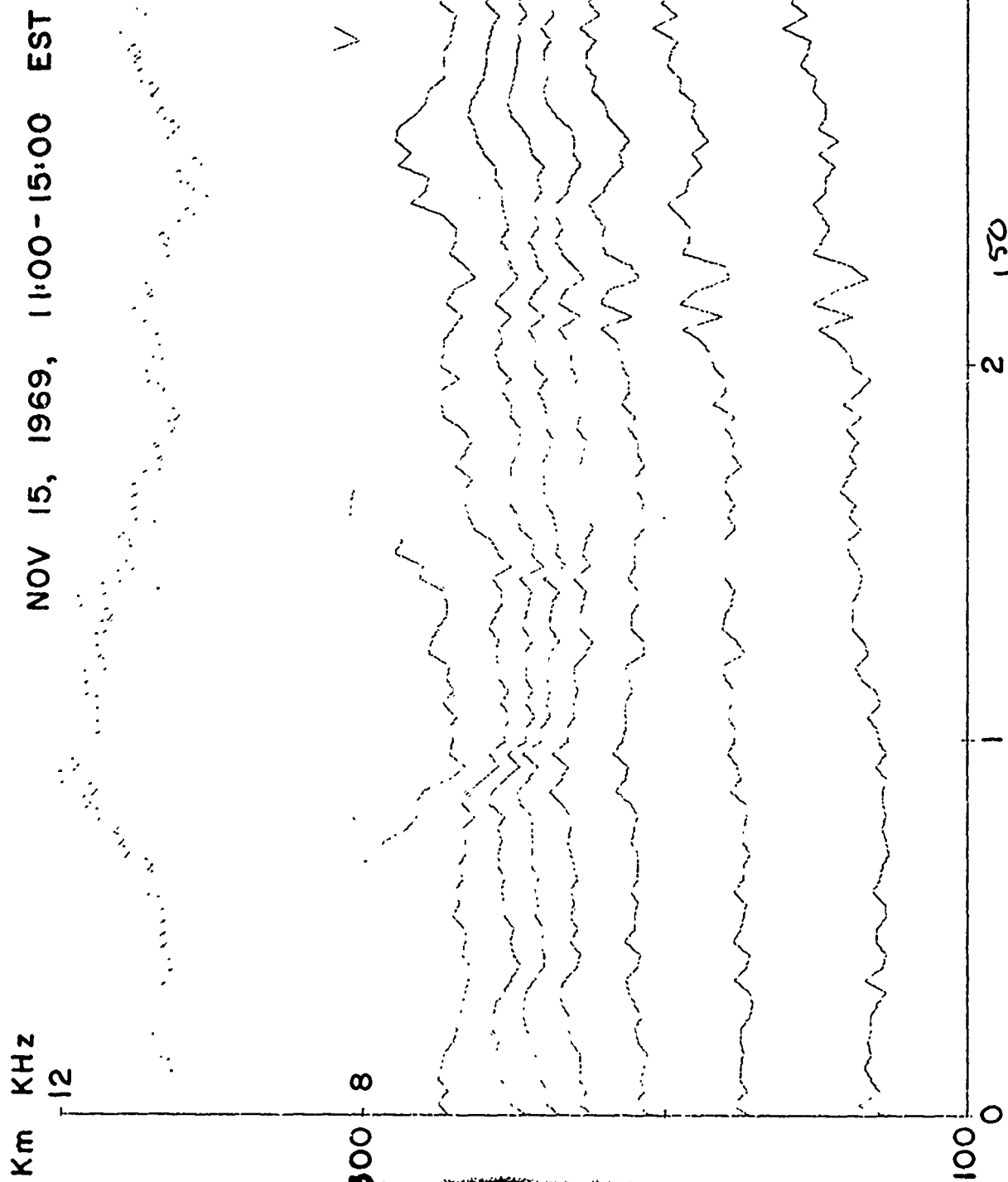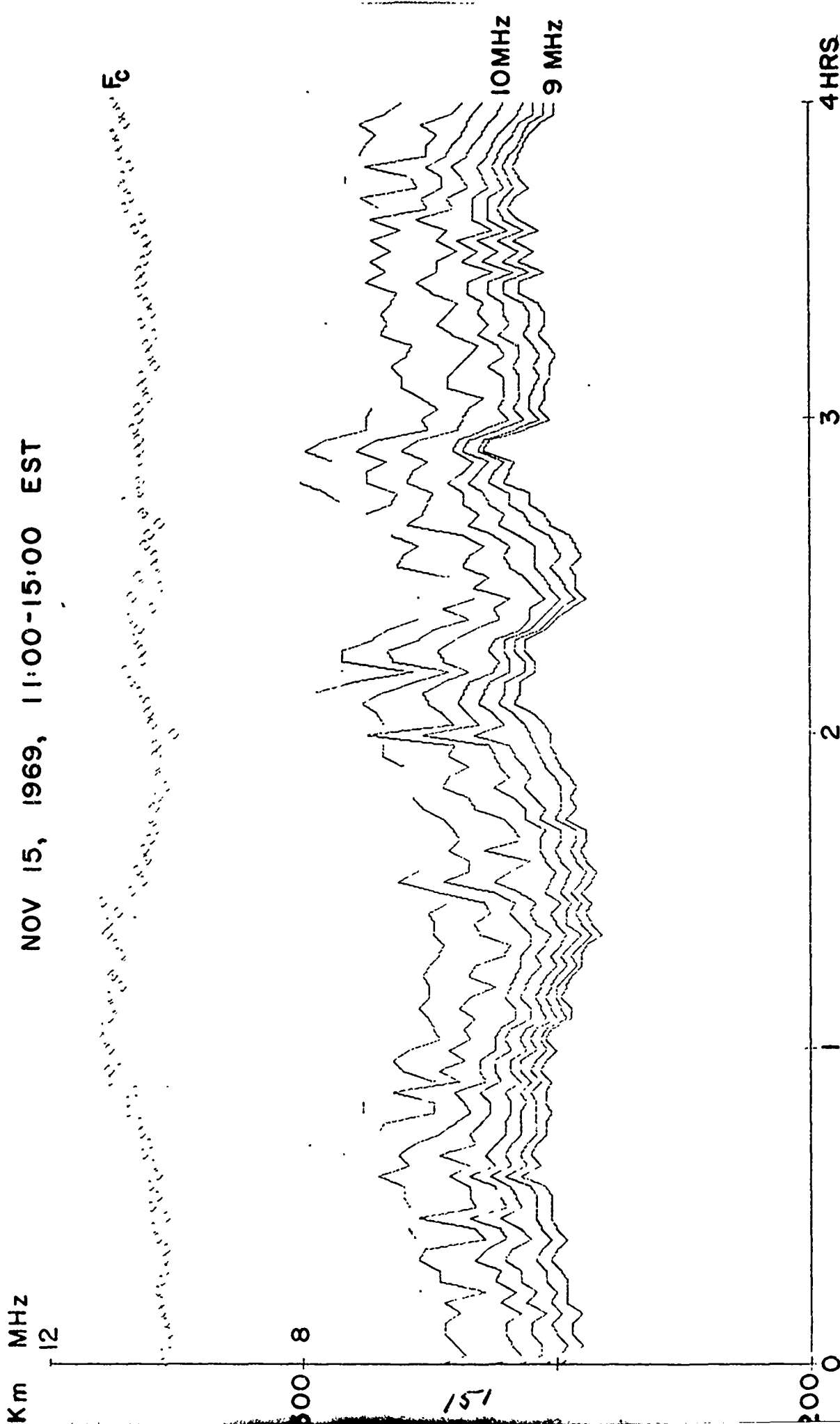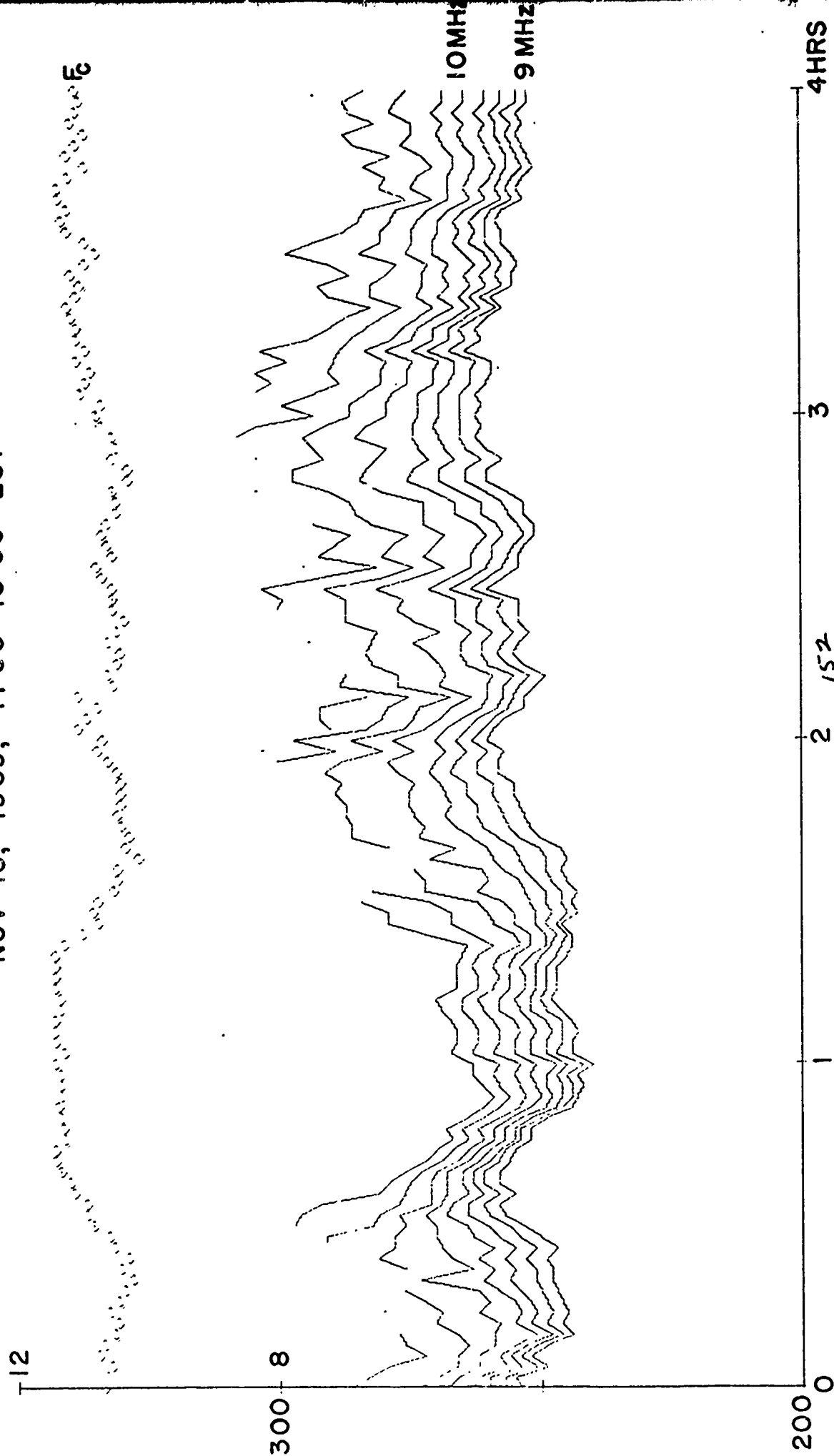FIGURE 62   CRITICAL FREQUENCIES AND ISOIONIC CONTOURS

ERROL

JAN 13, 1969, 10:00–14:00 EST
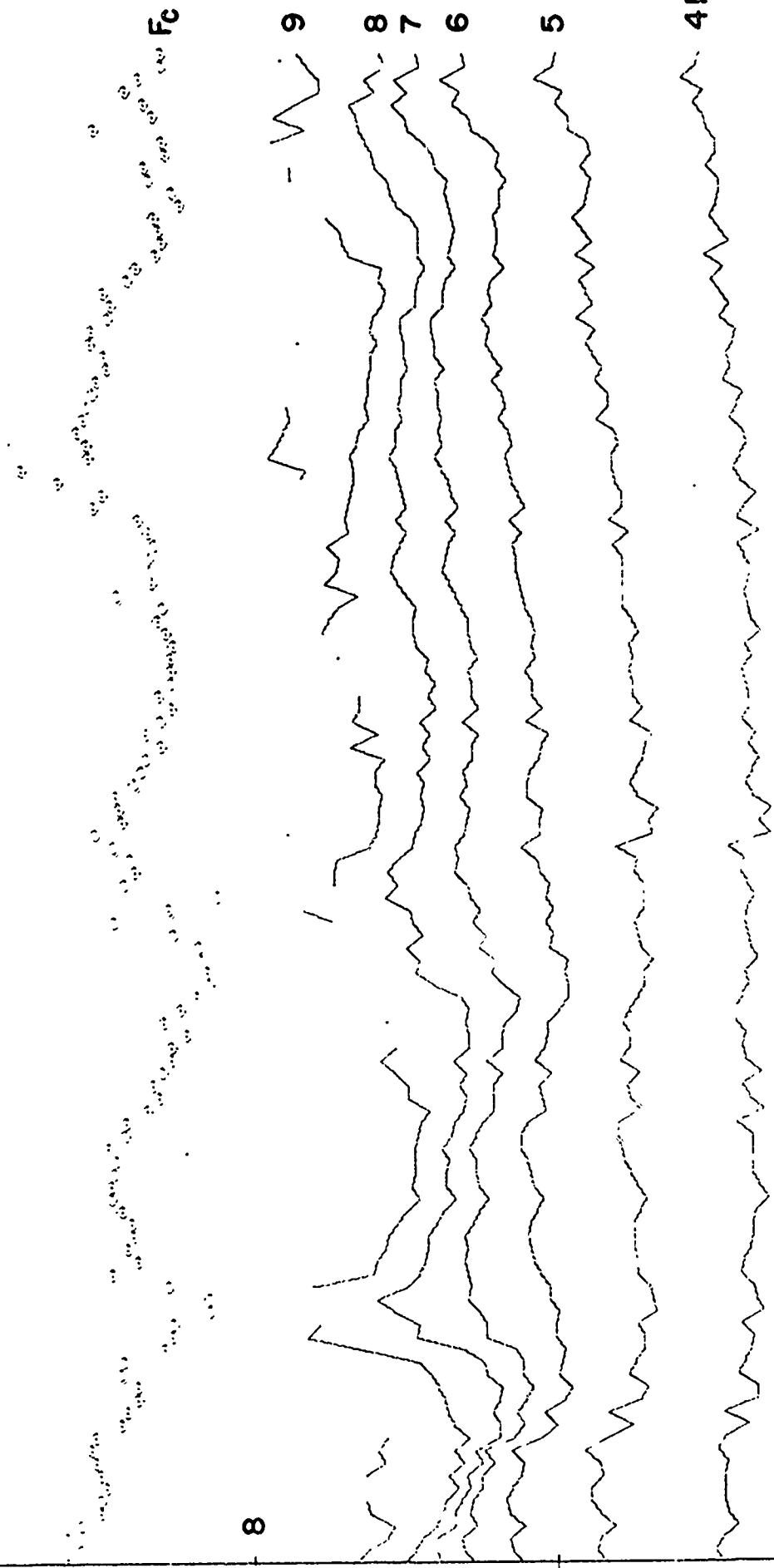
FIGURE 63   CRITICAL FREQUENCIES AND ISOIONIC CONTOURS
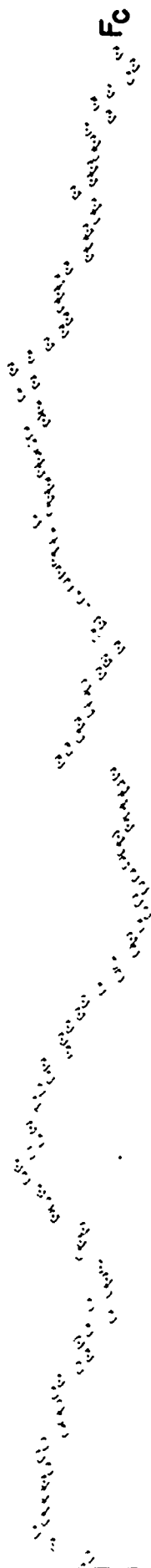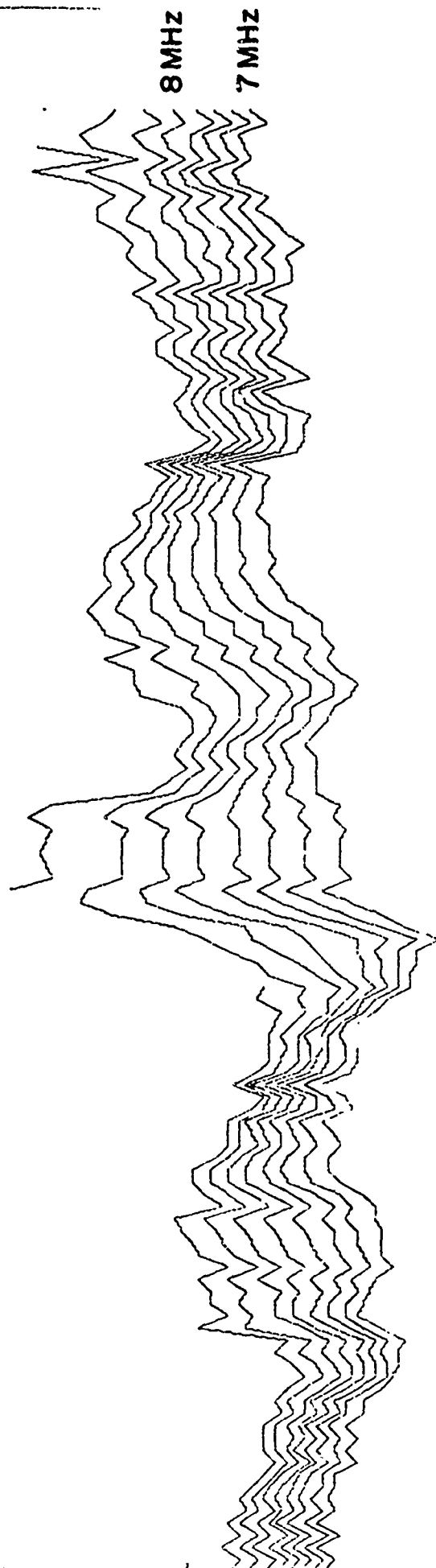
HANOVER

JAN 13, 1969, 10:00-14:00 EST

FIGURE 64   CRITICAL FREQUENCIES AND ISOIONIC CONTOURS

HIGHGATE SPRINGS

JAN 13, 1969, 10:00-14:00 EST
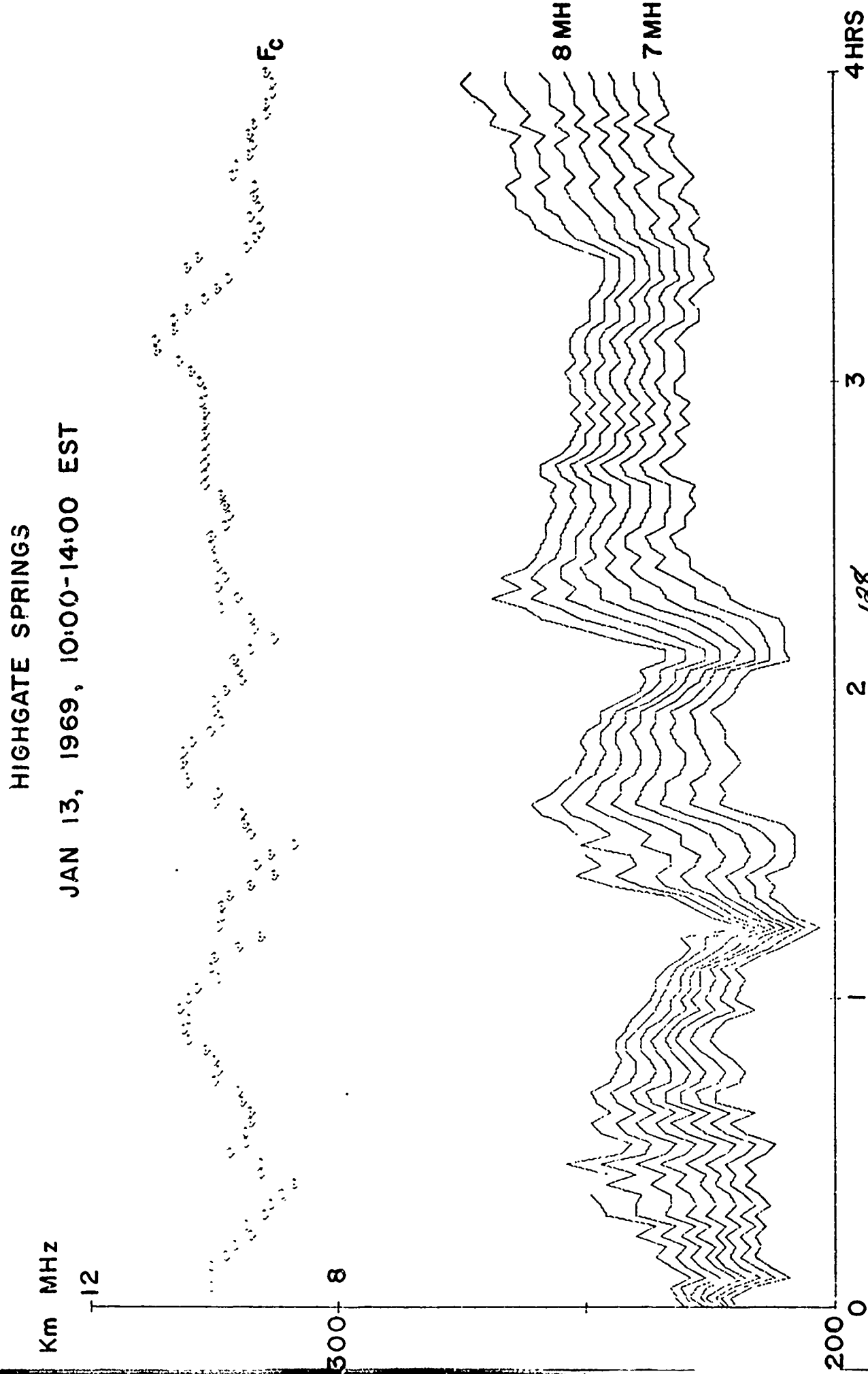
FIGURE 65   CRITICAL FREQUENCIES AND ISOIONIC CONTOURS
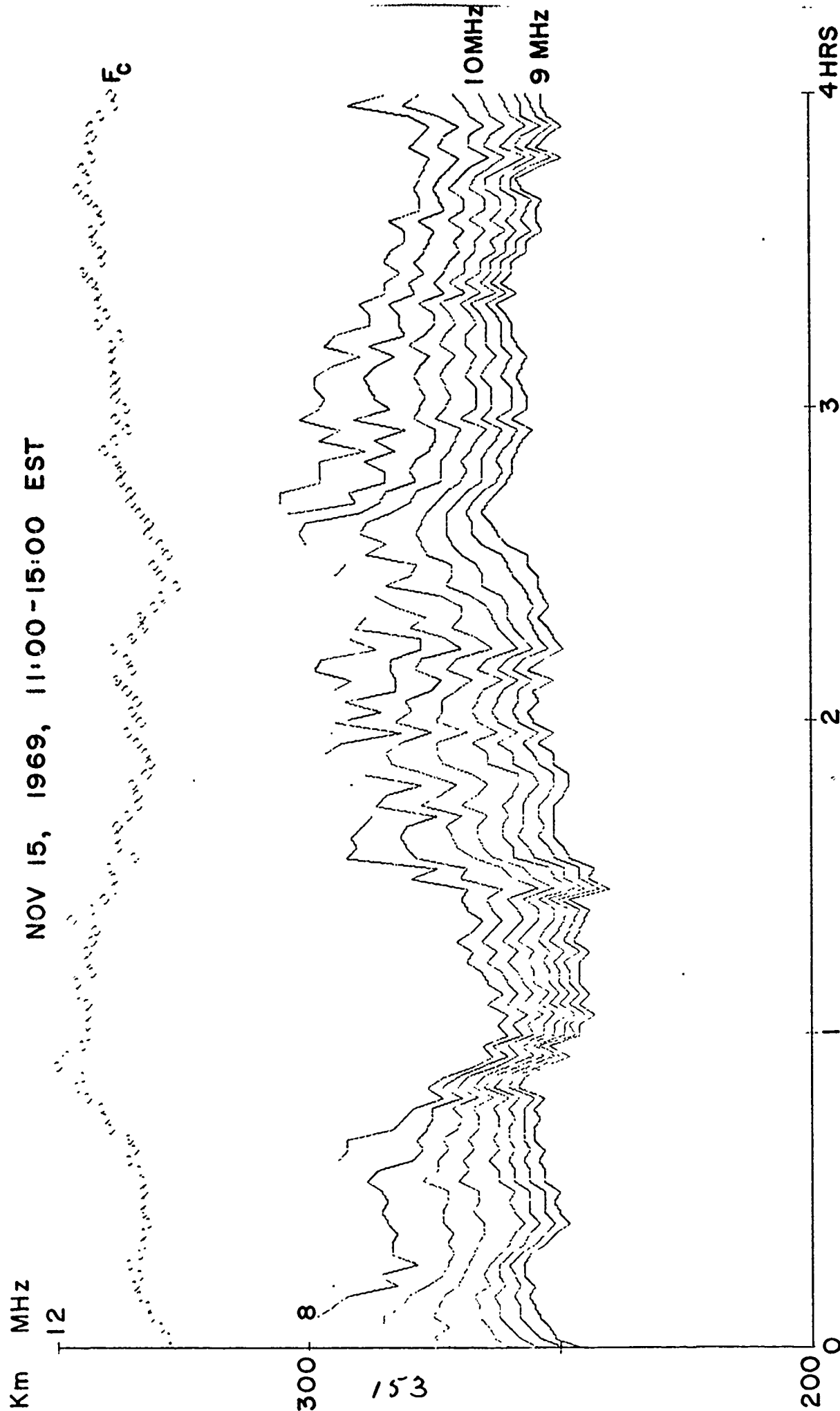
ERROL

JAN 13, 1969, 10:00–14:00 EST

FIGURE 66   CRITICAL FREQUENCIES AND ISOIONIC CONTOURS

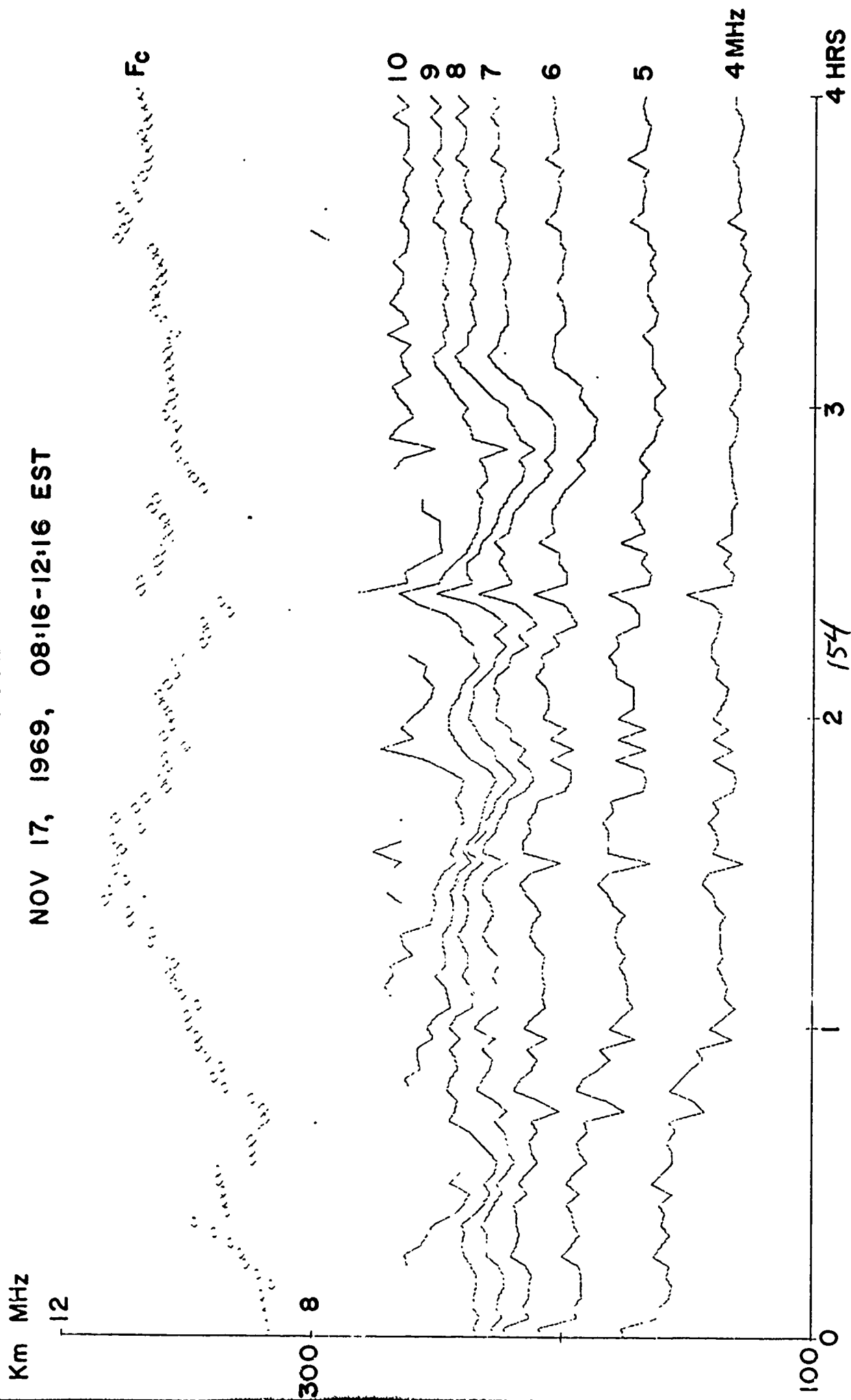HANOVER

MAR 02, 1969, 10:00 – 14:00 EST

FIGURE 67   CRITICAL FREQUENCIES AND ISOIONIC CONTOURS

HIGHGATE SPRINGS

MAR 02, 1969, 10:00-14:00 EST

FIGURE 68   CRITICAL FREQUENCIES AND ISOIONIC CONTOURS

ERROL

MAR 02, 1969, 10:00-14:00 EST

FIGURE 69   CRITICAL FREQUENCIES AND ISOIONIC CONTOURS

HANOVER

MAR 02, 1969, 10:00-14:00 EST

FIGURE 70   CRITICAL FREQUENCIES AND ISOIONIC CONTOURS

HIGHGATE SPRINGS
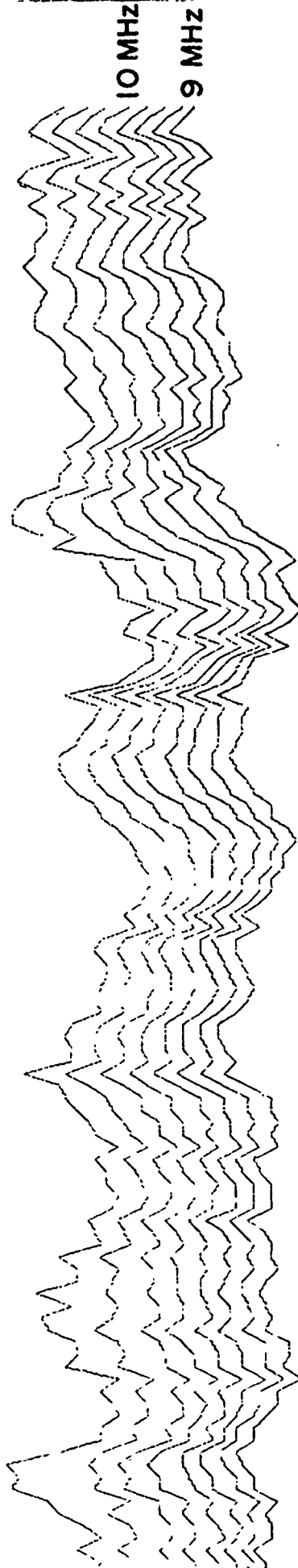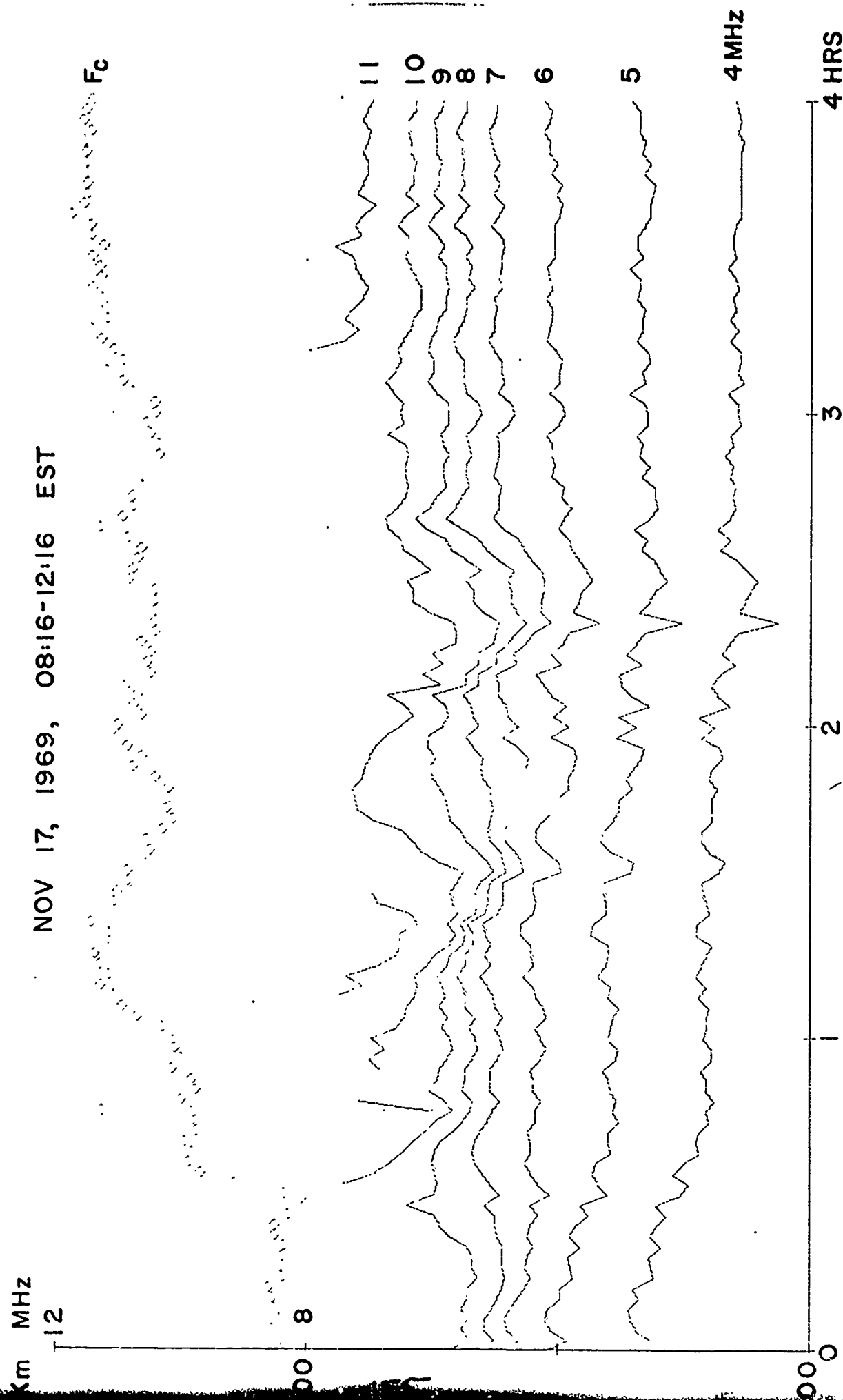
MAR 02, 1969, 10:00-14:00 EST

FIGURE 71   CRITICAL FREQUENCIES AND ISOIONIC CONTOURS
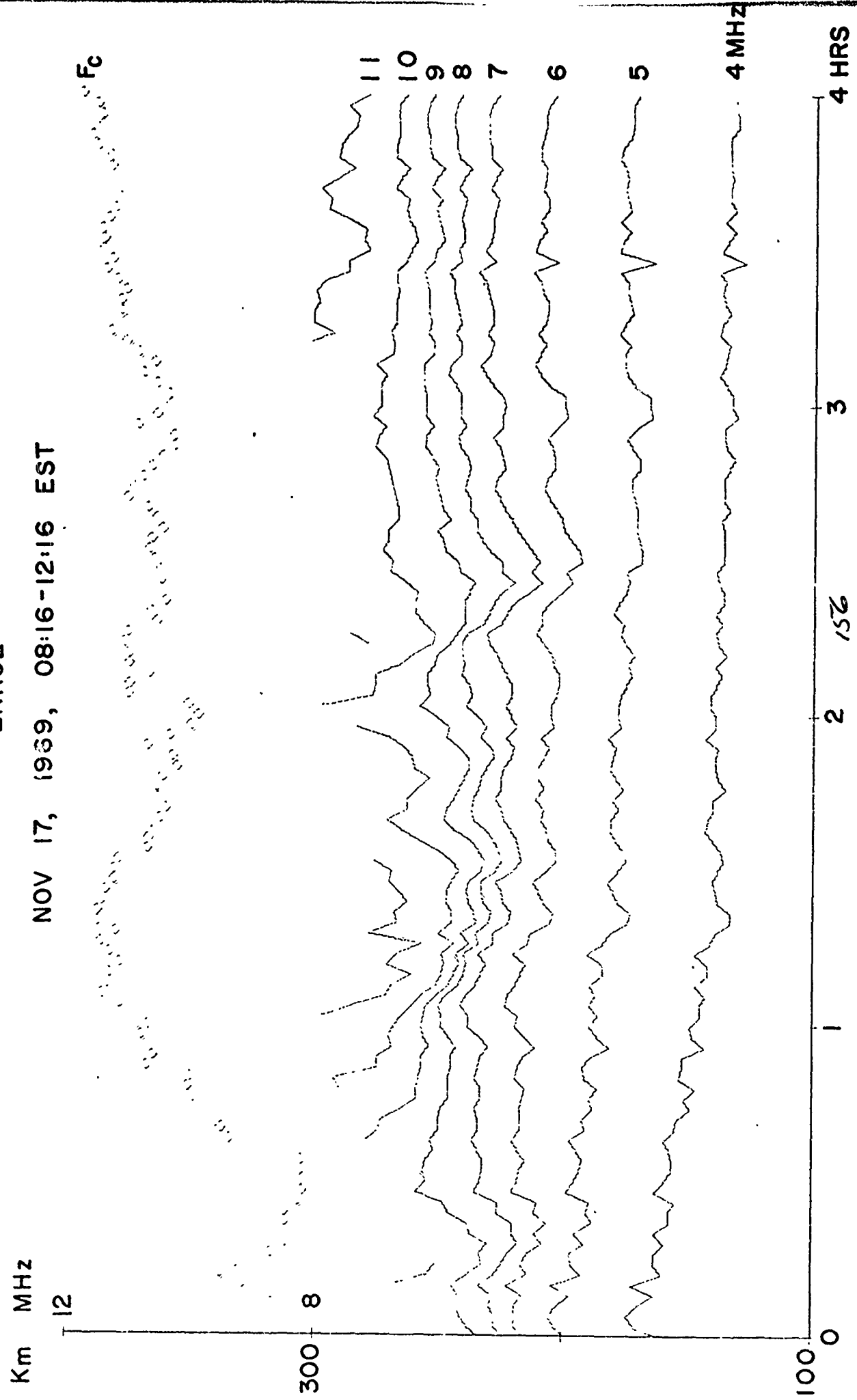
ERROL

MAR 02, 1969, 10:00-14:00 EST

FIGURE 72   CRITICAL FREQUENCIES AND ISOIONIC CONTOURS

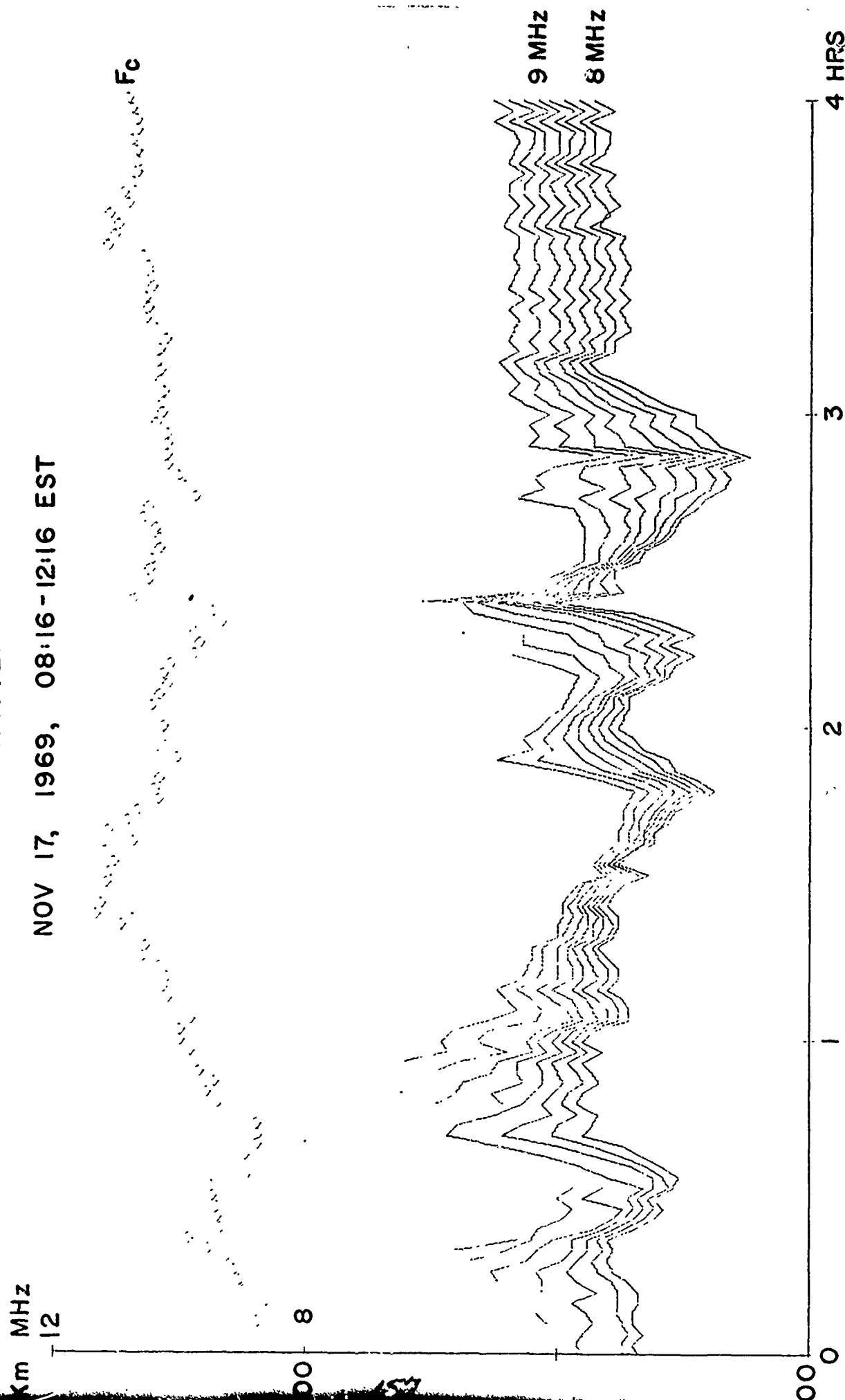HANOVER

APR 29, 1969, 13:30-17:30 EST

FIGURE 73   CRITICAL FREQUENCIES AND ISOIONIC CONTOURS

HIGHGATE SPRINGS

APR 29, 1969, 13:30-17:30 EST

137
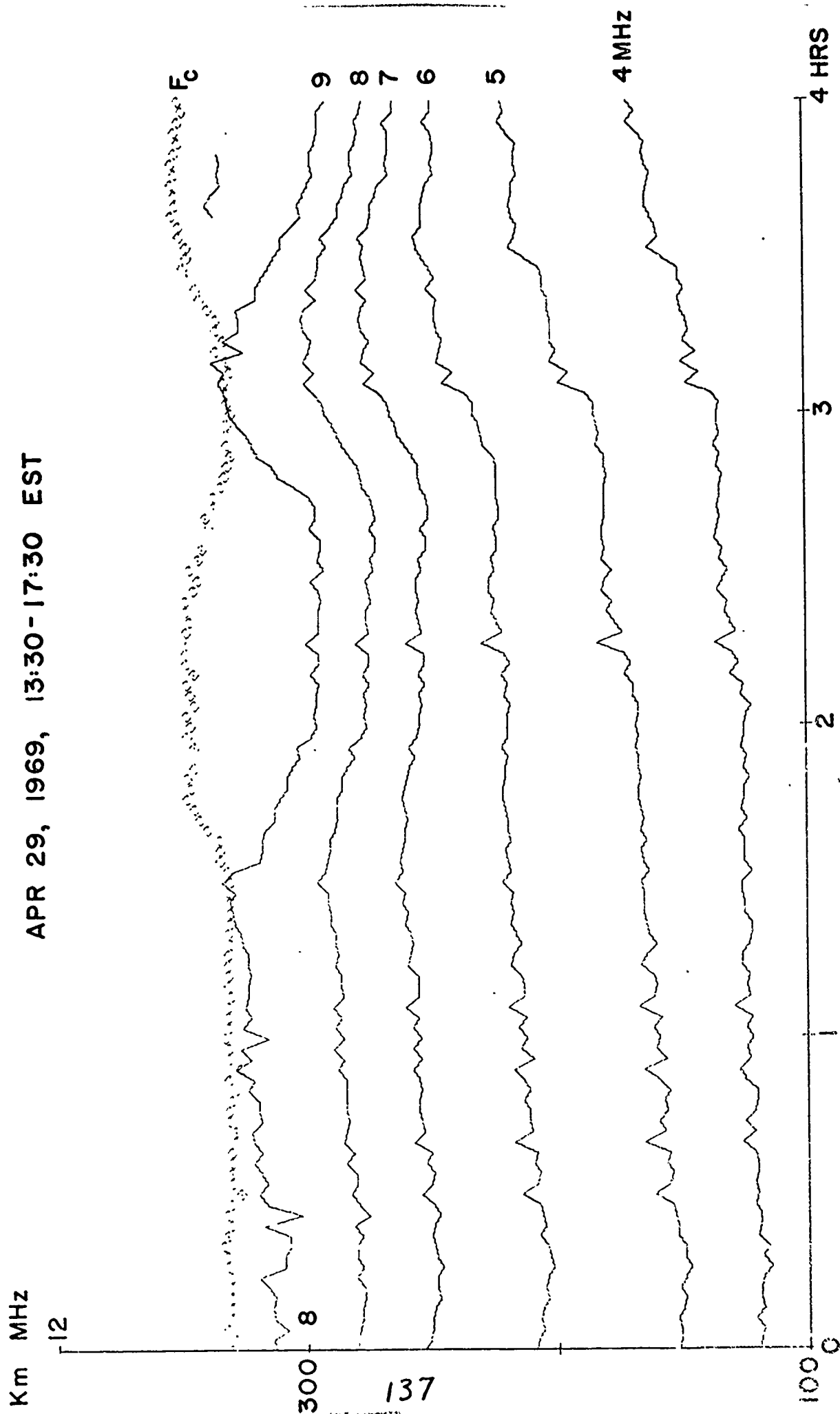
FIGURE 74

CRITICAL FREQUENCIES AND ISOIONIC CONTOURS

ERROL

APR 29, 1969, 13:30 - 17:30 EST

FIGURE 75   CRITICAL FREQUENCIES AND ISOIONIC CONTOURS

HANOVER

APR 29, 1969, 13:30-17:30 EST
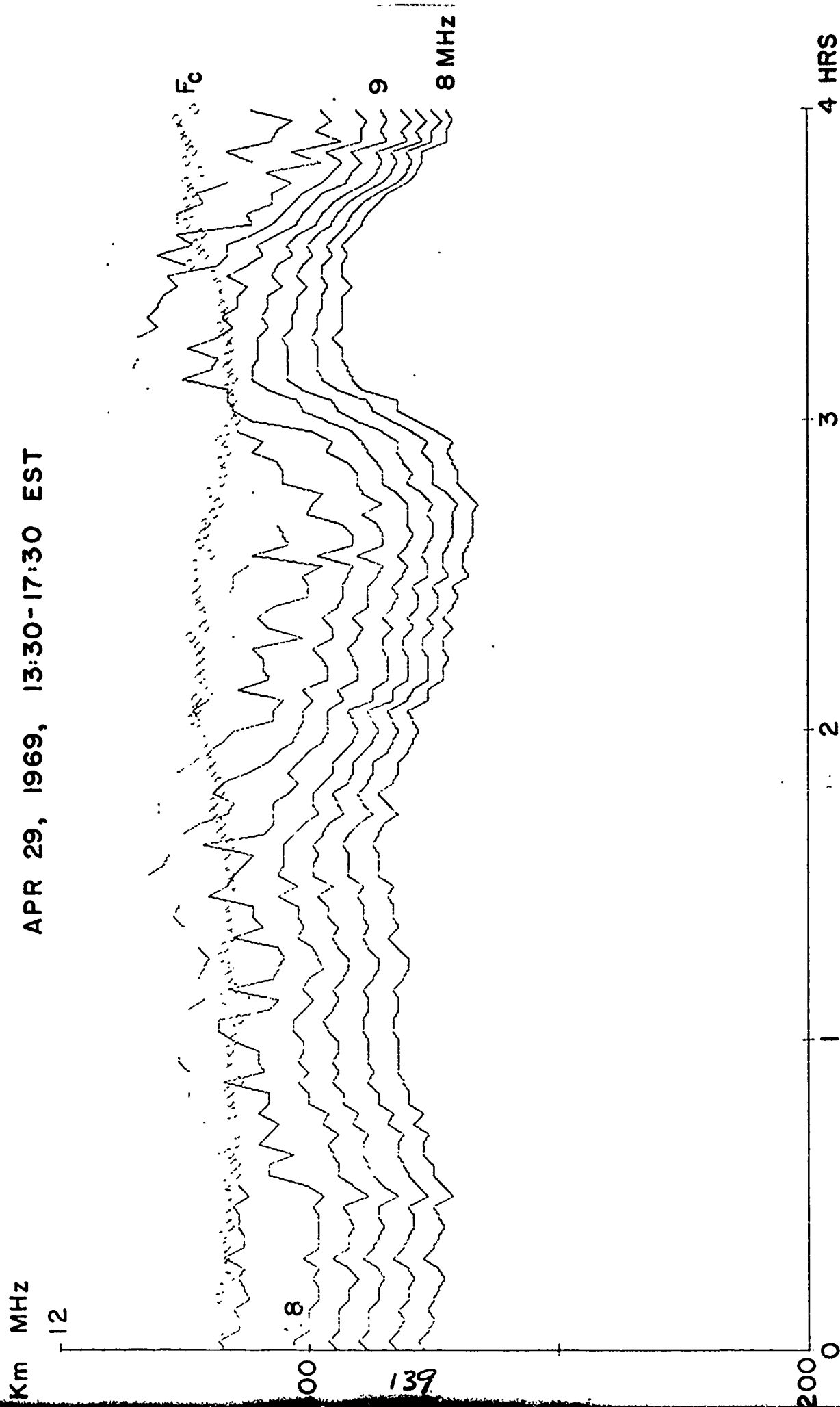
FIGURE 76   CRITICAL FREQUENCIES AND ISOIONIC CONTOURS

HIGHGATE SPRINGS

APR 29, 1969, 13:30-17:30 EST
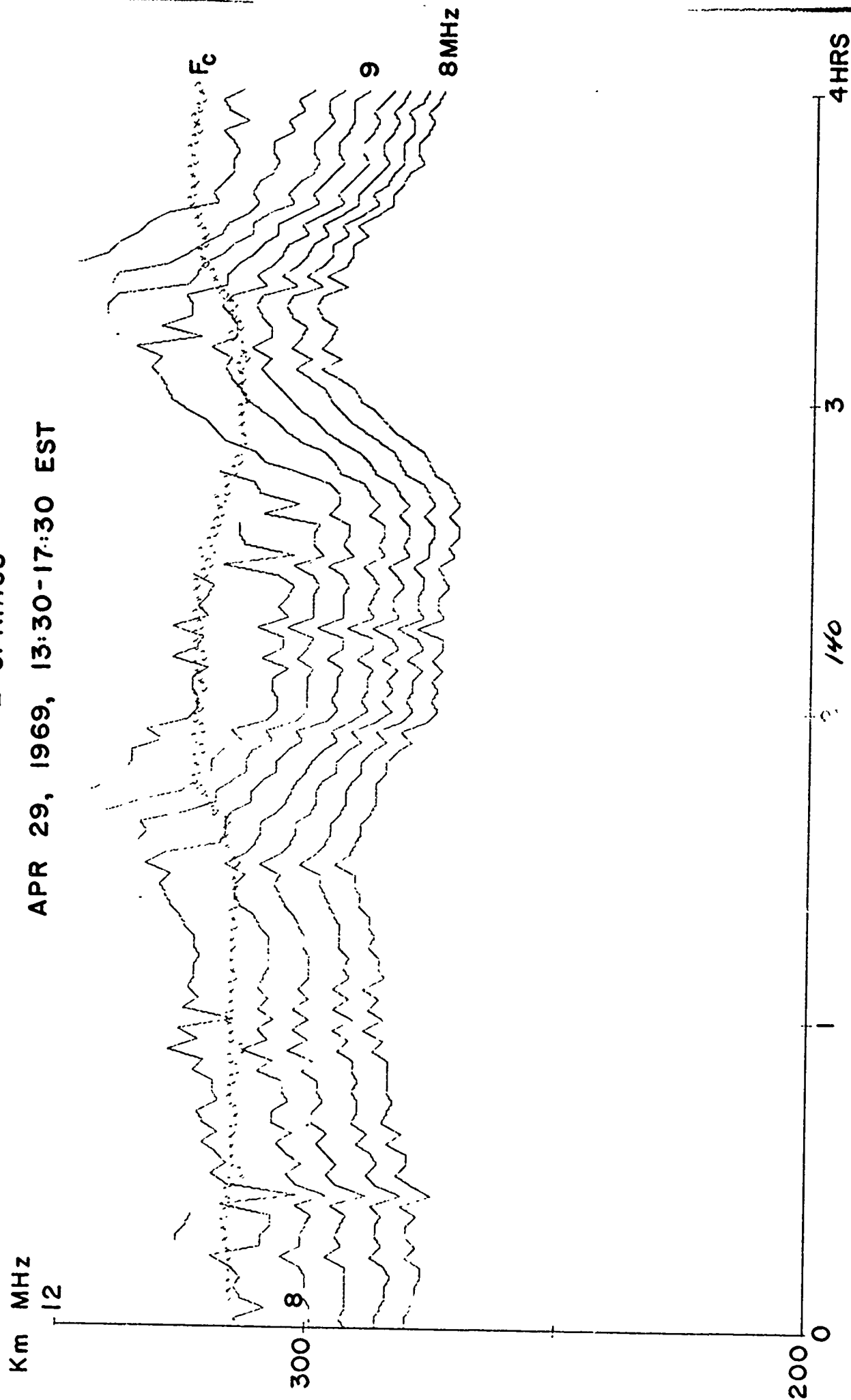
FIGURE 77   CRITICAL FREQUENCIES AND ISOIONIC CONTOURS

ERROL

APR 29, 1969, 13:30-17:30 EST
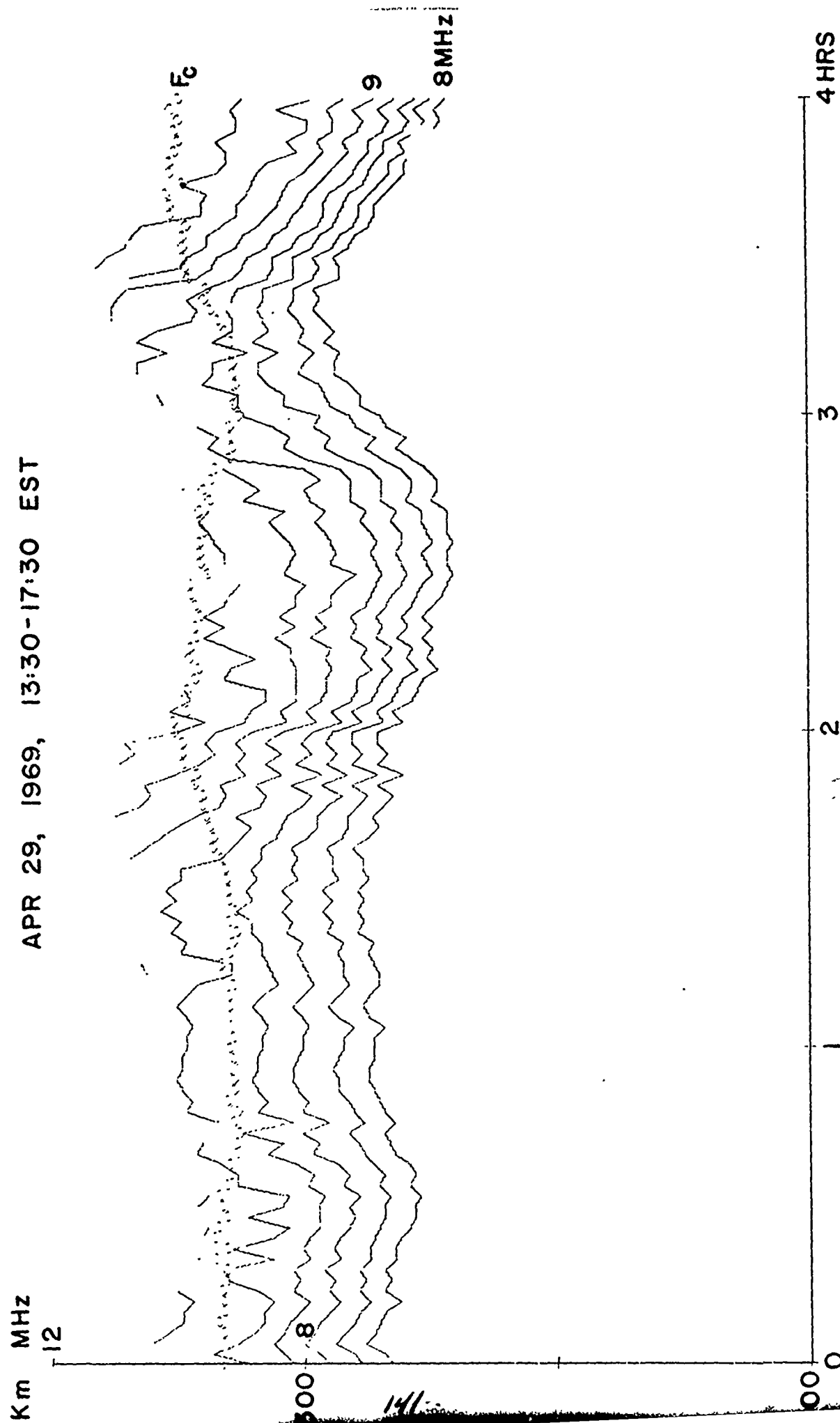
FIGURE 78   CRITICAL FREQUENCIES AND ISOIONIC CONTOURS

HANOVER

SEP 05, 1969, 09:00-13:00 EST
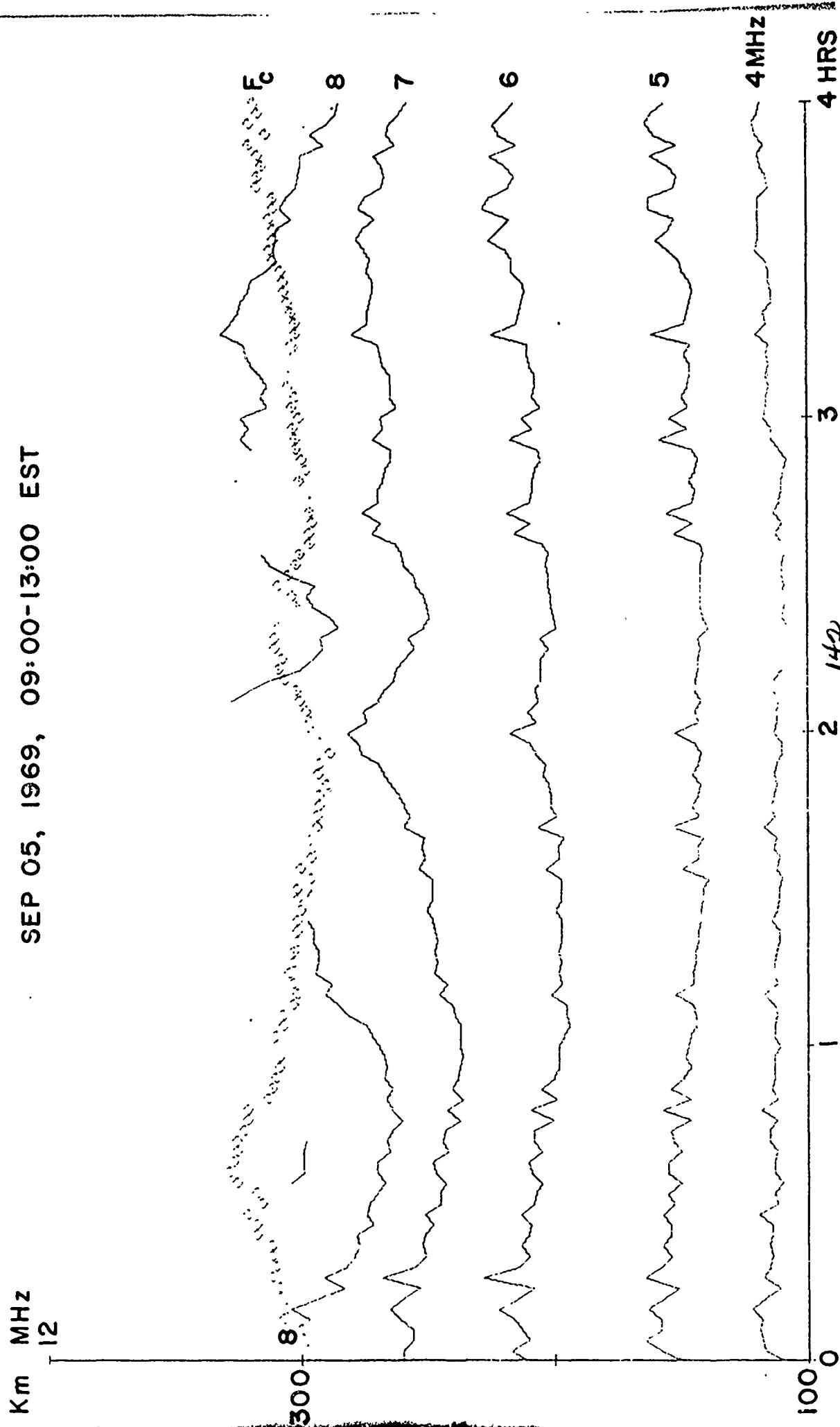
FIGURE 79   CRITICAL FREQUENCIES AND ISOIONIC CONTOURS

HIGHGATE SPRINGS

SEP 05, 1969, 09:00-13:00 EST
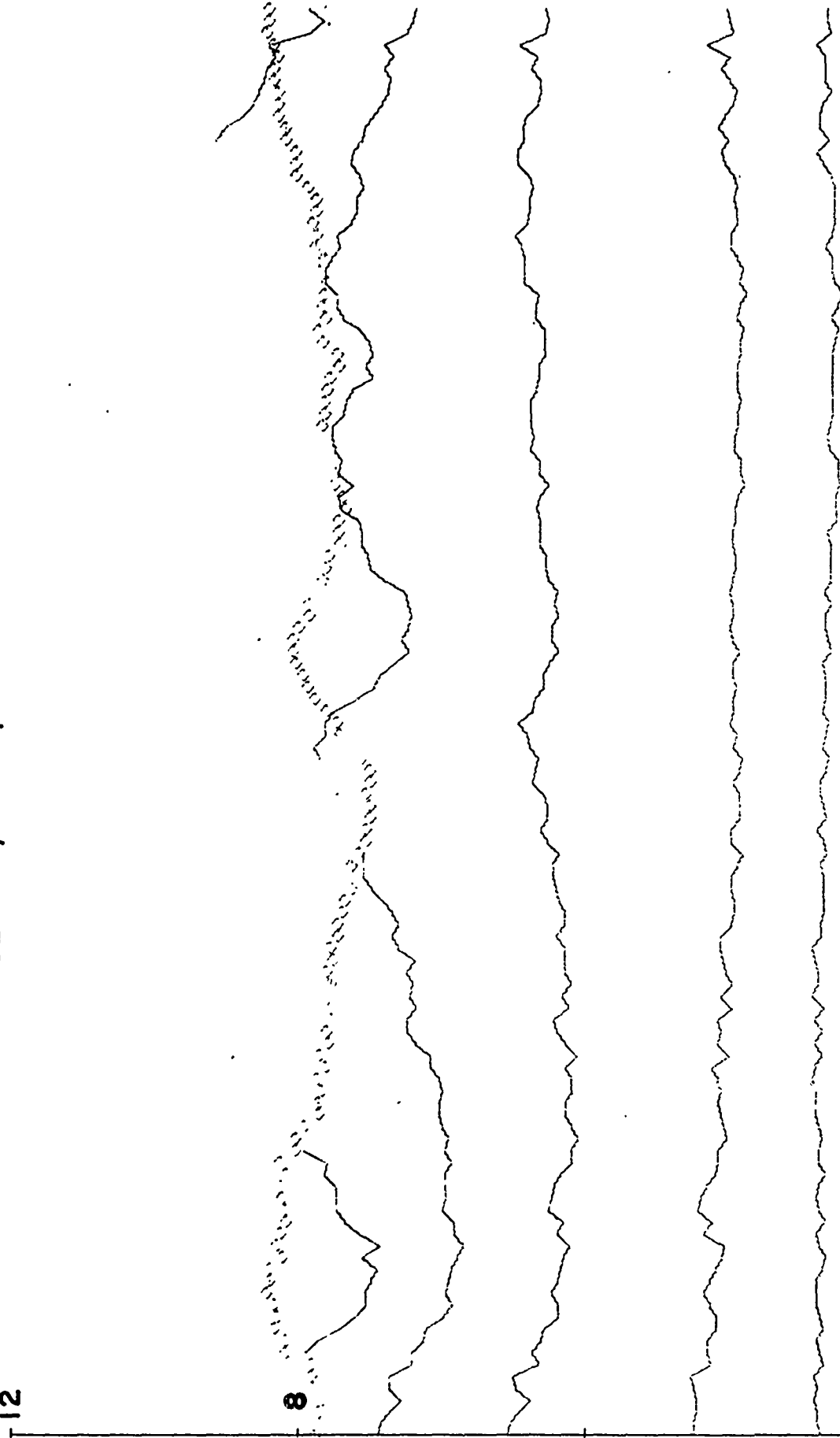
FIGURE 80   CRITICAL FREQUENCIES AND ISOIONIC CONTOURS

ERROL

SEP 05, 1969, 09:00-13:00 EST
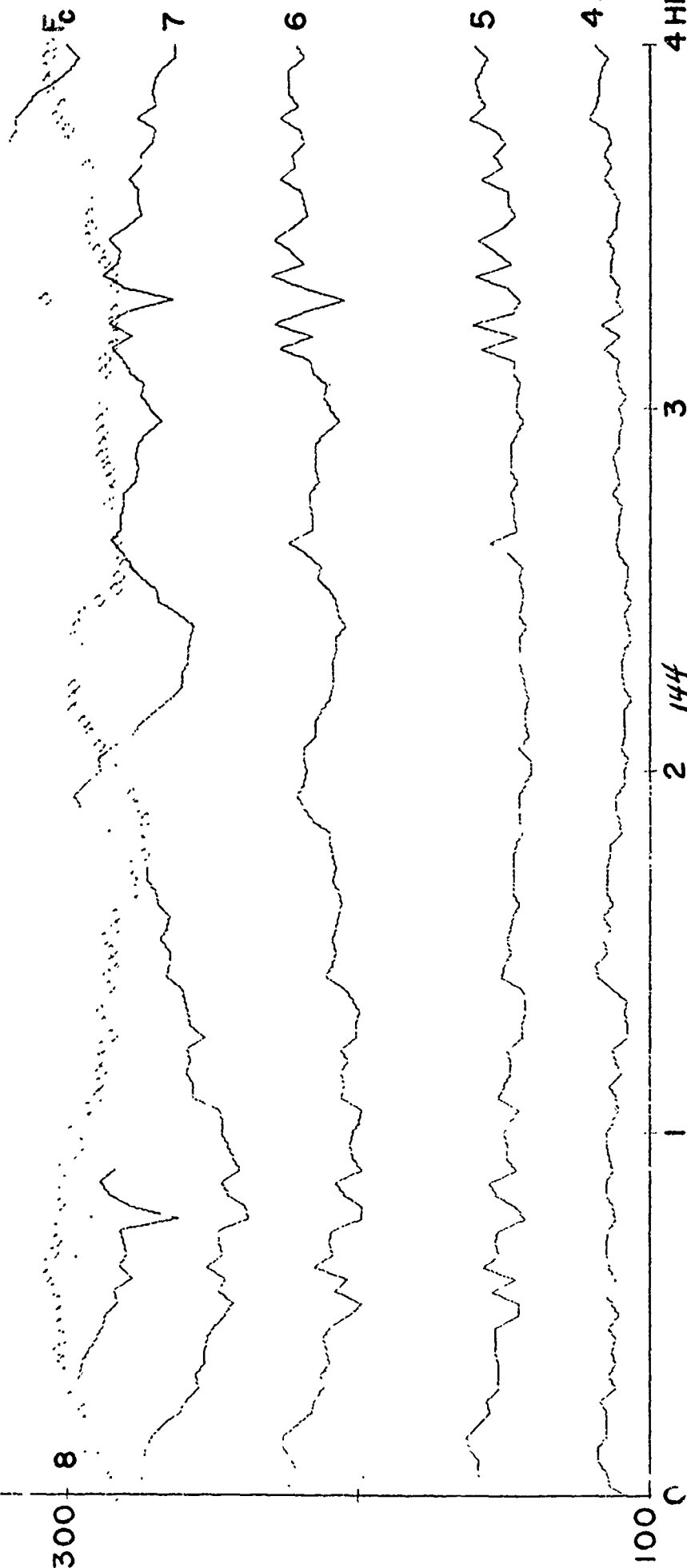
FIGURE 81   CRITICAL FREQUENCIES AND ISOIONIC CONTOURS

HANOVER

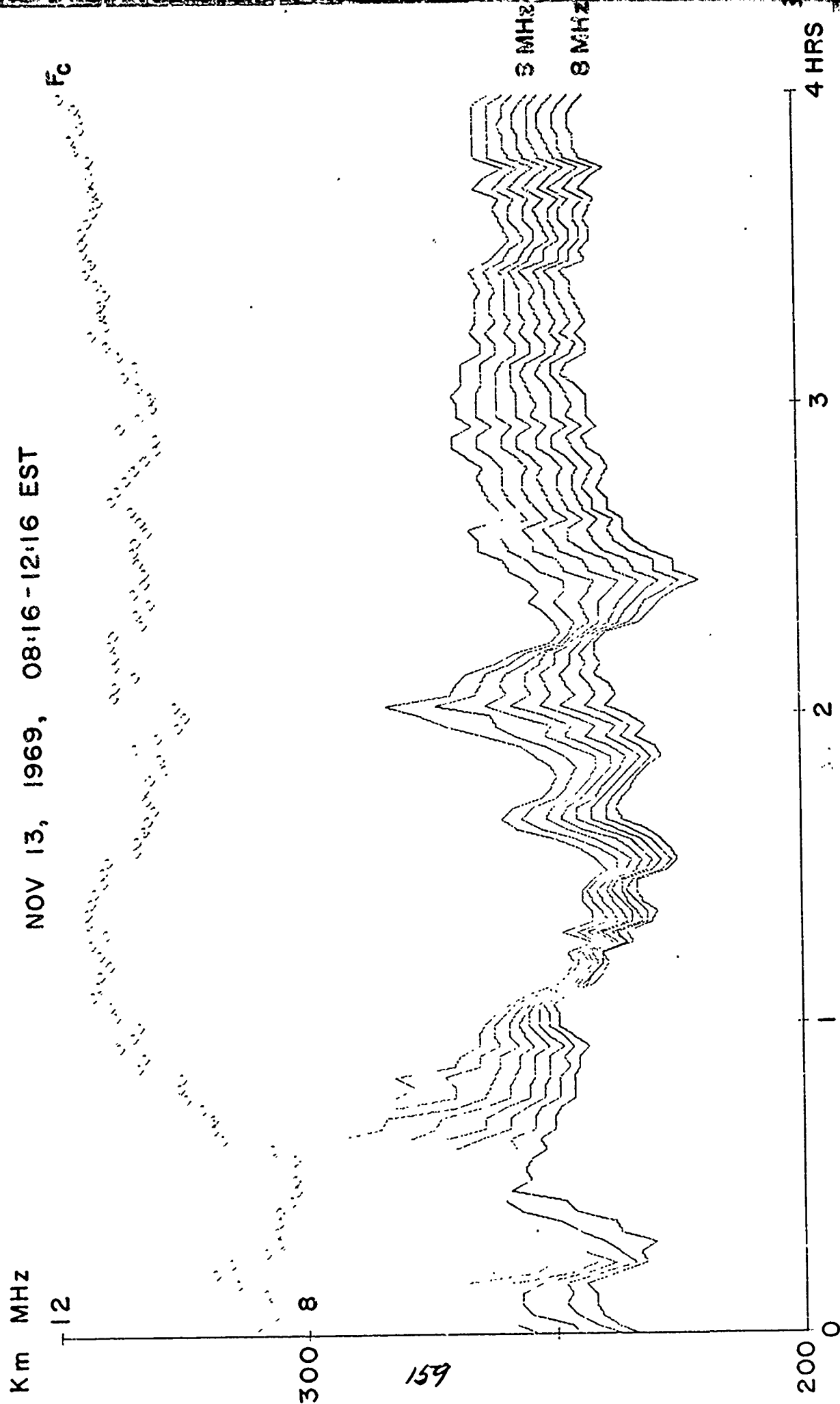SEP 05, 1969, 09:00–13:00 EST
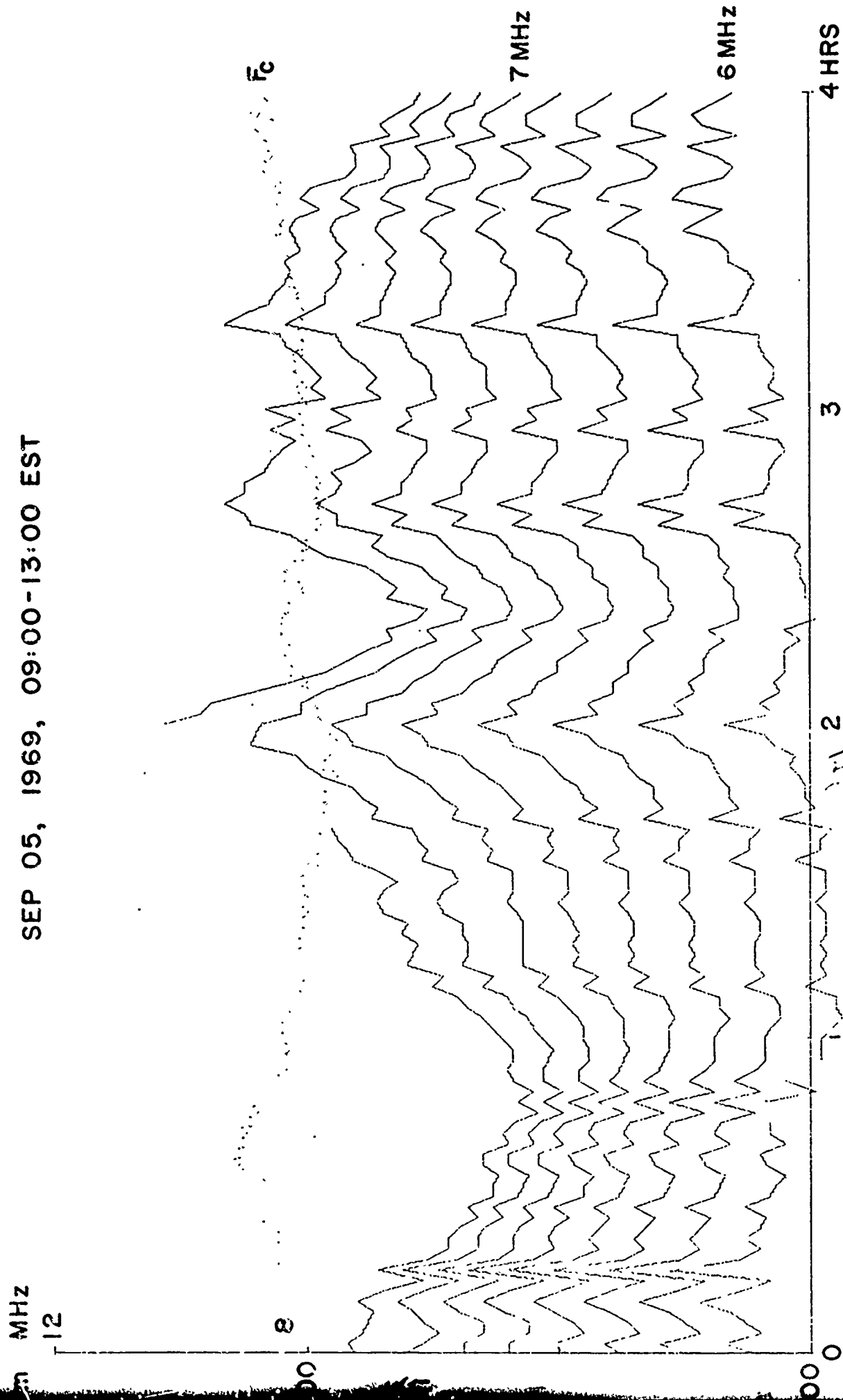
FIGURE 82   CRITICAL FREQUENCIES AND ISOIONIC CONTOURS

HIGHGATE SPRINGS

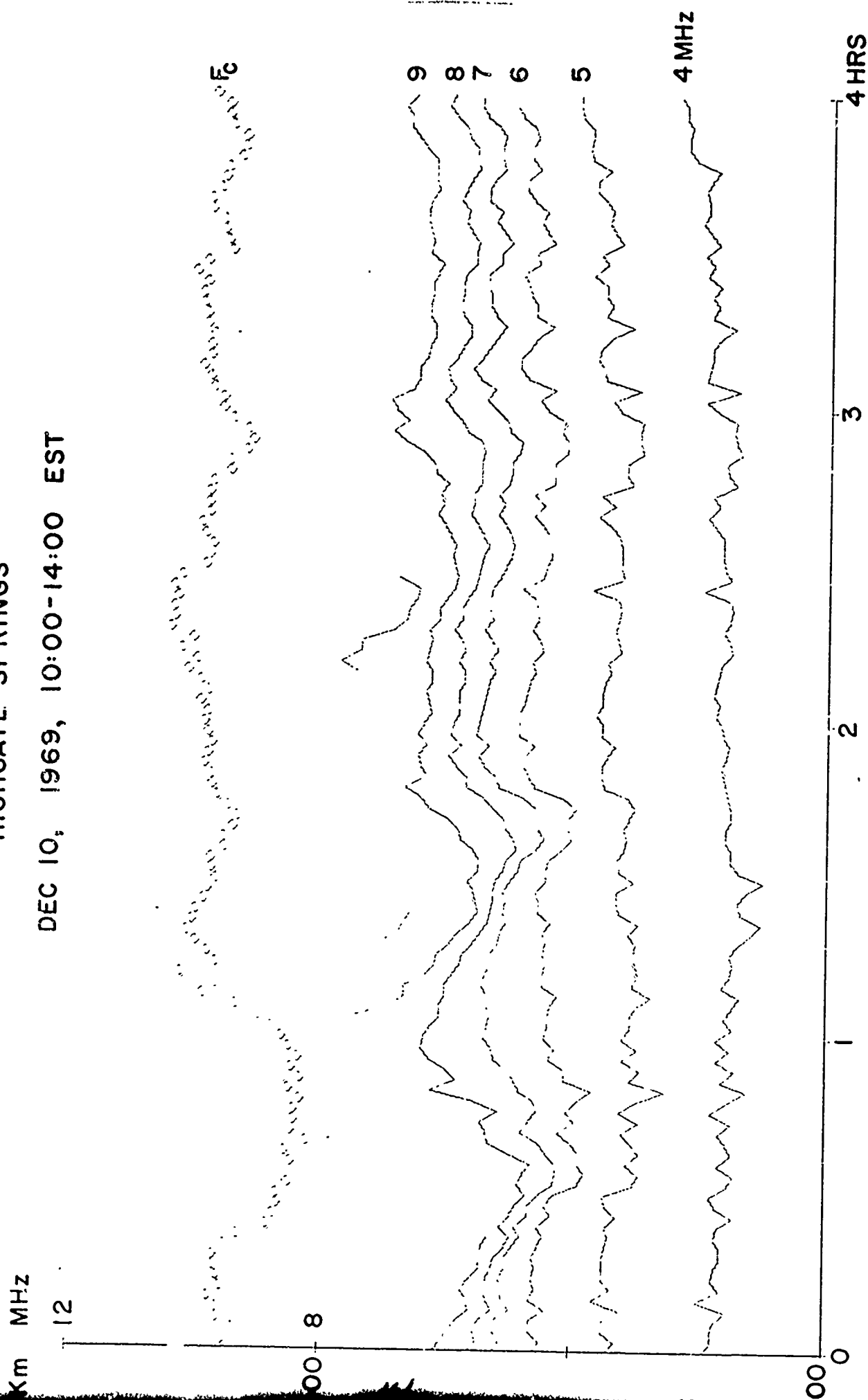SEP 05, 1969, 09:00-13:00 EST
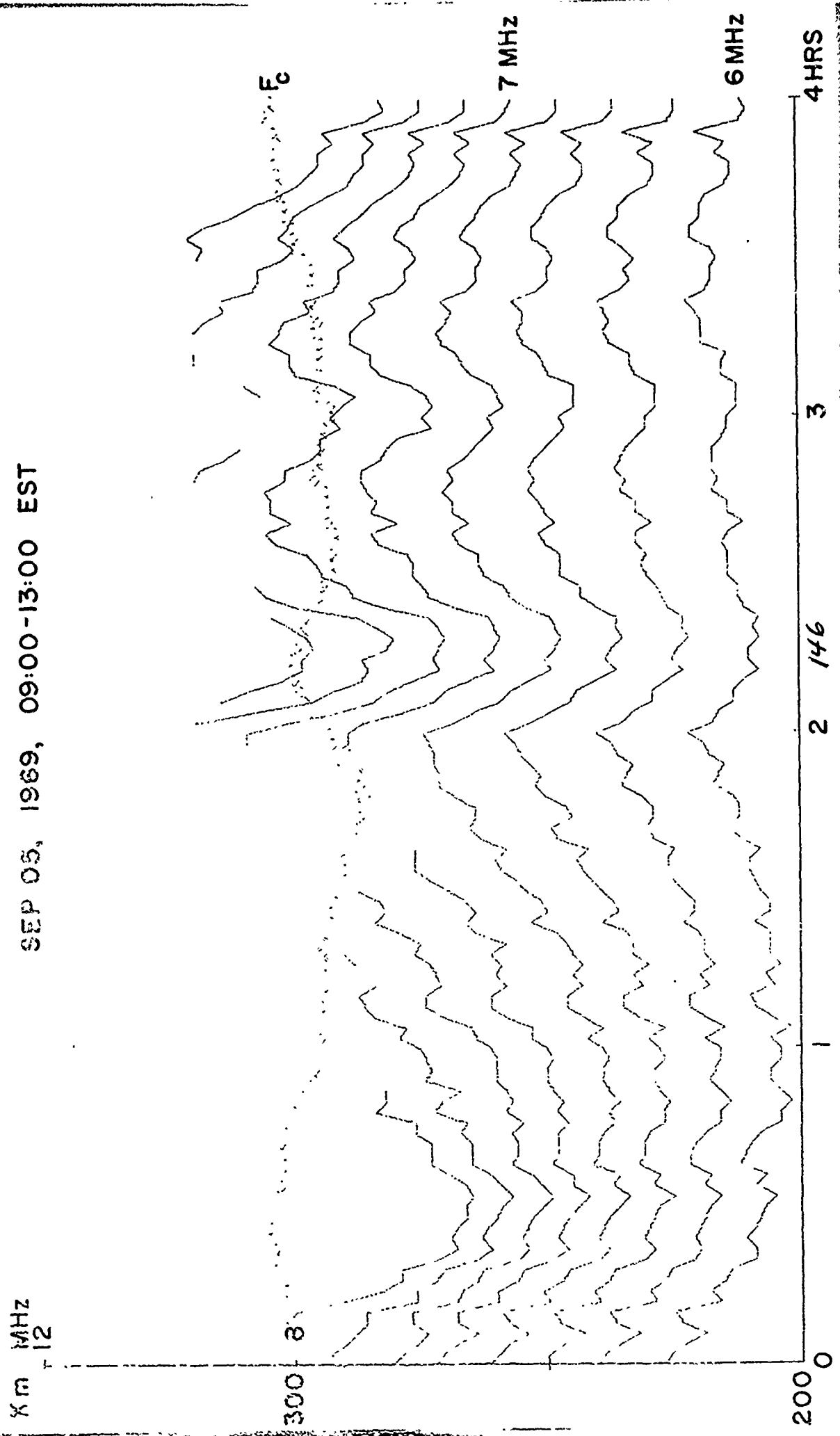
FIGURE 83   CRITICAL FREQUENCIES AND ISOIONIC CONTOURS

ERROL

SEP 05, 1969, 09:00-13:00 EST
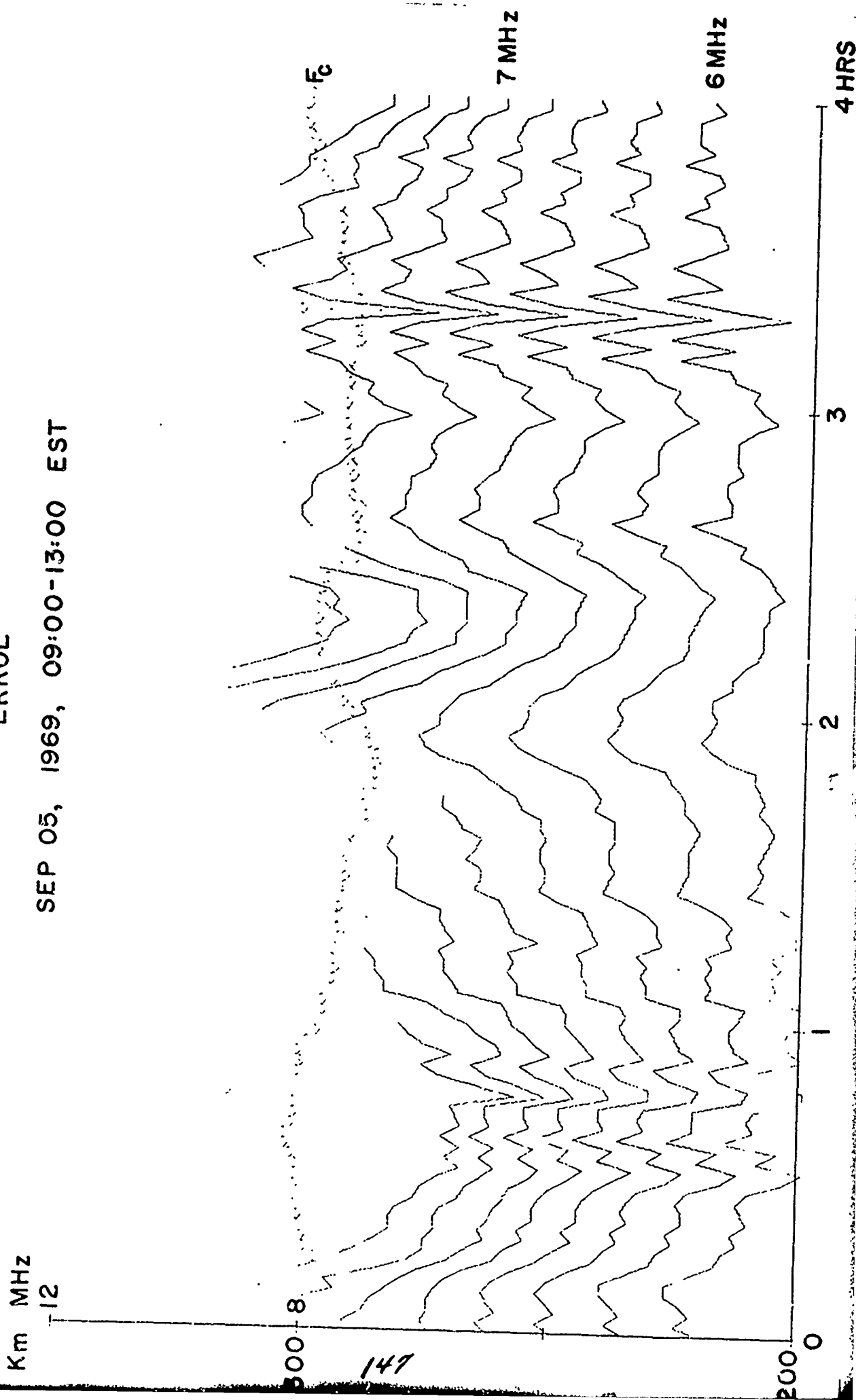
FIGURE 84   CRITICAL FREQUENCIES AND ISOIONIC CONTOURS

HANOVER

NOV 15, 1969, 11:00-15:00 EST
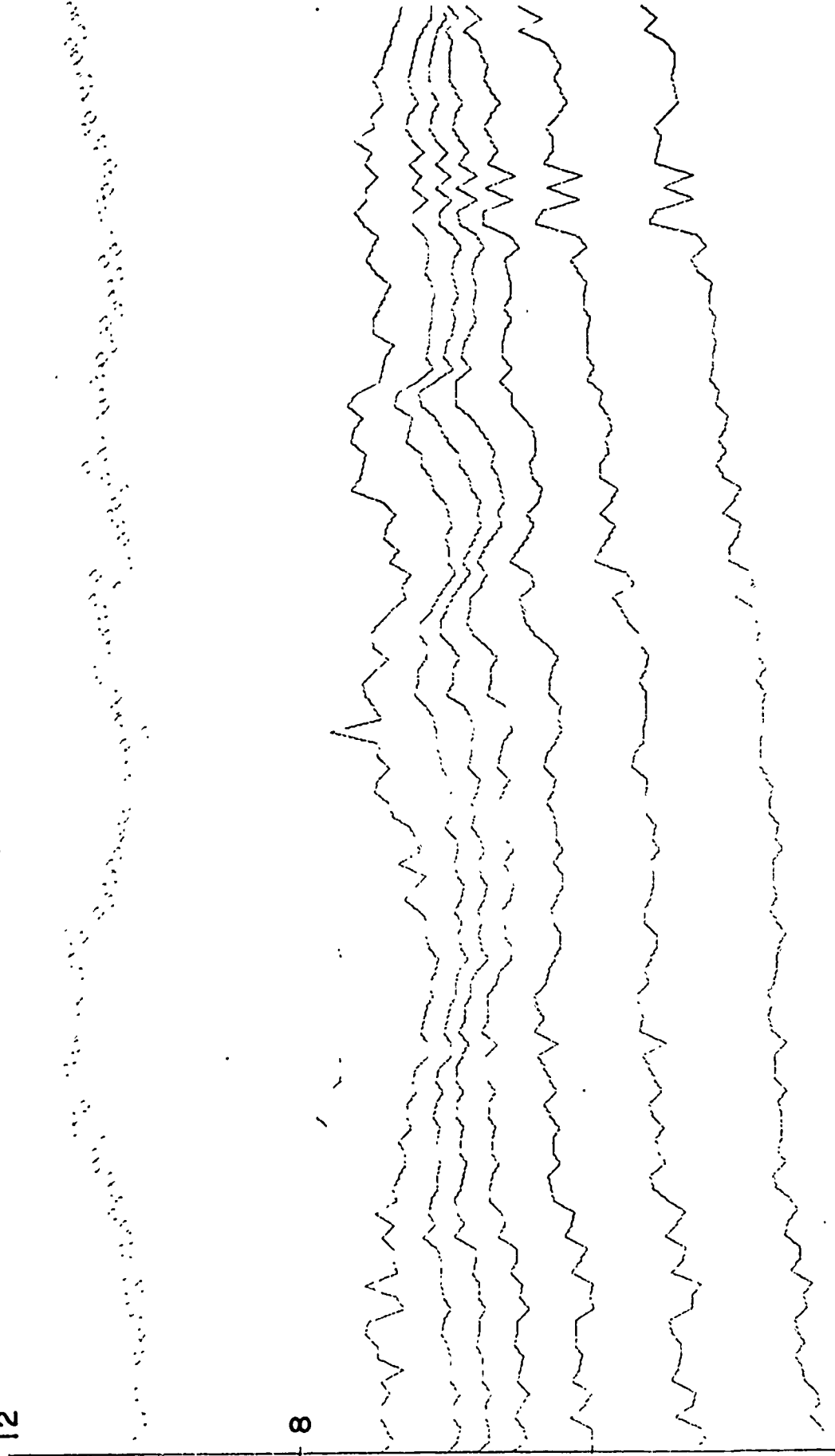
FIGURE 85   CRITICAL FREQUENCIES AND ISOIONIC CONTOURS

HIGHGATE SPRINGS

NOV 15, 1969, 11:00-15:00 EST
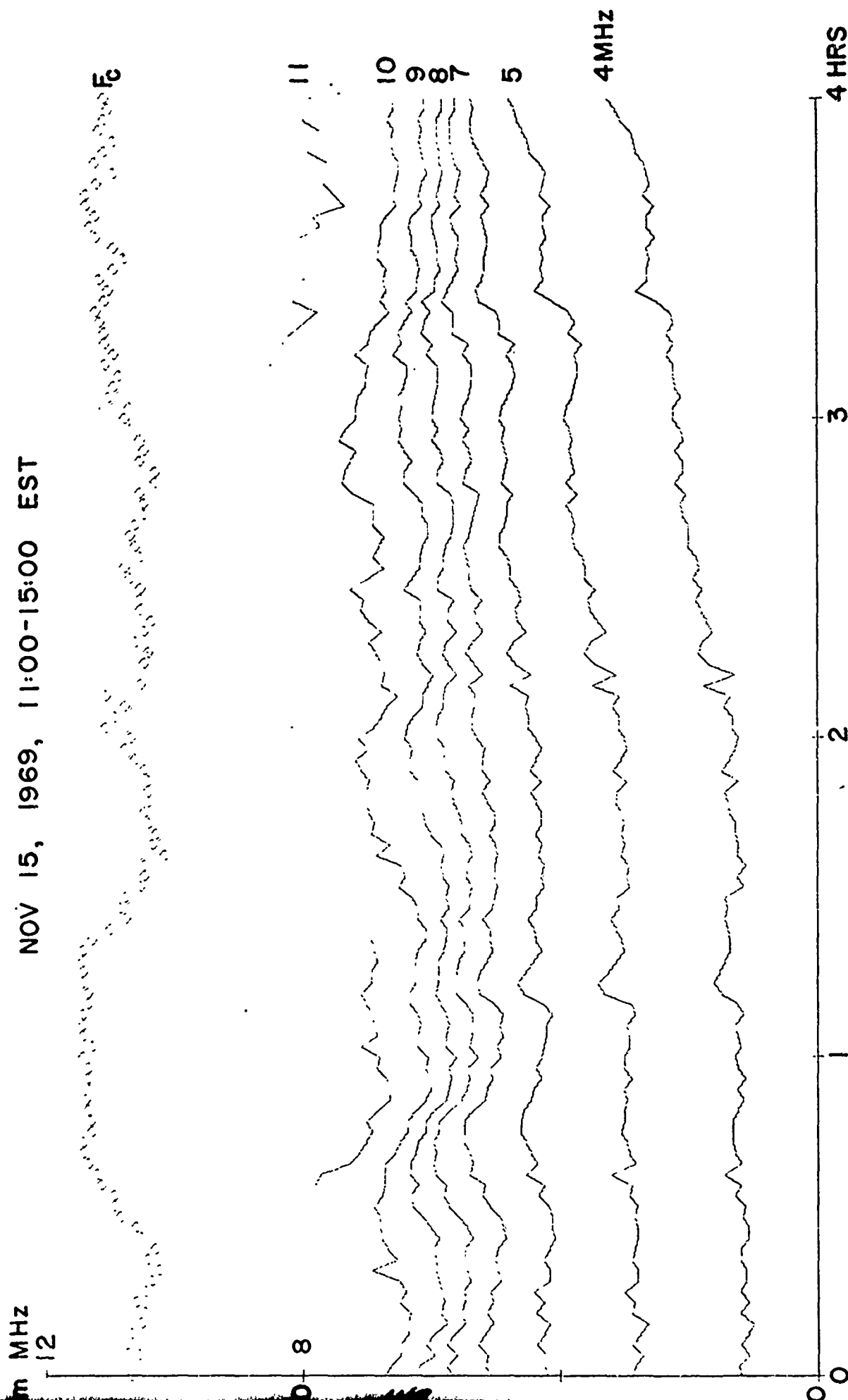
FIGURE 86   CRITICAL FREQUENCIES AND ISOIONIC CONTOURS
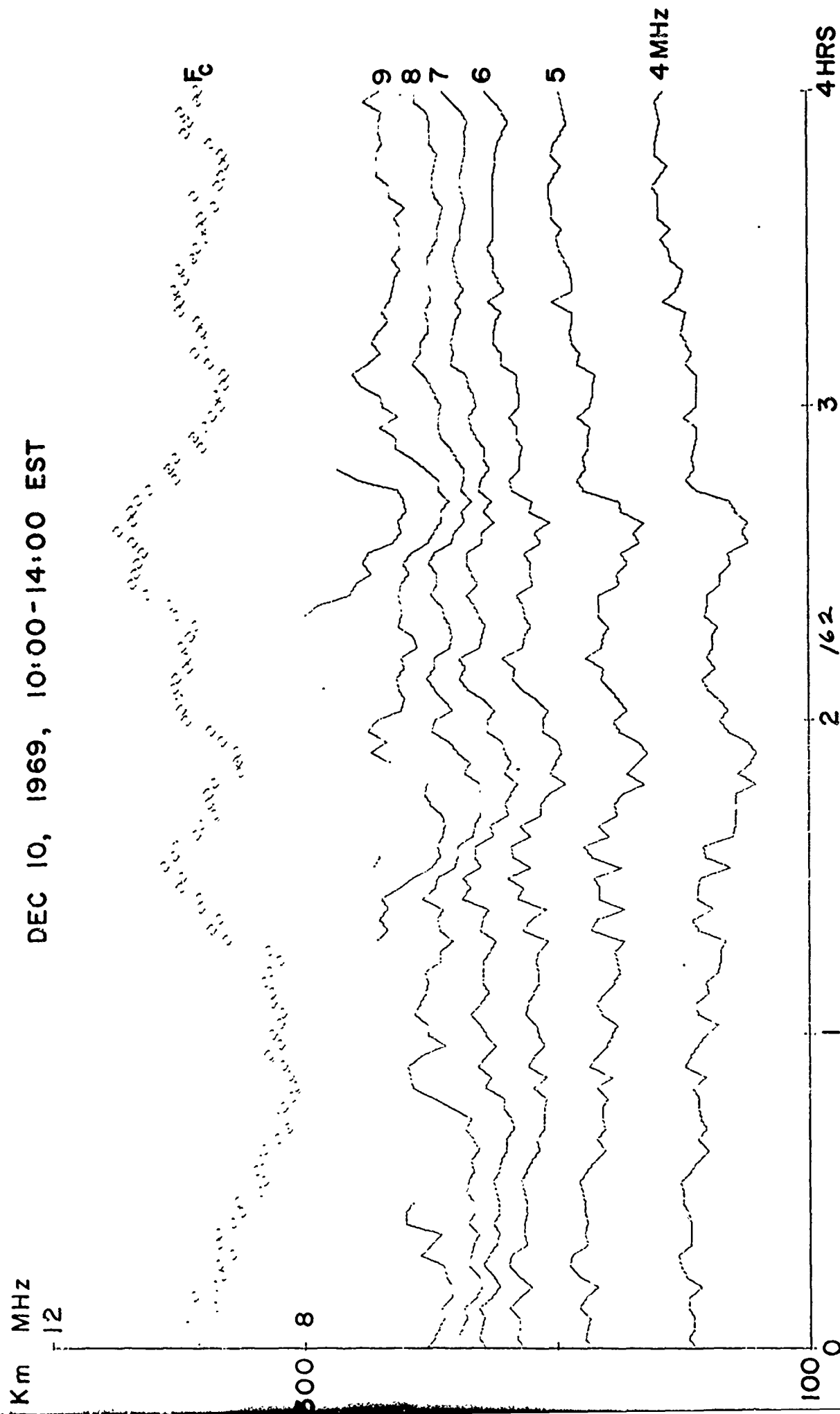
ERROL

NOV 15, 1969, 11:00-15:00 EST
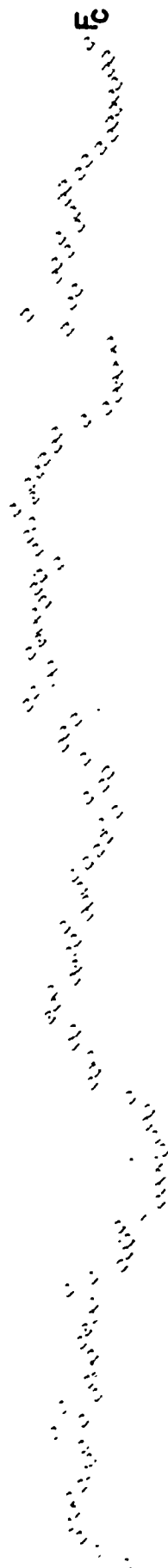
FIGURE 87   CRITICAL FREQUENCIES AND ISOIONIC CONTOURS

HANOVER

NOV 15, 1969, 11:00-15:00 EST

151

FIGURE 88   CRITICAL FREQUENCIES AND ISOIONIC CONTOURS

HIGHGATE SPRINGS

NOV 15, 1969, 11:00-15:00 EST

FIGURE 89   CRITICAL FREQUENCIES AND ISOIONIC CONTOURS

ERROL

NOV 15, 1969, 11:00-15:00 EST

FIGURE 90   CRITICAL FREQUENCIES AND ISOIONIC CONTOURS

HANOVER

NOV 17, 1969, 08:16-12:16 EST

FIGURE 91   CRITICAL FREQUENCIES AND ISOIONIC CONTOURS

HIGHGATE SPRINGS

NOV 17, 1969, 08:16-12:16 EST

Fc

Km MHz
    12

11
10
9
8
7
6
5
4 MHz

8

2   3   4 HRS

FIGURE 92   CRITICAL FREQUENCIES AND ISOIONIC CONTOURS

ERROL

NOV 17, 1969, 08:16-12:16 EST

FIGURE 93   CRITICAL FREQUENCIES AND ISOIONIC CONTOURS

HANOVER

NOV 17, 1969, 08:16–12:16 EST

FIGURE 94   CRITICAL FREQUENCIES AND ISOIONIC CONTOURS

HIGHGATE SPRINGS

NOV 17, 1969,   08:16 - 12:16 EST
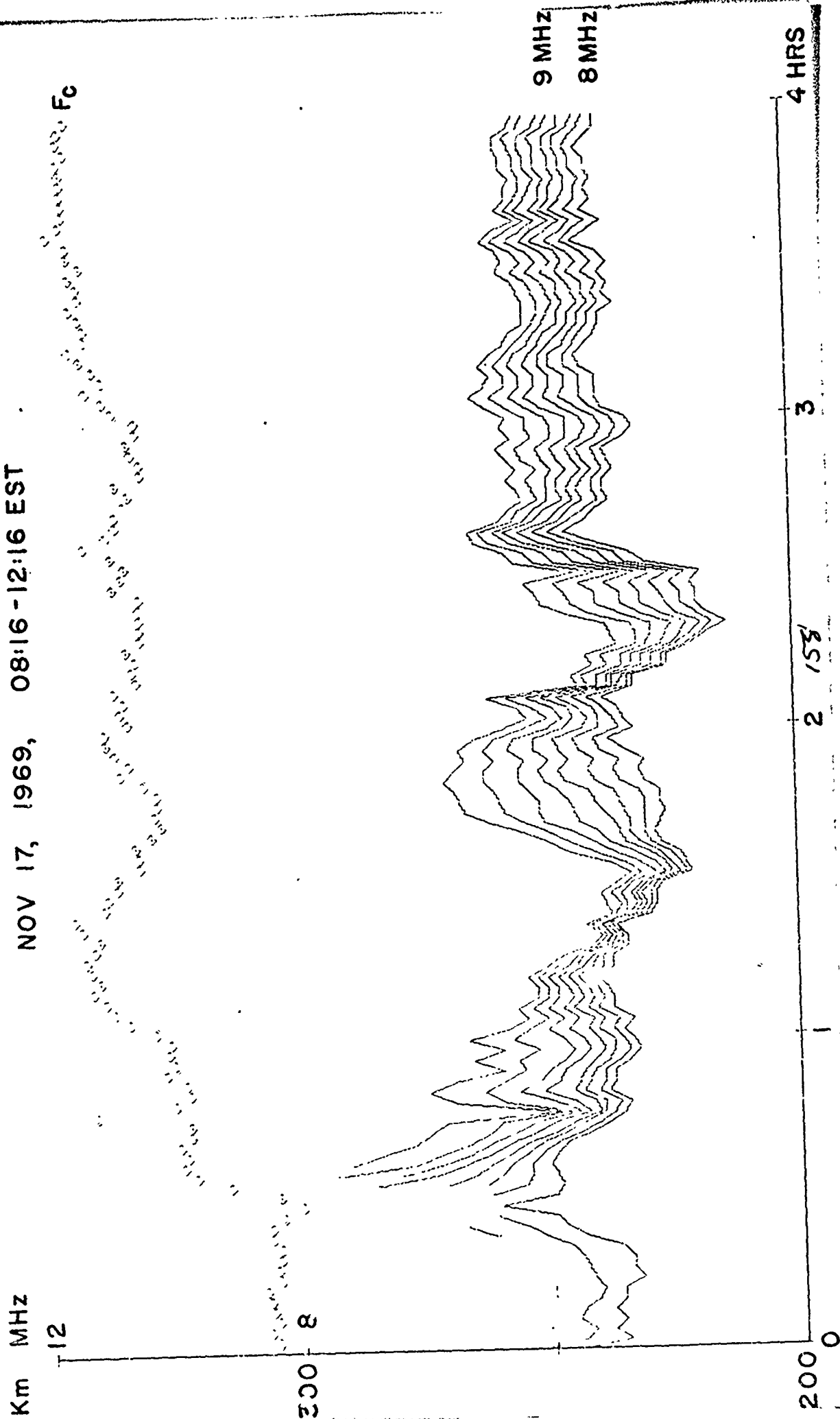
FIGURE 96   CRITICAL FREQUENCIES AND ISOIONIC CONTOURS

HANOVER
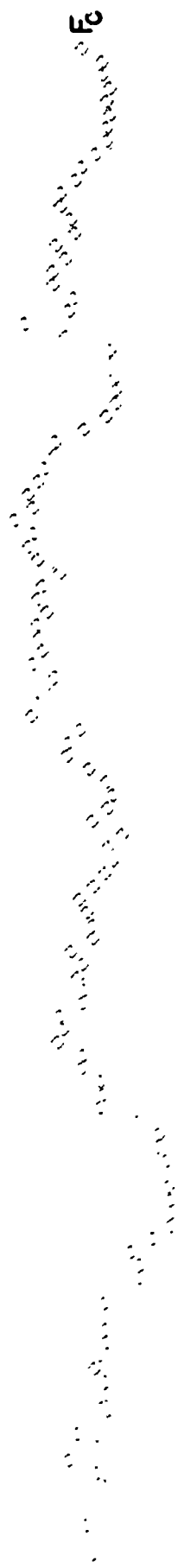
DEC 10, 1969, 10:00-14:00 EST

FIGURE 95   CRITICAL FREQUENCIES AND ISOIONIC CONTOURS

ERROL

NOV 13, 1969, 08:16 - 12:16 EST

159

FIGURE 97   CRITICAL FREQUENCIES AND ISOIONIC CONTOURS

HIGHGATE SPRINGS

DEC 10, 1969, 10:00-14:00 EST

FIGURE 98   CRITICAL FREQUENCIES AND ISOIONIC CONTOURS
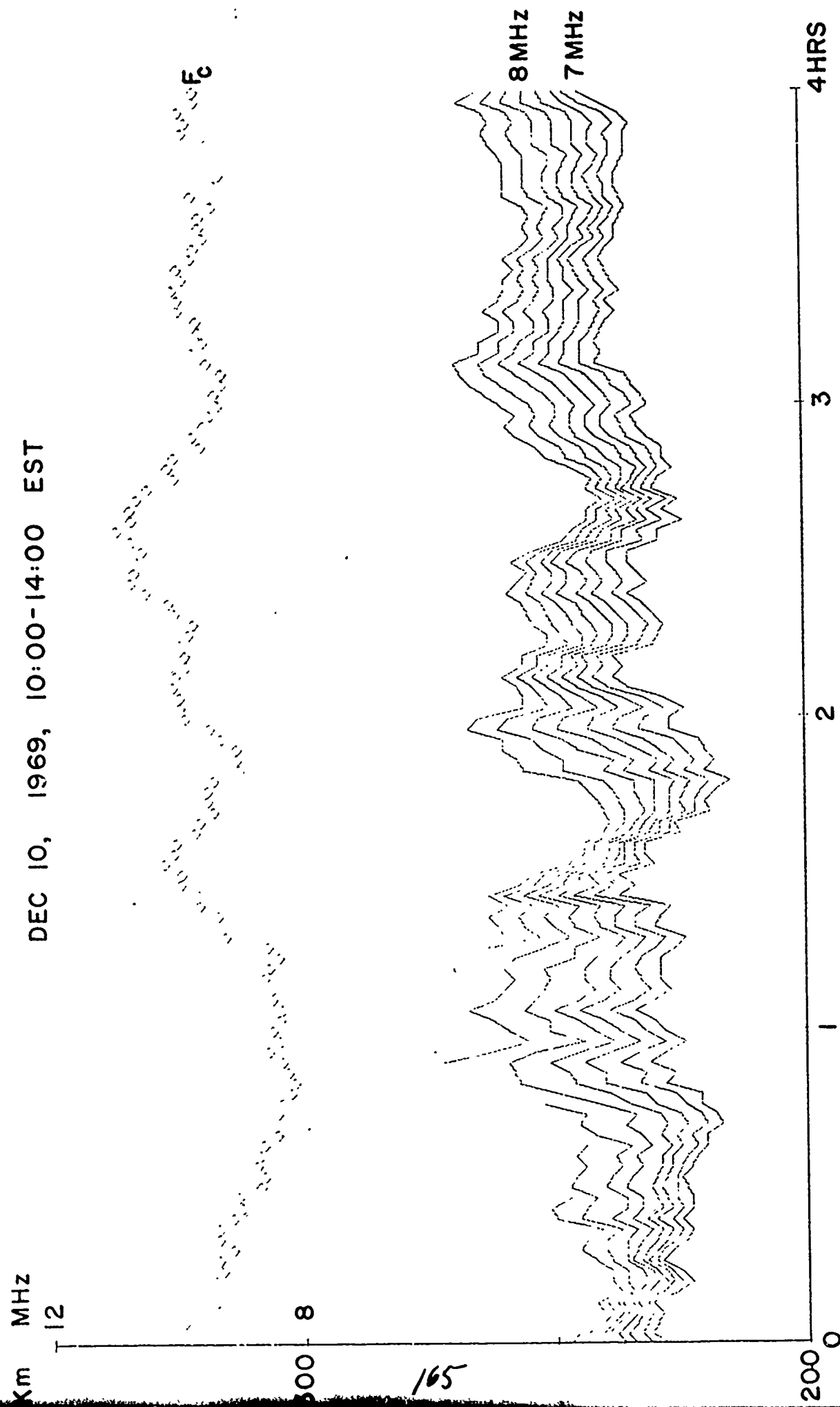
ERROL

DEC 10, 1969, 10:00–14:00 EST

FIGURE 99   CRITICAL FREQUENCIES AND ISOIONIC CONTOURS

HANOVER
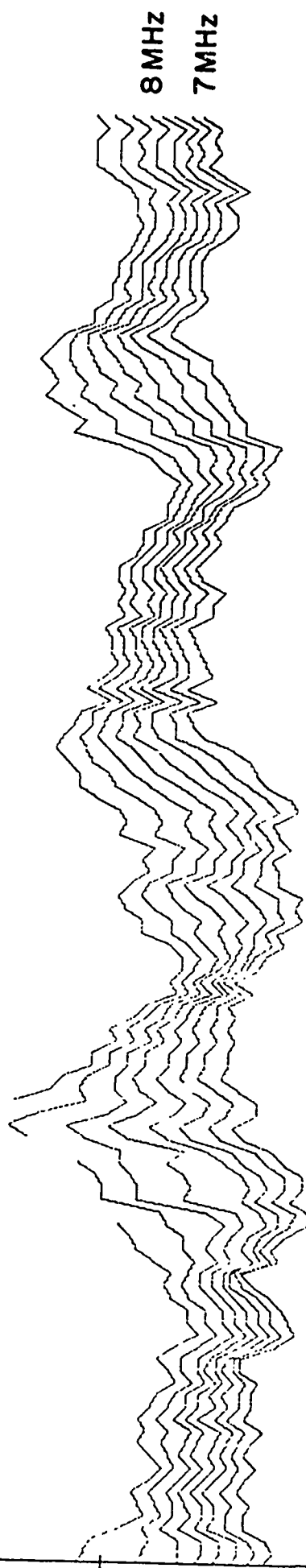
DEC 10, 1969, 10:00~14:00 EST

FIGURE 100   CRITICAL FREQUENCIES AND ISOIONIC CONTOURS

HIGHGATE SPRINGS
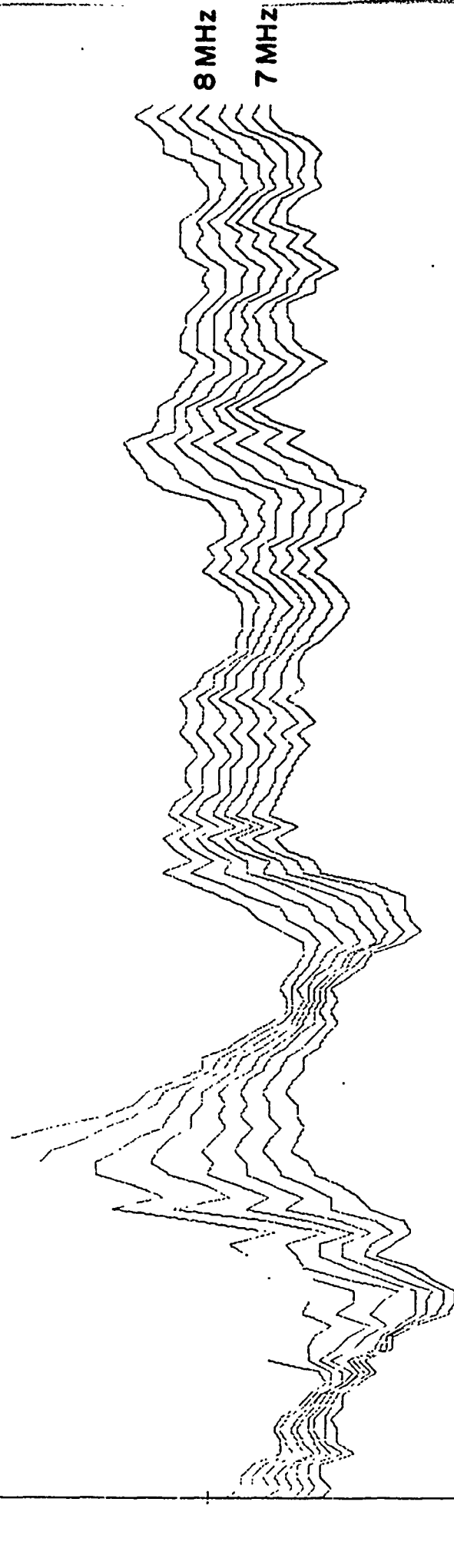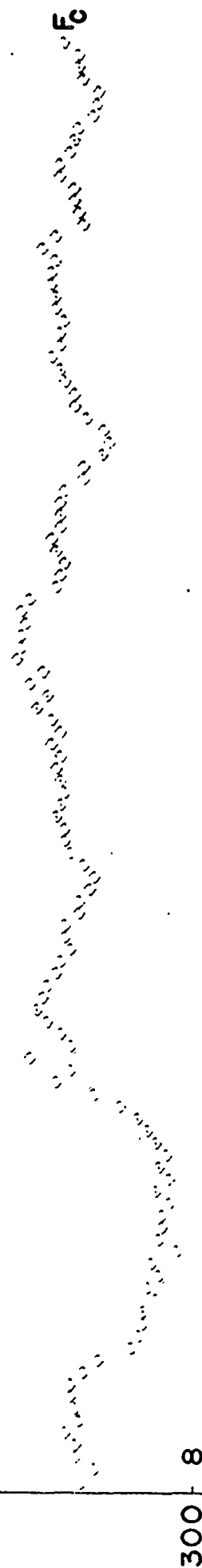
DEC 10, 1969, 10:00-14:00 EST

FIGURE 101   CRITICAL FREQUENCIES AND ISOIONIC CONTOURS

ERROL

DEC 10, 1969, 10:00-14:00 EST

FIGURE 102 VIRTUAL HEIGHTS AT 2 AT 2.5 MHZ
DARTMOUTH SYSTEM
MAY 29, 1970, 01:00 – 03:00 U.T.
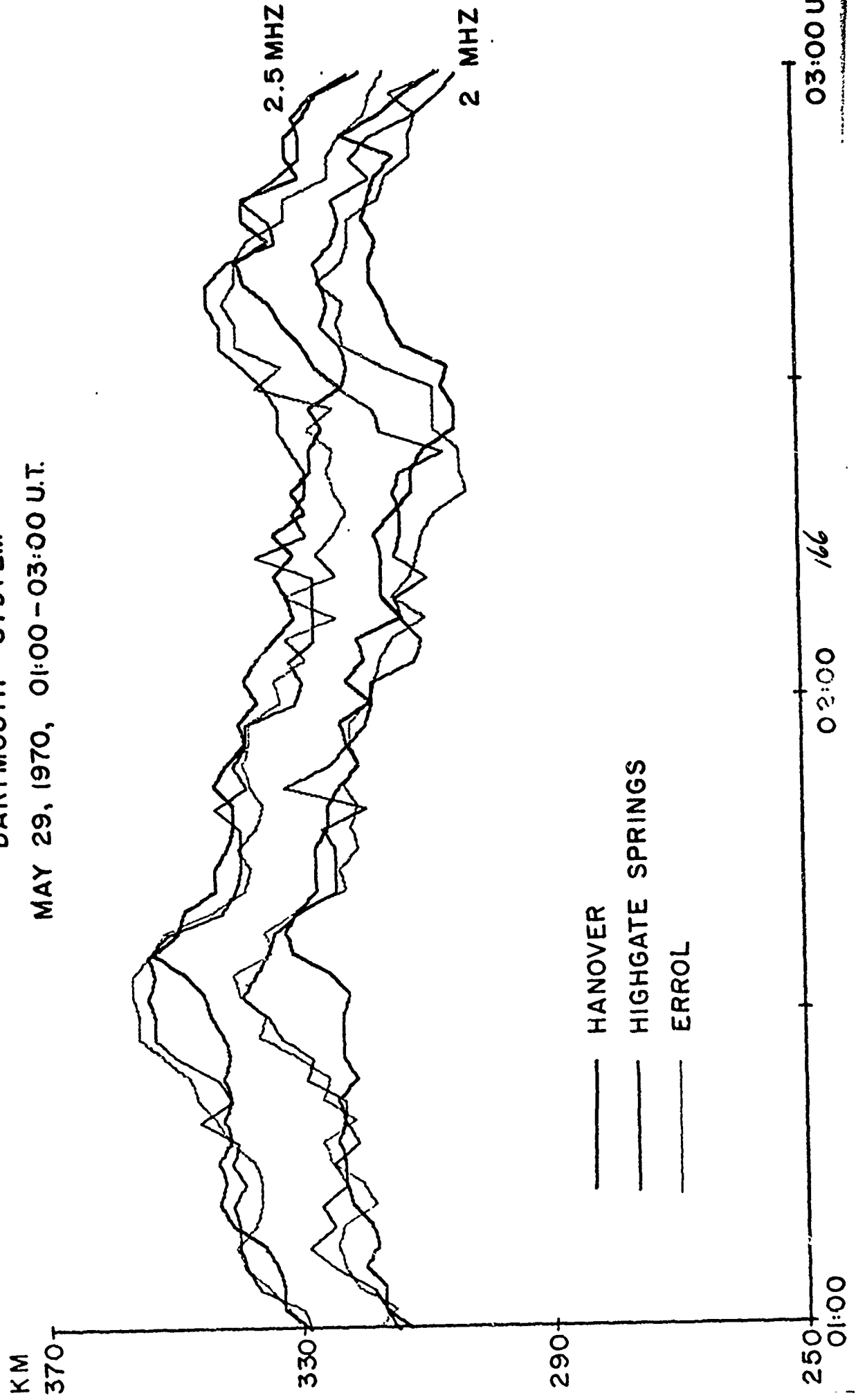
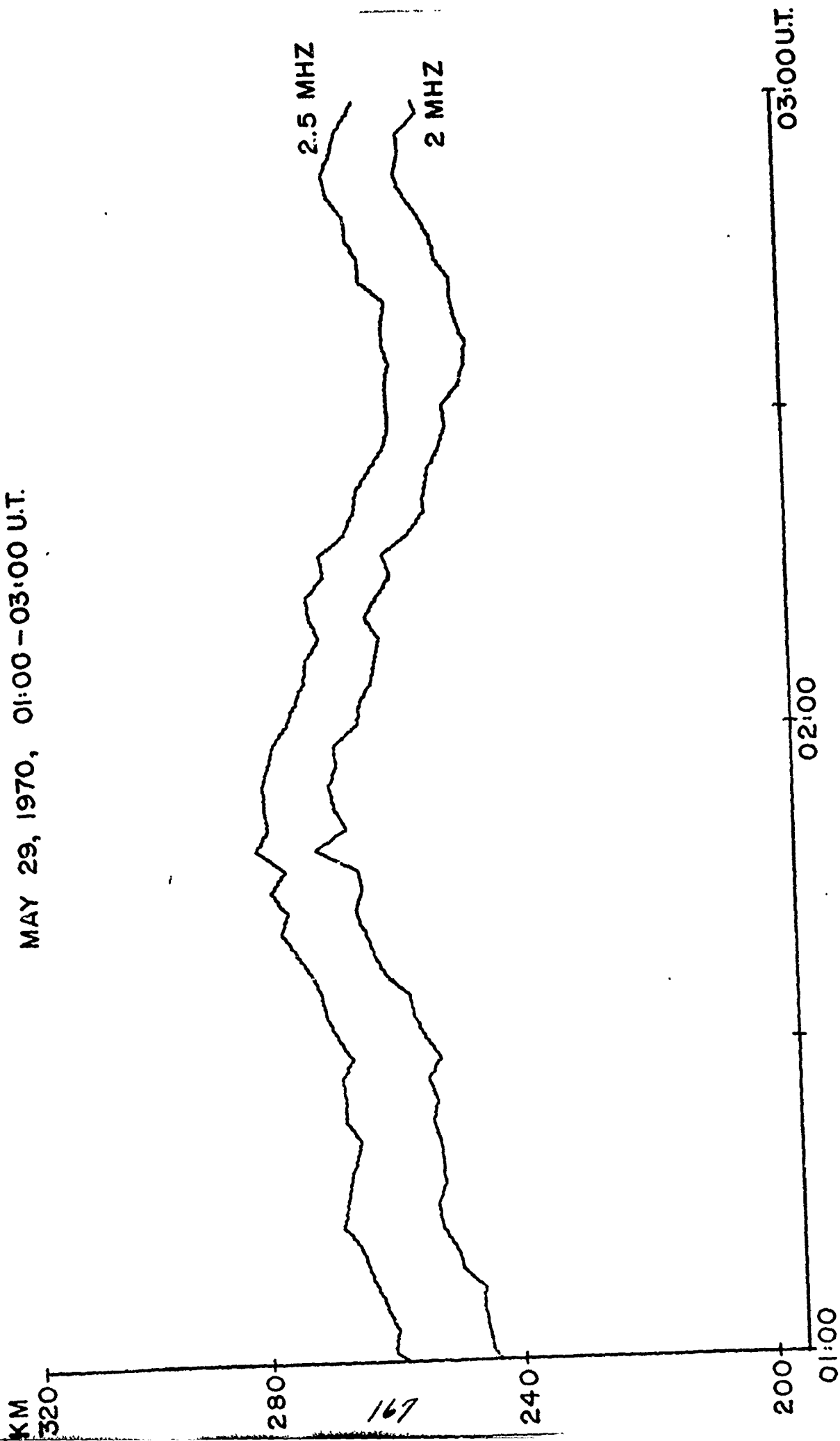FIGURE 103   REAL HEIGHTS AT 2 AND 2.5 MHZ
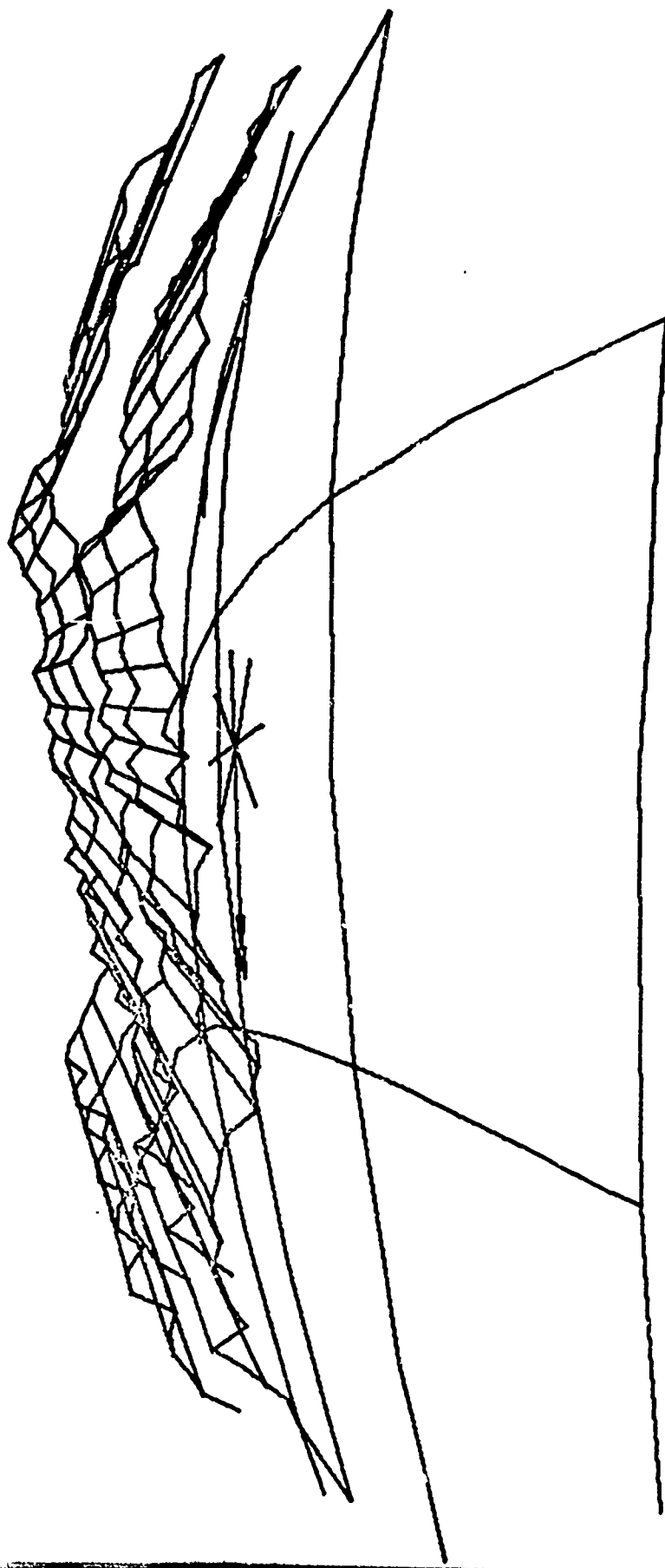MILLSTONE HILL
MAY 29, 1970, 01:00−03:00 U.T.

167

FIGURE 104 VIRTUAL HEIGHT CONTOURS AT 2 AND 2.5 MHZ

HANOVER, MAY 29, 1970, 02:00 UT

HANOVER 43° 41' 30"N 72° 11' 18" W
MILLSTONE HILL 42° 37' 04"N 71° 29' 26"W

HA
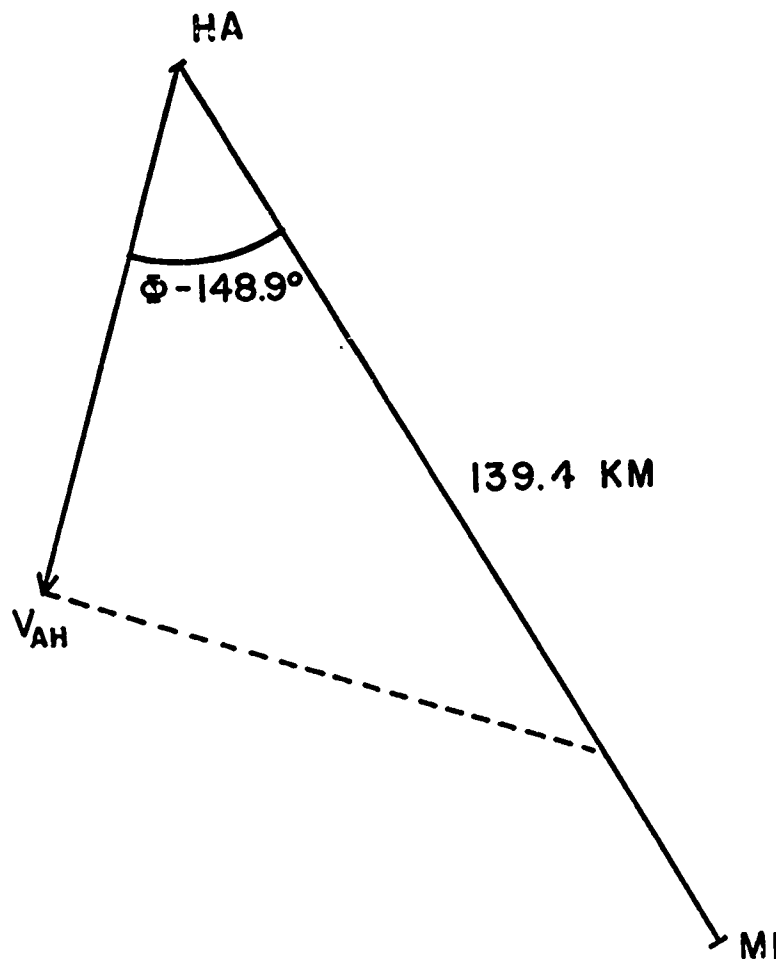
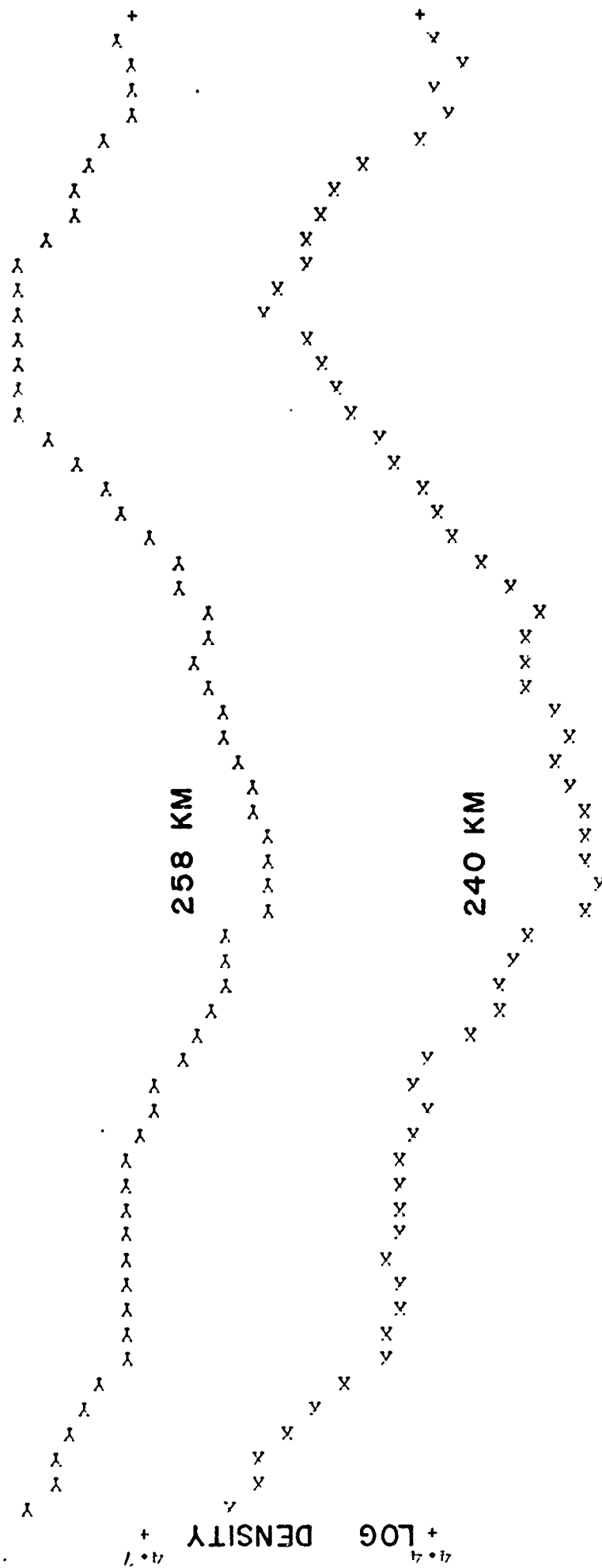Φ - 148.9°

139.4 KM

V$_{AH}$

MI

FIGURE 105   GEOMETRIC   DETERMINATION
OF THE TIME LAG BETWEEN
HANOVER AND MILLSTONE HILL
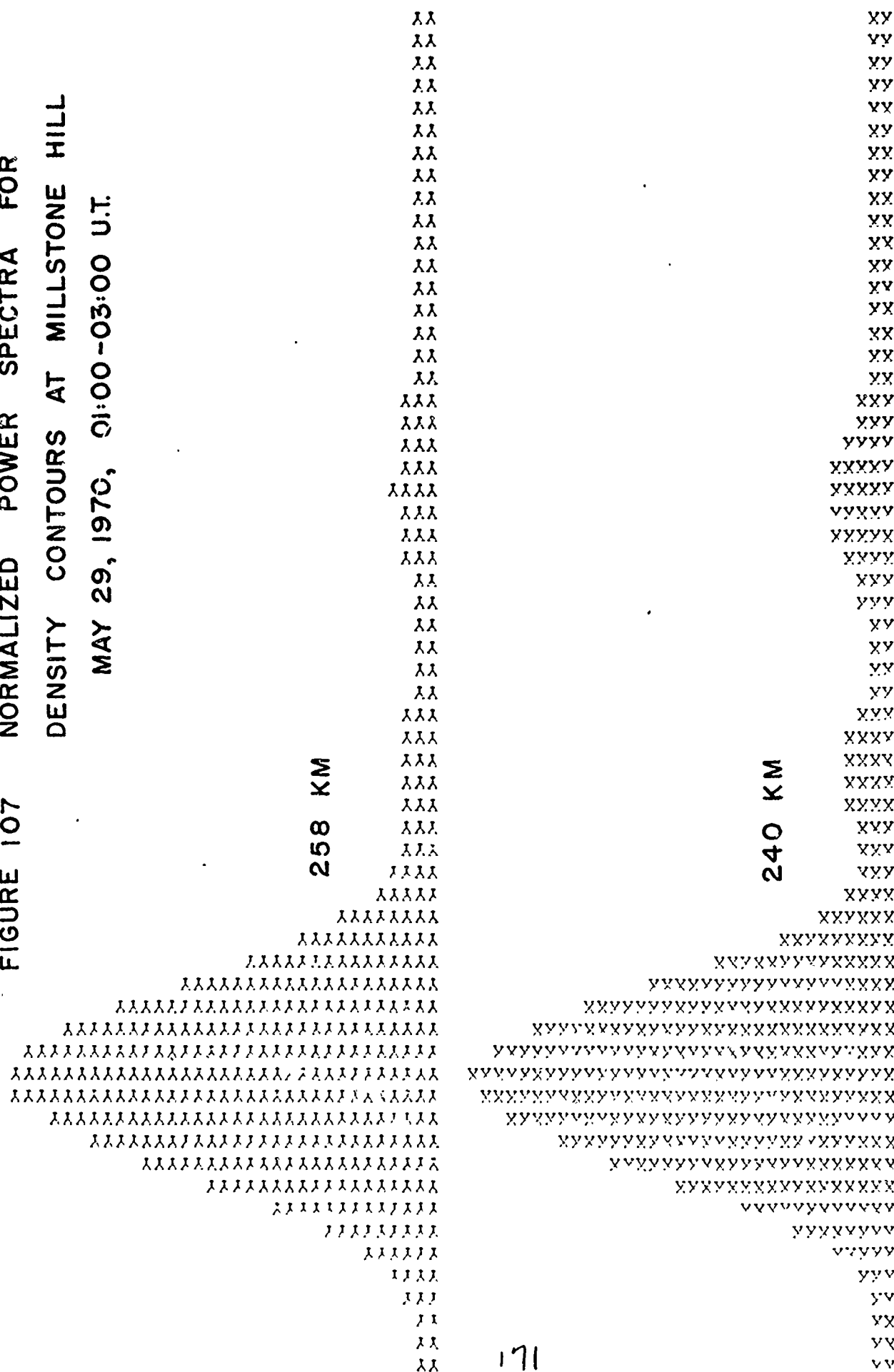
FIGURE 106   DENSITY CONTOURS FOR 240 AND 258 KM

MILLSTONE HILL

MAY 29, 1970, 01:00–03:00 U.T.

258 KM

240 KM

LOG DENSITY

UNIVERSAL TIME

01:00

03:00

170

FIGURE 107   NORMALIZED POWER SPECTRA FOR DENSITY CONTOURS AT MILLSTONE HILL MAY 29, 1970, 01:00-03:00 U.T.

258 KM

240 KM

1/20 MIN⁻¹

FREQUENCY

0

FIGURE 108 RATIO OF EXPERIMENTAL TO THEORETICAL VALUES OF $N'(Z_2)/N'(Z_1)$ FOR $Z_2 = 258$ KM AND $Z_1 = 240$ KM AT MILLSTONE HILL, MAY 29, 1970, 01:00-03:00 U.T.

PERIOD

N = 3600 POINTS

172